DISCLAIMER

This report was prepared as an account of work sponsored by an agency of the United States Government. Neither the United States Government nor any agency thereof, nor any of their employees, makes any warranty, express or implied, or assumes any legal liability or responsibility for the accuracy, completeness, or usefulness of any information, apparatus, product, or process disclosed, or represents that its use would not infringe privately owned rights. Reference herein to any specific commercial product, process, or service by trade name, trademark, manufacturer, or otherwise does not necessarily constitute or imply its endorsement, recommendation, or favoring by the United States Government or any agency thereof. The views and opinions of authors expressed herein do not necessarily state or reflect those of the United States Government or any agency thereof. Reference herein to any social initiative (including but not limited to Diversity, Equity, and Inclusion (DEI); Community Benefits Plans (CBP); Justice 40; etc.) is made by the Author independent of any current requirement by the United States Government and does not constitute or imply endorsement, recommendation, or support by the United States Government or any agency thereof.

A Comprehensive Study of the Impact of Inverter-Based Resource (IBR) Modeling and Control on Protection Relay Elements

Jing Wang,[1] Paulo Henrique Pinheiro,[2] Soham Chakraborty,[1] Brian Johnson,[2] Romulo Goncalves Bainy[2], and Andy Hoke[1]

1 National Renewable Energy Laboratory
2 University of Idaho

NREL is a national laboratory of the U.S. Department of Energy
Office of Energy Efficiency & Renewable Energy
Operated under Contract No. DE-AC36-08GO28308

This report is available at no cost from NREL at www.nrel.gov/publications.

Technical Report
NREL/TP-5D00-94430
November 2025

A Comprehensive Study of the Impact of Inverter-Based Resource (IBR) Modeling and Control on Protection Relay Elements

Jing Wang,[1] Paulo Henrique Pinheiro,[2] Soham Chakraborty,[1] Brian Johnson,[2] Romulo Goncalves Bainy[2], and Andy Hoke[1]

1 National Renewable Energy Laboratory
2 University of Idaho

Suggested Citation
Wang, Jing, Paulo Henrique Pinheiro, Soham Chakraborty, Brian Johnson, Romulo Goncalves Bainy, and Andy Hoke. 2025. *A Comprehensive Study of the Impact of Inverter-Based Resource (IBR) Modeling and Control on Protection Relay Elements*. Golden, CO: National Renewable Energy Laboratory. NREL/TP-5D00-94430. https://www.nrel.gov/docs/fy26osti/94430.pdf.

NREL is a national laboratory of the U.S. Department of Energy
Office of Energy Efficiency & Renewable Energy
Operated under Contract No. DE-AC36-08GO28308

This report is available at no cost from NREL at www.nrel.gov/publications.

Technical Report
NREL/TP-5D00-94430
November 2025

15013 Denver West Parkway
Golden, CO 80401
303-275-3000 • www.nrel.gov

NOTICE

This work was authored in part by NREL for the U.S. Department of Energy (DOE), operated under Contract No. DE-AC36-08GO28308. Funding for the NREL authors provided by U.S. Department of Energy Office of Energy Efficiency and Renewable Energy Solar Energy Technologies Office. The views expressed herein do not necessarily represent the views of the DOE or the U.S. Government.

This report is available at no cost from NREL at www.nrel.gov/publications.

U.S. Department of Energy (DOE) reports produced after 1991 and a growing number of pre-1991 documents are available free via www.OSTI.gov.

Cover photos (clockwise from left): Josh Bauer, NREL 61725; Visualization from the NREL Insight Center; Getty-181828180; Agata Bogucka, NREL 91683; Dennis Schroeder, NREL 51331; Werner Slocum, NREL 67842.

NREL prints on paper that contains recycled content.

Acknowledgments

This work is based upon work supported by the U.S. Department of Energy's Office of Energy Efficiency and Renewable Energy (EERE) under the Solar Energy Technologies Office Award Number 41215.

The authors thank Yi Yang of the U.S. Department of Energy's Solar Energy Technologies Office for her continuous support and her very helpful insights for this study.

In addition, we acknowledge the substantial contribution to this study provided by Scott Manson from Schweitzer Engineering Laboratories, Cameron Kruse from Kauai Island Utility Cooperative, Prashant Kansal and Sai Gopal Vennelaganti from Tesla, Manish Patel from Silicon Ranch, and Rich Bauer from the North American Electric Reliability Corporation. The project team is also grateful to colleagues Yaswanth Nag Velaga, Ben Kroposki, and Rasel Mahmud for their input, review, and feedback for this work.

List of Acronyms

AG	Phase-A-to-ground (fault)
BESS	battery energy storage system
dq	direct quadrature
EMT	electromagnetic transient
FID	fault identification logic
FRT	fault ride-through
GFL	grid-following
GFM	grid-forming
IBR	inverter-based resource
IEEE	Institute for Electrical and Electronics Engineers
KIUC	Kaui Island Utility Cooperation
MPPT	maximum power point tracking
NERC	North American Electric Reliability Corporation
PI	proportional-integral
PLL	phase-locked loop
POM	point of measurement
PR	proportional resonance
PV	photovoltaics
RMS	root mean square
SEL	Schweitzer Engineering Laboratories
VSM	virtual synchronous machine

Executive Summary

The increasing integration of inverter-based resources (IBRs) into power systems has challenged power system protection systems because of the different fault response behaviors these sources provide relative to the short circuit response of synchronous generators. The main challenges with respect to the IBR fault current response include the low level of fault current magnitude, unpredictable positive sequence current in the first two-three cycles, and the unpredictable angles and magnitudes of the negative sequence currents which combined can lead to the mis-operation of some classes of transmission system protection elements. These behaviors impact some distance elements and the elements that supervise them, such as directional elements and fault type identification logic, or those provide polarizing reference angle and frequency references. Today, researchers and engineers have a good understanding and knowledge of IBRs from the control perspective, but very few of them understand power system protection, especially how the various control/configuration aspects of IBRs affect the protective relay response. Similarly, power system protection engineers often lack in-depth knowledge and understanding of IBRs, making it challenging for them to configure protection relay settings correctly—even when they are aware that IBRs contribute lower fault currents and display inconsistent fault characteristics. Generally, there is a lack of coordination and understanding between the design of protection systems (protection engineers) and IBR controls (IBR engineers). Given the increasing share of IBRs in the global energy mix, it is essential to explore innovative solutions to enhance the performance and reliability of power system protection in the presence of high levels of inverter-based generation. To achieve this goal, existing protection technologies need to be revisited and redesigned based on an accurate understanding of the IBRs' fault responses, which are significantly different than the responses of synchronous generators; therefore, this study aims to investigate those challenges related to IBR-dependent transmission system protection. In this study, we perform a comprehensive study of the impact of IBR modeling and control on protection relay elements. This report offers recommendations for both IBR and protection engineers to improve IBR fault response and enhance the reliability of protection systems.

The study begins with an analysis to understand the gap between inverter fault behavior and relay efficacy. This results in the following four aspects of IBRs that need to be characterized and evaluated from the perspective of their impact on protective relay elements: (1) inverter model type (average model versus switching model), (2) sequence components, (3) control functions and current limiter, and (4) primary sources (battery, photovoltaics [PV], combined battery and PV, and an ideal DC source). Then, generic multifunctional grid-following (GFL) and grid-forming (GFM) IBR models are developed with configurable parameters and settings to select different DC sources, the average model versus the switching model, different power-level controls and current controls, and different current limiters, etc., to create models with different variations for the IBR characterization study. To support this characterization study, a protective relay model with all the relevant protection elements (distance elements, directional elements, differential elements, supervisory elements, and fault identification logic [FID]) used by our utility partner (KIUC) is implemented in MATLAB based on the relay manual and data sheet. The relay model is validated using field event data and verified against a commercial relay to ensure its proper functionality and accuracy.

For the characterization of the impact of IBR modeling and control on protection relay elements, only the dynamics of the first three cycles after the fault occur are analyzed because this is the

time window when the primary protective relays in transmission systems make decisions. Because IBR internal protection (e.g., AC overcurrent and DC undervoltage) and most controls that can cause an IBR to trip usually have a much longer window than the first three cycles (momentary cessation may happen within first three cycles), this study does not consider the impact of IBR internal protection and tripping controls on the protective relay and protection elements (momentary cessation is an exception). We use our utility partner's system, from Kauai Island Utility Cooperative, to perform simulation evaluations, including their power system model, IBR plant models, protective relay configurations and protection elements. A comprehensive simulated fault response dataset, including various aspects of IBR modeling and control (as well as some other aspects, such as momentary cessation; different IBR operating points; different grid strengths; and different fault locations, types, and impedances) is generated in PSCAD in COMTRADE format and passed into the protection elements and the relay model developed in MATLAB for the characterization and sensitivity analysis. The key learnings and findings are based on the system under study, and they are summarized as follows:

- Overall, GFM and GFL IBRs primarily impact traditional protection elements like distance protection, along with its supervising function, such as the directional elements and FID logic. This is due to IBR producing highly oscillatory fault currents with unpredictable angles and the absence of negative sequence current during faults. Differential protection remains reliable, with only fault with high fault resistance impacting its behavior by restraining its operation.
- Protection engineers need to understand the IBR fault response, particularly the negative-sequence current during the transient period (the window during the first three cycles when transmission protection relays make decisions) to ensure proper relay settings and coordination. Likewise, IBR engineers must understand how specific IBR controls and configurations influence IBR fault response and should set them to ensure consistent fault behavior during the transient period. Standards can be used to guide IBR control engineers towards designing fault responses that are conducive to proper transmission protection relay operation.
- The extensive characterization and the sensitivity study of the IBR modeling and control aspects impact on protection relay elements show that the inverter model (average model versus switching model), the DC source (PV, battery, and combined), and the power loop (PQ-dispatch versus Vdc-Vac control for GFL IBR and droop versus virtual synchronous machine for GFM IBR) do not significantly impact the sequence components and the protection elements. However, faster loop (current control), current limiter, and current-blocking time (momentary cessation) affect the protection elements and could affect the final protection relay decision.
- In particular, IBR negative-sequence current compliance with the Institute for Electrical and Electronics Engineers (IEEE) Std 2800-2022 is critical for the protection elements, and negative-sequence control should be included in the GFL and GFM inverter control to support protective relays' correct decision. We suggest disabling protection elements that need negative-sequence components when the fault response is dominated by IBRs that do not control negative-sequence current. This occurs because IBRs without negative-sequence current control can lead to incorrect calculations and decisions by those elements. Negative-sequence current should be higher than a certain threshold so that the supervisory overcurrent detectors enable the protection element that they are supervising (e.g., distance elements,

directional elements, and FID logic). Usually, this threshold checks that the current measurements are above currents due to untransposed lines or unbalanced loads, as well as the CT error (i.e., 10% of the rated secondary current during transient conditions). Along with the magnitude, the correct angle of the negative-sequence current contributed by the IBR with respect to the negative-sequence voltage is crucial for correct operation of any negative-sequence-based directional elements.

- If an IBR uses current blocking (momentary cessation) for undervoltage events, the duration of the minimum fault-ride-through (FRT) time before current blocking is allowed has an impact on the correct operation of the relay, especially for the negative-sequence directional element, the negative sequence current I2-polarized quadrilateral element, and the FID logic. In summary, if the element relies on the negative-sequence current, and if it is also supervised by the magnitude of I2, it will impact the relay response. If the IBR goes into current blocking too soon, the protection will not have sufficient time to pick up. When the IBR takes longer to block the current injection, the protection can respond properly if other protection criteria are met. If the blocking time is set to one cycle, the fault direction decision by the relay is significantly affected, whereas for longer times (e.g., four cycles), the relay elements correctly detect the fault direction, and, as a result, the relay is effective. One option is to disable the protection elements that require negative-sequence components if the blocking occurs too fast after the fault inception, but this is at the expense of the protection scheme reliability. Thresholds and delays related to IBR current blocking need to be considered in the IBR model. In future revisions, IEEE 2800 could require that current blocking, if used for undervoltage events, not take place until at least four cycles after the onset of an undervoltage condition.
- Different current-limiting schemes result in different fault responses. More specifically, based on the project team's field observation (including those from the advisor board members), the current limiter causes instantaneous angle shifts which deceive the relays and current limiting methods are sometimes the root of unpredictable negative sequence current production. The instantaneous dynamic current limiter shows more oscillations and needs more time to settle than the magnitude-based current limiter; therefore, the magnitude-based current limiter is more recommended.
- Even though GFM and GFL IBRs have different control strategies and may have different short-circuit capabilities, their fault currents are limited. Both GFL and GFM inverters can contribute consistent fault current for mho or quadrilateral distance elements supervised by negative sequence directional elements or using negative sequence polarization to make timely and correct decisions as long as they produce a reliable negative-sequence current that achieves appropriate magnitude and phase angle in the first cycles after the fault.
- Based on the learnings related to the impact of IBR response on the distance elements, the directional elements, and the FID logic, the recommendations are summarized as follows: (1) ground distance relays should avoid negative-sequence current polarization, protection engineers should use zero-sequence polarized quadrilateral elements and positive-sequence voltage-memory polarized mho elements; and negative-sequence current polarization should be replaced by loop-current polarization for ground and phase distance elements. (2) Zero-sequence polarized directional elements are preferred to supervise ground faults in a grounded system, and negative-sequence directional elements can be used to supervise phase faults if the IBR controls the negative-sequence current injection.

Table of Contents

Executive Summary ..... **v**
1 IBR Characterization Overview **1**
1.1 Background 1
1.2 Objectives and Overall Approach of the Study 1
1.3 Summary of the Study 3
2 Generic IBR Modeling **4**
2.1 Multifunctional EMT Model for GFL IBRs 4
2.1.1 Birds-Eye View of the EMT Model of GFL IBRs 5
2.1.2 Deep Dive Into the EMT Model of GFL IBRs 7
2.2 Multifunctional EMT Model for GFM IBRs 13
2.2.1 Birds-Eye View of the EMT Model of GFM IBRs 14
2.2.2 Deep Dive Into the EMT Model of GFM IBR 15
2.3 Additional Controls, Limiter Schemes, and Protection Logics 21
2.3.1 Negative-Sequence Component (IEEE Std 2800) 21
2.3.2 Update in the Current Limiter 23
2.3.3 Momentary Cessation 25
3 Protective Relay Modeling **28**
3.1 Background for Protection Element Modeling 28
3.2 Phasor-Based Protection Elements 31
3.2.1 Digital Signal Processing for Phasor-Based Protection Elements 31
3.2.2 Distance Protection: Mho Characteristic 32
3.2.3 Distance Protection: Quadrilateral Characteristic 33
3.2.4 Line Current Differential Protection in the Alpha Plane 36
3.2.5 Impedance-Based Directional Elements 37
3.2.6 FID Logic 39
3.3 Protection Elements Based on Time-Domain Superimposed Quantities 40
3.3.1 Digital Signal Processing for Time-Domain Elements 40
3.3.2 Time-Domain Distance Protection (TD21) 42
3.3.3 Time-Domain Directional Element (TD32) 43
3.3.4 Time-Domain FID Logic 44
4 Framework for Studying the Impact of IBRs on Protection Systems **45**
4.1 Motivation and List of IBR Modeling and Control Aspects 45
4.2 Power System Under Study 46
4.3 Scenarios and Dataset Creation 49
5 IBR Characterization Evaluation Results and Analysis **54**
5.1 Communication-Based Protection Scheme 56
5.2 Results for Distance Elements 57
5.2.1 IBR Aspects Not Affecting Relay Response 57
5.2.2 IBR Aspects Affecting Relay Response 67
5.2.3 Additional Analysis: Power System Conditions 101
6 Guidance and Suggested Requirements for IBR Modeling and Control **108**
6.1 GFL and GFM Modeling Aspects 108
6.2 Protection Setting Guidance Based on the Characterization Study 113
7 Conclusions and Future Work **115**
References **118**
Appendix **123**

List of Figures

Figure 1. Joint effort needed to achieve reliable grid protection and operation 2
Figure 2. Schematic diagram of the research approach of this study 3
Figure 3. Fundamental building blocks of the EMT model of GFL IBRs 5
Figure 4. Closed-loop PQ-dispatch control 8
Figure 5. $\boldsymbol{V}$dc-$\boldsymbol{V}$ac control 9
Figure 6. Current Limiter schemes 10
Figure 7. Current Limiter schemes with axis priority logic 10
Figure 8. Inner-current control in the dq domain 11
Figure 9. Inner-current control in the $\boldsymbol{\alpha\beta}$ domain 12
Figure 10. Inner-current control in the sequence domain 13
Figure 11. *P-f/Q-V* droop control 16
Figure 12. VSM control 17
Figure 13. Outer-voltage, inner-current controller designed in the dq domain 18
Figure 14. Outer-voltage, inner-current controller designed in the $\boldsymbol{\alpha\beta}$ domain 19
Figure 15. Outer-voltage, inner-current controller designed in the sequence domain 20
Figure 16. GFL and GFM IBR response under slow and fast IEEE Std 2800-compliant controllers 23
Figure 17. Initial saturation-based Current Limiter scheme 24
Figure 18. Modified priority-based Current Limiter scheme 25
Figure 19. Real-world example of IBR momentary cessation [46] 26
Figure 20. Logic diagram of the implemented momentary cessation in the IBR 27
Figure 21. KIUC transmission system 28
Figure 22. Active functions in the SEL-411L relay 30
Figure 23. Active functions in the SEL-T400L relay 30
Figure 24. Digital signal processing for phasor-based protection elements 31
Figure 25. Dynamic mho expansion due to memory polarization 32
Figure 26. Quadrilateral characteristics 33
Figure 27. Negative-sequence network diagram to compute the tilt angle of the quadrilateral characteristic 34
Figure 28. Logic diagram for the distance elements 35
Figure 29. Trip schematic diagram for Zone 1 using the quadrilateral characteristic 36
Figure 30. Rainbow characteristic for the line current differential protection in the alpha plane 37
Figure 31. General diagram for line current differential protection 37
Figure 32. Sequence component diagram showing the connections for forward and reverse faults 38
Figure 33. Diagram for the 32QG element 38
Figure 34. Operating principle for phasor-based FID logic 39
Figure 35. Superposition theorem 40
Figure 36. Digital signal processing stage 41
Figure 37. TD21 simplified logic diagram for the AG fault loop 43
Figure 38. TD32 principle of operation 43
Figure 39. Simplified logic for the TD32 element, AG loop 44
Figure 40. The inverter aspects under study 46
Figure 41. Figure showing the transmission system under study 46
Figure 42. The process flow diagram of the EMT study 50
Figure 43. Flow for scenario and dataset creation 50
Figure 44. Schematic for testing the IBR protection functions 54
Figure 45. Process flow diagram for EMT studies 55
Figure 46. Analysis framework 55
Figure 47. 87L elements using the alpha plane—all fault cases 57
Figure 48. Voltage and current signals for the AG fault case 58

Figure 49. Sequence current magnitudes 59
Figure 50. Sequence current angles 59
Figure 51. Voltage and current signals for the BC fault 60
Figure 52. Sequence current magnitudes 60
Figure 53. Sequence current angles 60
Figure 54. Sequence current magnitudes 62
Figure 55. Sequence current angles 62
Figure 56. Sequence currents magnitudes 63
Figure 57. Sequence currents angles 63
Figure 58. Sequence current magnitudes 64
Figure 59. Sequence current angles 64
Figure 60. Sequence current magnitudes 65
Figure 61. Sequence current angles 65
Figure 62. Sequence current magnitudes 66
Figure 63. Sequence current angles 66
Figure 64. Sequence current magnitudes 67
Figure 65. Sequence current angles 67
Figure 66. Effect of different current controllers in the quadrilateral characteristic polarized by the I2 – AG fault case 69
Figure 67. Effect of different current controllers in the quadrilateral characteristic polarized by the I2 – BC fault case 69
Figure 68. Quadrilateral characteristic behavior when using zero-sequence current polarization 70
Figure 69. Mho element behavior during an AG fault for different inner-current controllers 70
Figure 70 - Mho element behavior during AG fault (zoomed in). 70
Figure 71. Mho element behavior for a BC fault comparing the inner-current controllers 71
Figure 72. Comparing the dynamic mho expansion between the IBR end and the grid end of the line 71
Figure 73. Negative-sequence directional element response comparing the three current controllers 72
Figure 74. Overcurrent detectors that supervise the 32QG element 73
Figure 75. Zero-sequence restraining factor blocking the 32QG element 73
Figure 76. 32V element response 74
Figure 77. FID logic response for different current controllers 74
Figure 78. Three Current Limiter strategies for GFL IBRs 75
Figure 79. Example showing relay responses of the magnitude-based and latching-based current-limiting schemes under an (a) AG fault and a (b) BC fault 76
Figure 80. Current signals of two commonly used current limiters 77
Figure 81. Mho element for ground faults 78
Figure 82. I0-polarized quadrilateral element 79
Figure 83. I2-polarized quadrilateral element 79
Figure 84. Negative-sequence directional element (32QG) 80
Figure 85. Zero-sequence directional element (32V) 80
Figure 86. FID logic 81
Figure 87. Timing diagram 82
Figure 88. Instantaneous current signals of two typical current limiters 83
Figure 89. Mho element for ground faults 83
Figure 90. I0-polarized quadrilateral element 84
Figure 91. I2-polarized quadrilateral element 84
Figure 92. Negative-sequence directional element (32QG) 84
Figure 93. Zero-sequence directional element (32V) 85
Figure 94. FID logic response 85
Figure 95. Timing diagram 86
Figure 96. Instantaneous current signals 87

Figure 97. Mho element response for a BC fault 88
Figure 98. Quadrilateral characteristic with I2 polarization 89
Figure 99. Negative-sequence directional element (32Q) for phase faults 89
Figure 100. Timing diagram 90
Figure 101. Instantaneous current signals of two typical current limiters 91
Figure 102. Mho element for a phase fault 91
Figure 103. Quadrilateral characteristic with I2 polarization 92
Figure 104. Negative-sequence directional element (32Q) 92
Figure 105. Timing diagram 93
Figure 106. Timing diagrams to evaluate the impact of the current-blocking schemes on the relay response 94
Figure 107. I2-polarized quadrilateral element 95
Figure 108. 32QG element response 96
Figure 109. Sequence current-based FID logic 96
Figure 110. I2-polarized quadrilateral element for phase faults 97
Figure 111. 32Q directional element 98
Figure 112. Mho element response during the current-blocking scheme (BC loop) 98
Figure 113. I2-polarized quadrilateral element 99
Figure 114. 32QG directional element response 100
Figure 115. FID logic response 100
Figure 116. Timing diagram comparing the fast and slow response of the IBR's controllers 100
Figure 117. Quadrilateral relay behavior for resistive faults at 50% of the line with I2 polarization with IEEE Std 2800-compliant controller 102
Figure 118. Zero-sequence equivalent network to compute the tilt angle for zero-sequence current polarization 103
Figure 119. Mho element behavior for ground faults with different fault resistances 104
Figure 120. Comparing the effect of grid strength conditions for an AG fault with Rf 5 Ω at 50% of the line 105
Figure A-1. GFL (left) and GFM (right) IBR fault responses and the responses of the relay elements under an AG fault: (a) current and voltage, (b) I2-polarized quadrilateral element, (c) negative-sequence voltage-polarized directional element (32QG), (d) zero-sequence voltage-polarized directional element (32V), (e) memory-polarized mho element, (f) fault identification logic; and (g) relay trip signals 125
Figure A-2. GFL (left) and GFM (right) IBR fault responses and the responses of the relay elements under a BC fault: (a) current and voltage, (b) I2-polarized quadrilateral element, (c) negative-sequence voltage-polarized directional element (32QG), (d) memory-polarized mho element, and (e) relay trip signals 127
Figure A-3. GFL (left) and GFM (right) IBR fault responses and the responses of the relay elements under an AG fault (P* = 0.1 p.u. and Q* = 0 p.u.): (a) current and voltage, (b) I2-polarized quadrilateral element, (c) negative-sequence voltage-polarized directional element (32QG), (d) aero-sequence voltage-polarized directional element (32V), (e) memory-polarized mho element, (f) fault identification logic, (g) relay trip signals, and (h) sequence components of the fault current 130
Figure A-4. Current sequence components of GFL (left) and GFM (right) IBR fault responses under varying pre-fault operating points: (a) P* = 0.25 p.u. and Q*=0 p.u. under an AG fault, (b) P* = 0.25 p.u. and Q* = 0.15 p.u. under an AG fault, (c) P* = 0.1 p.u. and Q* = 0 p.u. under a BC fault, (d) P* = 0.25 p.u. and Q* = 0 p.u. under a BC fault, and (e) P* = 0.25 p.u. and Q* = 0.15 p.u. under a BC fault 132

List of Tables

Table 1. Parameters of the EMT Model of GFL IBRs 6
Table 2. Available Options in the Developed EMT Model of GFL IBRs for Selecting the DC Source Type and Inverter Model 6
Table 3. Available Options in the EMT Model of GFL IBRs for Selecting the Controller Logic 6
Table 4. Available Options in the EMT Model of GFL IBRs for Selecting the Current Limiter Protection Logic 7
Table 5. Available Options in the EMT Model of GFM IBRs for Selecting the Controller Logic 15
Table 6. Available Options in the EMT Model of GFM IBRs for Selecting the Current Limiter Protection Logic 15
Table 7. IEEE Std 2800-2022 Voltage Ride-Through Requirements for IBRs [5] 26
Table 8. Active Protection Elements in the SEL-411L Relay 29
Table 9. Active Time-Domain Protection Functions in the SEL-T400L Relay 29
Table 10. Detailed Voltage and Currents per Fault Loop 33
Table 11. Loop Incremental Voltages and Replica Currents 41
Table 12. Various Control and Current Limiter Schemes Under Study for GFL IBRs 47
Table 13. Various Control and Current Limiter Schemes Under Study for GFM IBRs 48
Table 14. Impedances of Various Lines of the Test System 48
Table 15. Fixed Parameters to Evaluate the Impact of Inverter Model on Protection Decisions 58
Table 16. Fixed Parameters to Analyze the Impact of Different Outer-Control Loops 63
Table 17. Fixed Parameters for the GFM Cases 65
Table 18. Case Study Settings to Evaluate IBR Aspects That Affect Relay Response 68
Table 19. Fixed Parameters in the Case Study 76
Table 20. Grid Strength Configuration 101
Table 21. Percentage of Operation for Distance Elements in Cases With Resistive Faults and Different Grid Strength Conditions 103
Table 22. Scenarios for Different Power Flow Conditions 105
Table 23. Performance of the Quadrilateral Element Operation for Different Power Flow Conditions and Fault Locations 106
Table 24. Performance of the Mho Element for Different Power Flow Conditions and Fault Locations 106
Table 25. Impact of Various GFL IBR Aspects on the Responses of Various Relay Elements 108
Table 26. Impacts of Various GFM IBR Aspects on the Response of Various Relays Elements 109
Table 27. Recommendations for IBR Modeling and Control From the Perspective of Protection Systems 110
Table 28. Recommendations for Protection Functions Impacted by IBRs 113

1 IBR Characterization Overview

1.1 Background

As the proportion of generation from inverter-based resources (IBRs), such as solar photovoltaics (PV) and wind, has increased, several challenges in transmission system protection have been observed. These include protective relay misoperations (mainly because of incorrect settings/logics/design errors) in reliability regions, according to a report by the North American Electric Reliability Corporation (NERC) [1]. These challenges have been shown to lead to unnecessary losses in generation that increase reliability risks [2]. One lesson learned from these events is that fault behaviors in high-IBR scenarios are becoming increasingly unpredictable, which has resulted in misoperation in protection and system-wide events, including outages [3]. In particular, the short-timescale transients of IBRs under fault scenarios (the first few cycles after fault events) are not accurately captured by phasor-based fault study simulation tools, which causes inaccurate fault study results and thus inaccurate protection design. As transmission systems rapidly transition toward IBR dependence, an inability to accurately predict and capture IBR fault responses could become a major barrier to transmission system protection and reliable grid operation.

In addition, there is a lack of coordination between the design of transmission system protection systems and the design of IBR controls, which is partly due to misunderstandings about how IBRs respond to faults. Today, researchers and engineers have a good understanding and knowledge of IBRs from the control perspective, but very few of them understand power system protection, especially how the various control/configuration aspects of IBRs affect the responses of protective relays and their protection elements. Similarly, power system protection engineers often lack in-depth knowledge and understanding of inverter-based resources (IBRs), making it challenging for them to configure protection relay settings correctly—even when they are aware that IBRs contribute lower fault currents and display inconsistent fault characteristics. Generally, there is a lack of coordination between the design of protection systems (protection engineers) and IBR controls (IBR engineers). Further, there are misunderstandings of how IBRs respond to faults because IBRs often operate with sophisticated control algorithms that can complicate fault identification (FID), isolation, and system recovery after disturbances. Given the increasing share of IBRs in the global energy mix, it is essential to adapt and modernize protection schemes to address these challenges. Researchers and engineers must explore innovative solutions to enhance the performance and reliability of power system protection in the presence of high levels of inverter-based generation. Also, existing protection technologies need to be revisited and redesigned based on an accurate understanding of IBRs' fault responses, which are significantly different than the responses of synchronous generators. These are urgent challenges to resolve to ensure IBR-dependent transmission system protection and to help maintain grid stability and reliability.

1.2 Objectives and Overall Approach of the Study

This goal of this study is to study and analyze the challenges associated with power system protection within the context of IBRs by identifying potential gaps in current protection schemes and proposing advancements that ensure grid stability, reliability, and resilience as inverter-based generation continues to increase. Toward this end, the study aims to achieve the following

three main objectives: (1) Perform a comprehensive study of the impact of IBR modeling and control on protection relay elements. (2) Provide recommendations for the characteristics of inverter fault responses to achieve reliable protection of IBR-dominant systems. (3) Develop enhanced protection schemes to resolve the protection challenges with systems with high IBRs. Importantly, the first two objectives serve as foundational research and educational work because they increase the fundamental understanding for protection and IBR engineers so that protection engineers know how to configure relays based on the understanding of IBR fault behavior and inverter engineers know how IBR controls affect the relay responses and decisions to design IBR controls. This report focuses on the first two objectives of the study: We perform a comprehensive study of the impact of IBR modeling and control on protection relay elements, and we provide guidance and suggested requirements of IBR modeling for fault studies and recommendations for protection settings. This comprehensive study will shed light on the misunderstandings between protection engineers and inverter engineers. As illustrated in Figure 1, the joint effort between protection engineers and inverter engineers will enable reliable grid protection and operation.

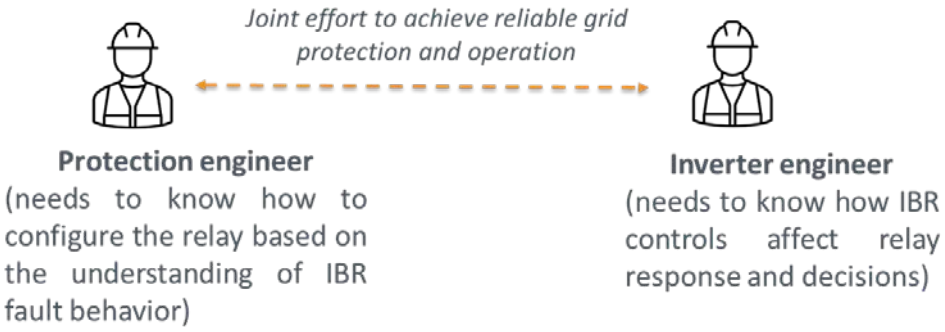

Figure 1. Joint effort needed to achieve reliable grid protection and operation

Figure 2 shows the schematic diagram of the research approach of this study. First, an analysis is performed to understand the gap between inverter fault behavior and relay efficacy. This results in the following four aspects of IBRs that need to be characterized and evaluated from the perspective of the protective relay elements: (1) inverter modeling (average model versus switching model), (2) sequence components, (3) control functions and current limiter, and (4) primary sources (battery, PV, combined battery and PV, and ideal DC source). Additionally, other aspects, such as momentary cessation and the fast/slow response of the output current, are found to be important factors as well, and they are included for a comprehensive study. The simulation evaluation of various aspects through protective relay elements is performed in a systematic way using existing relay models used in the field by our utility partner, Kauai Island Utility Cooperation (KIUC). Finally, as key contributions of this study, we provide guidance and suggested requirements of IBR modeling for fault studies and recommendations for protection engineers.

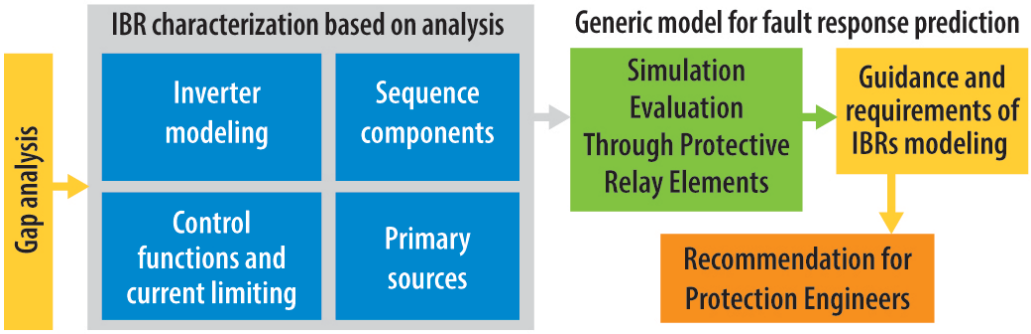

Figure 2. Schematic diagram of the research approach of this study

1.3 Summary of the Study

In this study, we use KIUC's system to perform the simulation evaluation, including their power system model, the IBR plant models, the protective relays, and the protection elements. For the IBR characterization and evaluation, only the dynamics of the first three cycles after the fault occurs are analyzed because this is the time window when the primary protective relays in transmission systems make decisions [3]. Because IBR internal protection (e.g., AC overcurrent and DC undervoltage) and undervoltage tripping controls usually have a much longer window than the first three cycles [4][5], this study does not consider the impact of IBR internal protection and tripping on the protective relay and protection elements. The simulation of the KIUC system with the IBR model is performed in an electromagnetic transient (EMT) simulation tool, PSCAD; and the protection elements and the relay models are developed in MATLAB. A comprehensive fault response dataset, including various aspects of IBR modeling and control, is generated in PSCAD in COMTRADE format and passed into the protection elements in the relay model developed in MATLAB for the characterization and sensitivity analysis. This study achieves the following outcomes:

- Develop generic multifunctional grid-following (GFL) and grid-forming (GFM) IBR models with configurable parameters and settings to select different DC sources, the average model versus the switching model, different power-level controls and current controls, and different current limiters, etc., to create models with different variations for the IBR characterization study.
- Implement the protective relay model with all the enabled protection elements (distance elements, direction elements, differential elements, supervisory elements, and FID logic) in MATLAB based on the relay manual and data sheet. The relay model is validated using the field event data and verified against a commercial relay to ensure its proper functions and accuracy in modeling.
- Perform a comprehensive IBR characterization evaluation using the protective relay model and protection elements and draw qualitative and quantitative conclusions based on the deep sensitivity analysis.
- Provide guidance and suggested requirements for IBR modeling for fault studies and protection design.
- Provide recommendations for protection relay settings for protection engineers based on the comprehensive study.
- Provide recommendations for IBR control design to facilitate proper transmission protection operation.

2 Generic IBR Modeling

The current state-of-the-art IBR models typically address only limited aspects of inverter-based resource modeling—such as various inverter power-level controls, device-level controls (current and/or voltage control), measurement and grid synchronization, grid compliance controls, and current limiters. However, these models lack the comprehensiveness needed for our IBR characterization and sensitivity study, which aims to assess how different modeling and control features influence protection elements and relay decision-making [7]. IBRs' negative-sequence current compliance with the Institute of Electrical and Electronics Engineers (IEEE) Std 2800 is a critical aspect to study from the protection perspective; therefore, this report goes beyond the state of the art and aims to develop a comprehensive GFL and GFM inverter model for transient stability studies, fault studies, and protection design. The GFL and GFM IBR models include variations, including different types of DC source, different types of inverter model, different inverter power-level control, different inverter device-level control (current and/voltage control), and current limiter strategies. The next two sections describe the EMT model of the GFL IBR and the GFM IBR.

2.1 Multifunctional EMT Model for GFL IBRs

The EMT model developed in this study using the PSCAD platform has the following characteristics:

1. It can be used as a single black box with flexibility in selecting the MVA rating.
2. It is suitable for interfacing transmission systems, and it complies with IEEE Std 2800; therefore, the model could be of use to transmission system planners to study site-specific performance with IBR integration.
3. It is suitable for interfacing various types and combinations of DC sources, including the PV module, the battery module, and an ideal voltage source; therefore, this model could be of use to different vendors of GFL IBRs with a variety of DC sources.
4. It covers both switching models and average models. This provides a benchmark platform to study the impact of inverter modeling on various aspects, such as fault behavior.
5. It includes large sets of control logic, which the user can select by choosing the correct flags. The control logic covers an exhaustive list of active power control, reactive power control, and inner-current control. The control architecture of commercial GFL IBRs is usually proprietary and can vary from one manufacturer to another. This generic EMT model can be used by both academia and industry to study the operation of systems with multivendor GFL IBRs.
6. It includes large sets of protection logic, which the user can select by choosing the correct flags. The protection logic covers an exhaustive list of the instantaneous current saturation limiter, the instantaneous circular current limiter, the current latching limiter, and anti-windup protections. It is well studied that the choice of limiter protection immensely impacts the fault behavior of IBRs; therefore, this model will be of use for protection system engineers to study and design suitable protection systems with GFL IBRs interfaced in the system.

2.1.1 Birds-Eye View of the EMT Model of GFL IBRs

The fundamental building blocks of the EMT model of GFL IBRs are shown in Figure 3. The power circuit consists of the inverter model interfaced with the DC source of the voltage, V_{dc}. At the output terminals, an LCL filter (L_f, C_f, L_g) and associated equivalent series resistances (R_f, R_g) of the inductors are connected and interfaced to the grid/network via a transformer. The main controller is responsible for generating the pulse-width modulated switching signals for the inverter based on processing the measurements (inner inductor current measurements, i_L^{abc}; output current measurements, i_O^{abc}; and capacitor voltage measurements, v_C^{abc}) via the controller logic and the protection logic.

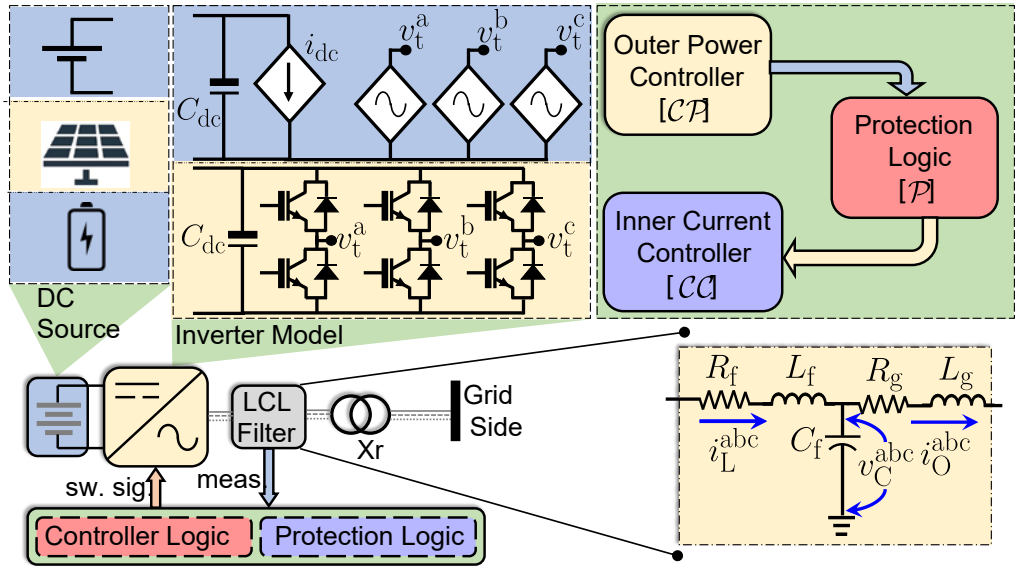

Figure 3. Fundamental building blocks of the EMT model of GFL IBRs

The rating and the parameters of the GFL IBR are tabulated in Table 1. Note that the MVA rating is user-defined and can be changed based on the end-user requirement. The EMT model is connected to a 57.1-kV grid via a step-up transformer of the rating of the three-phase, 0.48/57.1-kV, 1.5-MVA, $Y-\Delta$ transformer; however, this external circuit is independent of the model of the GFL IBRs. The main features of the EMT model of GFL IBRs are as follows:

1. From the DC source model side, the developed EMT model has the flexibility to select various types of DC sources (single or a combination) by choosing the flag, S, externally, as tabulated in Table 2. For example, $S = S_1$ enables connecting to a single PV module on the DC side; $S = S_2$ enables connecting to a single battery module on the DC side; $S = S_3$ enables connecting to a single ideal DC module on the DC side; and $S = S_4$ enables connecting to any combination of PV, battery, and ideal DC module on the DC side.
2. From the inverter model side, the developed EMT model has the flexibility to select two types of models by choosing the flag, M, externally, as tabulated in Table 2. For example, $M = M_1$ enables the switching model, and $M = M_2$ enables the average model of the inverter [8],[9].
3. From the controller logic side, the developed EMT model has the flexibility to select various types of controls, as tabulated in Table 3. For example, in the outer-power

controller (indicated by CP), for active power control, open-loop P dispatch ($CPP = CPP_1$), closed-loop P dispatch ($CPP = CPP_2$), and DC-bus voltage control ($CPP = CPP_3$) are available. Similarly, for reactive power control, open-loop ($CPQ = CPQ_1$) Q dispatch, closed-loop ($CPQ = CPQ_2$) Q dispatch, and AC terminal voltage control ($CPQ = CPQ_3$) are available. In the inner-current controller (CC), the controller in the direct quadrature (dq) domain ($CC = CC_1$), the controller in the $\alpha\beta$ domain ($CC = CC_2$), and the controller in the sequence domain ($CC = CC_3$) are available. The mathematical models of all these control logics are discussed later.

4. From the Current Limiter side, the developed EMT model has the flexibility to select various types of protections, as tabulated in Table 4. For example, in the current limiter (PC), the model has a current saturation-based ($PC = PCS$) and a current latching-based ($PC = PCL$) protection. To have d-axis priority in the limiter, $PCS = PCS_1$ for the saturation-based and $PCL = PCL_1$ for the latching-based limiter can be selected. Similarly, to have q-axis priority in the limiter (as recommended in IEEE Std 2800), $PCS = PCS_2$ for the saturation-based and $PCL = PCL_2$ for the latching-based limiter can be selected. The mathematical models of all these control logics are discussed next.

Table 1. Parameters of the EMT Model of GFL IBRs

Inverter	Value of the Parameters
Ratings (3-ϕ)	480 V (L-L), 60 Hz, 1.25 MVA
DC side	$V_{\mathrm{dc}} = 1200\mathrm{V}$, $f_{\mathrm{sw}} = 5$ kHz
LCL filter	$L_{\mathrm{f}} = 15\mu H, L_{\mathrm{g}} = 1.5\mu H, C_{\mathrm{f}} = 280\mu F$

Table 2. Available Options in the Developed EMT Model of GFL IBRs for Selecting the DC Source Type and Inverter Model

DC Source (S)	Inverter Model (M)
$\boldsymbol{S_1}$: PV module $\boldsymbol{S_2}$: battery module	M_1: switching model
$\boldsymbol{S_3}$: ideal voltage source $\boldsymbol{S_4}$: any combination	M_2: average model

Table 3. Available Options in the EMT Model of GFL IBRs for Selecting the Controller Logic

Controller Logic ($\boldsymbol{C}$)		
Outer-Power Controller ($\boldsymbol{CP}$)		**Inner Current ($\boldsymbol{CC}$)**
Active power (CPP)	Reactive power (CPQ)	CC_1: dq domain
CPP_1: open-loop P dispatch	CPQ_1: open-loop Q dispatch	CC_2: $\alpha\beta$ domain
CPP_2: closed-loop P dispatch	CPQ_2: closed-loop Q dispatch	CC_3: sequence domain
CPP_3: V_{dc} control	CPQ_3: V_{ac} control	

Table 4. Available Options in the EMT Model of GFL IBRs for Selecting the Current Limiter Protection Logic

Current Limiter (PC)		Windup (PW)
Saturation-based (PCS)		PW_1: anti-windup for PI controller
PCS_1: d-axis priority	PCS_2: q-axis priority	
Latching-based (PCL)		PW_2: anti-windup for PR controller
PCL_1: d-axis priority	PCL_2: q-axis priority	

2.1.2 Deep Dive Into the EMT Model of GFL IBRs

Since modeling the DC source and inverter model is very straightforward, this section does not cover these two aspects. Instead, this section discusses the mathematical and computational models of the EMT model of GFL IBRs. In particular, the controller logic and the Current Limiter protection logic are discussed in detail while referring to Table 3, Table 4, and Figure 3.

2.1.2.1 Outer-Power Controller

As mentioned in the previous section, the outer-power controller consists of the following controls: (1) open-loop PQ-dispatch control, (2) closed-loop PQ-dispatch control, and (3) DC-bus voltage (V_{dc}) and AC terminal voltage (V_{ac}) control.

2.1.2.1.1 Open-Loop PQ-Dispatch Control (CPP_1 and CPQ_2)

An open-loop PQ-dispatch controller generates the reference current signals for the inner-current controller of the GFL IBR. The objective is to regulate the active and reactive power of the GFL IBR to a prespecified reference active power, P_{ref}, and reactive power, Q_{ref}, defined either locally or remotely. The power references, P_{ref} , Q_{ref}, and the output of the synchronous reference frame phase-locked loop (PLL) [10],[11] with $v_{\mathrm{C}}^{\mathrm{abc}}$as the input are used to set the references for the current controllers [12],[13],[14]. The synchronous reference frame PLL is based on aligning in closed-loop control the angle of the dq-transformation such that $v_{\mathrm{C}}^{\mathrm{abc}}$ has no q-axis component. A proportional-integral (PI) regulator acts on the alignment error to set the rotation frequency. The desired output current references are calculated using the following pair of equations:

- For CPP_1, CPQ_1 with CC_1: $i_{\mathrm{L,ref}}^{\mathrm{d}'} = \frac{v_{\mathrm{C}}^{\mathrm{d}} P_{\mathrm{ref}} + v_{\mathrm{C}}^{\mathrm{q}} Q_{\mathrm{ref}}}{\left(v_{\mathrm{C}}^{\mathrm{d}}\right)^2 + \left(v_{\mathrm{C}}^{\mathrm{q}}\right)^2}$, $i_{\mathrm{L,ref}}^{\mathrm{q}'} = \frac{v_{\mathrm{C}}^{\mathrm{q}} P_{\mathrm{ref}} - v_{\mathrm{C}}^{\mathrm{d}} Q_{\mathrm{ref}}}{\left(v_{\mathrm{C}}^{\mathrm{d}}\right)^2 + \left(v_{\mathrm{C}}^{\mathrm{q}}\right)^2}$
- For CPP_1, CPQ_1 with CC_2: $i_{\mathrm{L,ref}}^{\alpha'} = \frac{v_{\mathrm{C}}^{\alpha} P_{\mathrm{ref}} + v_{\mathrm{C}}^{\beta} Q_{\mathrm{ref}}}{\left(v_{\mathrm{C}}^{\alpha}\right)^2 + \left(v_{\mathrm{C}}^{\beta}\right)^2}$, $i_{\mathrm{L,ref}}^{\beta'} = \frac{v_{\mathrm{C}}^{\beta} P_{\mathrm{ref}} - v_{\mathrm{C}}^{\alpha} Q_{\mathrm{ref}}}{\left(v_{\mathrm{C}}^{\alpha}\right)^2 + \left(v_{\mathrm{C}}^{\beta}\right)^2}$
- For CPP_1, CPQ_1 with CC_3: Using the synchronous reference frame PLL output, θ_{pll} and $-\theta_{\mathrm{pll}}$, the positive- and negative-sequence components of the voltage ($v_{\mathrm{C}}^{\mathrm{d}+}, v_{\mathrm{C}}^{\mathrm{d}-}, v_{\mathrm{C}}^{\mathrm{q}+}, v_{\mathrm{C}}^{\mathrm{q}-}$) and the current ($i_{\mathrm{L}}^{\mathrm{d}+}, i_{\mathrm{L}}^{\mathrm{d}-}, i_{\mathrm{L}}^{\mathrm{q}+}, i_{\mathrm{L}}^{\mathrm{q}-}$) are calculated [15]. For unbalanced voltage conditions, the following equation is used to create the commanded references for the current regulators:

$$\begin{bmatrix} i_{\mathrm{L,ref}}^{\mathrm{d+}} \\ i_{\mathrm{L,ref}}^{\mathrm{q+}} \\ i_{\mathrm{L,ref}}^{\mathrm{d-}} \\ i_{\mathrm{L,ref}}^{\mathrm{q-}} \end{bmatrix} = \begin{bmatrix} v_{\mathrm{C}}^{\mathrm{d+}} & v_{\mathrm{C}}^{\mathrm{q+}} & v_{\mathrm{C}}^{\mathrm{d-}} & v_{\mathrm{C}}^{\mathrm{q-}} \\ v_{\mathrm{C}}^{\mathrm{q+}} & -v_{\mathrm{C}}^{\mathrm{d+}} & v_{\mathrm{C}}^{\mathrm{q-}} & -v_{\mathrm{C}}^{\mathrm{d-}} \\ v_{\mathrm{C}}^{\mathrm{d-}} & v_{\mathrm{C}}^{\mathrm{q-}} & v_{\mathrm{C}}^{\mathrm{d+}} & v_{\mathrm{C}}^{\mathrm{q+}} \\ v_{\mathrm{C}}^{\mathrm{q-}} & -v_{\mathrm{C}}^{\mathrm{d-}} & -v_{\mathrm{C}}^{\mathrm{q+}} & v_{\mathrm{C}}^{\mathrm{d+}} \\ v_{\mathrm{C}}^{\mathrm{q-}} & -v_{\mathrm{C}}^{\mathrm{d-}} & v_{\mathrm{C}}^{\mathrm{q+}} & -v_{\mathrm{C}}^{\mathrm{d+}} \\ -v_{\mathrm{C}}^{\mathrm{d-}} & -v_{\mathrm{C}}^{\mathrm{q-}} & v_{\mathrm{C}}^{\mathrm{d+}} & v_{\mathrm{C}}^{\mathrm{q+}} \end{bmatrix}^{-1} \begin{bmatrix} P \\ Q \\ P_{\mathrm{c}} \\ P_{\mathrm{s}} \\ Q_{\mathrm{c}} \\ Q_{\mathrm{s}} \end{bmatrix} \quad (1)$$

where P and Q are the average real and reactive powers injected into the grid; and $P_{\mathrm{c}}, P_{\mathrm{s}}, Q_{\mathrm{c}}, Q_{\mathrm{s}}$ are the magnitude of the double fundamental frequency oscillating real and reactive powers as quadrature components referenced to the synchronous rotating frame. The EMT model of the GFL IBRs has flexibility in selecting the following types of sequence reference generation methods:

- Active power ripple control generates $i_{\mathrm{L,ref}}^{\mathrm{d+}}, i_{\mathrm{L,ref}}^{\mathrm{d-}}, i_{\mathrm{L,ref}}^{\mathrm{q+}}, i_{\mathrm{L,ref}}^{\mathrm{q-}}$ by setting $P_{\mathrm{c}} = P_{\mathrm{s}} = 0$.
- Reactive power ripple control generates $i_{\mathrm{L,ref}}^{\mathrm{d+}}, i_{\mathrm{L,ref}}^{\mathrm{d-}}, i_{\mathrm{L,ref}}^{\mathrm{q+}}, i_{\mathrm{L,ref}}^{\mathrm{q-}}$ by setting $Q_{\mathrm{c}} = Q_{\mathrm{s}} = 0$.
- Balanced current control generates $i_{\mathrm{L,ref}}^{\mathrm{d+}}, i_{\mathrm{L,ref}}^{\mathrm{d-}}, i_{\mathrm{L,ref}}^{\mathrm{q+}}, i_{\mathrm{L,ref}}^{\mathrm{q-}}$ by setting $P_{\mathrm{c}} = P_{\mathrm{s}} = Q_{\mathrm{c}} = Q_{\mathrm{s}} = 0$.

2.1.2.1.2 Closed-Loop PQ-Dispatch Control (CPP_2 and CPQ_2)

Two PI controllers are used in the closed-loop PQ-dispatch control, as shown Figure 4. The set points are the commanded active power, P_{ref}, and the reactive power, Q_{ref}; however, at the beginning, $v_{\mathrm{C}}^{\mathrm{abc}}$and $i_{\mathrm{O}}^{\mathrm{abc}}$are used to determine the instantaneous active power, p, and the instantaneous reactive power, q, and then are passed through low-pass filters with the time constant, $\tau_{\mathrm{S}} \in \mathbb{R}_{>0}$, to obtain the average value of the active power, P, and the reactive power, Q. The desired output current references are calculated using the following pair of equations:

- For CPP_2, CPQ_2 with CC_1: The output of the PI regulators is directly used as $i_{\mathrm{L,ref}}^{\mathrm{d}'}, i_{\mathrm{L,ref}}^{q'}$.
- For CPP_2, CPQ_2 with CC_2: $i_{\mathrm{L,ref}}^{\mathrm{d}'}, i_{\mathrm{L,ref}}^{q'}$ are transformed into $i_{\mathrm{L,ref}}^{\alpha'}, i_{\mathrm{L,ref}}^{\beta'}$ using θ_{pll}.

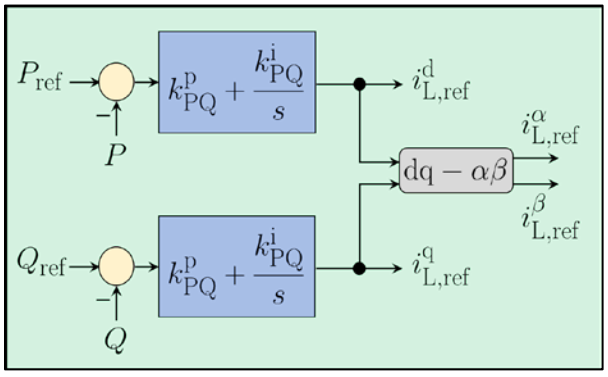

Figure 4. Closed-loop PQ-dispatch control

2.1.2.1.3 V_{dc}-V_{ac} Control (CPP_3 and CPQ_3)

The main objective of control is to regulate the DC-bus voltage, V_{dc}, and the AC terminal voltage, as shown in Figure 5. The kernel of the voltage control is the real/reactive power controller by which P and Q can be independently controlled; therefore, to regulate the DC-bus voltage and the AC terminal voltage, a feedback mechanism compares V_{dc} with its reference command, V_{dc}^{ref}, and V_{ac} with its reference command, V_{ac}^{ref} . Accordingly, it adjusts P_{ref} and Q_{ref} such that the net power exchanged with the DC-bus capacitor is kept at zero and the required reactive power support is provided to regulate the terminal AC voltage. In this application, when the DC source is the PV module, the V_{dc}^{ref} is the output of the maximum power point tracking (MPPT) controller, V_{mppt}. Here, the perturb and observe method of MPPT is used [16].

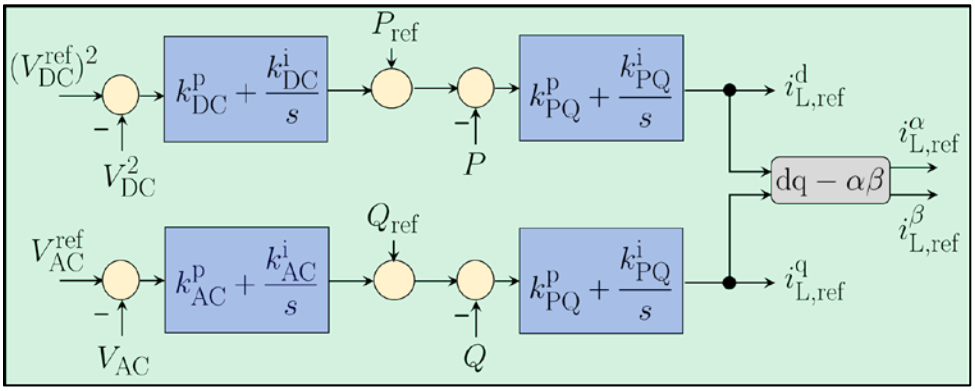

Figure 5. V_{dc}-V_{ac} control

2.1.2.2 Current Limiter

The fault current-limiter strategies employed for the GFL IBR model are described in the following sections.

2.1.2.2.1 Saturation-Based Current Limiter (PCS)

The instantaneous current saturation limiter [17], as shown in Figure 6, sets hard limits on the inductor current references, $i_{L,ref}^{d'}$ and $i_{L,ref}^{q'}$, for CC_1. Whereas for CC_2, the hard limit is on $i_{L,ref}^{\alpha'}$ and $i_{L,ref}^{\beta'}$. The d-axis priority-based instantaneous current saturation limiter, as shown in Figure 7, PCS_1, for CC_1 follows the following equations [18],[19],[20]:

$$\left|i_{L,ref}^{d}\right| = \min\left(i_{sat}, \left|i_{L,ref}^{d'}\right|\right), \left|i_{L,ref}^{q}\right| = \min\left(i'_{sat}, \left|i_{L,ref}^{q'}\right|\right), \quad (2)$$

where $i'_{sat} = \sqrt{i_{sat}^2 - \left(i_{L,ref}^{d}\right)^2}$. Similarly, the q-axis priority-based instantaneous current saturation limiter, PCS_2, for CC_1 is implemented too [21],[22], as shown in Figure 7. An instantaneous hard current saturation limiter will clip the peak of the sinusoidal signal in case of CC_2. This will result in distortional output currents. A magnitude-based circular current saturation limiter is usually implemented for CC_2 with the following equations [23],[24],[25]:

$$i_{L,ref}^{\alpha\beta} = i_{L,ref}^{\alpha'\beta'} \quad \text{if} \quad \sqrt{\left(i_{L,ref}^{\alpha}\right)^2 + \left(i_{L,ref}^{\beta}\right)^2} \le i_{sat} \quad (3)$$

$$i_{\mathrm{L,ref}}^{\alpha\beta} = i_{\mathrm{L,ref}}^{\alpha'\beta'} \frac{i_{\mathrm{sat}}}{\sqrt{\left(i_{\mathrm{L,ref}}^{\alpha'}\right)^2 + \left(i_{\mathrm{L,ref}}^{\beta'}\right)^2}} \quad \text{otherwise} \tag{4}$$

where i_{sat} is usually selected as 1.2–1.5 p.u. of the nominal current of the IBR.

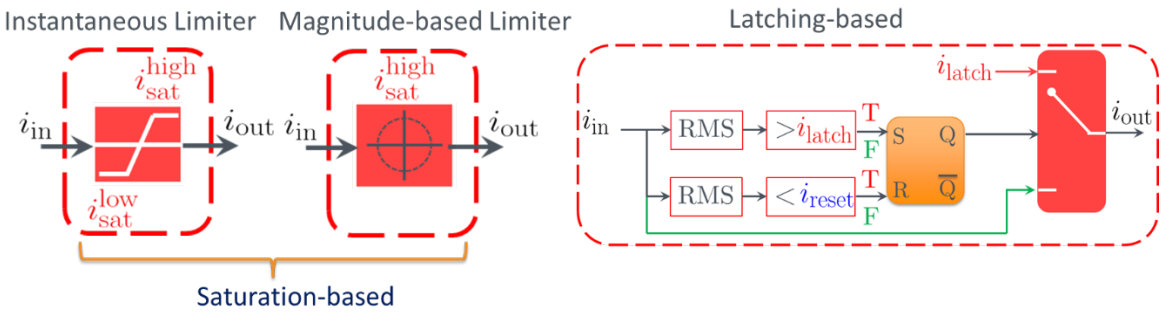

Figure 6. Current Limiter schemes

	d-axis Priority (P priority)	q-axis Priority (Q priority)
Saturation	$\lvert i_{\mathrm{L,ref}}^{\mathrm{d,lim}}\rvert = \mathbf{min}(i_{\mathrm{sat}}, \lvert i_{\mathrm{L,ref}}^{\mathrm{d}}\rvert)$ $\lvert i_{\mathrm{L,ref}}^{\mathrm{q,lim}}\rvert = \mathbf{min}(\sqrt{i_{\mathrm{sat}}^2 - (i_{\mathrm{L,ref}}^{\mathrm{d,lim}})^2}, \lvert i_{\mathrm{L,ref}}^{\mathrm{q}}\rvert)$	$\lvert i_{\mathrm{L,ref}}^{\mathrm{d,lim}}\rvert = \mathbf{min}(\sqrt{i_{\mathrm{sat}}^2 - (i_{\mathrm{L,ref}}^{\mathrm{q,lim}})^2}, \lvert i_{\mathrm{L,ref}}^{\mathrm{d}}\rvert)$ $\lvert i_{\mathrm{L,ref}}^{\mathrm{q,lim}}\rvert = \mathbf{min}(i_{\mathrm{sat}}, \lvert i_{\mathrm{L,ref}}^{\mathrm{q}}\rvert)$
Latching	$i_{\mathrm{L,ref}}^{\mathrm{d,sat}} = \frac{i_{\mathrm{L,ref}}^{\mathrm{d}}}{\lvert i_{\mathrm{L,ref}}^{\mathrm{d}}\rvert} \times \mathbf{min}(\lvert i_{\mathrm{L,ref}}^{\mathrm{d}}\rvert, i_{\mathrm{sat}})$ $i_{\mathrm{L,ref}}^{\mathrm{q,sat}} = \frac{i_{\mathrm{L,ref}}^{\mathrm{q}}}{\lvert i_{\mathrm{L,ref}}^{\mathrm{q}}\rvert} \times \mathbf{min}(\lvert i_{\mathrm{L,ref}}^{\mathrm{q}}\rvert, \sqrt{(i_{\mathrm{sat}})^2 - (i_{\mathrm{L,ref}}^{\mathrm{d,sat}})^2})$	$i_{\mathrm{L,ref}}^{\mathrm{q,sat}} = \frac{i_{\mathrm{L,ref}}^{\mathrm{q}}}{\lvert i_{\mathrm{L,ref}}^{\mathrm{q}}\rvert} \times \mathbf{min}(\lvert i_{\mathrm{L,ref}}^{\mathrm{q}}\rvert, i_{\mathrm{sat}})$ $i_{\mathrm{L,ref}}^{\mathrm{d,sat}} = \frac{i_{\mathrm{L,ref}}^{\mathrm{d}}}{\lvert i_{\mathrm{L,ref}}^{\mathrm{d}}\rvert} \times \mathbf{min}(\lvert i_{\mathrm{L,ref}}^{\mathrm{d}}\rvert, \sqrt{(i_{\mathrm{sat}})^2 - (i_{\mathrm{L,ref}}^{\mathrm{q,sat}})^2})$

Figure 7. Current Limiter schemes with axis priority logic

2.1.2.2.2 Latching-Based Current Limiter (*PCL*)

The latching current limiter, as shown in Figure 6, allows a mode change in the current values in which the GFL IBR control switches to a predefined inductor fault current reference, i_{latch}, instead of the reference current signals [23],[24],[26]. It is held at that value until the inductor current reference magnitude drops below a reset threshold,i_{reset}. For CC_1, the limiter follows the following equations [27]:

$$i_{\mathrm{L,ref}}^{\mathrm{d}}, i_{\mathrm{L,ref}}^{\mathrm{q}} = i_{\mathrm{L,ref}}^{\mathrm{d,sat}}, i_{\mathrm{L,ref}}^{\mathrm{q,sat}} \quad \text{if } i_{\mathrm{L,ref}} \geq i_{\mathrm{sat}} \tag{5}$$

$$i_{\mathrm{L,ref}}^{\mathrm{d}}, i_{\mathrm{L,ref}}^{\mathrm{q}} = i_{\mathrm{L,ref}}^{\mathrm{d'}}, i_{\mathrm{L,ref}}^{\mathrm{q'}} \quad \text{if } i_{\mathrm{L,ref}} \leq i_{\mathrm{sat}} \tag{6}$$

where $i_{\mathrm{L,ref}} = \sqrt{\left(i_{\mathrm{L,ref}}^{\mathrm{d'}}\right)^2 + \left(i_{\mathrm{L,ref}}^{\mathrm{q'}}\right)^2}$. Also, the selection of $i_{\mathrm{L,ref}}^{\mathrm{d,sat}}, i_{\mathrm{L,ref}}^{\mathrm{q,sat}}$ should satisfy $\sqrt{\left(i_{\mathrm{L,ref}}^{\mathrm{d,sat}}\right)^2 + \left(i_{\mathrm{L,ref}}^{\mathrm{q,sat}}\right)^2} = i_{\mathrm{sat}}$. In case of d-axis priority-based latching [24]:

$$i_{\mathrm{L,ref}}^{\mathrm{d,sat}} = \frac{i_{\mathrm{L,ref}}^{\mathrm{d}'}}{\left|i_{\mathrm{L,ref}}^{\mathrm{d}'}\right|}\min\left(i_{\mathrm{L,ref}}^{\mathrm{d}'}, i_{\mathrm{sat}}\right), i_{\mathrm{L,ref}}^{\mathrm{q,sat}} = \frac{i_{\mathrm{L,ref}}^{\mathrm{q}'}}{\left|i_{\mathrm{L,ref}}^{\mathrm{q}'}\right|}\min\left(i_{\mathrm{L,ref}}^{\mathrm{q}'}, \sqrt{i_{\mathrm{sat}}^2 - \left(i_{\mathrm{L,ref}}^{\mathrm{d}}\right)^2}\right). \quad (7)$$

Similarly, the q-axis priority-based latching is implemented too, as shown in Figure 7. The latching equation for CC_2 is selected as follows [26],[27]:

$$i_{\mathrm{L,ref}}^{\alpha\beta,\mathrm{lim}} = i_{\mathrm{L,ref}}^{\alpha'\beta'}\frac{i_{\mathrm{sat}}}{i_{\mathrm{L,ref}}} \quad \text{if} \quad \sqrt{\left(i_{\mathrm{L,ref}}^{\alpha}\right)^2 + \left(i_{\mathrm{L,ref}}^{\beta}\right)^2} \geq i_{\mathrm{sat}} \quad (8)$$

$$i_{\mathrm{L,ref}}^{\alpha\beta} = i_{\mathrm{L,ref}}^{\alpha'\beta'} \quad \text{if} \quad \sqrt{\left(i_{\mathrm{L,ref}}^{\alpha}\right)^2 + \left(i_{\mathrm{L,ref}}^{\beta}\right)^2} \leq i_{\mathrm{reset}} \quad (9)$$

To prevent the limit cycle behavior of the inserted nonlinearity, i_{latch} is selected to be less than i_{sat} yet greater than the current magnitude at rated power operation at the lowest nominal voltage [27].

2.1.2.3 Inner-Current Controller Logic

As mentioned in the previous section, the inner-current controller consists of the inner-current control in the dq domain (CC_1), the $\alpha\beta$ domain (CC_2), and the sequence domain (CC_3).

2.1.2.3.1 Inner-Current Control in the dq Domain (CC_1) [Figure 8]

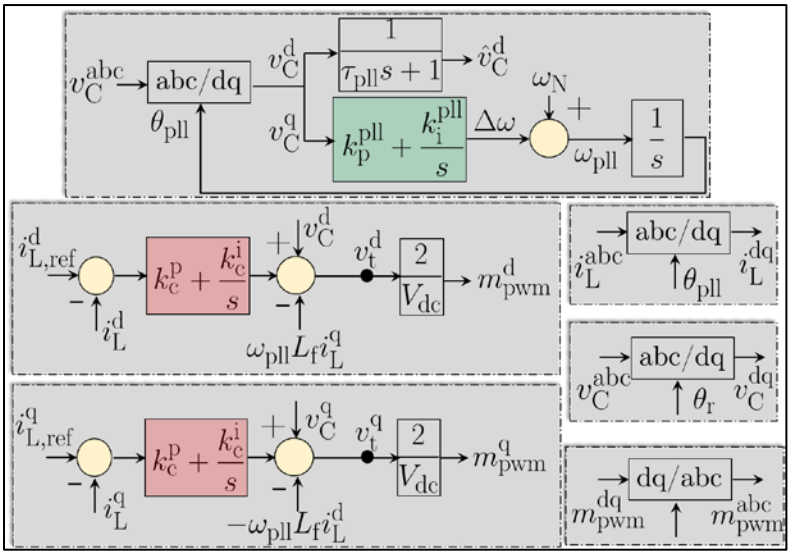

Figure 8. Inner-current control in the dq domain

For GFL IBRs, the conventional inner-current controller in the synchronous reference frame (i.e., dq-domain) architecture is employed [31]. For the inner-current controller, $i_{\mathrm{L,ref}}^{\mathrm{d}}$ and $i_{\mathrm{L,ref}}^{\mathrm{q}}$ are provided as the reference signals to be tracked by the output signals, $i_{\mathrm{L}}^{\mathrm{d}}$ and $i_{\mathrm{L}}^{\mathrm{q}}$, respectively. A PI compensator is used to track the reference of the dq-axis inductor current. For a desired time constant, τ_{c}, the parameters of the current controller are selected as $k_{\mathrm{c}}^{\mathrm{p}} = \frac{L_{\mathrm{f}}}{\tau_{\mathrm{c}}}$ and $k_{\mathrm{c}}^{\mathrm{i}} = \frac{R_{\mathrm{f}}}{\tau_{\mathrm{c}}}$. Depending on the switching frequency, τ_{c} is typically selected to range from 0.5–2 ms [9]. Additional feed-forward voltage signals, $v_{\mathrm{C}}^{\mathrm{d}}$ and $v_{\mathrm{C}}^{\mathrm{q}}$, and cross-coupling signals, $-\omega_{\mathrm{N}}L_{\mathrm{f}}i_{\mathrm{L}}^{\mathrm{q}}$ and $\omega_{\mathrm{N}}L_{\mathrm{f}}i_{\mathrm{L}}^{\mathrm{d}}$, facilitate the disturbance rejection capability. Here, ω_{N} is the nominal frequency in rad/s.

2.1.2.3.2 Inner-Current Control in the $\alpha\beta$ Domain (CC_2) [Figure 9]

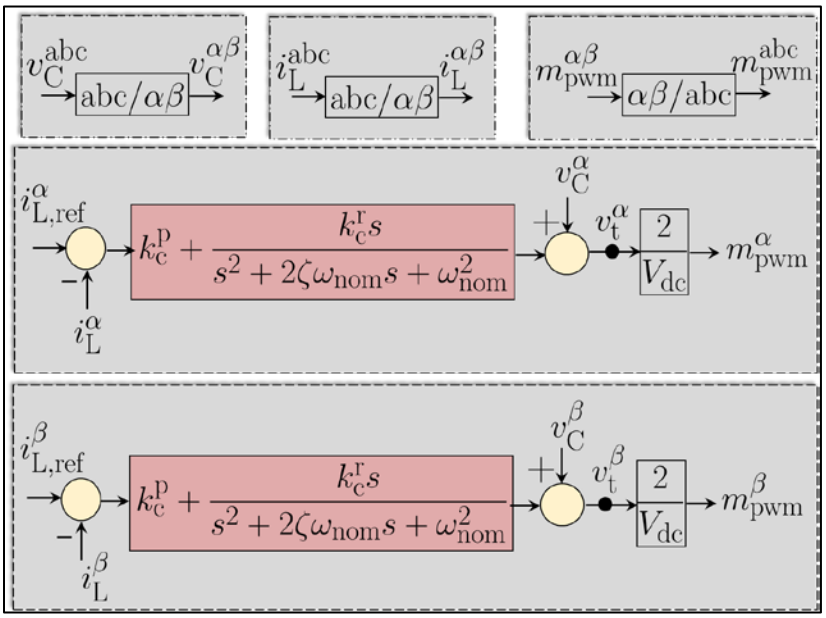

Figure 9. Inner-current control in the $\alpha\beta$ domain

For GFL IBRs, the conventional inner-current controller in the stationary reference frame (i.e., $\alpha\beta$ −domain) architecture is employed [32]. For the inner-current controller for GFL IBRs, $i_{L,ref}^{\alpha}$and $i_{L,ref}^{\beta}$ are provided as the reference signals to be tracked by the signals i_L^{α} and i_L^{α}, respectively. Following the internal-model principle, the PR controller's only two gain parameters, k_c^p and k_c^r, have been used. For a desired phase margin and to gain crossover frequency, the parameters of the voltage controller (k_c^p and k_c^r) can be designed [9]. Similarly, feed-forward voltage signals, v_C^{α} and v_C^{β}, facilitate the disturbance rejection capability.

2.1.2.3.3 Inner-Current Control in the Sequence Domain (CC_3) [Figure 10]

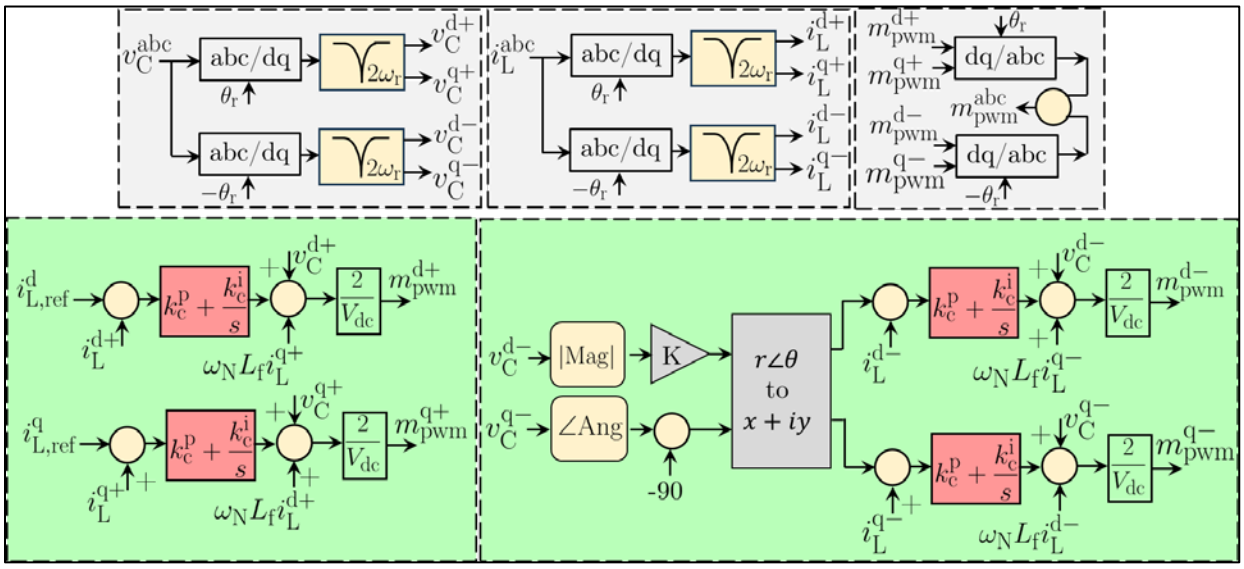

Figure 10. Inner-current control in the sequence domain

For GFL IBRs, the sequence-domain inner-current controller in the synchronous reference frame (i.e., dq-domain) architecture is employed [33]. For the inner-current controller, $i_{\mathrm{L,ref}}^{\mathrm{d+}}$, $i_{\mathrm{L,ref}}^{\mathrm{d-}}$, $i_{\mathrm{L,ref}}^{\mathrm{q+}}$, $i_{\mathrm{L,ref}}^{\mathrm{q-}}$ are provided as the reference signals to be tracked. The output signals are $i_{\mathrm{L}}^{\mathrm{d+}}$, $i_{\mathrm{L}}^{\mathrm{d-}}$, $i_{\mathrm{L}}^{\mathrm{q+}}$, $i_{\mathrm{L}}^{\mathrm{q-}}$, and these are the notch filter outputs (resonant frequency at $2\omega_{\mathrm{pll}}$). The compensator and feed-forward signals are used here with the similar phenomenon of CC_1.

2.2 Multifunctional EMT Model for GFM IBRs

The EMT model developed in this study using the PSCAD platform has the following characteristics [34]:

1. It can be served as a versatile single black box, offering the flexibility to choose the MVA rating as needed.
2. It is well suited for integrating with transmission systems, and it adheres to the guidelines outlined in IEEE Std 2800; hence, it is applicable for transmission system interconnection studies to assess site-specific performance implications associated with IBR integration with the grid.
3. It is well suited for interfacing with different types and combinations of DC sources, such as PV, battery, and ideal DC sources. As a result, it could prove valuable to various vendors of GFM IBRs that use a range of DC source configurations.
4. It covers both switching and average models. This framework offers a benchmark platform for scrutinizing the effects of inverter modeling on diverse aspects.
5. It incorporates extensive sets of control logic. Users can tailor their selections by toggling the appropriate flags. This control logic includes a comprehensive array of droop control; virtual synchronous machine (VSM) control; and outer-voltage, inner-current control. Given that the control architectures of commercial GFM IBRs are typically proprietary and vary among manufacturers, this generic EMT model serves as a valuable tool for both academic and industrial entities seeking to explore systems' operation involving multivendor GFM IBRs.

6. It contains comprehensive sets of current-limiter logic. Users can customize their choices by selecting the appropriate flags. This inclusive limiter logic encompasses an exhaustive range of features, including current saturation, latching, a virtual impedance-based limiter, and anti-windup. It is widely acknowledged that the selection of limiters significantly influences the fault behavior of IBRs; therefore, this model is invaluable for protection system engineers seeking to analyze and design suitable protection systems for systems incorporating GFM IBRs.

2.2.1 Birds-Eye View of the EMT Model of GFM IBRs

Like the GFL IBR, the fundamental building blocks of the EMT model of GFM IBRs are shown in Figure 3. The power circuit consists of the inverter model interfaced with the DC source of voltage, V_{dc}. At the output terminals, an LCL filter ($L_{\mathrm{f}}, C_{\mathrm{f}}, L_{\mathrm{g}}$, and the associated equivalent series resistances, $R_{\mathrm{f}}, R_{\mathrm{g}}$, of the inductors) are connected and interfaced to the grid/network via a transformer. The main controller is responsible for generating the pulse-width-modulated switching signals for the inverter based on processing the measurements (inner inductor current measurements, $i_{\mathrm{L}}^{\mathrm{abc}}$, output current measurements, $i_{\mathrm{O}}^{\mathrm{abc}}$, and capacitor voltage measurements, $v_{\mathrm{C}}^{\mathrm{abc}}$) via the controller logic and protection logic. The rating and the parameters of the GFM IBR are tabulated in Table 1. Note that the MVA rating is user-defined and can be changed based on the end-user requirement. The EMT model is connected to a 57.1-kV grid via a step-up transformer of the rating of the three-phase, 0.48/57.1-kV, 1.5-MVA, Y − Δ transformer; however, this external circuit is independent of the model of the GFM IBRs. The main features of the EMT model of the GFM IBRs are as follows:

1. From the DC source model side, the developed EMT model has the flexibility to select various types of DC sources (single or combination) by choosing the flag, S, externally, as tabulated in Table 2.
2. From the inverter model side, the developed EMT model has the flexibility to select two types of models by choosing the flag, M, externally, as tabulated in Table 2. The selection of the options is like that of the cases of the GFL IBR model.
3. From the controller logic side, the developed EMT model has the flexibility to select various types of controls, as tabulated in Table 5. For example, in the primary controller (PC), P-f/Q-V-based droop control ($PC = PC_1$) and VSM-based control ($PC = PC_2$) are available. In both the outer-voltage (VC) and inner-current controller (CC), the controller in the dq domain ($VC = VC_1, CC = CC_1$), the controller in the $\alpha\beta$ domain ($VC = VC_2, CC = CC_2$), and the controller in the sequence domain ($VC = VC_3, CC = CC_3$) are available. The mathematical models of all these control logics are discussed later.
4. From the limiter logic side, the developed EMT model has the flexibility to select various types of limiters, as tabulated in Table 6. For example, in the current limiter (LC), the model has a current saturation-based ($LC = LCS$) and current latching-based ($LC = LCL$) limiter. To have d-axis priority in the limiter, $LCS = LCS_1$ for the saturation-based and $LCL = LCL_1$ for the latching-based limiter can be selected. Similarly, to have q-axis priority in the limiter (as recommended in IEEE Std 2800), $LCS = LCS_2$ for the saturation-based and $LCL = LCL_2$ for the latching-based limiter can be selected. The models of all these control logics are discussed next. For the virtual impedance-based limiter, $LC = LCV$.

Table 5. Available Options in the EMT Model of GFM IBRs for Selecting the Controller Logic

Controller Logic (C)		
Primary Controller (PC)	**Outer Voltage (VC)**	**Inner Current (CC)**
PC_1: P-f/Q-V droop	VC_1: dq domain	CC_1: dq domain
PC_2: VSM	VC_2: $\alpha\beta$ domain	CC_2: $\alpha\beta$ domain
PC_3 : constant voltage source	VC_3: sequence domain	CC_3: sequence domain

Table 6. Available Options in the EMT Model of GFM IBRs for Selecting the Current Limiter Protection Logic

Current Limiter (LC)		**Windup (PW)**
Saturation-based (LCS)		PW_1: anti-windup for PI controller
LCS_1: d-axis priority	LCS_2: q-axis priority	
Latching-based (LCL)		PW_2: anti-windup for PR controller
LCL_1: d-axis priority	LCL_2: q-axis priority	
Virtual Impedance-based (LCV)		-

2.2.2 Deep Dive Into the EMT Model of GFM IBR

This section discusses the mathematical and computational models of the EMT model of GFM IBRs. In particular, the controller logic and the limiter logic are discussed in detail while referring to Table 2.

2.2.2.1 Primary Controller

As mentioned in the previous section, the outer-power controller consists of the following controls: (1) Pf/QV-based droop control and (2) VSM-based control.

2.2.2.1.1 *P-f/Q-V* Droop Control (PC_1)

Droop control involves using active and reactive power as the control variables [35], where the droop gains determine the steady-state power sharing among the inverters, as shown in Figure 11. Here, the $P-f$ and $Q-V$ droop controls are treated as proportional controllers with coefficients n_{P} and m_{Q}, respectively. The error signals $e_{\mathrm{P}} := P_{\mathrm{ref}} - P$ and $e_{\mathrm{Q}} := Q_{\mathrm{ref}} - Q$ are defined, where P and Q are the control variables, and P_{ref}, and Q_{ref} are the references. Initially $v_{\mathrm{C}}^{\mathrm{abc}}$and $i_{\mathrm{O}}^{\mathrm{abc}}$are used to determine the instantaneous active power, p, and the instantaneous reactive power, q, and then are passed through low-pass filters with the time constant, $\tau_{\mathrm{S}} \in \mathbb{R}_{>0}$, to obtain the average value of the active power, P, and the reactive power, Q. The following equations are used for the calculations:

$$p := [v_{\mathrm{C}}^{\mathrm{a}} i_{\mathrm{O}}^{\mathrm{a}} + v_{\mathrm{C}}^{\mathrm{b}} i_{\mathrm{O}}^{\mathrm{b}} + v_{\mathrm{C}}^{\mathrm{c}} i_{\mathrm{O}}^{\mathrm{c}}],\ P := \frac{1}{\tau_{\mathrm{S}} s+1} p, \tag{10}$$

$$q := \frac{1}{\sqrt{3}} [i_{\mathrm{O}}^{\mathrm{a}} (v_{\mathrm{C}}^{\mathrm{b}} - v_{\mathrm{C}}^{\mathrm{c}}) + i_{\mathrm{O}}^{\mathrm{b}} (v_{\mathrm{C}}^{\mathrm{c}} - v_{\mathrm{C}}^{\mathrm{a}}) + i_{\mathrm{O}}^{\mathrm{c}} (v_{\mathrm{C}}^{\mathrm{a}} - v_{\mathrm{C}}^{\mathrm{b}})],\ Q := \frac{1}{\tau_{\mathrm{S}} s+1} q. \tag{11}$$

In summary, the droop law is as follows:

$$\omega_{\mathrm{r}} = \omega_{\mathrm{N}} - n_{\mathrm{P}} (P - P_{\mathrm{ref}}), \tag{12}$$

$$V_{\mathrm{r}} = V_{\mathrm{N}} - m_{\mathrm{Q}}(Q - Q_{\mathrm{ref}}). \quad (13)$$

where $\dot{\theta}_{\mathrm{r}} = \omega_{\mathrm{r}}$, ω_{N} and V_{N} are the nominal frequency and the voltage.

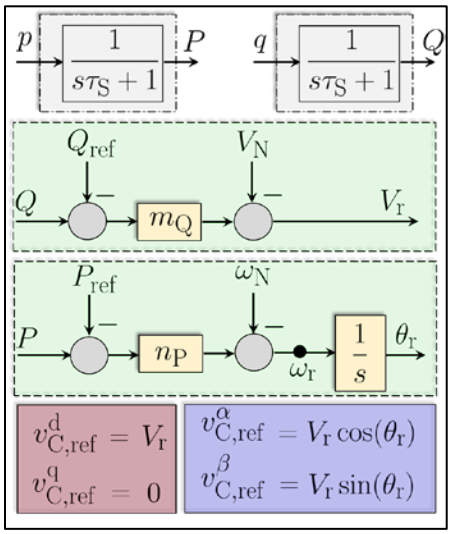

Figure 11. *P-f/Q-V* droop control

2.2.2.1.2 VSM Control (PC_2)

Emulating a synchronous machine, known as a VSM, is a direct method to integrate GFM capabilities into an IBR. VSM-based IBRs employ the swing equation and damping of virtual mass inertia, akin to synchronous machines [33], as shown in Figure 12. The VSM uses the following swing equation with proper damping:

$$T_{\mathrm{a}} \frac{\mathrm{d}\omega_{\mathrm{r}}}{\mathrm{d}t} = P_{\mathrm{ref}} - p - P_{\mathrm{D}}. \quad (14)$$

where $P_{\mathrm{D}} = k_{\mathrm{pf}}[\omega_{\mathrm{N}} - \omega_{\mathrm{r}}]$. Here, p is the measured instantaneous output active power of the IBR. P_{ref} and P_{D} are the reference and damping power, respectively. Here, T_{a} denotes the virtual inertia in the swing equation, which can be adjusted as needed. Although the damping coefficient is typically fixed in physical synchronous machines, in VSM IBRs, this parameter can be freely chosen. It directly influences the relationship between active power and frequency, defining the slope of the $P - f$ characteristic, denoted as k_{pf} . Additionally, a forward damping constant, k_{df}, is introduced to dampen the oscillations between generators, affecting the oscillatory angle output according to the form of $\theta_{\mathrm{r}} = \int \omega_{\mathrm{r}}\mathrm{d}t + k_{\mathrm{df}}[\omega_{\mathrm{N}} - \omega_{\mathrm{r}}]$. In the Q-V loop, k_{v} is chosen as the slope of the $Q - V$ characteristic, and τ_{S} is the excitation time constant. Finally, it is ascribed in the form of $V_{\mathrm{r}} = [V_{\mathrm{N}} - k_{\mathrm{v}}(Q_{\mathrm{ref}} - q)]\frac{1}{\tau_{\mathrm{S}}s+1}$. Here, q is the measured instantaneous output reactive power of the IBR, and Q_{ref} is the reference.

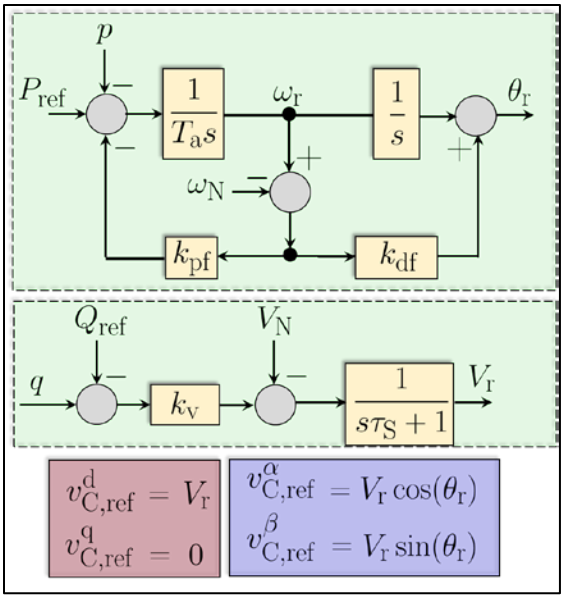

Figure 12. VSM control

2.2.2.1.3 Constant Voltage Reference Control (PC_3)

This control, called isochronous mode, is the same as the droop control, with $n_{\text{P}} = m_{\text{Q}} = 0$. The reference signals for the voltage controller are generated using $v^{\text{d}}_{\text{C,ref}} = V_{\text{r}}, v^{\text{q}}_{\text{C,ref}} = 0$, $v^{\alpha}_{\text{C,ref}} = V_{\text{r}}\cos\theta_{\text{r}}$, $v^{\beta}_{\text{C,ref}} = V_{\text{r}}\sin\theta_{\text{r}}$, and $v^{\text{d}^+}_{\text{C,ref}} = V_{\text{r}}, v^{\text{d}^-}_{\text{C,ref}} = 0, v^{\text{q}^+}_{\text{C,ref}} = 0, v^{\text{q}^-}_{\text{C,ref}} = 0$.

2.2.2.2 Outer-Voltage and Inner-Current Controller

The following outer-voltage and inner-current control for the GFM IBR model is employed:

2.2.2.2.1 dq-Domain Control (VC_1, CC_1)

The conventional outer-voltage, inner-current controller operates within the synchronous reference frame (i.e., dq-domain) architecture [9], as shown in Figure 13. In the inner-current controller, $i^{\text{d}}_{\text{L,ref}}$ and $i^{\text{q}}_{\text{L,ref}}$ are provided as the reference signals to be tracked by the output signals i^{d}_{L} and i^{q}_{L}, respectively. A PI compensator is used to track the reference of the dq-axis inductor current. For a desired time constant, τ_{c}, the parameters of the current controller are selected as $k^{\text{p}}_{\text{c}} = \frac{L_{\text{f}}}{\tau_{\text{c}}}$ and $k^{\text{i}}_{\text{c}} = \frac{R_{\text{f}}}{\tau_{\text{c}}}$. Depending on the switching frequency, τ_{c} is typically selected to range from 0.5–2 ms. Additional feed-forward voltage signals, v^{d}_{C} and v^{q}_{C}, and cross-coupling signals, $-\omega_{\text{N}}L_{\text{f}}i^{\text{q}}_{\text{L}}$ and $\omega_{\text{N}}L_{\text{f}}i^{\text{d}}_{\text{L}}$, facilitate the disturbance rejection capability. Here, ω_{N} is the nominal frequency in rad/s. In the outer-voltage controller, $v^{\text{d}}_{\text{C,ref}}$ and $v^{\text{q}}_{\text{C,ref}}$ are the reference signals tracked by v^{d}_{C} and v^{q}_{C}, respectively. A PI compensator enables reference tracking, with the parameters (k^{p}_{v} and k^{i}_{v}) determined based on the symmetrical optimum method to achieve the desired phase margin and to gain crossover frequency. Current feed-forward signals, i^{d}_{O} and i^{q}_{O}, and cross-coupling signals, $-\omega_{\text{N}}C_{\text{f}}v^{\text{q}}_{\text{C}}$ and $\omega_{\text{N}}C_{\text{f}}v^{\text{d}}_{\text{C}}$, facilitate the disturbance rejection capability.

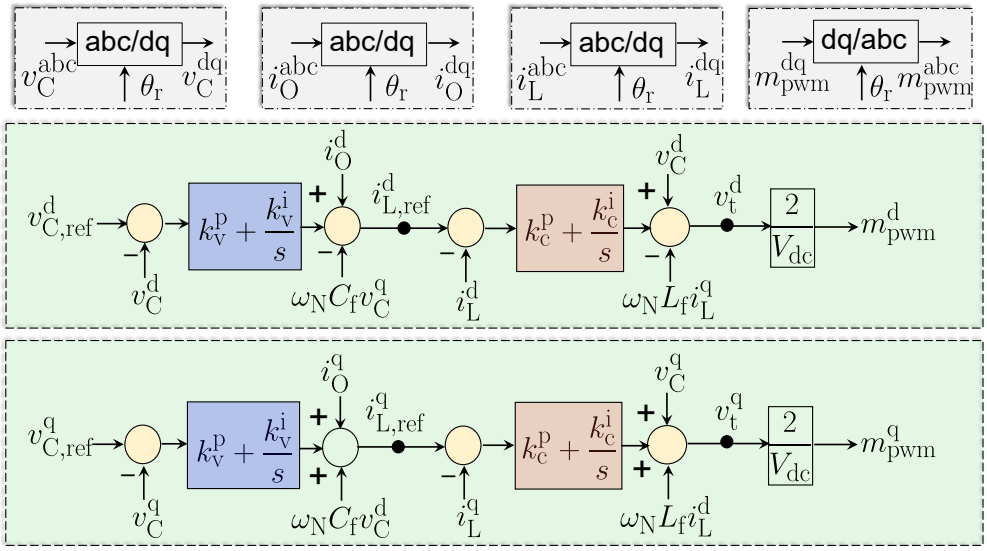

Figure 13. Outer-voltage, inner-current controller designed in the dq domain

2.2.2.2.2 $\alpha\beta$-Domain Control

The conventional outer-voltage, inner-current controller operates within the stationary reference frame (i.e., $\alpha\beta$ domain) architecture, as shown in Figure 14. The inner-current controllers for the GFM IBRs, $i_{\mathrm{L,ref}}^{\alpha}$and $i_{\mathrm{L,ref}}^{\beta}$, are provided as the reference signals to be tracked by the signals i_{L}^{α} and i_{L}^{α}, respectively. A PI compensator is used to track the reference of the dq-axis inductor current. For a desired time constant, τ_{c}, the parameters of the current controller are selected as $k_{\mathrm{c}}^{\mathrm{p}} = \frac{L_{\mathrm{f}}}{\tau_{\mathrm{c}}}$ and $k_{\mathrm{c}}^{\mathrm{i}} = \frac{R_{\mathrm{f}}}{\tau_{\mathrm{c}}}$. Depending on the switching frequency, τ_{c} is typically selected to range from 0.5–2 ms. For the outer-voltage controller for GFM IBRs, $v_{\mathrm{C,ref}}^{\alpha}$and $v_{\mathrm{C,ref}}^{\beta}$ are provided as the reference signals to be tracked by the signals v_{C}^{α} and v_{C}^{α}, respectively. Following the internal-model principle [9], the PR controller's only two gain parameters, $k_{\mathrm{v}}^{\mathrm{p}}$ and $k_{\mathrm{v}}^{\mathrm{r}}$, are used. For a desired phase margin and to gain crossover frequency, the parameters of the voltage controller ($k_{\mathrm{v}}^{\mathrm{p}}$ and $k_{\mathrm{v}}^{\mathrm{r}}$) can be designed. Similarly, feed-forward voltage signals, i_{O}^{α} and i_{O}^{β}, facilitate the disturbance rejection capability.

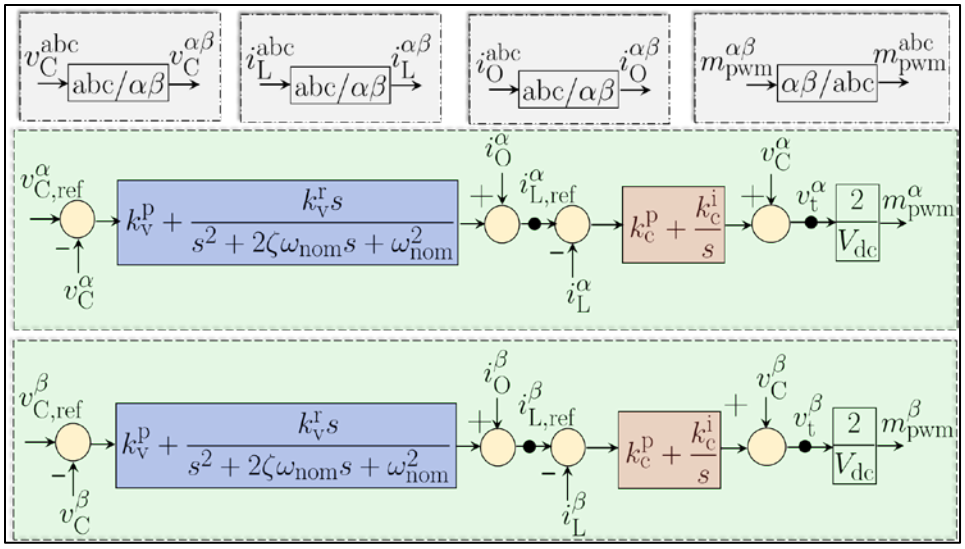

Figure 14. Outer-voltage, inner-current controller designed in the $\alpha\beta$ domain

2.2.2.2.3 Sequence-Domain Control

The sequence-domain outer-voltage, inner-current controller in the synchronous reference frame (i.e., dq-domain) architecture is shown in Figure 15 [37]. The inner-current controllers, $i_{L,ref}^{d+}, i_{L,ref}^{d-}, i_{L,ref}^{q+}, i_{L,ref}^{q-}$, are provided as the reference signals to be tracked. The output signals are $i_L^{d+}, i_L^{d-}, i_L^{q+}, i_L^{q-}$, and these are the notch filter outputs (resonant frequency at $2\omega_{pll}$). The compensator and feed-forward signals are used here with a similar phenomenon of CC_1. In the outer-voltage controller, $v_{C,ref}^{d+}, v_{C,ref}^{d-}, v_{C,ref}^{q+}, v_{C,ref}^{q-}$ are the reference signals tracked by $v_C^{d+}, v_C^{d-}, v_C^{q+}, v_C^{q-}$, respectively. A PI compensator enables reference tracking, with the parameters (k_v^p and k_v^i) determined based on the symmetrical optimum method to achieve the desired phase margin and to gain crossover frequency [9]. Current feed-forward signals, $i_O^{d+}, i_O^{d-}, i_O^{q+}, i_O^{q-}$ are also present here. To enable negative-sequence current injection by the GFM IBR in compliance with IEEE Std 2800 [43], the $i_{L,ref}^{d-}, i_{L,ref}^{q-}$ are generated using the logic:

$$i_{L,ref}^{d-}, +j i_{L,ref}^{q-} = K\sqrt{\left(v_C^{d-}\right)^2 + \left(v_C^{q-}\right)^2}\angle\left[\text{atan}\left(\frac{v_C^{q-}}{v_C^{d-}}\right) - \frac{\pi}{2}\right] \quad (15)$$

where the factor K can be selected based on the user.

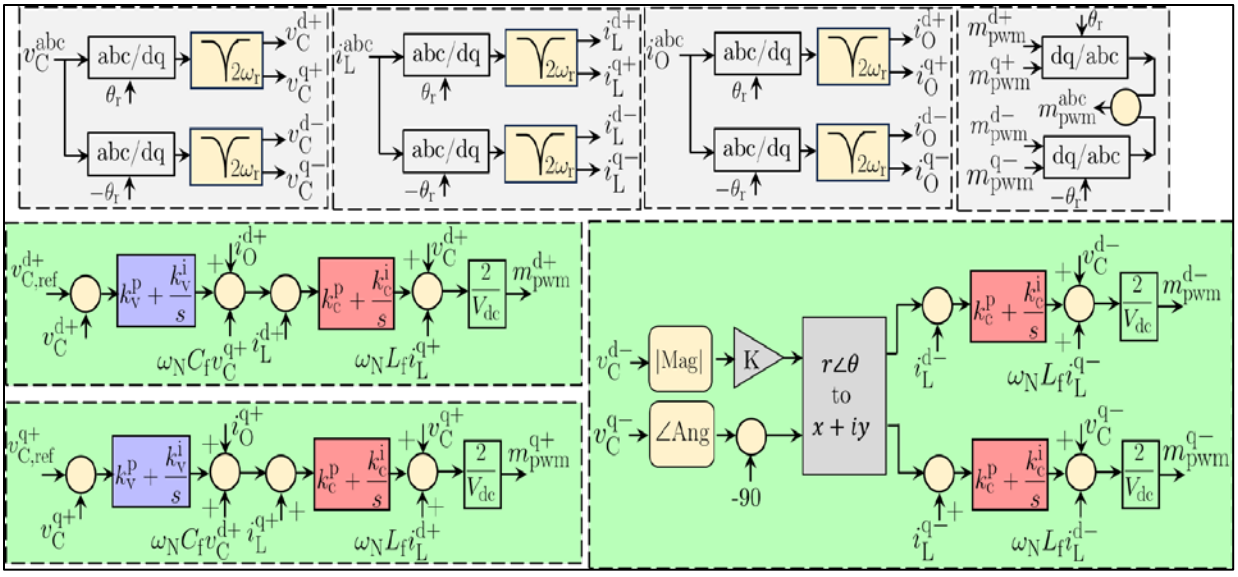

Figure 15. Outer-voltage, inner-current controller designed in the sequence domain

2.2.2.3 Limiter Logic

The current saturation-based and current-latching-based limiter logic employed in the GFM IBR are the same as the limiter logic of the GFL IBR, described earlier. The additional virtual impedance-based limiter logic is described here.

2.2.2.3.1 Virtual Impedance-Based Current Limiter (*LCV*)

Unlike the saturation and latching-based current limiters, the virtual impedance-based limiter is applied to the voltage reference signals rather than the inductor current reference signals and is primarily used for GFM IBRs. This is achieved by integrating a complex-valued fault-current-dependent feed-forward term into the voltage control loop [40]. The expressions for the virtual resistance, R_{vir}, and the virtual inductance, L_{vir}, are given by:

$$R_{\text{vir}} = k_{\text{p}}^{R_{\text{vir}}} [\text{RMS}(i_{\text{L}}) - i_{\text{sat}}] \text{ if } \text{RMS}(i_{\text{L}}) - i_{\text{sat}} \geq 0 \tag{16}$$

$$R_{\text{vir}} = 0 \, otherwise. \tag{17}$$

And $\omega_{\text{N}} L_{\text{vir}} = X_{\text{vir}} = \sigma_{\text{X/R}} R_{\text{vir}}$. Here, $\text{RMS}(i_{\text{L}}) \coloneqq \sqrt{\left(i_{\text{L}}^{\text{d}}\right)^2 + \left(i_{\text{L}}^{\text{q}}\right)^2} = \sqrt{(i_{\text{L}}^{\alpha})^2 + \left(i_{\text{L}}^{\beta}\right)^2}$. $k_{\text{p}}^{R_{\text{vir}}}$ and $\sigma_{\text{X/R}}$ are the virtual impedance proportional gain and the X/R ratio of the virtual impedance, respectively. The parameter $k_{\text{p}}^{R_{\text{vir}}}$ is tuned to limit the current magnitude to a suitable level during the overcurrent in steady state, while $\sigma_{\text{X/R}}$ ensures good system dynamics during the overcurrent. When the virtual impedance-based limiter in dq-domain is activated, the following equations are used in the voltage control loop [38],[39]:

$$v_{\text{C,ref}}^{\text{d,lim}} = v_{\text{C,ref}}^{\text{d}} - R_{\text{vir}} i_{\text{O}}^{\text{d}} + X_{\text{vir}} i_{\text{O}}^{\text{q}} \tag{18}$$

$$v_{\text{C,ref}}^{\text{q,lim}} = v_{\text{C,ref}}^{\text{q}} - R_{\text{vir}} i_{\text{O}}^{\text{q}} - X_{\text{vir}} i_{\text{O}}^{\text{d}} \tag{19}$$

Similarly, when the virtual impedance-based limiter in $\alpha\beta$-domain is activated, the following equations are used in the voltage control loop:

$$v_{\mathrm{C,ref}}^{\alpha,\mathrm{lim}} = v_{\mathrm{C,ref}}^{\alpha} - (R_{\mathrm{vir}} + sL_{\mathrm{vir}})i_{\mathrm{O}}^{\alpha} \quad (20)$$

$$v_{\mathrm{C,ref}}^{\beta,\mathrm{lim}} = v_{\mathrm{C,ref}}^{\beta} - (R_{\mathrm{vir}} + sL_{\mathrm{vir}})i_{\mathrm{O}}^{\beta} \quad (21)$$

2.3 Additional Controls, Limiter Schemes, and Protection Logics

2.3.1 Negative-Sequence Component (IEEE Std 2800)

Figure 10 and Figure 15 show the sequence-domain inner-current controller and outer-voltage, inner-current controller in the synchronous reference frame (i.e., dq domain) for GFL IBRs and GFM IBRs in compliance with the IEEE Std 2800, respectively. For the current controller $i_{\mathrm{L,ref}}^{\mathrm{d+}}$, $i_{\mathrm{L,ref}}^{\mathrm{q+}}$, $i_{\mathrm{L,ref}}^{\mathrm{d-}}$, and $i_{\mathrm{L,ref}}^{\mathrm{q-}}$ are provided as the reference signals to be tracked by $i_{\mathrm{L}}^{\mathrm{d+}}$, $i_{\mathrm{L}}^{\mathrm{q+}}$, $i_{\mathrm{L}}^{\mathrm{d-}}$, and $i_{\mathrm{L}}^{\mathrm{q-}}$, respectively. A PI compensator is used, with the parameters $k_{\mathrm{c}}^{\mathrm{p}} = L_{\mathrm{f}}/\tau_{\mathrm{c}}$ and $k_{\mathrm{c}}^{\mathrm{i}} = R_{\mathrm{f}}/\tau_{\mathrm{c}}$ selected for a desired time constant τ_{c}, typically ranging from 0.5 to 2 ms. The feed-forward voltage signals, $v_{\mathrm{C}}^{\mathrm{d+}}, v_{\mathrm{C}}^{\mathrm{q+}}, v_{\mathrm{C}}^{\mathrm{d-}}, v_{\mathrm{C}}^{\mathrm{q-}}$, and the cross-coupling signals, $\omega_{\mathrm{N}}L_{\mathrm{f}}i_{\mathrm{L}}^{\mathrm{q+}}, -\omega_{\mathrm{N}}L_{\mathrm{f}}i_{\mathrm{L}}^{\mathrm{d+}}$, $-\omega_{\mathrm{N}}L_{\mathrm{f}}i_{\mathrm{L}}^{\mathrm{q-}}, \omega_{\mathrm{N}}L_{\mathrm{f}}i_{\mathrm{L}}^{\mathrm{d-}}$, enhance the disturbance rejection capability, where ω_{N} denotes the nominal frequency in rad/s. In the outer-voltage controller, $v_{\mathrm{C,ref}}^{\mathrm{d+}}, v_{\mathrm{C,ref}}^{\mathrm{q+}}, v_{\mathrm{C,ref}}^{\mathrm{d-}}, v_{\mathrm{C,ref}}^{\mathrm{q-}}$ are the reference signals tracked by $v_{\mathrm{C}}^{\mathrm{d+}}, v_{\mathrm{C}}^{\mathrm{q+}}, v_{\mathrm{C}}^{\mathrm{d-}}, v_{\mathrm{C}}^{\mathrm{q-}}$ respectively. A PI compensator enables reference tracking, with the parameters ($k_{\mathrm{v}}^{\mathrm{p}}$ and $k_{\mathrm{v}}^{\mathrm{i}}$) determined based on the symmetrical optimum method to achieve the desired phase margin and to gain crossover frequency. The current feed-forward signals, $i_{\mathrm{O}}^{\mathrm{d+}}, i_{\mathrm{O}}^{\mathrm{q+}}, i_{\mathrm{O}}^{\mathrm{d-}}$, and $i_{\mathrm{O}}^{\mathrm{q-}}$, and the cross-coupling signals, $\omega_{\mathrm{N}}C_{\mathrm{f}}v_{\mathrm{C}}^{\mathrm{q+}}, -\omega_{\mathrm{N}}C_{\mathrm{f}}v_{\mathrm{C}}^{\mathrm{d+}}, -\omega_{\mathrm{N}}C_{\mathrm{f}}v_{\mathrm{C}}^{\mathrm{q-}}$, $\omega_{\mathrm{N}}C_{\mathrm{f}}v_{\mathrm{C}}^{\mathrm{d-}}$, bolster the disturbance rejection capability for the voltage control loop. The output signals, $v_{\mathrm{C}}^{\mathrm{d+}}, v_{\mathrm{C}}^{\mathrm{q+}}, v_{\mathrm{C}}^{\mathrm{d-}}, v_{\mathrm{C}}^{\mathrm{q-}}, i_{\mathrm{L}}^{\mathrm{d+}}, i_{\mathrm{L}}^{\mathrm{q+}}, i_{\mathrm{L}}^{\mathrm{d-}}, i_{\mathrm{L}}^{\mathrm{q-}}, i_{\mathrm{O}}^{\mathrm{d+}}, i_{\mathrm{O}}^{\mathrm{q+}}, i_{\mathrm{O}}^{\mathrm{d-}}$, and $i_{\mathrm{O}}^{\mathrm{q-}}$ are the notch filter outputs (resonant frequency at $2\omega_{\mathrm{N}}$); however, to enable negative-sequence current injection by the GFL IBRs and GFM IBRs in compliance with IEEE Std 2800, the $i_{\mathrm{L,ref}}^{\mathrm{d-}}$, and $i_{\mathrm{L,ref}}^{\mathrm{q-}}$ are generated using the logic $i_{\mathrm{L,ref}}^{\mathrm{d-}} + ji_{\mathrm{L,ref}}^{\mathrm{q-}} = K\sqrt{\left(v_{\mathrm{C}}^{\mathrm{d-}}\right)^2 + \left(v_{\mathrm{C}}^{\mathrm{q-}}\right)^2}\angle\left[\mathrm{atan}\left(\frac{v_{\mathrm{C}}^{\mathrm{q-}}}{v_{\mathrm{C}}^{\mathrm{d-}}}\right) + \frac{\pi}{2}\right]$, where the factor K can be selected based on the user. To ensure that the negative-sequence injection control complies with IEEE Std 2800, for GFL IBRs, the following rules of thumb for controller tuning are followed:

- τ_{c} is the desired closed-loop time constant for the inner-current controller.
- $k_{\mathrm{c}}^{\mathrm{p}}$ and $k_{\mathrm{c}}^{\mathrm{i}}$ need to be tuned accordingly.
- The nonideal notch filter is given by $\mathcal{G}(s) = \frac{s^2+2k_{\mathrm{notch}}\zeta\omega s+\omega^2}{s^2+2\zeta\omega s+\omega^2}$, $\omega = 2\pi \times 120$ rad/s.
- ζ and k_{notch} determine the dynamic response.
- τ_{LPF} needs to be tuned. τ_{LPF} (not shown in Figure 10),

To ensure that the negative-sequence injection control complies with IEEE Std 2800, for GFM IBRs, the following rules of thumb for controller tuning are followed:

- τ_{c} is the desired closed-loop time constant for the inner-current controller.
- $k_{\mathrm{c}}^{\mathrm{p}}$ and $k_{\mathrm{c}}^{\mathrm{i}}$ need to be tuned accordingly.
- Symmetrical optimum is utilized for tuning $k_{\mathrm{v}}^{\mathrm{p}}$ and $k_{\mathrm{v}}^{\mathrm{i}}$
- Proper time scale separation is maintained (selection of τ_{v})

- The nonideal notch filter is given by $\mathcal{G}(s) = \frac{s^2+2k_{\text{notch}}\zeta\omega s+\omega^2}{s^2+2\zeta\omega s+\omega^2}$, $\omega = 2\pi \times 120$ rad/s.
- ζ and k_{notch} determine the dynamic response.
- τ_{LPF} needs to be tuned. τ_{LPF} (not shown in the Figure 15).

With the selected choice of the controller parameters, the positive- and negative-sequence components of the IBR output current is shown in Figure 16. The pre-fault power set points of both the GFL IBR and the GFM IBR are $P_{\text{ref}} = 0.25$ p.u. and $Q_{\text{ref}} = 0.15$ p.u. The GFL IBR and the GFM IBR are operating in the sequence-domain inner-current controller and the sequence-domain outer-voltage, inner-current controller, with a closed-loop PQ-dispatch controller and a $P - f\ /Q - V$-based droop controller in the outer-power control layer, respectively. The current limiter for both the GFL IBR and the GFM IBR are selected as a q-priority saturation-based limiter scheme. On the DC side, battery and the PV source are interfaced, and the voltage source inverter (VSI) model is taken as a switch-average model. The fault scenario is the same for both IBRs, and it is a bolted AG fault that occurs at $t = 5$ s. Here, $I_{\text{P}}^{+} \coloneqq |\bar{I}^{+}|\cos(\angle\bar{V}^{+} - \bar{I}^{+})$, $I_{\text{Q}}^{+} \coloneqq |\bar{I}^{+}|\sin(\angle\bar{V}^{+} - \bar{I}^{+})$, $I_{\text{P}}^{-} \coloneqq |\bar{I}^{-}|\cos(\angle\bar{V}^{-} - \bar{I}^{-})$, and $I_{\text{Q}}^{-} \coloneqq |\bar{I}^{-}|\sin(\angle\bar{V}^{-} - \bar{I}^{-})$. $\bar{V}^{+}$, $\bar{V}^{-}$, $\bar{I}^{+}$, and $\bar{I}^{-}$ are the positive-sequence and negative-sequence components of the output voltage and the current of the IBR. As observed, in both IBR cases, the active component of the positive-sequence post-fault current output of the IBRs, I_{P}^{+}, drops to zero, and the reactive component of the positive-sequence post-fault current output of the IBRs, I_{Q}^{+}, increases to 1.2 p.u. This is because of the current-limiter scheme with q priority, and 1.2 p.u. is the saturation current limit, I_{sat}, selected for the IBRs. On the other hand, the active component of the negative-sequence post-fault current output of the IBRs, I_{P}^{-}, stays at zero, and the reactive component of the negative-sequence post-fault current output of the IBRs, I_{Q}^{-}, increases to 0.45 p.u., depending on the K factor selected in the negative-sequence current controller (here, $K = 5$). This signifies that the negative-sequence current magnitude is dependent on the magnitude of the negative-sequence voltage at the terminal of the IBR, and the angle of the negative-sequence output current leads the negative-sequence voltage by 90^{o}. This aligns with IEEE Std 2800. Note that for both tuned parameters, the steady-state values of the positive- and negative-sequence current components (both in magnitude and angle) follow IEEE Std 2800. But the slower tuned controller results in an initial transient that is much higher than the faster controller response, and during that period, the angle convention of the negative-sequence current output of the IBR is significantly different than the steady-state values; therefore, from the manufacturer's perspective, there are multiple parameters to be tuned when the IBR is claimed to comply with IEEE Std 2800.

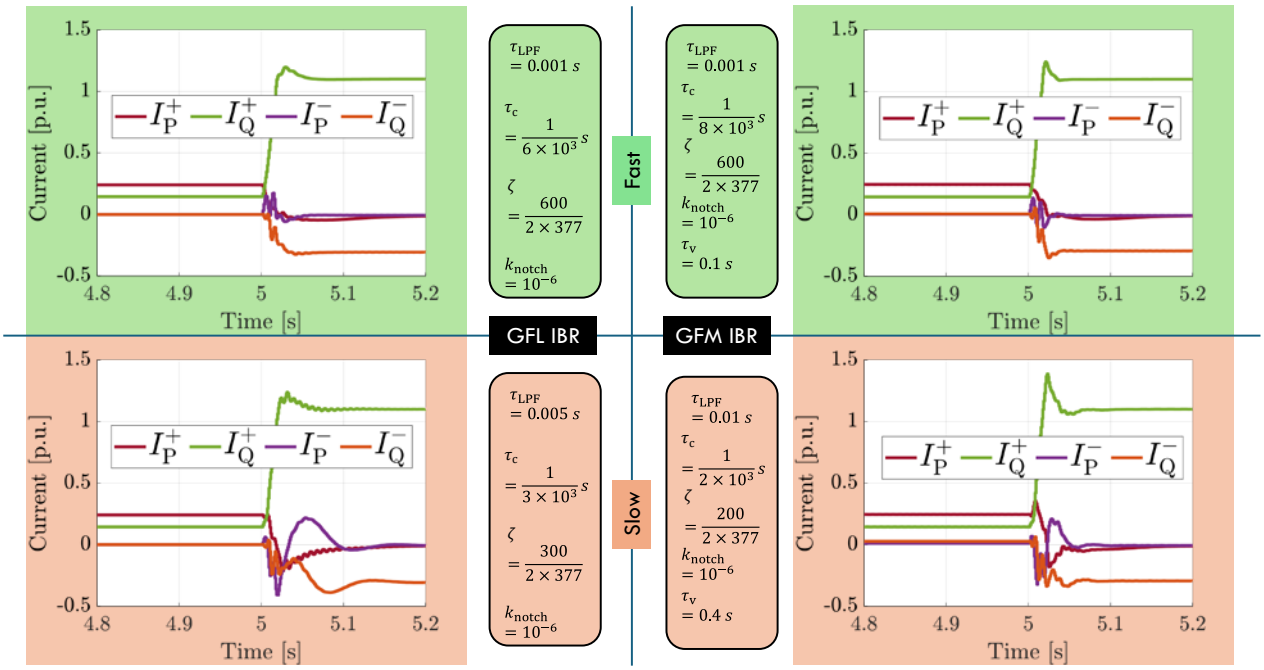

Figure 16. GFL and GFM IBR response under slow and fast IEEE Std 2800-compliant controllers

2.3.2 Update in the Current Limiter

The original instantaneous current saturation limiter sets hard limits on the inductor current references, $i_{L,ref}^{d'}$ and $i_{L,ref}^{q'}$, following (22) and (23):

$$\left|i_{L,ref}^{d,lim}\right| = \min\left(i_{sat}, \left|i_{L,ref}^{d}\right|\right), \left|i_{L,ref}^{q,lim}\right| = \min\left(\sqrt{i_{sat}^2 - \left(i_{L,ref}^{d,lim}\right)^2}, \left|i_{L,ref}^{q}\right|\right), \tag{22}$$

$$\left|i_{L,ref}^{d,lim}\right| = \min\left(\sqrt{i_{sat}^2 - \left(i_{L,ref}^{q,lim}\right)^2}, \left|i_{L,ref}^{d}\right|\right), \left|i_{L,ref}^{q}\right| = \min\left(i_{sat}, \left|i_{L,ref}^{q}\right|\right) \tag{23}$$

The implementation of the current saturation limiter is shown in Figure 17. An instantaneous hard current saturation limiter will clip the peak of the sinusoidal. This will result in distortional output currents; therefore, the dynamic limiter logic is adapted in general. The following procedures will follow:

1. When d-axis/P priority is selected, the following two situations can occur:
   A. In case $i_{L,ref}^{d} \geq i_{sat}$, i.e., the limiter is hit due to a fault condition, $i_{L,ref}^{d,lim} = i_{sat}$. As a result, $\sqrt{i_{sat}^2 - \left(i_{L,ref}^{d,lim}\right)^2} = 0$. So, the limiter values in the q-axis loop are 0, and as a result $i_{L,ref}^{q,lim} = 0$.

B. In case $i^{d}_{L,ref} < i_{sat}$, i.e., the limiter is not hit due to a fault condition, $i^{d,lim}_{L,ref} = i^{d}_{L,ref}$. As a result, $\sqrt{i^2_{sat} - \left(i^{d,lim}_{L,ref}\right)^2} = \sqrt{i^2_{sat} - \left(i^{d}_{L,ref}\right)^2}$. So, the limiter values in the q-axis loop are $\pm\sqrt{i^2_{sat} - \left(i^{d}_{L,ref}\right)^2}$.

2. When q-axis/q priority is selected, the following two situations can occur:

A. In case $i^{q}_{L,ref} \geq i_{sat}$, i.e., the limiter is hit due to a fault condition, $i^{q,lim}_{L,ref} = i_{sat}$. As a result, $\sqrt{i^2_{sat} - \left(i^{q,lim}_{L,ref}\right)^2} = 0$. So, the limiter values in the d-axis loop are 0, and as a result $i^{d,lim}_{L,ref} = 0$.

B. In case $i^{q}_{L,ref} < i_{sat}$, i.e., the limiter is not hit due to a fault condition, $i^{q,lim}_{L,ref} = i^{q}_{L,ref}$. As a result, $\sqrt{i^2_{sat} - \left(i^{q,lim}_{L,ref}\right)^2} = \sqrt{i^2_{sat} - \left(i^{q}_{L,ref}\right)^2}$. So, the limiter values in the d-axis loop are $\pm\sqrt{i^2_{sat} - \left(i^{q}_{L,ref}\right)^2}$.

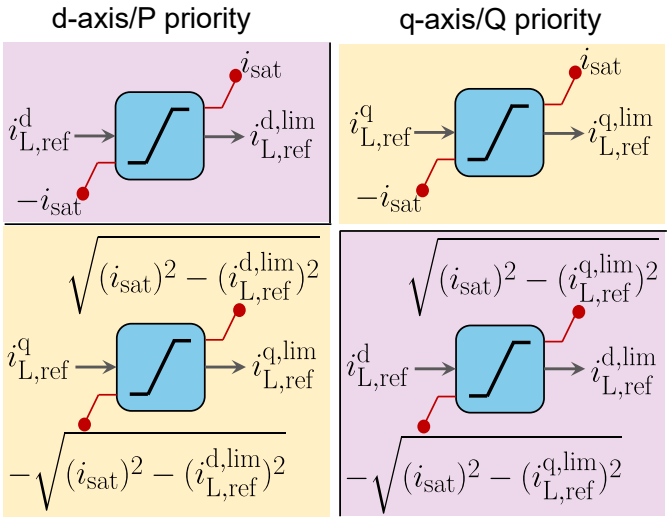

Figure 17. Initial saturation-based Current Limiter scheme

As a result, the limiter value (upper and lower limit) is dynamically determined based on the limit hit/not hit condition. In case of an unbalanced fault, depending on the current reference generation scheme adapted in the inverter control system, there is a possibility of the presence of a 2ω component along with a DC value in $i^{d}_{L,ref}$ and $i^{q}_{L,ref}$. For instance, in the case of the GFL IBR, the outer closed-loop PQ controller is responsible for generating $i^{d}_{L,ref}$ and $i^{q}_{L,ref}$. Whereas in the case of the GFM IBR, the outer-voltage controller is responsible for generating $i^{d}_{L,ref}$ and $i^{q}_{L,ref}$. As a result, in case of an unbalanced fault condition without the limit-hitting situation, the calculated limiter value, such as $\sqrt{i^2_{sat} - \left(i^{d}_{L,ref}\right)^2}$ or $\sqrt{i^2_{sat} - \left(i^{q}_{L,ref}\right)^2}$, will not be constant, and a dynamic fluctuating limiter value (upper and lower limit) can be present in the control system. This is the potential cause of the chattering phenomena (the presence of high-frequency

chattering in the fault current) that is usually observed during the initial fractions of power cycles after the fault.

The limiting scheme results in an inevitable and undesired distortion in the current waveform of the IBR during the initial few fractions of cycles, which is mainly caused by the dynamically fluctuating limit range due to the operation of the root square. To avoid that, the following modified priority selection logic is added, as shown in Figure 18. The logic is as follows:

$$i_{\mathrm{L,ref}}^{\mathrm{d,lim}} + j i_{\mathrm{L,ref}}^{\mathrm{d,lim}} = i_{\mathrm{L,ref}}^{\mathrm{d}} + j i_{\mathrm{L,ref}}^{\mathrm{d}}, \text{ if } i_{\mathrm{M}} < i_{\mathrm{sat}} \quad (24)$$

$$i_{\mathrm{L,ref}}^{\mathrm{d,lim}} + j i_{\mathrm{L,ref}}^{\mathrm{d,lim}} = i_{\mathrm{M}}^{\mathrm{lim}} e^{j\phi}, \text{ if } i_{\mathrm{M}} \geq i_{\mathrm{sat}} \quad (25)$$

$$\phi = 0^{\mathrm{o}} \text{ if d} - \text{axis priority is selected} \quad (26)$$

$$\phi = 90^{\mathrm{o}} \text{ if q} - \text{axis priority is selected} \quad (27)$$

This limiting scheme avoids the dynamic allocation of the limiter range based on the limited current magnitude, like the original priority logics.

$$i_{\mathrm{L,ref}}^{\mathrm{d,lim}} + j i_{\mathrm{L,ref}}^{\mathrm{d,lim}} = i_{\mathrm{L,ref}}^{\mathrm{d}} + j i_{\mathrm{L,ref}}^{\mathrm{d}} \quad \text{if } i_{\mathrm{M}} < i_{\mathrm{sat}}$$

$$i_{\mathrm{L,ref}}^{\mathrm{d,lim}} + j i_{\mathrm{L,ref}}^{\mathrm{d,lim}} = i_{\mathrm{M}}^{\mathrm{lim}} e^{j\phi} \quad \text{if } i_{\mathrm{M}} \geq i_{\mathrm{sat}}$$

$\phi = 0^{\mathrm{o}}$ for P priority
$\phi = 90^{\mathrm{o}}$ for Q priority

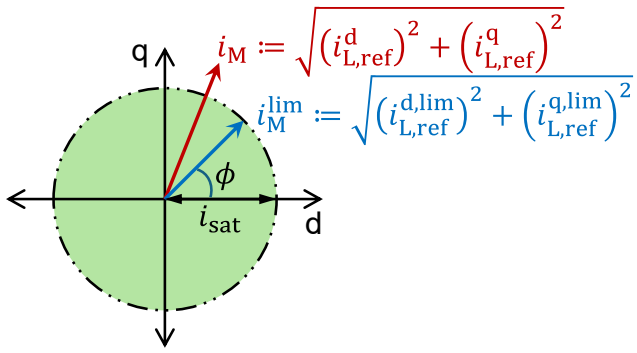

Figure 18. Modified priority-based Current Limiter scheme

2.3.3 Momentary Cessation

The IEEE Std 2800 voltage ride-through requirements for IBRs are shown in Table 7. If the point of measurement (POM) voltage drops below 0.1 p.u., the IBR must ride through for at least 0.32 s (20 cycles) before entering momentary cessation or remaining connected. The POM refers to the transmission-side connection of the IBR transformer. This requirement ensures current injections at low-voltage levels to aid fault detection and clearing, but it is highly demanding for IBRs. Figure 19 shows an IBR entering momentary cessation just one cycle after the fault inception, ceasing current injection and potentially affecting the protection relay operation. Determining the minimal ride-through time needed for reliable relay performance without damaging inverters is essential. This duration must be shorter than the IBR's internal protection time to prevent issues such as synchronization loss, temporary overvoltages, and DC voltage control challenges [4].

Table 7. IEEE Std 2800-2022 Voltage Ride-Through Requirements for IBRs [4]

Applicable Voltage (p.u.) at POM	Operating Mode/Response	Minimal Ride-Through Time (s) (Design Criteria)
V>1.20	May ride through or trip	N/A
V>1.10	Mandatory operation	1.0
V>1.05	Continuous operation	18000
V<0.90	Mandatory operation	6.00
V<0.70	Mandatory operation	3.0
V<0.50	Mandatory operation	1.20
V<0.25	Mandatory operation	0.32
V<0.1	Permissive operation	0.32

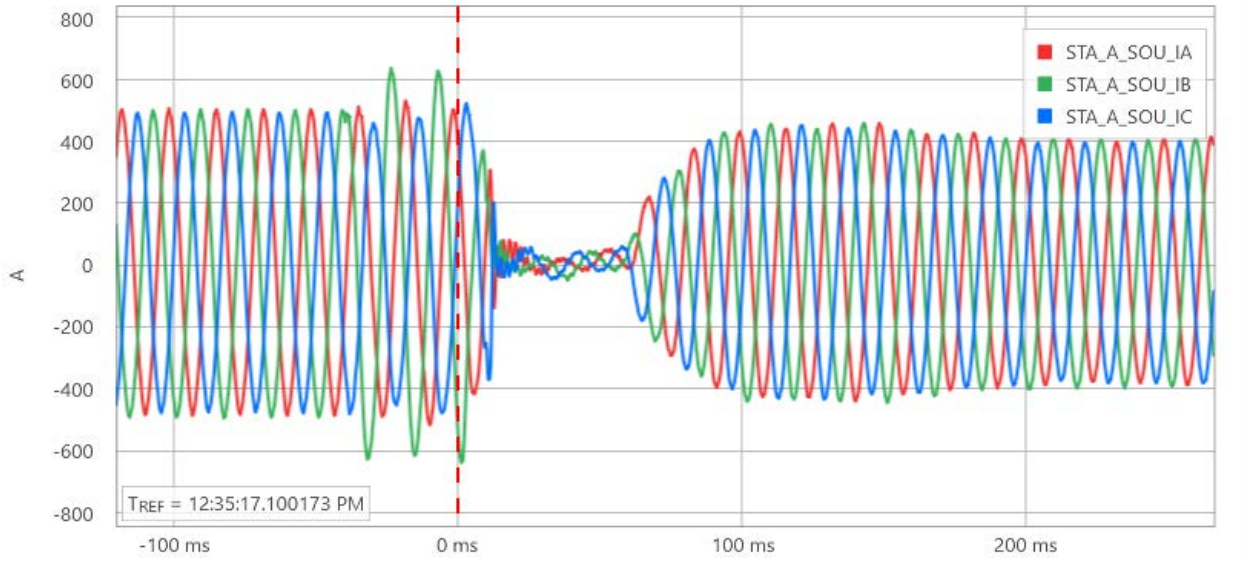

Figure 19. Real-world example of IBR momentary cessation [46]

Figure 20 illustrates this logic. It includes the following, which are continuously monitored: (1) undervoltage conditions—five threshold levels, U_1, U_2, …, U_5, corresponding to the IEEE Std 2800 undervoltage criteria (Table 7); (2) overvoltage conditions—three levels, O_1, O_2, O_3, also defined by IEEE Std 2800; and (3) the unbalanced factor condition—the ratio V_2/V_1 (where V_1 is the root-mean-square [RMS] positive-sequence voltage, and V_2 is the RMS negative-sequence voltage). If this ratio exceeds m%, the IBR ceases operation after t_{UB} seconds. The RMS POM voltage is used to assess whether any thresholds are exceeded. Note that the unbalanced factor condition is considered as a supervised component on the top of the undervoltage and overvoltage conditions. Unlike the undervoltage and overvoltage conditions, the unbalanced factor condition is based on the IBR terminal voltage, not the POM. This additional condition check protects the IBR from internal faults and prevents damage. Standards define the following:

- The V is defined as the min (V_N^{POM}, V_L^{POM}) or $avg(V_N^{POM}, V_L^{POM})$.
- V_N^{POM} and V_L^{POM} are the phase-to-neutral and phase-to-phase voltage at the POM.

- Table 7 from IEEE Std 2800 mentions U_n, $t_{U_n}(n = 1,2,\ldots,5)$, O_n, t_{O_n} $(n = 1,2,3)$.

Theoretically, if the POM voltage falls below 10%, the actual voltage at the IBR terminal (the capacitor voltage of the LC filter) is slightly higher due to the voltage drop across the transformer. Consequently, an IBR might enter momentary cessation even when its terminal voltage is slightly above 10%. For testing purposes, the implemented logic allows flexibility in selecting the momentary cessation entry time and enables or disables the cessation function for the IBR. Once momentary cessation is triggered, the gate pulse-width modulation signals are blocked, halting current generation. Note that only undervoltage situations caused by faults are studied in this work.

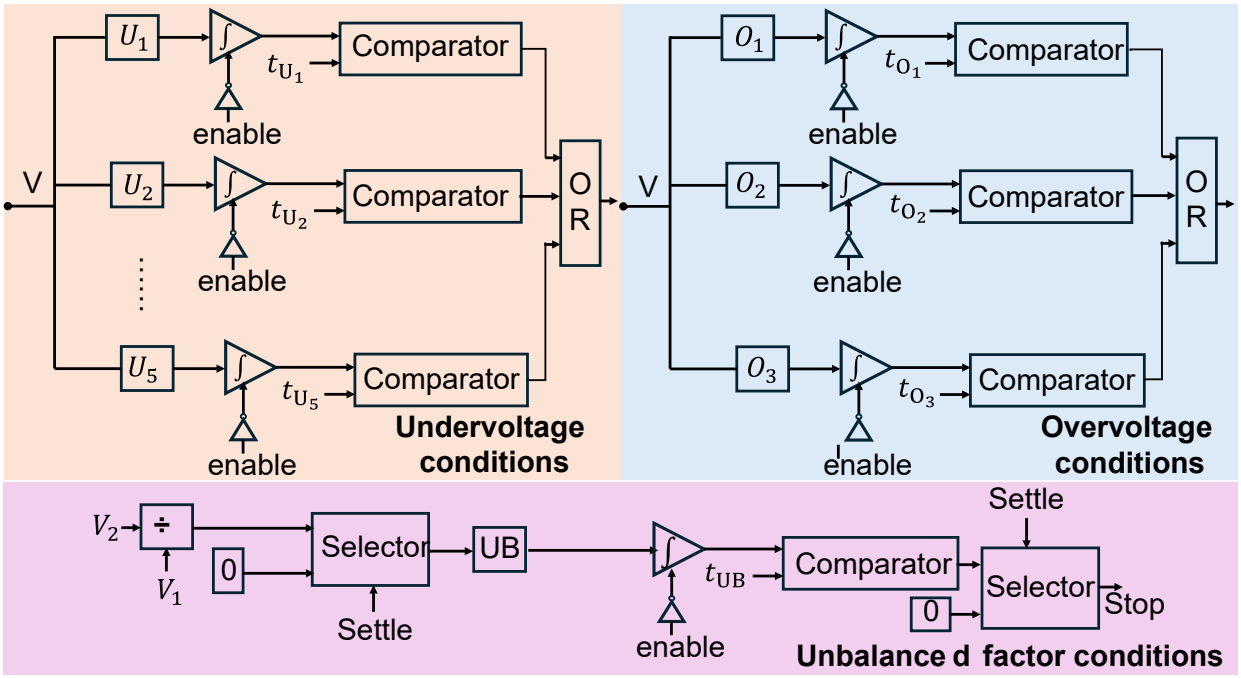

Figure 20. Logic diagram of the implemented momentary cessation in the IBR

3 Protective Relay Modeling

This section describes the protective relay models developed in MATLAB. The model development represents algorithms in real protection devices. All the algorithms were implemented using publicly available literature, such as conference and journal papers, instructions manuals, and patent publications. Protective relay modeling includes phasor-based protection elements and time-domain elements based on superimposed quantities. For organization, each protection element is described in a separate section. The protection element models are based on the protection schemes applied in relays used by the utility partners for the study.

3.1 Background for Protection Element Modeling

The KIUC transmission system is analyzed in this study. This study selected a specific transmission line that interconnects two substations, referred to as Substation 1 and Substation 2. Substation 1 represents a bus fed by the main power grid, dominated by synchronous machines, whereas Substation 2 is connected to an IBR. The transmission line under study is rated at 57.1 kV and spans 4.6 miles. Figure 21 illustrates the reduced version of the KIUC system evaluated in this study.

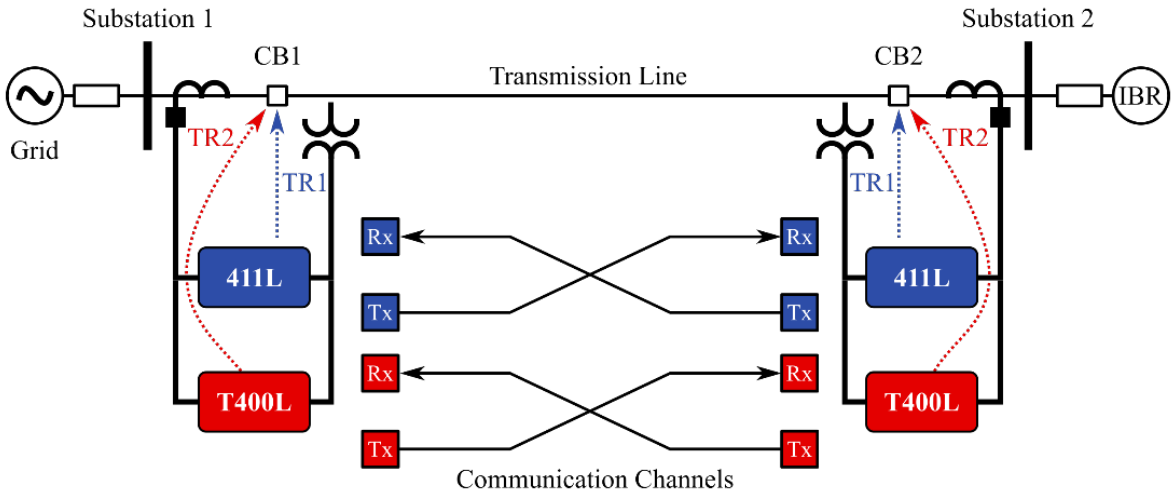

Figure 21. KIUC transmission system

Each substation is equipped with two Schweitzer Engineering Laboratories (SEL) protective relays: a SEL-411L and a SEL-T400L. The SEL-411L supports phasor-based protection elements, whereas the SEL-T400L implements time-domain protection functions. The time-domain functions are superimposed quantity-based and traveling wave-based protection elements. Table 8 details the protection elements that are actively set in the SEL-411L relay at each substation, and Table 9 lists the active elements in the SEL-T400L relay.

Table 8. Active Protection Elements in the SEL-411L Relay

Element	Name	Sub. 1	Sub. 2
87P	Phase current differential	1	1
87N	Negative-sequence differential	1	1
87G	Ground differential	1	1
21P	Mho phase distance	2	2
21G	Mho ground distance	2	2
21G	Quadrilateral ground distance	2	2
32QG	Negative-sequence voltage-polarized directional (ground)	1	1
32Q	Negative-sequence voltage-polarized directional (phase)	1	1
32V	Zero-sequence voltage-polarized directional	1	1
32SPO	Open-pole directional	1	1
32P	Voltage-polarized phase directional	1	1

Table 9. Active Time-Domain Protection Functions in the SEL-T400L Relay

Element	Name	Sub. 1	Sub. 2
TD32	Time-domain directional	1	1
TD21P	Time-domain distance (phase)	1	1
TD21G	Time-domain distance (ground)	1	1
TW32	Traveling wave directional	1	1
TW87	Traveling wave differential	1	1

A protection relay operates by measuring the voltage and currents at a specific point of a power system. The measurements from the current transformers and the voltage transformers go to the relay, which samples the measurements and performs the digital signal processing required for each protection function. The trip decision is taken according to the activate functions in the device. For instance, Figure 22 details the active elements in SEL-411L at each substation. These elements are classified into three primary types:

1. Line current differential: 87P (phase currents), 87Q (negative-sequence currents), and 87G (zero-sequence currents)
2. Distance elements: 21P and 21G with the mho characteristic, and 21G with the quadrilateral characteristic
3. Directional elements: 32Q, 32QG, 32V, and 32P.

The line current differential protection is a communication-based protection scheme, whereas the distance and directional elements are stand-alone elements. Note that 67G is not enabled.

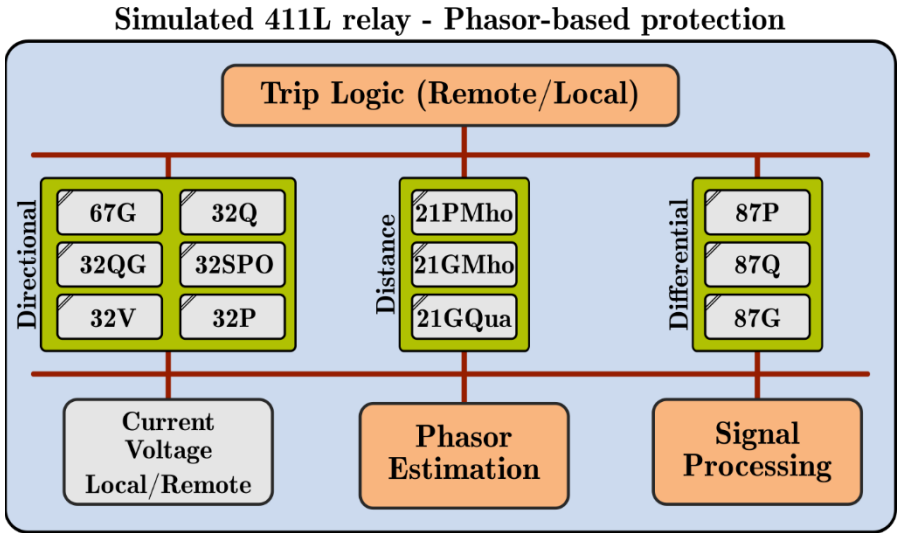

Figure 22. Active functions in the SEL-411L relay

The second relay, SEL-T400L, shown in Figure 23, employs time-domain protection functions for high-speed protection using either superimposed quantities or traveling wave-based protection elements. The superimposed quantity-based elements operate on the principle of superposition theorem, which isolates the pure-fault network by applying delta and replica filters to the voltage and current signals. The relay also contains the following traveling wave-based protection functions:

- TW32: traveling wave-based directional element
- TW87: traveling wave-based line current differential protection.

Sections 3.2 and 3.3 provides detailed descriptions of the protection elements and their modeling, and Section 5 presents how IBRs can influence the protective relay decisions considering different aspects regarding their modeling and control.

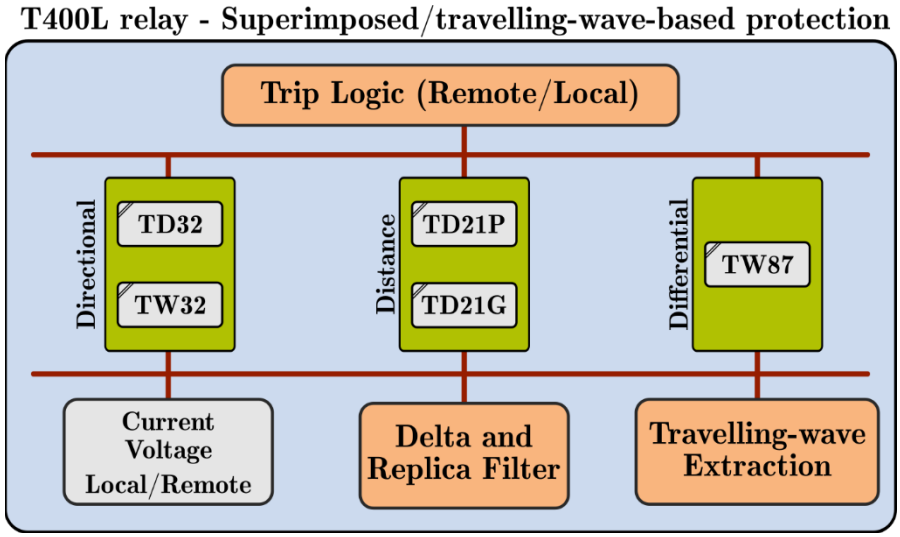

Figure 23. Active functions in the SEL-T400L relay

3.2 Phasor-Based Protection Elements

First, we define in detail the phasor-based protection elements enabled in the protection scheme.

3.2.1 Digital Signal Processing for Phasor-Based Protection Elements

The digital signal processing for the phasor-based protection elements includes a phasor estimation process based on a fundamental frequency one-cycle cosine filter and a symmetrical components filter. Figure 24 presents the logic diagram for this stage. The inputs are the instantaneous voltage and current signals, v_{abc} and i_{abc}, generated by the PSCAD/EMTDC simulation, and the outputs are the voltage and current RMS phasors, V_{abc} and I_{abc}, output by the full-cycle cosine filter.

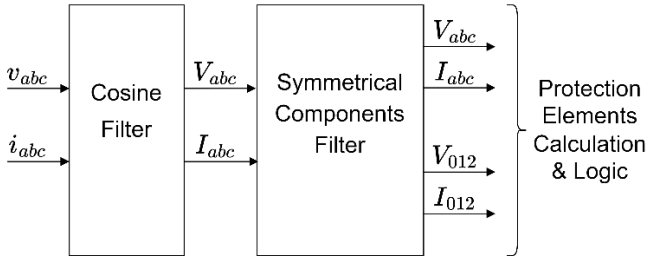

Figure 24. Digital signal processing for phasor-based protection elements

A phasor is a complex number formed by real and imaginary parts. The cosine filter computes the real part of the phasor using (28). The imaginary part is obtained by adding a one-quarter-cycle-delayed cosine term, $j\,X_{r\left(n-\frac{N}{4}\right)}$, as detailed in (29). The time-delayed cosine term replaces a sine filter because it provides better rejection of the decaying DC offset terms in fault currents:

$$X_{r(n)} = \frac{\sqrt{2}}{N}\sum_{n=0}^{N-1} x_{(n)} \cdot \cos\left(\frac{2\pi n}{N}\right) \tag{28}$$

$$X_{(n)} = X_{r(n)} + j\,X_{r\left(n-\frac{N}{4}\right)} \tag{29}$$

In (28) and (29), $X_{r\,(n)}$ is the real term of the phasor, n represents the current sample, N is the total number of samples in the window, and $x_{(n)}$ is the instantaneous voltage/current signal. After obtaining the phasors, the relay applies the Fortescue transformation to obtain the symmetrical component quantities in the Phase A reference frame using (30):

$$\begin{bmatrix} X_{A0} \\ X_{A1} \\ X_{A2} \end{bmatrix} = \begin{bmatrix} 1 & 1 & 1 \\ 1 & a^2 & a \\ 1 & a & a^2 \end{bmatrix} \cdot \begin{bmatrix} X_a \\ X_b \\ X_c \end{bmatrix} \tag{30}$$

To obtain the symmetrical components for the phase B and C reference frames, a phase shift element, $a = 1\angle 120^{\circ}$ is added to the components in the Phase A reference frame. The protection elements use phase and symmetrical component quantities in their algorithms for relay decisions. These protection functions include specific equations according to each fault loop for the

protection decisions, and they are supervised by additional elements, such as current-level detectors, directional elements, and fault type selection logic.

3.2.2 Distance Protection: Mho Characteristic

The mho characteristic implemented in this study uses positive-sequence memory voltage polarization, where the polarizing quantity serves as an angle reference [49]. The use of voltage memory polarization provides more security, especially for three-phase close-in bolted faults, where all the voltages drop to zero. The memory filter guarantees that the positive-sequence voltage angle is reliable information as long as the voltage memory does not expire. As a side benefit, the polarizing element causes a dynamic mho response. The effective mho circle for the zone dynamically expands the circle approximately toward the equivalent source impedance for forward faults with low power flow, which improve fault resistance coverage, and it contracts for reverse direction faults to improve security. Figure 25 presents a comparison of the memory polarized with the circle expansion with the self-polarized (static circle) element. Similar dynamic behavior occurs in a cross-polarized mho element, which replaces the memory voltages with line to ground voltages from phases not involved with the fault loop, such as the V_{BG} and V_{CG} voltages as a reference for the AG fault loop.

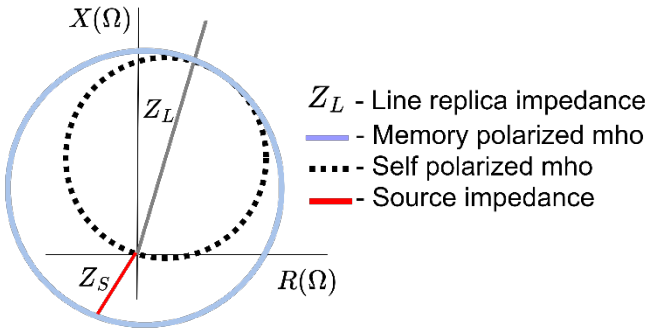

Figure 25. Dynamic mho expansion due to memory polarization

The positive-sequence memory voltage comes from a moving-window finite impulse response filter using (31). Usually, $\alpha = 1/16$ [50]:

$$V_{A1mem\,(k)} = \alpha \cdot V_{A1\,(k)} - (1-\alpha) \cdot V_{A1mem\,(k-half\ cycle)}\ (V) \tag{31}$$

To obtain the positive-sequence memory-polarized voltage for the other two phases (B and C), we apply the proper phase shift in the balanced positive-sequence voltage, V_{A1mem}, for each phase. The memory-polarized mho distance element uses the m equation in (32) to estimate the distance to the fault for the six fault loops listed in Table 10 [57]. The six fault loops include phase-to-ground elements, one on each phase, to respond to single-line-to-ground faults, and phase-to-phase loops to respond to the rest of the fault types. The m equation, described in (32), computes the effective distance to the fault from the relay location. It is a magnitude-based approach that compares the estimated fault distance with the protection zone settings (e.g., Zone 1 or Zone 2 reach):

$$m = \frac{Re[V \cdot V_{1mem}^{*}]}{Re[1\angle Z_{1L} \cdot I \cdot V_{1mem}^{*}]} \ (\Omega) \tag{32}$$

Table 10. Detailed Voltage and Currents per Fault Loop

Fault Loop	V	I	V_{1mem}
AG	V_A	$I_A + k_0 \cdot I_R$	V_{A1mem}
BG	V_B	$I_B + k_0 \cdot I_R$	V_{B1mem}
CG	V_C	$I_C + k_0 \cdot I_R$	V_{C1mem}
AB	$V_A - V_B$	$I_A - I_B$	$V_{A1mem} - V_{B1mem}$
BC	$V_B - V_C$	$I_B - I_C$	$V_{B1mem} - V_{C1mem}$
CA	$V_C - V_A$	$I_C - I_A$	$V_{C1mem} - V_{A1mem}$

If the estimated distance, *m,* from (32) is less than the protection zone setting thresholds and greater than 0, the fault is inside the protection zone. This study concentrates on forward direction Zone 1 and Zone 2 elements.

3.2.3 Distance Protection: Quadrilateral Characteristic

The quadrilateral (quad) characteristic improves the fault resistance coverage for faults involving a ground loop (e.g., AG, BG, and CG loops). Phase-to-phase quadrilateral elements are available as well. The relay implements the characteristic in Figure 26 using four comparators to create a quasi-rectangular polygon (one comparator for each side). The four sides are a reactance element, two fault resistance blinders (left and right), and directional supervision.

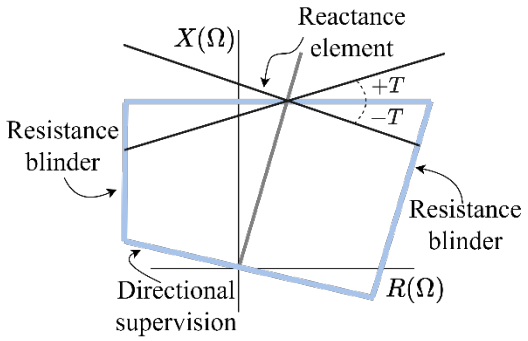

Figure 26. Quadrilateral characteristics

The relay implements reactance and fault resistance elements for ground and phase faults with some differences based on the fault type, similar to the mho element. The directional element supervises these two elements to guarantee the correct fault direction; it is described in detail in Section 3.2.5. The reactance characteristic uses (33) to estimate the distance to the fault:

$$X = \frac{Im[V \cdot (I_{POL} \cdot 1\angle T)^{*}]}{Im[1\angle Z_{1L} \cdot I \cdot (I_{POL} \cdot 1\angle T)^{*}]} \ (\Omega) \tag{33}$$

where *V* and *I* are the loop voltage and current phasor quantities from Table 10; $1\angle Z_{1L}$ is the positive-sequence impedance angle of the protected line; I_{POL} is a polarizing current that can be

I_0 or I_2 for ground faults and only I_2 for phase faults that do not involve a ground path, i.e., phase-to-phase; and T is the tilt angle for compensating the phase shift between the polarizing current and the total fault current in nonhomogeneous power systems. The tilt angle improves the security and the reliability of the element by reducing possible misoperations.

Figure 27 presents the negative-sequence network used to derive the tilt angle computation for single-line configurations in conventional power systems (i.e., it does not apply for systems fed by IBRs).

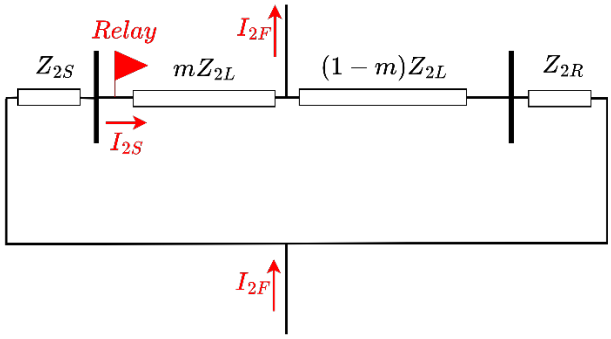

Figure 27. Negative-sequence network diagram to compute the tilt angle of the quadrilateral characteristic

By applying the current divider rule, engineers can use (34) to compute T for the negative-sequence current polarization case. The same network applies for the zero-sequence network, and (35) can compute T for the zero-sequence current polarization case. The polarizing current is chosen in a manner to better approximate the total fault current angle because the relay does not have access to current measurements from the remote end of the line [52]:

$$T_2 = \frac{Z_{2S} + Z_{2L} + Z_{2R}}{(1-m)\cdot Z_{2L} + Z_{2R}} \tag{34}$$

$$T_0 = \frac{Z_{0S} + Z_{0L} + Z_{0R}}{(1-m)\cdot Z_{0L} + Z_{0R}} \tag{35}$$

The fault resistance is computed for ground and phase loops in a way that is similar to what happens with the reactance element. The fault resistance estimation for ground and phase loops uses (36) and (37), respectively [52],[55],[56]:

$$R_{\phi g} = \frac{Im\left[V_\phi \cdot \left(1\angle Z_{1L} \cdot \left(I_\phi + k_0 I_R\right)\right)^*\right]}{Im\left[\frac{3}{2}(I_2 + I_0)\left(1\angle Z_{1L} \cdot \left(I_\phi + k_0 I_R\right)\right)^*\right]}\ (\Omega) \tag{36}$$

$$R_{\phi\phi} = \frac{Im\left[V_{\phi\phi} \cdot \left(1\angle Z_{1L} \cdot I_{\phi\phi}\right)^*\right]}{Im\left[\left(j\sqrt{2}\cdot I_2\right)\cdot\left(1\angle Z_{1L} \cdot I_{\phi\phi}\right)^*\right]}\ (\Omega) \tag{37}$$

The fault is declared inside the protection zone if the reactance estimation is smaller than its threshold and if the fault resistance estimation is also between the left and right resistance

blinders. In addition, the directional element must assert for forward faults, and the FID logic must select the correct fault loop by identifying the faulted phases.

Figure 28 presents a general diagram for the distance elements including both the mho and quadrilateral characteristics. In summary, the phasors and symmetrical component quantities are used to compute the abovementioned elements for each protection characteristic, and they are also used in directional supervision and the FID logic. After computing the elements, the relay logic checks if there is a fault condition to send a trip signal for the respective circuit breakers.

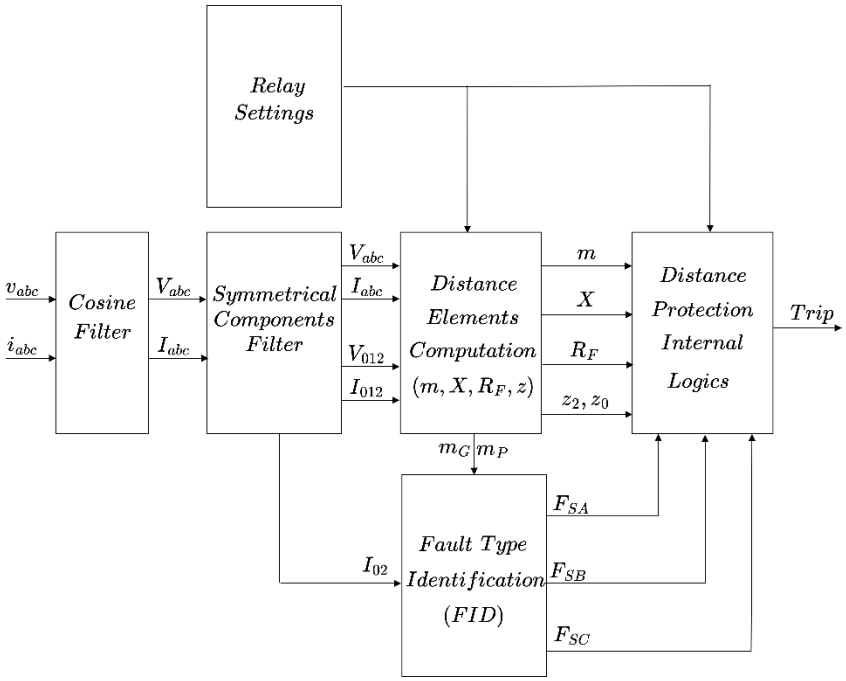

Figure 28. Logic diagram for the distance elements

Figure 29 presents the schematic diagram for the quadrilateral characteristic using Zone 1 of a Phase-A-to-ground (AG) fault as an example. Similar diagrams describe other fault types or zones. For the quadrilateral element to pick up, the reactance measurement for the AG loop, X_{AG}, needs to be smaller than its threshold, X_{set}. The estimated fault resistance, R_F, must be between the left and right resistive blinders (i.e., $-R_{set}$ and R_{set}, respectively). The 32GF bit indicates a forward fault signal generated by the impedance-based directional elements. The FID logic outputs the Phase A-to-ground fault loop selection bit to classify an AG fault, with similar outputs for other phases. The overcurrent level detectors verify the magnitude of the phase current, the negative-sequence current, and the zero-sequence current, I_A, $3I_{A2}$, and $3I_{A0}$, respectively.

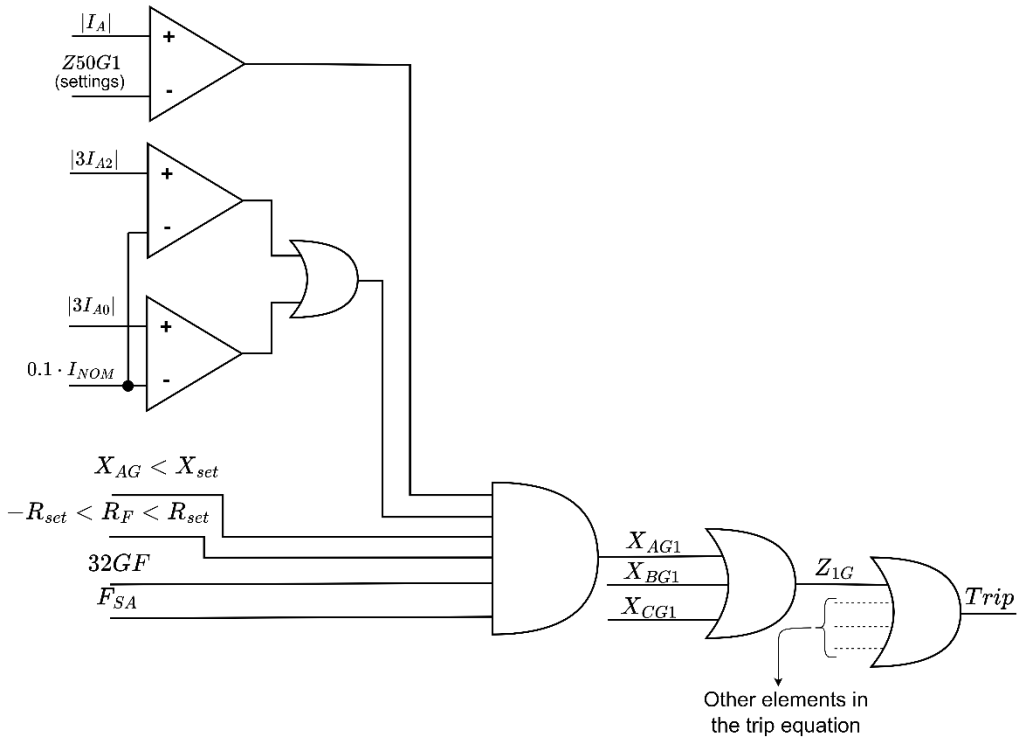

Figure 29. Trip schematic diagram for Zone 1 using the quadrilateral characteristic

3.2.4 Line Current Differential Protection in the Alpha Plane

The line current differential protection considers the generalized alpha plane formulation for the phase (87LP), negative-sequence (87LQ), and ground (87LG) elements. The alpha plane defines a complex variable given by the ratio of the remote current to the local current (i.e., I_R / I_L), as shown in (38). It uses the rainbow characteristic shown in Figure 30 to check the operating and restraining conditions [57],[58]:

$$\frac{\overrightarrow{I_R}}{\overrightarrow{I_L}} = a + jb = \vec{r} = re^{j\theta} \tag{38}$$

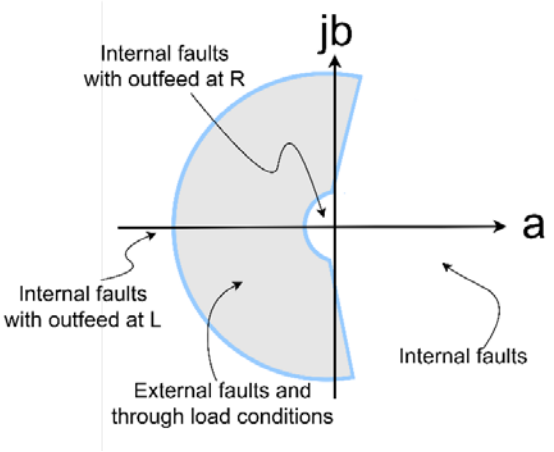

Figure 30. Rainbow characteristic for the line current differential protection in the alpha plane

If the calculated quantity lies inside the shaded area, the differential element based on the alpha plane will restrain (not generate) a trip output. On the other hand, if it lies outside the shaded area, it means there is an internal fault in the protected area, leading to a trip decision. For through load conditions (during steady-state), the I_R/I_L ratio equals $1\angle 180°$, and plots in one unit to the left of the alpha plane origin (i.e., a = -1) [58]. Because during steady state, the differential computation is basically a point at the real axis at a = -1. Its coordinates would be real axis = -1 and imaginary axis = 0. This is a region of restraining in the alpha plane. Figure 31 presents the general diagram for the line current differential protection.

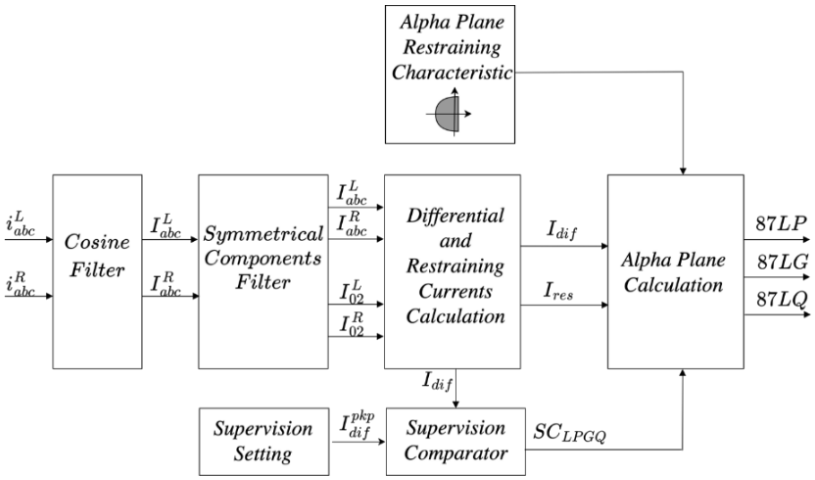

Figure 31. General diagram for line current differential protection

3.2.5 Impedance-Based Directional Elements

The impedance-based directional elements estimate the equivalent impedance seen by the protective device to indicate forward or reverse faults. Figure 32 presents the equivalent diagrams for the negative-sequence network during forward and reverse fault conditions. In ideal conditions, the protective relay estimates an equivalent impedance equal to $-|Z_{2S}|$ for forward faults, whereas for reverse fault conditions, it estimates an impedance equal to $+|Z_{2L} + Z_{2R}|$. A similar analysis applies for the zero-sequence network. Because there is a large difference between these thresholds, the setting thresholds of zone elements typically start with 50% of the

line impedance. This practice is also useful because the local and remote end source impedances are not known with a high degree of accuracy.

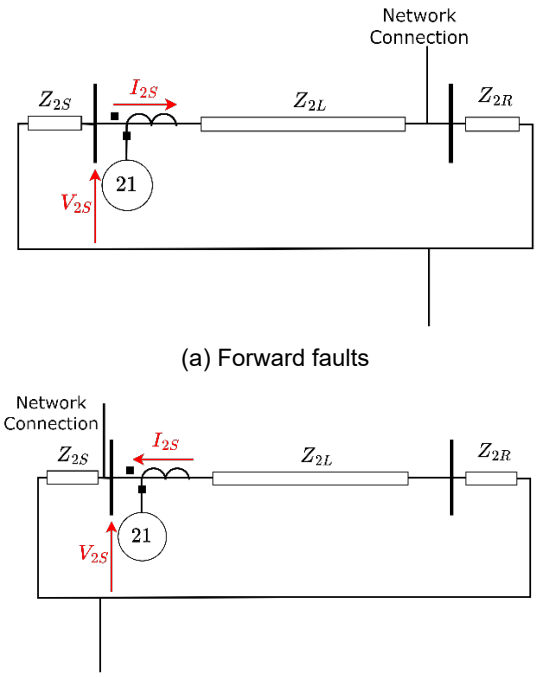

Figure 32. Sequence component diagram showing the connections for forward and reverse faults

The relay has the 32Q and 32QG elements that are based on the negative-sequence network (32Q is used for unbalanced phase faults and 32QG for ground faults). In addition, the relay model can also use the 32V element based on the zero-sequence network for ground faults. Figure 33 presents the schematic diagram for the 32QG element.

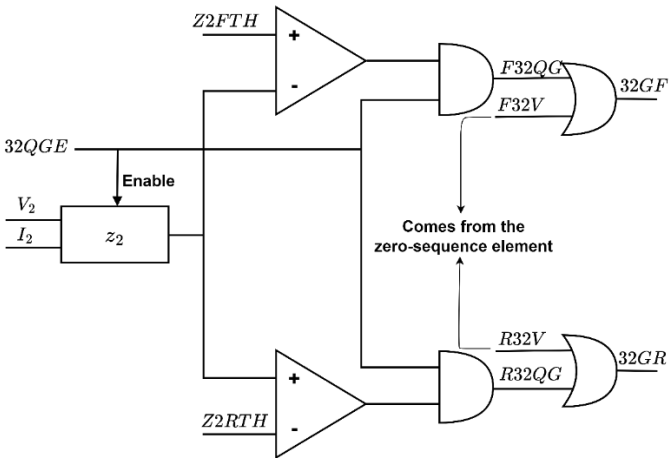

Figure 33. Diagram for the 32QG element

The directional element 32QG estimates the equivalent impedance using (39), and it compares the z2 impedance with the dynamic forward (Z2FTH) and dynamic reverse (Z2RTH) thresholds to determine the fault direction [59]. The 32QG element indicates a forward fault if z2 < Z2FTH.

In this case, the F32QG bit asserts. On the other hand, for a reverse fault, then z2 > Z2RTH; therefore, the R32QG bit asserts, indicating a reverse fault. Z2FTH starts with |Z2L|/2 - ε, with some additional calculations to enhance security. Similarly, Z2FTH starts with |Z2L|/2 + ε, with some additional calculations to enhance security, where ε is a security margin:

$$z2 = \frac{Re[V_2 \cdot (I_2 \cdot 1\angle Z_{1L})^*]}{|I_2|^2} \ (\Omega) \tag{39}$$

A similar diagram in Figure 33 applies for the 32V element. In this case, the element indicates a forward fault by asserting the F32V bit if the z0 impedance is smaller than the forward threshold Z0FTH. The element will indicate a reverse fault by asserting the R32V bit if z0 > Z0RTH [65]:

$$z0 = \frac{Re[V_0 \cdot (I_0 \cdot 1\angle Z_{0L})^*]}{|I_0|^2} \ (\Omega) \tag{40}$$

3.2.6 FID Logic

The phasor-based FID logic classifies the fault type by checking the angle difference between the zero-sequence and the negative-sequence currents on Phase A reference frame [61]. It separates three 60° angle regions to differentiate between the single-phase-to-ground and double-line-to-ground faults. From the principle presented in Figure 34, if the angle difference between I_{A0} and I_{A2} is within -30° and 30°, the relay classifies a fault as either an AG or a BCG fault. If this angle difference is between 90° and 150°, it classifies the event as a BG or a CAG fault. If this angle ranges from -150° to -90°, it is classified as a CG or an ABG fault.

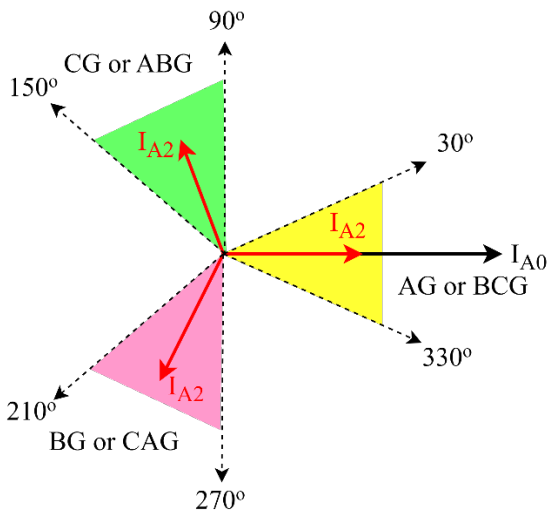

Figure 34. Operating principle for phasor-based FID logic

To differentiate between phase-to-ground and double-line-to-ground faults, the relay checks the absolute value of the mho element with smaller reach. For instance, if the fault is AG, the angle difference between I_{A0} and I_{A2} will lie inside the region from -30° to 30°, and also the absolute value of the mho element for AG will be smaller than the mho element for BC faults; therefore, the relay will classify the fault as an AG [61]. Other possibilities include checking the reactance

element for the ground and phase loops with smaller reach as well as the total current method implemented in [66].

3.3 Protection Elements Based on Time-Domain Superimposed Quantities

The time-domain protection elements that operate based on superimposed, or incremental, quantities apply the superposition theorem of electrical circuits. These elements consider removing the effects of the pre-fault circuit to obtain the fault-generated signals (i.e., voltages and current) to create the operating and restraining quantities of the following protection elements: distance protection (TD21), directional element (TD32), and FID logic. Figure 35 shows that the pre-fault circuit considers the operating equivalent voltage sources and the pre-fault voltage at the fault location, *m,* determined by $v_{pre}(t) = V \cdot cos\ (\omega t + \phi)$. By applying the delta filter, we obtain the superimposed quantities and remove the pre-fault condition, thus isolating the faulted circuit. In this case, the pre-fault sources are shorted, and at the fault point, there is an equivalent source with the same magnitude and opposite polarity of the pre-fault voltage. Note that in the faulted circuit, the protection relay measures the delta voltages and the currents signals, referred to as $\Delta v(t)$ and $\Delta i(t)$, respectively.

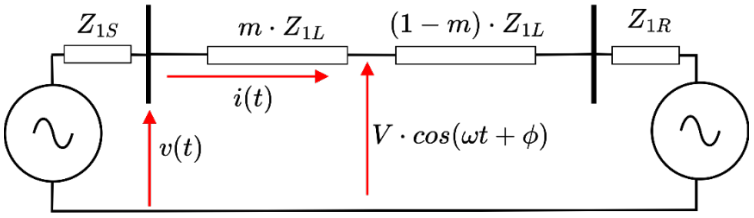

(a) Pre-fault circuit

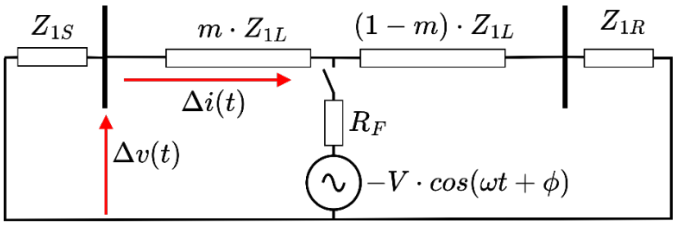

(b) Faulted circuit

Figure 35. Superposition theorem

3.3.1 Digital Signal Processing for Time-Domain Elements

The superimposed protection elements work with a sampling frequency of 10 kHz. Usually, time-domain protection relays sample the voltage and current signals at a rate of 1 MHz to use in other protection functions (e.g., traveling wave-based elements). For the incremental quantities, these signals pass through an anti-aliasing filter, and they are decimated to a 10-kHz sampling rate. Figure 36 presents a general diagram for the digital signal processing occurring in time-domain protection relays.

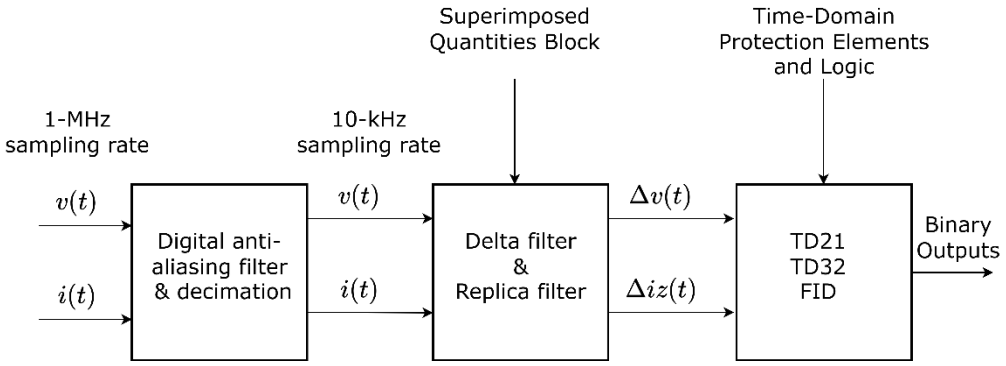

Figure 36. Digital signal processing stage

After the anti-aliasing filter and decimation stages, the delta filter outputs the incremental voltage and current signals, $\Delta v(t)$ and $\Delta i(t)$, respectively. The delta filter subtracts the most recent sample by a one-cycle delayed sample, as expressed by (41):

$$\Delta x(n) = x(n) - x(n - 1\ cycle) \tag{41}$$

$\Delta x(n)$ is the delta voltage or current signal, $x(n)$ is the most recent sample of the signal, and $x(n - 1\ cycle)$ is the delayed sample. The delta quantities are specified per fault loop in a similar way on the phasor-based elements. Table 11 details the loop incremental voltages and the replica currents.

Table 11. Loop Incremental Voltages and Replica Currents

Fault Loop	Voltage (Δv)	Replica Current (Δiz)
AG	Δ_{VA}	$\Delta i_{ZA} - \Delta i_{Z0}$
BG	Δ_{VB}	$\Delta i_{ZB} - \Delta i_{Z0}$
CG	Δ_{VC}	$\Delta i_{ZC} - \Delta i_{Z0}$
AB	$\Delta_{VA} - \Delta_{VB}$	$\Delta i_{ZA} - \Delta i_{ZB}$
BC	$\Delta_{VB} - \Delta_{VC}$	$\Delta i_{ZB} - \Delta i_{ZC}$
CA	$\Delta_{VC} - \Delta_{VA}$	$\Delta i_{ZC} - \Delta i_{ZA}$

The replica current calculation removes the decaying DC offset from the delta currents. This filter mimics the transmission line impedance represented as an RL circuit. It is effectively measuring a voltage drop through the transmission line by multiplying the current signals by the line impedance with the unit gain in the fundamental frequency. The replica current is represented by $\Delta i_z(t)$, as shown in (42). The i_z label refers to the math operation between the current signal and the impedance:

$$\Delta i_z(t) = \frac{R_S}{|Z_S|}\Delta i(t) + \frac{L_s}{|Z_S|}\frac{d}{dt}\Delta i(t) \tag{42}$$

The delta zero-sequence current is obtained using (43), and the replica zero-sequence current is obtained using (44) [62]:

$$\Delta i_0(t) = \frac{1}{3}\left(\Delta i_A(t) + \Delta i_B(t) + \Delta i_C(t)\right) \tag{43}$$

$$\Delta i_{Z0}(t) = \frac{R_1}{|Z_1|}\Delta i_0(t) + \frac{L_1}{|Z_1|}\frac{d}{dt}\,\Delta i_0(t) - \frac{|Z_0|}{|Z_1|}\left(\frac{R_0}{|Z_0|}\Delta i_0(t) + \frac{L_0}{|Z_0|}\frac{d}{dt}\,\Delta i_0(t)\right) \tag{44}$$

3.3.2 Time-Domain Distance Protection (TD21)

The time-domain distance protection provides an instantaneous underreaching element for the protected line. This function calculates the change in the voltage at the set reach point, $v_{OP}(t)$ and compares it with the pre-fault voltage at the reach point, $v_{RT}(t)$. $v_{OP}(t)$ is also referred to as the operating quantity, whereas $v_{RT}(t)$ is the restraining quantity. They are shown in (45) and (46), respectively:

$$v_{OP}(t) = \Delta v(t) - m \cdot |Z_{1L}| \cdot \Delta i_Z(t) \tag{45}$$

$$v_{RT}(t) = v\,(t - 1\ cycle) - m \cdot |Z_{1L}| \cdot i\,(t - 1\ cycle) \tag{46}$$

The computation for these quantities is performed on a per-fault-loop basis following Table 11. The TD21 logic compares the operating and restraining signals considering the relative signs of these quantities as follows:

1. If the restraining signal is positive, the fault occurred on the positive half of the voltage wave, and the voltage will move down toward zero in response to the fault. In this case, the incremental change in voltage is negative.
2. If the restraining signal is negative, the fault occurs on the negative half of the voltage wave, and the voltage will move up toward zero in response to the fault. In this case, the incremental change in voltage is positive.

The TD21 element requires that the absolute value of the operating quantity surpasses the absolute value of the restraining quantity while maintaining opposite polarities. The TD21 logic also requires a minimum level of restraining quantity to address when the pre-fault voltage signal crosses zero. Figure 37 presents a simplified logic diagram for the TD21 element for the AG fault loop.

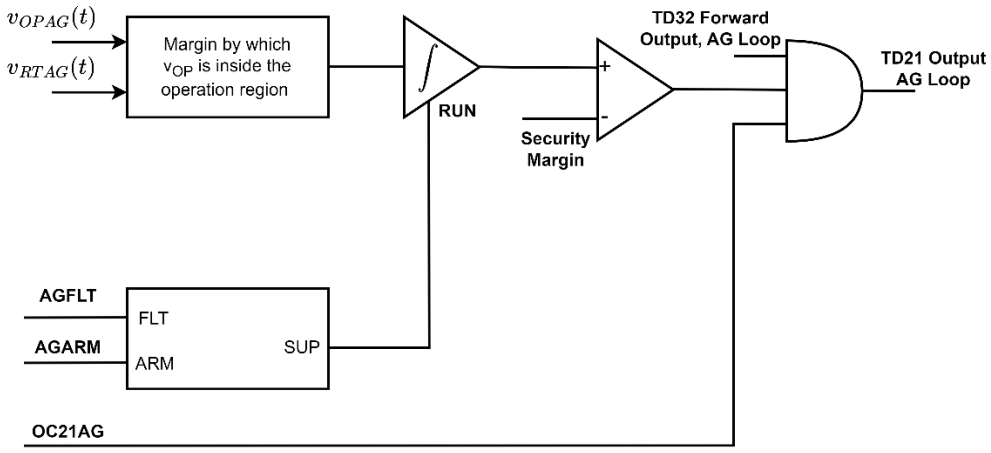

Figure 37. TD21 simplified logic diagram for the AG fault loop

3.3.3 Time-Domain Directional Element (TD32)

The time-domain directional element (TD32) is intended for use with the permissive overreaching transfer trip scheme and to supervise other protection elements, such as TD21. The TD32 element compares the polarities of the incremental loop voltage (Δv) and the incremental replica loop current (Δi_z). The relationship between the incremental loop voltage and the incremental replica loop current for a purely resistive circuit is shown in Figure 38. Figure 39 presents the simplified logic diagram for the TD32 element.

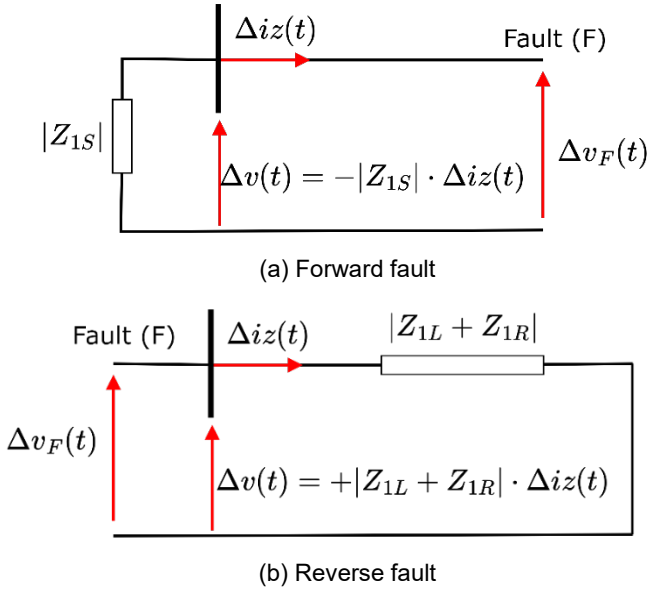

Figure 38. TD32 principle of operation

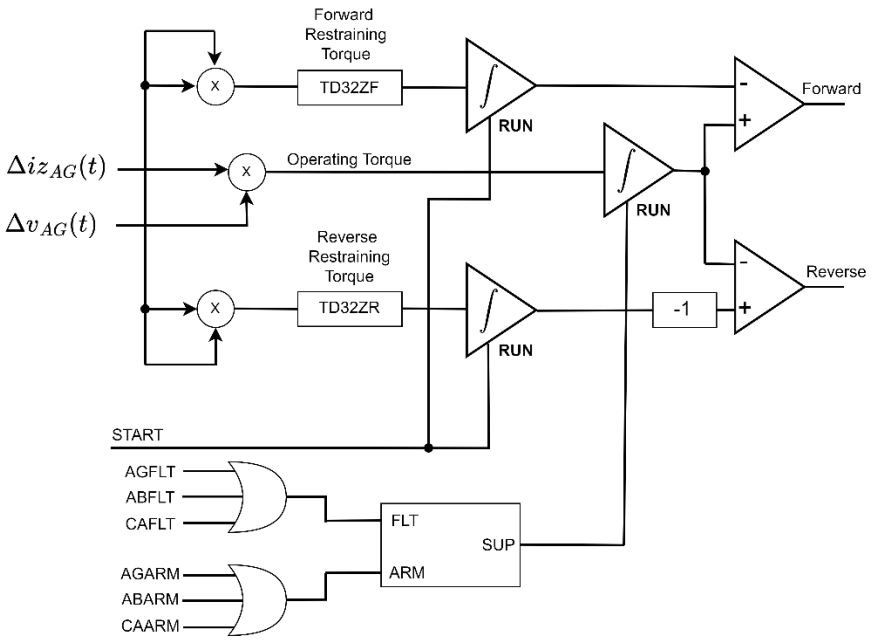

Figure 39. Simplified logic for the TD32 element, AG loop

The TD32 element operates independently for each of the six fault loops. First, the TD32 logic computes the operating torque as a product of the incremental loop voltage and the incremental replica loop current. It inverts the sign of the product so that a positive torque indicates forward direction. The forward restraining torque is always positive, and the reverse restraining torque is always negative. The TD32 element asserts in the forward direction if the integrated operating torque is positive and greater than the integrated forward restraining torque. The TD32 element asserts in the reverse direction if the integrated operating torque is negative and greater (in terms of absolute values) than the integrated reverse restraining torque. Both thresholds are dynamically calculated because they are a function of the loop current squared.

3.3.4 Time-Domain FID Logic

The time-domain FID logic analyzes the output of the starting logic and the output from the raw TD32 incremental quantity directional element. Both logics operate on a per-loop basis, and by inspecting both outputs, the FID logic distinguishes between a single multiphase fault and an evolving external/internal fault.

The starting logic will check which of the six protection measurement loops are involved in a fault. The logic uses the incremental loop voltage (Δv) and the incremental replica loop current (Δiz) to compute the starting voltage (Δv_{START}) according to (47). The starting voltage is a voltage change at an electrical distance Z_X away from the relay:

$$\Delta v_{START} = |\Delta v| + Z_X \cdot |\Delta iz| \tag{47}$$

The distance, Z_X, is the positive-sequence line impedance magnitude, Z1MAG, plus margin for dependability. The starting logic determines the loop involved in a fault if the starting voltage exceeds a threshold. In addition, the logic compares the six starting voltages for each protection measurement loop with one another to identify the loops involved in the fault.

4 Framework for Studying the Impact of IBRs on Protection Systems

This section covers the motivation and lists the impacts of IBR modeling and control aspects on protective relay decisions (Section 4.1), the power system under study for the validation of the IBR impact study (Section 4.2), and the scenarios and dataset creation for the validation (Section 4.3). Each subsection will be discussed in detail.

4.1 Motivation and List of IBR Modeling and Control Aspects

To our knowledge, it is not well studied how different modeling aspects (DC source, inverter model, power control, current/voltage control, and Current Limiter) qualitatively and quantitatively affect the response and trip decisions of the protective relay elements. It is important to answer the following pertinent questions:

1. How does the type of primary source at the DC side of the IBRs impact the functionality of the protective relay elements?
2. How does the type of VSI modeling of the IBRs impact the functionality of the protective relay elements?
3. How does the type of control scheme of the IBRs impact the functionality of the protective relay elements?
4. How does the type of fault current-limiter scheme of the IBRs impact the functionality of the protective relay elements?

This report classifies the aspects of IBR modeling into five categories for detailed understanding, as shown in Figure 40. An extensive EMT simulation study is conducted, and the captured IBR response characterizations consider both GFL IBRs and GFM IBRs as evaluated using the real-world network to quantitatively assess and prioritize their impacts on the system's protection performance. The main contributions of this work are to address the research gaps and to benefit power system protection engineers. Toward that end, we:

- Identify the dominant factors among the IBR modeling aspects, both qualitatively and quantitatively, that impact the functionalities of relay elements.
- Provide some required modifications in the fault prediction algorithms to be included in the fault study software.
- Provide a platform to modify settings for the existing protection schemes or design new protection algorithms.

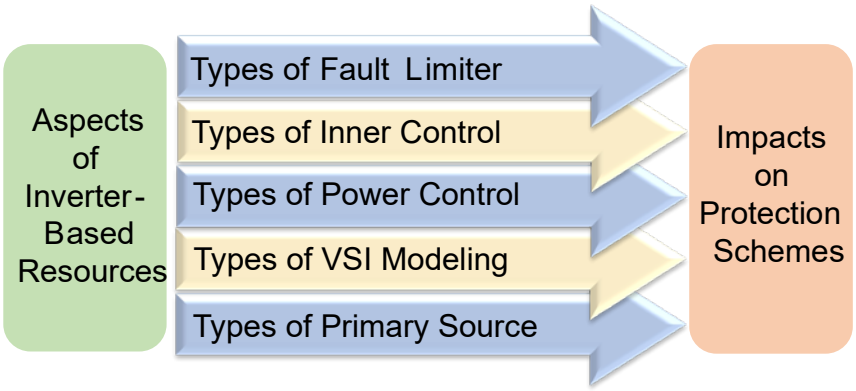

Figure 40. The inverter aspects under study

4.2 Power System Under Study

The power system under study is shown in Figure 41 and is adapted from an existing transmission system. Here, the equivalent grid is modeled as either a three-phase, 57.1-kV, stiff voltage source or a non-stiff synchronous generator behind the equivalent line impedance at the point of interconnection. The equivalent grid is connected to Bus-1 via Line-1 and is paralleled with a three-phase, 6.9-kV, 7.5-MVA hydro turbine generator connected to the bus via a three-phase, Y-Δ, 57.1/6.9-kV, 7.5-MVA step-up transformer (TF1). The transmission line under study, Line-2, connects Bus-1 and Bus-2. At Bus-2, a three-phase, 0.48-kV, 15 MVA IBR is connected at the point of common coupling via a three-phase, Δ-Y (or Y-Δ), 57.1/0.48-kV, 15-MVA step-up transformer (TF2).

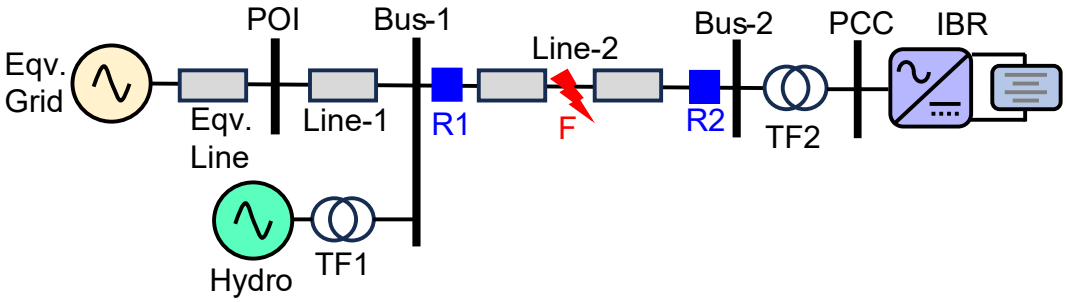

Figure 41. Figure showing the transmission system under study

The generic IBR model is developed in this study considering the following configurations:

- The IBR can operate either as a GFL IBR or a GFM IBR.
- The VSI topology is modeled using a switching model or a switch-average model.
- The DC side is terminated by either a PV or a battery source or both.
- The GFL IBR is configured with PQ-dispatch control and $V_{dc} - V_{ac}$ control in the outer-power-control layer, with inner-control in the dq domain, the $\alpha\beta$ domain, and the sequence domain in the inner-current-control layer, as shown in Table 12.
- The GFM IBR is configured with $P - f$ and $Q - V$ droop control, with VSM control in the outer-power-control layer; multi-loop-based control in the dq domain, $\alpha\beta$ domain, and sequence domain; and single-loop-based control in the inner-voltage-control layer, as shown in Table 13.

- For both GFL IBRs and GFM IBRs, instantaneous current saturation-based and latching-based fault current-limiter logic is employed with configurable d-axis and q-axis priority. For the GFM IBR, virtual impedance-based fault limiter logic is also employed.

Table 12. Various Control and Current Limiter Schemes Under Study for GFL IBRs

<table>
<tr><th rowspan="2">DC Source</th><th colspan="2">GFL Control Scheme</th><th rowspan="2">Current Limiter</th></tr>
<tr><th>Outer Power Control</th><th>Current Control</th></tr>
<tr><td>Ideal DC source</td><td rowspan="4">fP-VQ dispatch control (IEEE 2800 compliant)
❑ Open-loop dispatch control
❑ Closed-loop dispatch control</td><td rowspan="2">Conventional DQ-domain current control</td><td rowspan="2">Instantaneous saturation limit
❑ D-axis priority-based (act. power)
❑ Q-axis priority based (VAr)</td></tr>
<tr><td>PV source</td></tr>
<tr><td>Battery source</td><td rowspan="2">Conventional $\alpha\beta$-domain current control</td><td rowspan="2">Current Latching
❑ D-axis priority-based
❑ Q-axis priority based</td></tr>
<tr><td>Any Combination</td></tr>
<tr><th>VSC Model</th><td rowspan="3">V_{dc}-Q control
❑ MPPT-based V_{dc} control</td><td rowspan="3">+ve and –ve sequence DQ-domain current control</td><td rowspan="3">Anti-wind-up Protection for
❑ Proportional-Integral (PI) Regulators
❑ Proportional-Resonant (PR) Regulators</td></tr>
<tr><td>Switched-averaged model</td></tr>
<tr><td>Switch Model</td></tr>
</table>

Table 13. Various Control and Current Limiter Schemes Under Study for GFM IBRs

<table>
<tr><th rowspan="2">DC Source</th><th colspan="2">GFM Control Scheme</th><th rowspan="2">Current Limiter</th></tr>
<tr><th>Outer Control</th><th>Voltage Control</th></tr>
<tr><td>Ideal DC source</td><td rowspan="3">Pf-QV droop Control</td><td rowspan="3">Conventional DQ-domain control
❑ Outer-voltage-inner-current control
❑ Single-loop voltage control</td><td>Instantaneous saturation limit
❑ D-axis priority-based
❑ Q-axis priority based</td></tr>
<tr><td>PV source</td><td>Current Latching
❑ D-axis priority-based
❑ Q-axis priority based</td></tr>
<tr><td>Battery source</td><td rowspan="2">Virtual Impedance-based limit</td></tr>
<tr><td>Any Combination</td><td rowspan="4">Virtual Synchronous Machine Control (VSM)</td><td rowspan="2">Conventional $\alpha\beta$-domain outer-voltage-inner-current control</td></tr>
<tr><td>VSC Model</td><td rowspan="3">Anti-wind-up Protection for
❑ Proportional-Integral (PI) Regulators
❑ Proportional-Resonant (PR) Regulators</td></tr>
<tr><td>Switched-averaged model</td><td rowspan="2">+ve and –ve sequence DQ-domain outer-voltage-inner-current control</td></tr>
<tr><td>Switch Model</td></tr>
</table>

Table 14 shows the various selected impedances of the test system, where $Z_{\mathrm{KP}}^{\mathrm{p}}$ and Z_{KP}^{0} are the positive-sequence and zero-sequence line impedances between Bus-1 and Bus-2 in Figure 41. $Z_{\mathrm{eq}}^{\mathrm{p}}$ and Z_{eq}^{0} are the positive-sequence and zero-sequence line impedance between the equivalent grid and the point of interconnection in Figure 41. Note that the test system under study now incorporates the equivalent grid impedance, determined from a real event captured from our utility partner at the KIUC transmission system. The numbers of $Z_{\mathrm{eq}}^{\mathrm{p}}$ and Z_{eq}^{0} are the computed line impedances based on the field event data provided by KIUC, as shown in Table 14.

Table 14. Impedances of Various Lines of the Test System

$Z_{\mathrm{KP}}^{\mathrm{p}} = 1.0433 + \mathrm{j}3.218$	$Z_{\mathrm{KP}}^{0} = 1.5649 + \mathrm{j}4.827$
$Z_{\mathrm{eq}}^{\mathrm{p}} = 5.91 + \mathrm{j}12.53$	$Z_{\mathrm{eq}}^{0} = 5.65 + \mathrm{j}18.93$

4.3 Scenarios and Dataset Creation

Extensive EMT simulation studies are carried out to understand the impacts of various aspects of IBR modeling, shown in Figure 42, on the protection schemes. The hierarchical framework is shown in Figure 43. The system under study is modeled using the PSCAD/EMTDC platform. A Python-based automated script is the central unit that links the PSCAD model, the input configuration file, and the data acquisition process. The input configuration file contains the scenario details that cover the following top hierarchy of scenarios:

1. AG fault at 'F' with $R_f = 0.01\Omega$ with TF2 as Y-Δ
2. AG fault at 'F' with $R_f = 0.01\Omega$ with TF2 as Δ-Y,
3. BC fault at 'F' with $R_f = 0.01\Omega$ with TF2 as Δ-Y.

Under each scenario is the next layer of hierarchical scenarios, which covers all combinations inside:

A. {# types of DC source} × {# type of VSI model} × {# type of outer-power control} for GFL IBR cases with a fixed type of inner-current control and current-limiter scheme
B. {# types of inner-current control} × {# type of current-limiter scheme} for GFL IBR cases with a fixed type of DC source, a VSI model, and outer-power control
C. {# type of outer-power control} for GFM IBR cases with a fixed type of DC source, a VSI model, inner-voltage control, and a current-limiter scheme
D. {# types of inner-voltage control} × {# type of current-limiter scheme} for GFM IBR cases with a fixed type of DC source, a VSI model, and outer-power control.

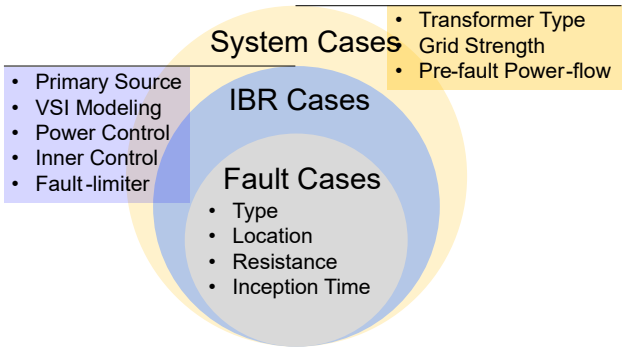

Figure 42. The process flow diagram of the EMT study

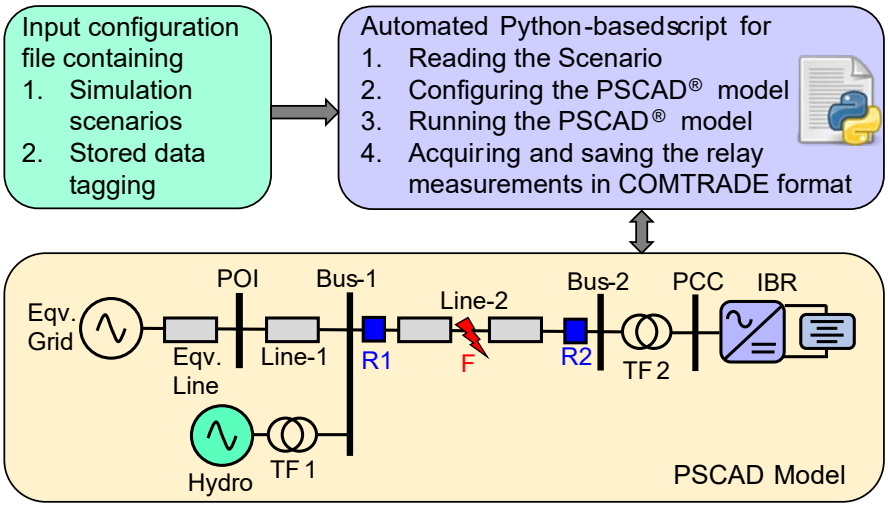

Figure 43. Flow for scenario and dataset creation

The automated Python-based script reads the scenario file and configures the PSCAD model accordingly by using the PSCAD Automation Library and running the model. The same script acquires the instantaneous voltage waveforms at relay R1 (i.e., $v_{\mathrm{A}}^{\mathrm{R1}}(t), v_{\mathrm{B}}^{\mathrm{R1}}(t), v_{\mathrm{C}}^{\mathrm{R1}}(t)$) and at R2 (i.e., $v_{\mathrm{A}}^{\mathrm{R2}}(t), v_{\mathrm{B}}^{\mathrm{R2}}(t), v_{\mathrm{C}}^{\mathrm{R2}}(t)$), and the instantaneous current waveforms at relay R1, from Bus-1 to Bus-2 (i.e., $i_{\mathrm{A}}^{\mathrm{R1}}(t), i_{\mathrm{B}}^{\mathrm{R1}}(t), i_{\mathrm{C}}^{\mathrm{R1}}(t)$), and at relay R2, from Bus-2 to Bus-1 (i.e., $i_{\mathrm{A}}^{\mathrm{R2}}(t), i_{\mathrm{B}}^{\mathrm{R2}}(t), i_{\mathrm{C}}^{\mathrm{R2}}(t)$), and saves it in COMTRADE-99 format with a sample time step, $T_{\mathrm{s}} = 2084\ \mu\mathrm{s}$. This results in eight samples per cycle, which is a common sampling rate that protection relays use. The case studies are as follows:

1. In the system cases, TF2 in Figure 41 was selected as either a YgD transformer (Yg facing the transmission) or a DYg transformer (D facing the transmission).
2. In the fault cases, we selected a bolted AG fault for both TF2 connections (i.e., the YgD transformer and the DYg transformer).
3. The fault location was always at F in Figure 41.

A few additional case studies are summarized as follows:

1. Grid strength: This contains an additional 24 cases.
   A. $Z_{\mathrm{eq}}^{\mathrm{p}} = 5.91 + \mathrm{j}12.53$, $Z_{\mathrm{eq}}^{0} = 5.65 + \mathrm{j}18.93$ in Figure 41.

B. With hydro online (high grid impedance) and with hydro offline (low grid impedance)

C. Bolted fault at F3 of:

   i. AG fault with TF2 as YgD (D facing IBR)
   ii. BC fault with TF2 as DYg (Yg facing IBR).

D. For each fault case, GFL with PV+battery, average model, PQ-dispatch outer control, $P_{\text{ref}} = 1.0\ \text{p.u.}$, $Q_{\text{ref}} = 0.0\ \text{p.u.}$:

   i. dq-based current controller with q-priority saturation limiter
   ii. $\alpha\beta$-based current controller with q-priority saturation limiter
   iii. Sequence-domain control with q-priority saturation limiter.

E. For each fault case, GFM with PV+battery, average model, droop-based outer control, $P_{\text{ref}} = 0.8\ \text{p.u.}$, $Q_{\text{ref}} = 0.0\ \text{p.u.}$:

   i. dq-based current controller with q-priority saturation limiter
   ii. $\alpha\beta$-based current controller with q-priority saturation limiter
   iii. Sequence-domain control with q-priority saturation limiter.

2. Pre-fault operating point of IBR: This contains an additional 36 cases:

A. $Z_{\text{eq}}^{\text{p}} = 5.91 + \text{j}12.53$, $Z_{\text{eq}}^{0} = 5.65 + \text{j}18.93$ in Figure 41.

B. With two different pre-fault operating points:

   i. $P_{\text{ref}} = 0.1\ \text{p.u.}$, $Q_{\text{ref}} = 0.0\ \text{p.u.}$
   ii. $P_{\text{ref}} = 0.25\ \text{p.u.}$, $Q_{\text{ref}} = 0.0\ \text{p.u.}$

C. Bolted fault at F3 of

   i. AG fault with TF2 as YgD (D facing IBR)
   ii. BC fault with TF2 as DYg (Yg facing IBR).

D. For each fault case, GFL with PV+battery, average model, PQ-dispatch outer control:

   i. dq-based current controller with q-priority saturation limiter
   ii. $\alpha\beta$-based current controller with q-priority saturation limiter
   iii. Sequence-domain control with q-priority saturation limiter.

E. For each fault case, GFM with PV+battery, average model, droop-based outer control:

   i. dq-based current controller with q-priority saturation limiter
   ii. $\alpha\beta$-based current controller with q-priority saturation limiter
   iii. Sequence-domain control with q-priority saturation limiter.

3. The momentary cessation logic of the IBR is active: This contains an additional 10 cases:

A. $Z_{\text{eq}}^{\text{p}} = 5.91 + \text{j}12.53$, $Z_{\text{eq}}^{0} = 5.65 + \text{j}18.93$ in Figure 41.

B. GFL with PV+battery, average model, PQ-dispatch outer control, $P_{\text{ref}} = 1\ \text{p.u.}$, $Q_{\text{ref}} = 0\ \text{p.u.}$:

i. Sequence-domain control with momentary cessation disabled and enabled with FRT time = 1, 2 and 4 cycles with q-priority saturation limiter.

C. Bolted fault at F3 of:

i. AG fault with TF2 as YgD (D facing IBR)
ii. BC fault with TF2 as DYg (Yg facing IBR).

D. IEEE Std 2800 provides the minimum fault ride-through (FRT) capability for IBRs; cessation is designed based on that, but with less withstanding time.

E. $\frac{|V_2|}{|V_1|} > 5\%$ as trigger is also added in the logic.

F. GFL with PV+battery, average model, PQ-dispatch outer control, $P_{\text{ref}} = 1\ \text{p.u.}$, $Q_{\text{ref}} = 0\ \text{p.u.}$, FRT= 1 cycle:

i. dq-based current controller with q-priority saturation limiter
ii. $\alpha\beta$-based current controller with q-priority saturation limiter
iii. Sequence-domain control with q-priority saturation limiter.

4. Slow/fast IEEE Std 2800-compliant sequence-domain controller of IBRs: This contains an additional eight cases:

A. GFM with PV+battery, average model, droop-based outer control, $P_{\text{ref}} = 0.25\ \text{p.u.}$, $Q_{\text{ref}} = 0.15\ \text{p.u.}$

i. Sequence-domain control with q-priority saturation limiter:

a. Slow
b. Fast.

B. Bolted fault at F3 of:

ii. AG fault with TF2 as YgD (D facing IBR)
iii. BC fault with TF2 as DYg (Yg facing IBR).

C. GFL with PV+battery, average model, PQ-dispatch outer control, $P_{\text{ref}} = 0.25\ \text{p.u.}$, $Q_{\text{ref}} = 0.15\ \text{p.u.}$

i. Sequence-domain control with q-priority saturation limiter:

a. Slow
b. Fast.

5. Additional fault impedance, fault types, and fault locations: This contains an additional 100 cases:

A. IBR as GFL with PV+battery, average model, PQ-dispatch outer control, $P_{\text{ref}} = 0.25\ \text{p.u.}$, $Q_{\text{ref}} = 0.0\ \text{p.u.}$, dq-based and sequence-based current controller with q-priority saturation limiter:

i. F3, type = AG, R_{f} = 1 Ω, 5 Ω, and 10 Ω, with TF2 as DYg (Yg facing IBR):

a. m = 10%, 20% and 50%.
b. With and without IBR.

ii. F3, type = ABC, R_f = 0.01 Ω with TF2 as DYg (Yg facing IBR)
iii. F1, type = BC, R_f = 0.01 Ω with TF2 as DYg (Yg facing IBR):

    a. With hydro online and with hydro offline.

B. IBR as GFM with PV+battery, average model, droop-based outer control, $P_{ref} = 0.25$ p.u., $Q_{ref} = 0.0$ p.u., dq-based and sequence-based current controller with q-priority saturation limiter:

iv. F3, type = AG, R_f = 1 Ω, 5 Ω, and 10 Ω, with TF2 as DYg (Yg facing IBR):

    a. m = 10%, 20% and 50%.

v. F3, type = ABC, R_f = 0.01 Ω with TF2 as DYg (Yg facing IBR)
vi. F1, type = BC, R_f = 0.01 Ω with TF2 as DYg (Yg facing IBR):

    a. With hydro online and with hydro offline.

5 IBR Characterization Evaluation Results and Analysis

This section evaluates the fault response of IBRs and how their modeling aspects can affect the protection element decisions. To characterize the IBR fault response and evaluate the protection elements response, the PSCAD simulation described in Section 4.2 stores the instantaneous voltage and current signals in two COMTRADE files with sampling rates of 480 Hz and 10 kHz. The 480-Hz file is used to evaluate the phasor-based protection elements, and the 10-kHz file is used to evaluate the time-domain protection elements. Figure 44 presents a schematic diagram to evaluate the protection function response according to the scenarios described in Section 4.3.

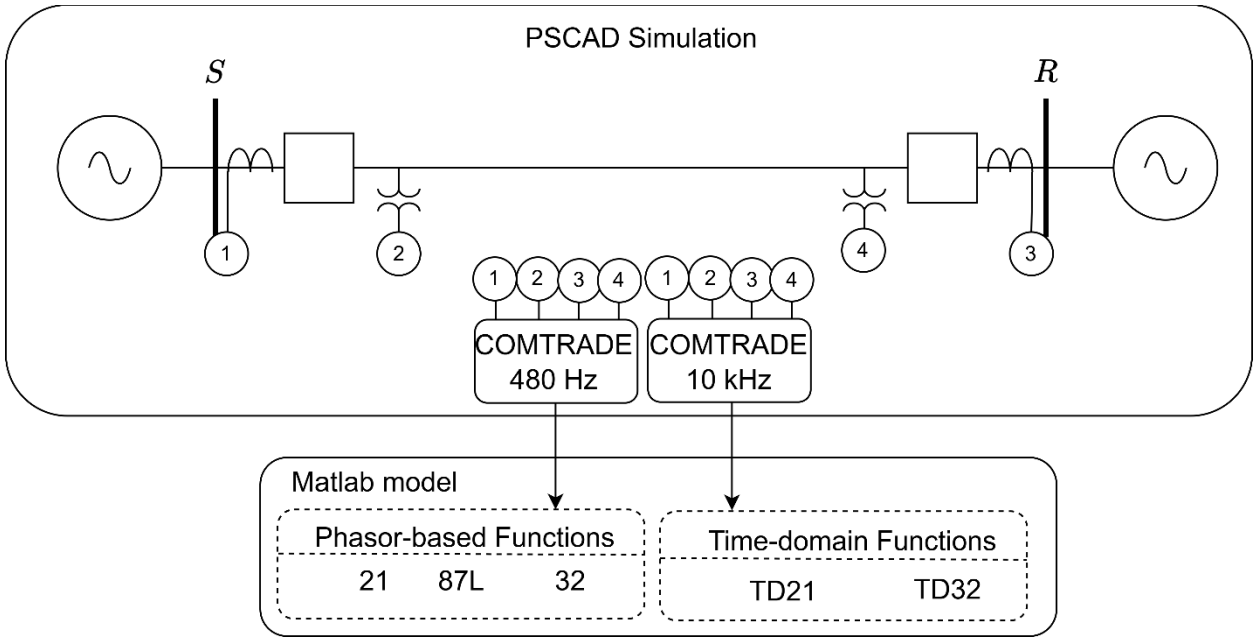

Figure 44. Schematic for testing the IBR protection functions

Figure 45 presents the layer diagram for the EMT simulation creation designed for evaluating the protective relay response against various configurations for IBR controllers (outer loop, inner loop, current limiters, etc.). First, the scenario is defined considering the system-level configurations, such as grid strength and power transformer connections. Then, the IBR model is defined according to its internal structure for controls and topology. Finally, the third layer covers fault parameters, such as fault type, resistance, and location.

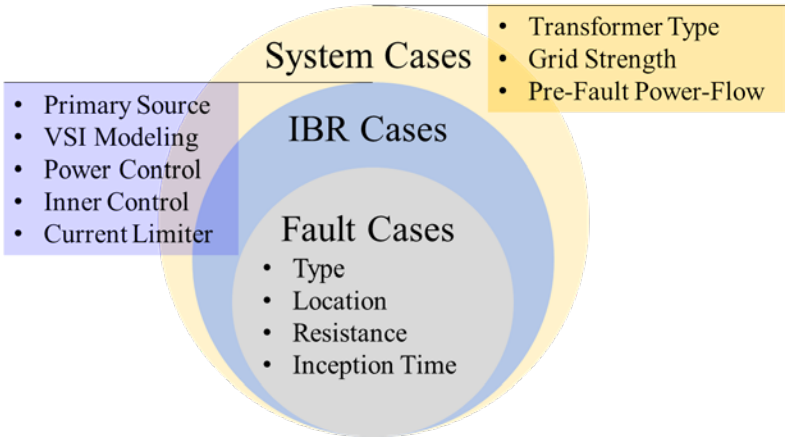

Figure 45. Process flow diagram for EMT studies

Figure 46 presents the framework used to characterize the relay response considering the various IBR modeling aspects. The initial step focuses on symmetrical components analysis by computing the magnitude and angle of sequence components quantities and comparing their behavior for different IBR modeling aspects, such as current limiters.

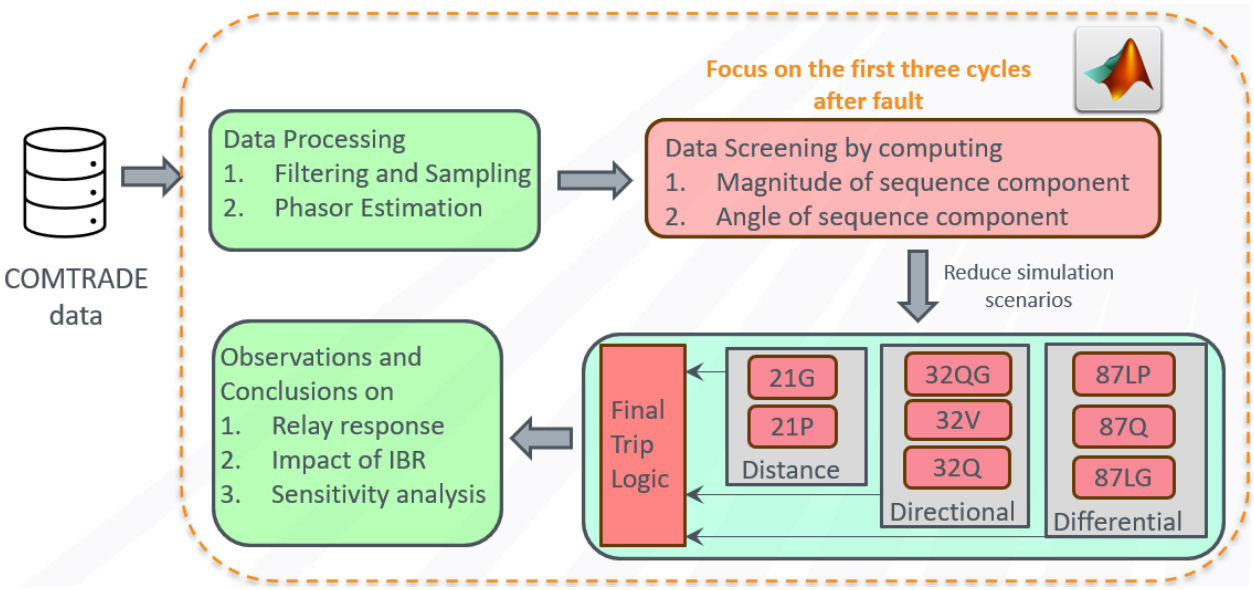

Figure 46. Analysis framework

This screening of sequence component quantities is used to evaluate which modeling aspects affect the protection relay response. Then, a reduced number of simulation scenarios, considering only those aspects affecting the relay response, are replayed in the relay model developed in MATLAB while considering the following phasor-based elements:

- Distance element 1: I0- and I2-polarized quadrilateral characteristics
- Distance element 2: V1-polarized mho element
- Directional elements: negative (32Q and 32QG) and zero (32V)-sequence voltage-polarized elements

- Line current differential: phase (87LP), negative (87LQ), and zero (87LG)-sequence elements
- Additional supervising functions: FID logic based on sequence currents.

The protection element response studies highlight which elements are affected by the IBR model aspects, therefore aiding in setting up conventional phasor-based elements to remain reliable when interfacing with inverters. Section 5.1 presents the results for the communication-based protection scheme using the 87L function. Section 5.2 presents the results for the stand-alone elements, which do not rely on a communication channel presence, in two parts: Section 5.2.1 presents the aspects that do not compromise the protection scheme behavior, and Section 5.2.2 presents the aspects that affect the protection response.

5.1 Communication-Based Protection Scheme

The line current differential protection is in the group of communication-based protection schemes because it transfers information from both ends of a transmission line between substations. Section 3.2.4 presents the operating principle for the line current differential protection, 87L. This function uses current phasor measurements from the local and the remote end of the line to distinguish between in-zone and out-of-zone faults. This function is influenced by the source types that are connected at both ends of the line, whether these sources are inverter-based generation or conventional synchronous machines.

For the KIUC case study, the local end is fed by an inverter-based generation, and the remote end is fed by a conventional synchronous machine; therefore, the 87L element response is dominated by the remote source feeding the fault. This is valid for the phase, zero, and negative-sequence elements (i.e., 87LP, 87LG and 87LQ, respectively). For the KIUC test system, the different IBR modeling aspects studied in this report did not impact the 87L function response. Figure 47 presents the 87L element response for the various fault cases. As shown, the complex gamma variables that are outside of the gray area indicate a fault condition and the relay trips. Cases where the gamma variables are plotted inside the gray area indicate a restraining condition and the relay does not operate. The restraining conditions were primarily due to a very high fault resistance, where there was insufficient fault current to trip the element. The IBR does not play a significant role in these cases, and the relay would fail to detect the fault even if a conventional generator of the same MVA rating replaced the IBR.

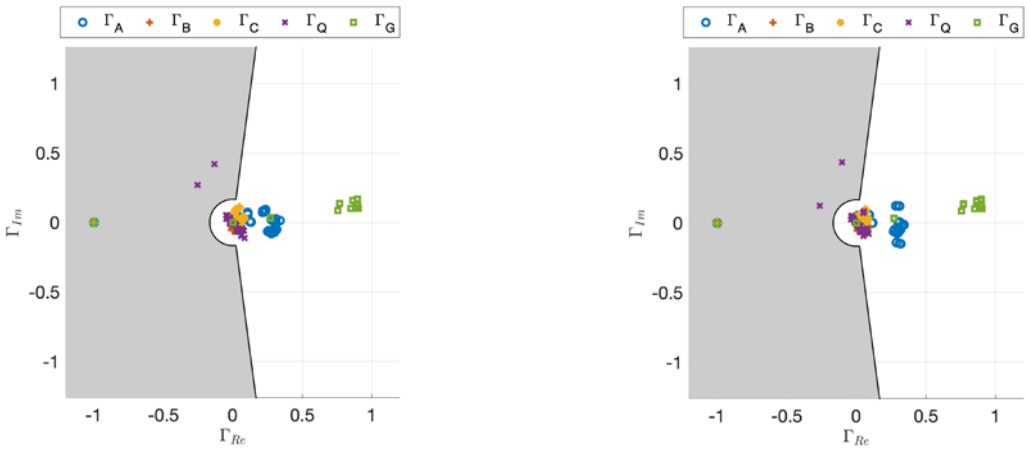

(a) GFL (b) GFM

Figure 47. 87L elements using the alpha plane—all fault cases

5.2 Results for Distance Elements

This section describes the results for the distance elements, their supervising functions (i.e., directional supervision), and the FID logic. These functions rely on local measurements to detect faults; therefore, their operation is influenced by the inverter-based generation differently than what occurs with the 87L elements. Section 5.2.1 describes the IBR aspects that do not affect the relay response, and Section 5.2.2 describes the aspects that influence the protection decisions. Section 5.2.3 presents additional analysis for different power system conditions and their influence on protection decisions. All results are obtained from the relay R2 which is close to the IBR side.

5.2.1 IBR Aspects Not Affecting Relay Response

The analysis is centered on analyzing three responses: (1) effective impedance estimated by the distance elements, (2) directional element decision, and (3) proper fault identified by the FID logic. The aspects that did not influence the relay decisions are the (1) inverter model (i.e., switching model or average model), (2) DC primary source type, and (3) outer-loop controllers for GFL and GFM operating modes.

5.2.1.1 Inverter Model (Switching Model or Average Model)

The analysis of the impact of the inverter model type considers the parameters shown in Table 15 as fixed. In this case, the fault type (i.e., AG fault and BC fault) and the type of inverter model vary.

Table 15. Fixed Parameters to Evaluate the Impact of Inverter Model on Protection Decisions

Fixed Parameter	Description
Transformer TF1 connection	ΔYg – Δ connection facing the power system
Transformer TF2 connection	YgΔ for ground faults and ΔYg for phase faults
DC source	Combination of PV+BESS
Power control	PQ dispatch
Current control	Phase currents in dq synchronous reference frame
Current-limiting logic	Saturation on q-axis
Fault location	5% referred to as the IBR end

5.2.1.1.1 Phase-A-to-Ground Fault Case

Figure 48 presents the voltage and current signals for the AG fault case at 5% of the line referred to as the IBR end. One observation that applies is that despite the fault type (AG), all the phase currents showed an increase in magnitude. In addition, they are in phase during the fault. This is a characteristic of a fault response dominated by a zero-sequence current. Because the IBR control limits the phase currents to 1.2 p.u., and the transformer TF2 has a Y grounded connection facing the power system, the incoming zero-sequence current from the other side of the line (conventional grid) dominates the fault response.

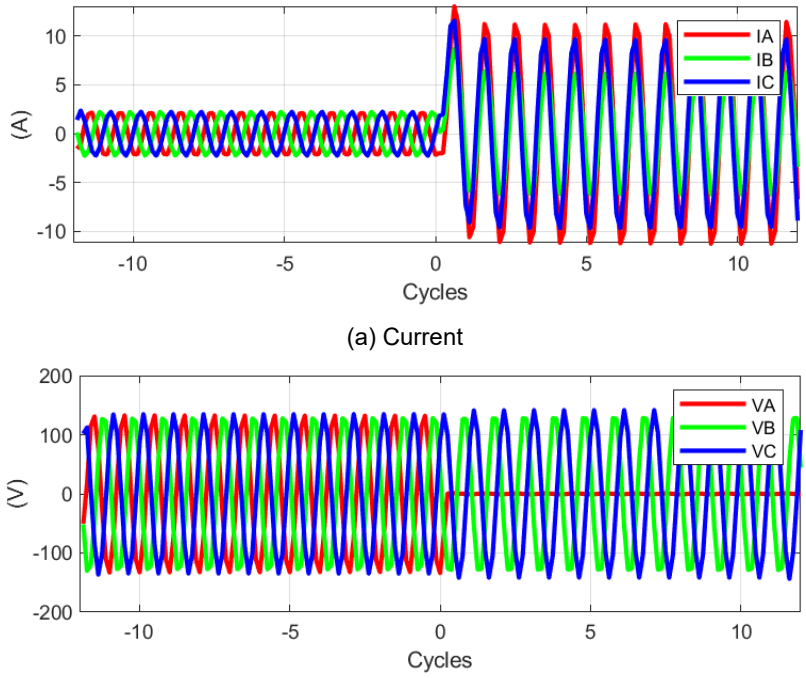

(a) Current

(b) Voltage

Figure 48. Voltage and current signals for the AG fault case

Figure 49 presents the sequence current magnitudes measured by the relay located at the end fed by an IBR. Figure 50 presents the sequence current angles. These plots compare the calculated

sequence currents by changing the IBR model between switching (detailed) and average models. The goal is to evaluate possible changes in the calculated sequence currents (I_0, I_1, and I_2). The term Avg refers to the average model, and Sw refers to the switching model. A comparison of the curves shows that they are identical; therefore, the inverter model did not influence the fault response for ground faults.

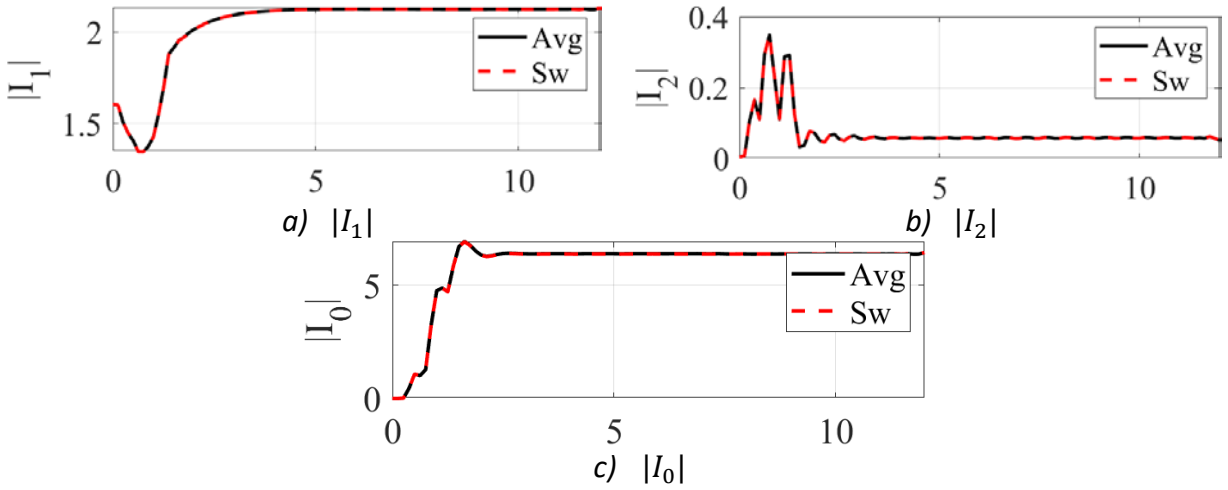

Figure 49. Sequence current magnitudes

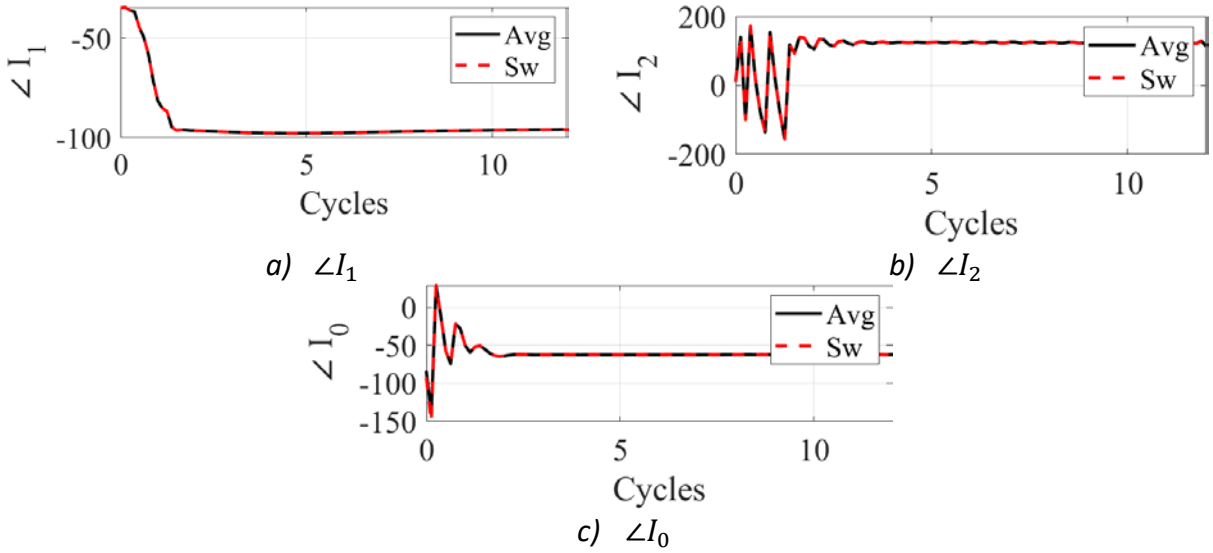

Figure 50. Sequence current angles

5.2.1.1.2 BC Fault Case

Figure 51 presents the current and voltage signals for the IBR end. An interesting behavior occurs in the phase currents controlled by the inverter, where the inverter injects balanced phase currents, even during a BC fault.

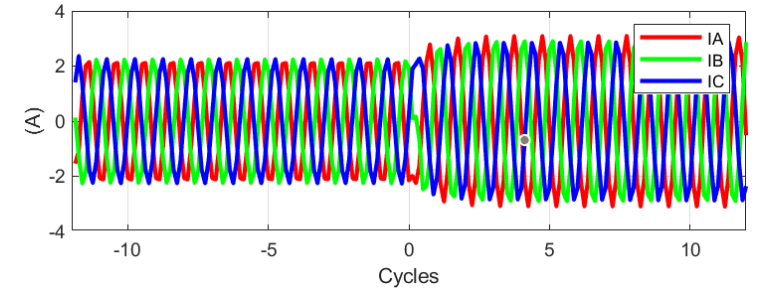

(a) Current

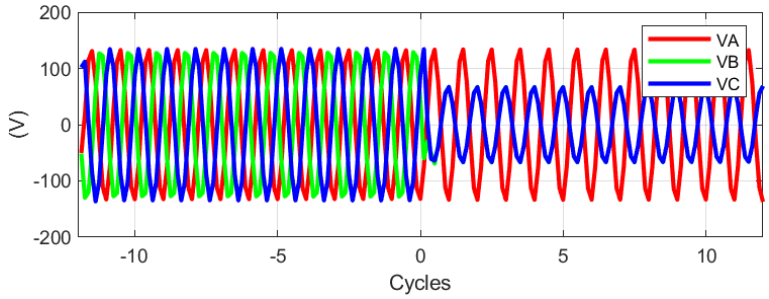

(b) Voltage

Figure 51. Voltage and current signals for the BC fault

Figure 52 shows the sequence currents magnitudes, while Figure 53 presents the sequence current angles to compare the effects of changing the inverter models in the fault current response. Similar to the AG fault case, the inverter models did not impact the fault response for phase faults. The zero-sequence current is not shown because BC faults do not involve the ground; thus, no zero-sequence current is present.

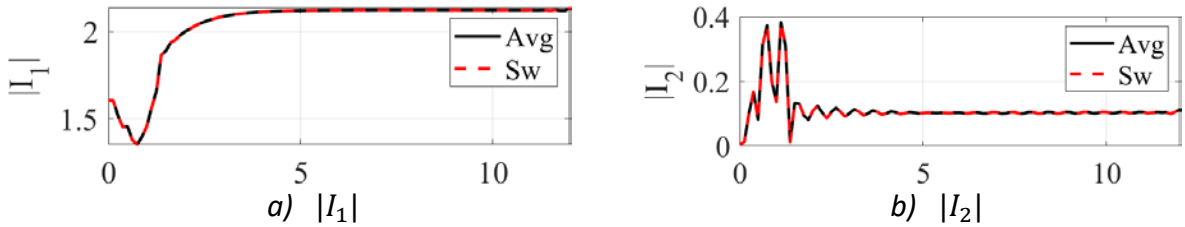

a) $|I_1|$ *b)* $|I_2|$

Figure 52. Sequence current magnitudes

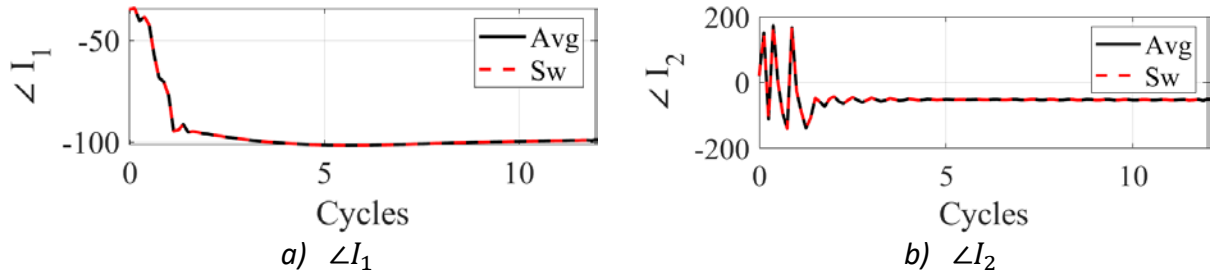

a) $\angle I_1$ *b)* $\angle I_2$

Figure 53. Sequence current angles

The results in this section support the conclusion that the chosen inverter model (Avg or Sw) does not play a significant role in the fault current response from the IBR, nor the sequence

current estimated by the relay; however, using an inverter average model aids in reducing the computational burden for EMT simulations.

5.2.1.2 DC Primary Source

The analysis for the effects of DC primary sources considers the same fixed parameters shown in Table 15. The comparison is made for three combinations of DC source types: (1) PV array, (2) battery energy storage system (BESS), and (3) PV+BESS.

5.2.1.2.1 Phase-A-to-Ground Fault Case

The voltage and current signals are equal to those shown in Figure 48. Figure 54 presents the sequence current magnitudes during the fault for the three different DC primary sources from the inverter. Figure 55 presents the sequence current angles for the AG fault case. Similar to the inverter model, the DC primary source did not affect the inverter fault response.

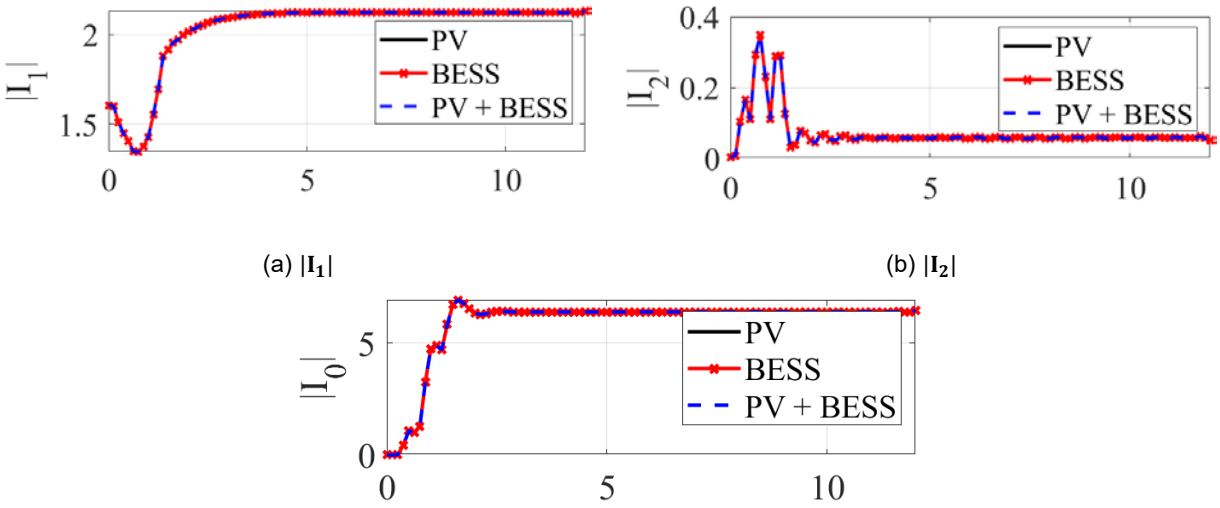

(a) $|\mathbf{I_1}|$ (b) $|\mathbf{I_2}|$

(c)$|\mathbf{I_0}|$

Figure 54. Sequence current magnitudes

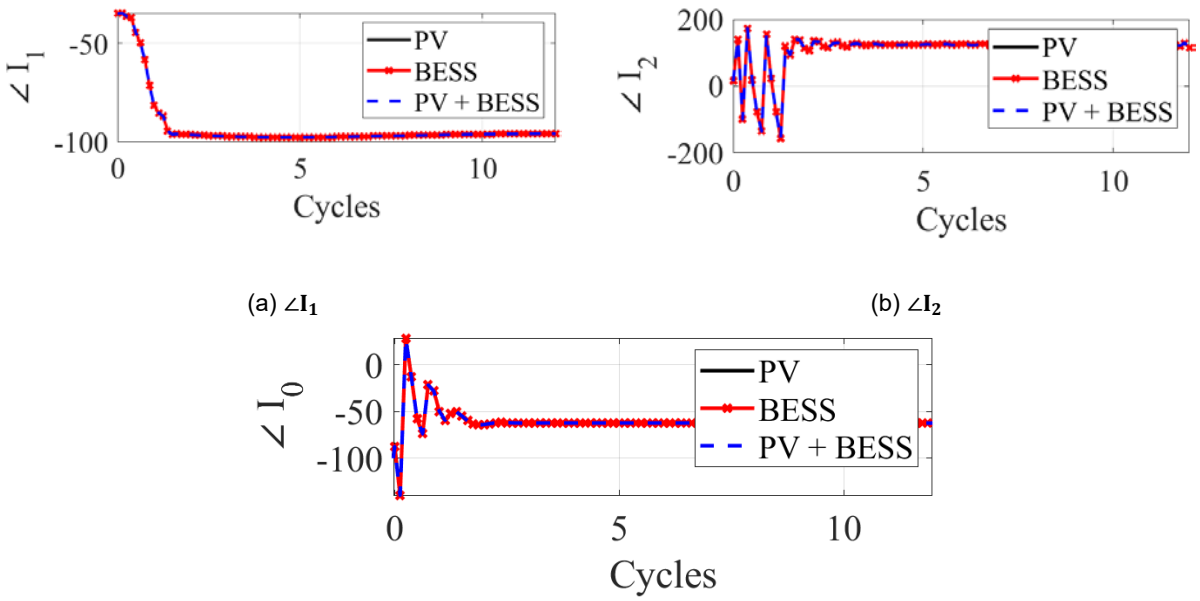

(a) $\angle\mathbf{I_1}$ (b) $\angle\mathbf{I_2}$

(c)$\angle\mathbf{I_0}$

Figure 55. Sequence current angles

5.2.1.2.2 BC Fault Case

For the BC fault case, the voltage and current signals are shown in Figure 51. Figure 56 presents the sequence current magnitudes, and Figure 57 presents the sequence current angles for the BC fault case. Like the previous case (ground fault), the DC primary sources did not change the inverter response for the phase faults.

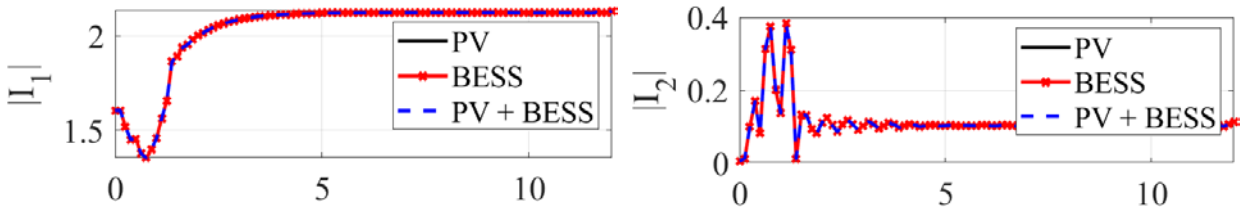

(a) $|\mathbf{I_1}|$ (b) $|\mathbf{I_2}|$

Figure 56. Sequence currents magnitudes

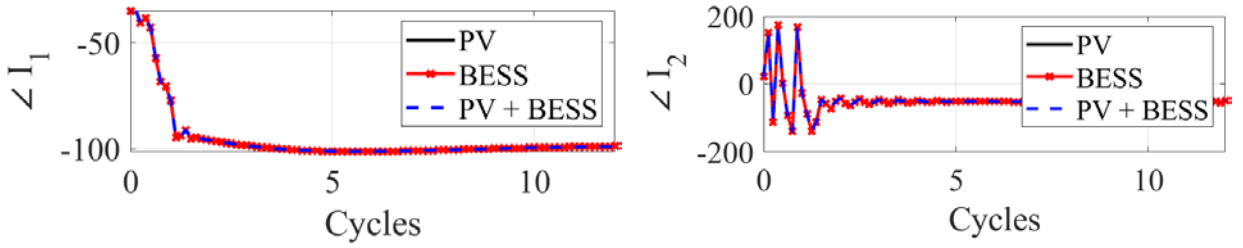

(a) $\angle \boldsymbol{I_1}$ (b) $\angle \boldsymbol{I_2}$

Figure 57. Sequence currents angles

5.2.1.3 Outer-Loop Controllers—GFL Inverters

This section provides an analysis of the impact of different outer-loop controllers on the IBRs during GFL operating mode. The options are: (1) PQ-dispatch and (2) DC-voltage/AC-voltage control. Table 16 presents the fixed settings used in the simulation to analyze the impacts of different outer-control loops on the inverter fault response.

Table 16. Fixed Parameters to Analyze the Impact of Different Outer-Control Loops

Fixed Parameter	Description
IBR model	Average
Transformer TF1 connection	ΔYg – Δ connection facing the power system
Transformer TF2 connection	YgΔ for ground faults and ΔYg for phase faults
DC source	Combination of PV+BESS
Current control	Phase currents in dq synchronous reference frame
Current-limiting logic	Saturation on q-axis
Fault location	5% referred to as the IBR end

5.2.1.3.1 Phase-A-to-Ground Fault

Figure 58 presents the sequence current magnitudes, and Figure 59 presents the sequence current angles for the ground fault case. The inverter fault response was not affected by the outer-loop controllers during the ground fault because the curves are identical.

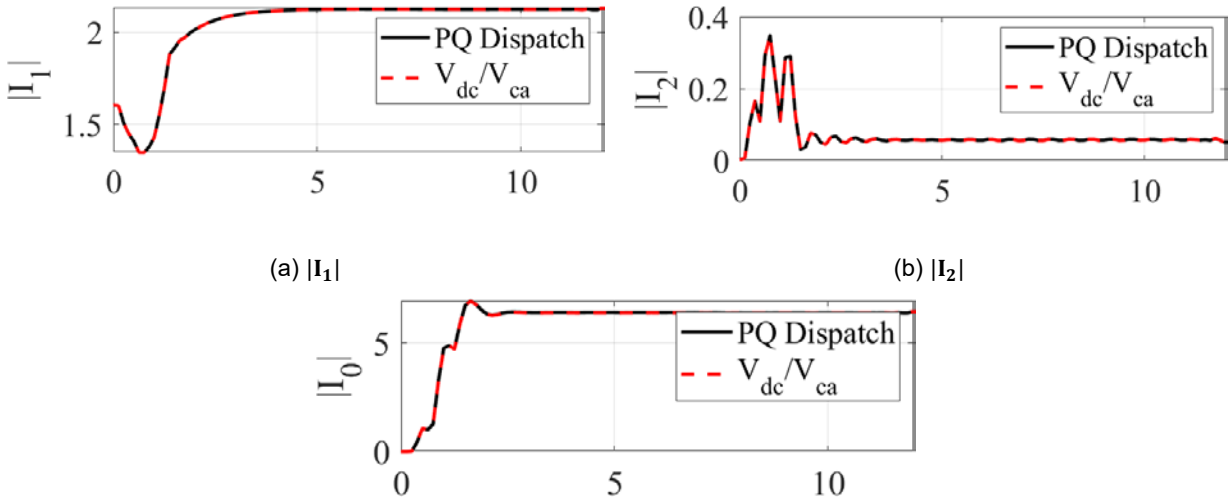

(a) $|\mathbf{I_1}|$ (b) $|\mathbf{I_2}|$

(c) $|\mathbf{I_0}|$

Figure 58. Sequence current magnitudes

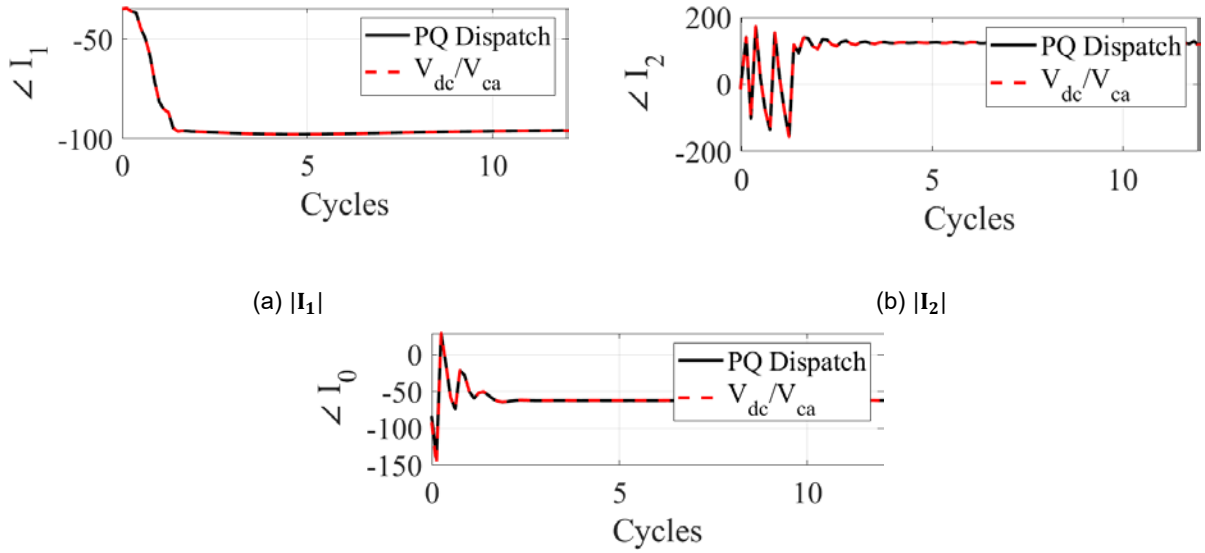

(a) $|\mathbf{I_1}|$ (b) $|\mathbf{I_2}|$

(c) $|\mathbf{I_0}|$

Figure 59. Sequence current angles

5.2.1.3.2 BC Fault

For the phase fault, Figure 60 presents the sequence current magnitudes, and Figure 61 presents the sequence current angles. A comparison of the closeness of the curves shows that the GFL outer-loop controllers did not impact the inverter fault response.

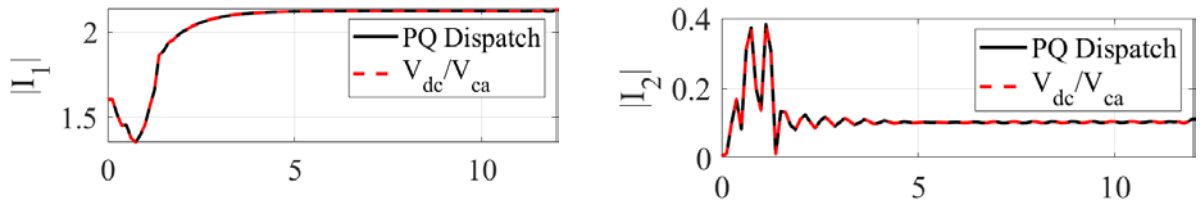

(a) $|\mathbf{I_1}|$ (b) $|\mathbf{I_2}|$

Figure 60. Sequence current magnitudes

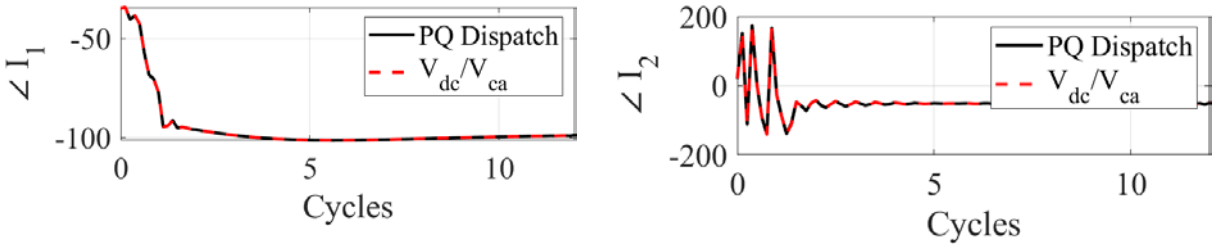

(a) $\angle \boldsymbol{I_1}$ (b) $\angle \boldsymbol{I_2}$

Figure 61. Sequence current angles

Neither the ground nor phase faults were impacted by the GFL outer-loop controllers.

5.2.1.4 Outer-Loop Controllers—GFM Inverters

The evaluation of the effects of the outer-loop controllers of GFM inverters on the protection relay response considers the following options: (1) droop and (2) VSM. Table 17 presents the fixed setting parameters considered in the simulation. Only the outer-loop controllers vary in this analysis.

Table 17. Fixed Parameters for the GFM Cases

Fixed Parameter	Description
IBR model	Average
Transformer TF1 connection	ΔYg – Δ connection facing the power system
Transformer TF2 connection	YgΔ for ground faults and ΔYg for phase faults
DC source	Combination of PV+BESS
Voltage control	Phase voltages in dq synchronous reference frame
Current control	Phase currents in dq synchronous reference frame
Current-limiting logic	Saturation on q-axis
Fault location	5% referred to as the IBR end

5.2.1.4.1 Phase-A-to-Ground Fault

Figure 62 presents the sequence current magnitudes, and Figure 63 presents the sequence current angles. The GFM outer-loop controllers (i.e., droop or VSM) did not impact the inverter fault response for ground faults.

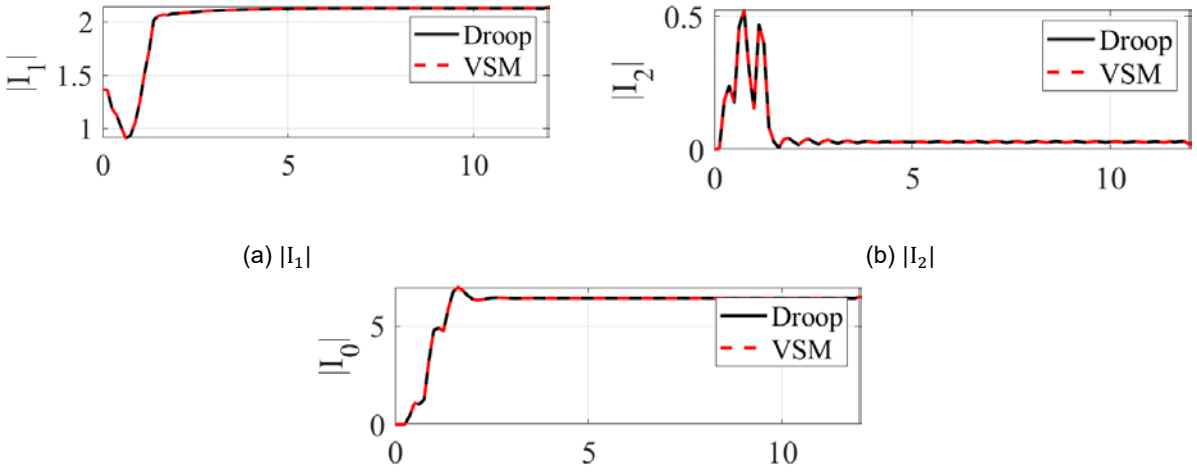

(a) $|I_1|$ (b) $|I_2|$

(c) $|I_0|$

Figure 62. Sequence current magnitudes

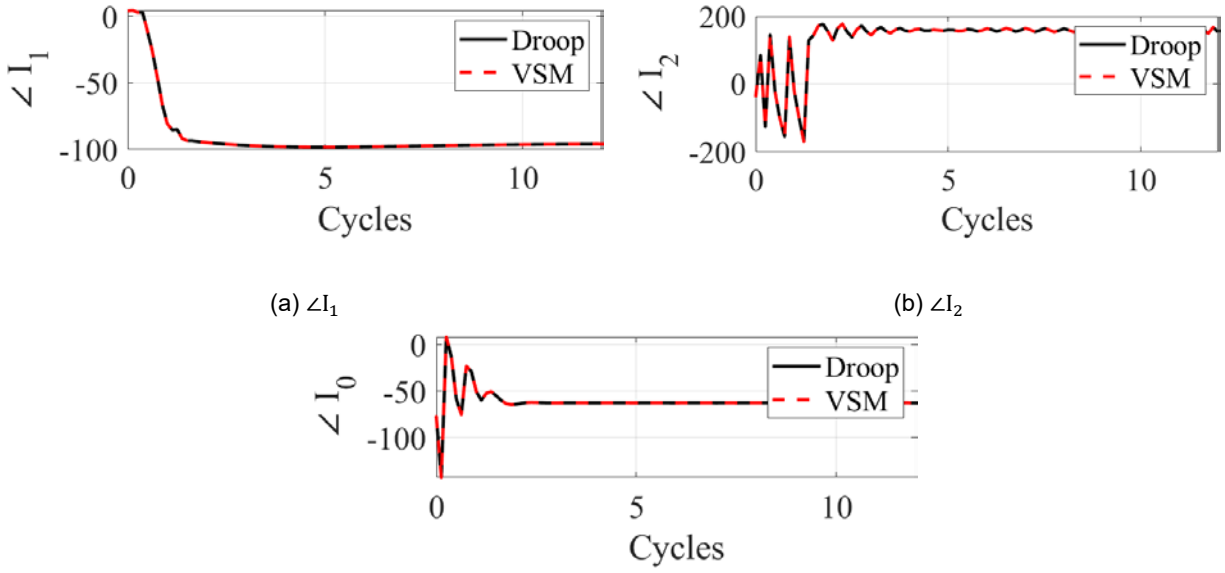

(a) $\angle I_1$ (b) $\angle I_2$

(c) $\angle I_0$

Figure 63. Sequence current angles

5.2.1.4.2 BC Fault

For the phase fault, Figure 64 presents the sequence current magnitudes, and Figure 65 presents the sequence current angles. Similar to what was observed in ground faults, the outer-loop controllers in GFM mode did not impact the inverter fault response.

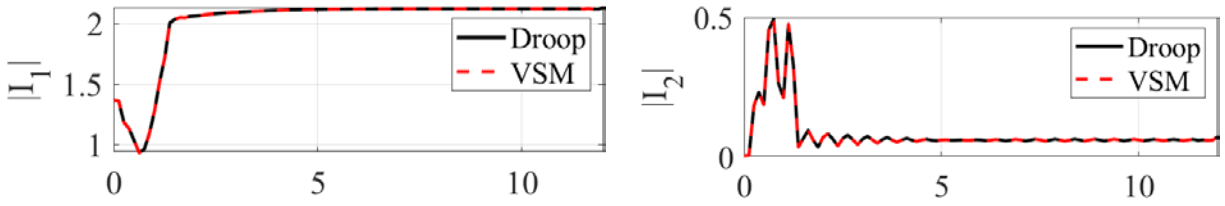

(a) $|\mathbf{I_1}|$ (b) $|\mathbf{I_2}|$

Figure 64. Sequence current magnitudes

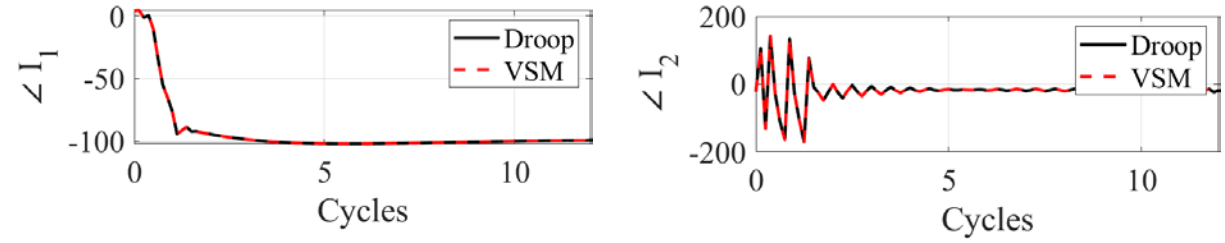

(a) $\angle\mathbf{I_1}$ (b) $\angle\mathbf{I_2}$

Figure 65. Sequence current angles

5.2.2 IBR Aspects Affecting Relay Response

This section presents the IBR modeling aspects that affect the protection element response. The main items include the (1) inner-current control loops, (2) current-limiting logic schemes, (3) current-blocking schemes (or momentary cessation), and (4) time constant of the IBR controllers. There are some elements where the response does not depend on the inverter control options, and others that are dependent. The following sections present that comparison, and Table 18 describes the case study settings.

Table 18. Case Study Settings to Evaluate IBR Aspects That Affect Relay Response

Fixed Parameter	Description
Transformer TF1 connection	ΔYg connection
Transformer TF2 connection	1. YgΔ connection for ground faults 2. ΔYg connection for phase faults
IBR model	Average
DC source	PV+BESS
Power control	1. PQ dispatch for GFL 2. Droop for GFM
Current control	1. Phase currents—dq domain 2. Phase currents—αβ domain 3. Sequence currents—dq domain
Current limiter	1. Saturation q/d-axis 2. Latching q/d-axis 3. Saturation/latching αβ
Fault location	5% of the line (referred to the IBR bus)
Fault type	1. AG 2. BC

5.2.2.1 Effect of Inner-Current Control Loops

The current controllers impact the protection elements that depend on current signals either to polarize the distance elements or to estimate the equivalent impedance to determine the fault direction. We present these issues in detail for each protection element affected.

5.2.2.1.1 Distance Elements

The distance element affected by the inner-current controllers is the quadrilateral element polarized by the negative-sequence current. This element is used to detect ground and unbalanced phase faults. Figure 66 presents the comparison of the quadrilateral element response for the current controllers during an AG fault. Figure 67 presents the same comparison but for a BC fault. By analyzing the plots in the R-X plan, when the inverter is controlling the phase currents in either the dq or αβ domain, the effective impedance computed by the relay is oscillatory, and it is not reliable for protection decisions. This is because in this case the relay is using negative-sequence current polarization, and for phase currents control in either dq or alpha beta domain, there is no control over the negative sequence current, which means its angle might not have a consistent behavior. A more stable behavior is observed when the inverter regulates the sequence currents, therefore injecting a controlled negative-sequence current, in compliance with IEEE Std 2800-2022 [63].

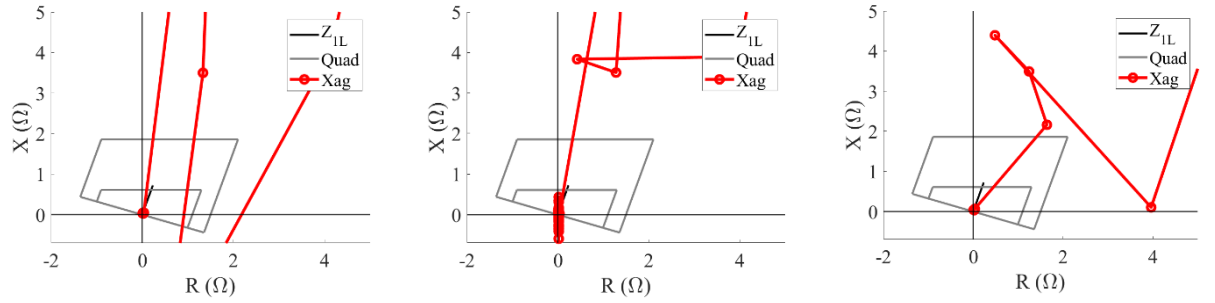

(a) Phase currents—dq domain (b) Phase currents—αβ domain (c) Sequence currents—dq domain

Figure 66. Effect of different current controllers in the quadrilateral characteristic polarized by the I2 – AG fault case

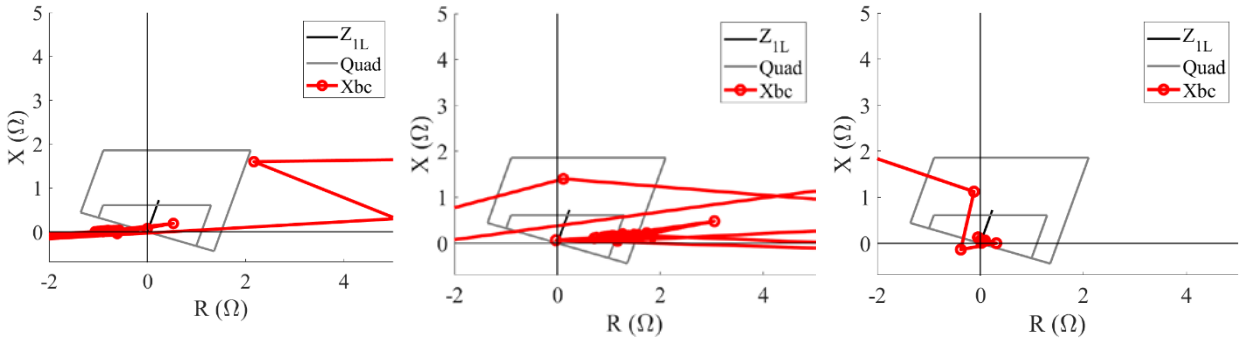

(a) Phase currents—dq domain (b) Phase currents—αβ domain (c) Sequence currents—dq domain

Figure 67. Effect of different current controllers in the quadrilateral characteristic polarized by the I2 – BC fault case

The case shown in Figure 66 and Figure 67 is polarized by the negative-sequence current; however, it is possible to polarize using the zero-sequence current for ground faults. For this condition, the element presents a reliable behavior, similar to what is observed in terminations fed by a conventional source, as shown in Figure 68. Note that the main requirement to use zero-sequence current polarization is the presence of a ground path behind the relay. Commonly, substations interconnecting IBRs to the power grid have power transformers to step up the voltage to the transmission level with a Y grounded connection facing the system.

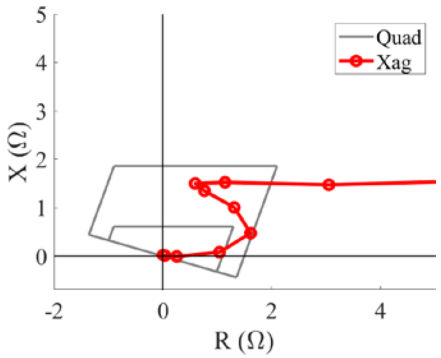

Figure 68. Quadrilateral characteristic behavior when using zero-sequence current polarization

The other distance element that presented reliable behavior in the evaluated cases is the memory-polarized mho element for ground faults. Figure 69 presents the element response comparing the three current controllers available in the IBR model. Figure 70 presents the zoomed in mho element for easy the visualization of zone 1 and zone 2 reach, set as Z1 = 0.61 Ω and Z2 = 1.10 Ω, respectively. Since the IBRs behave as weak sources, the memory polarized element has a greater expansion towards the third quadrant in the R-X plan.

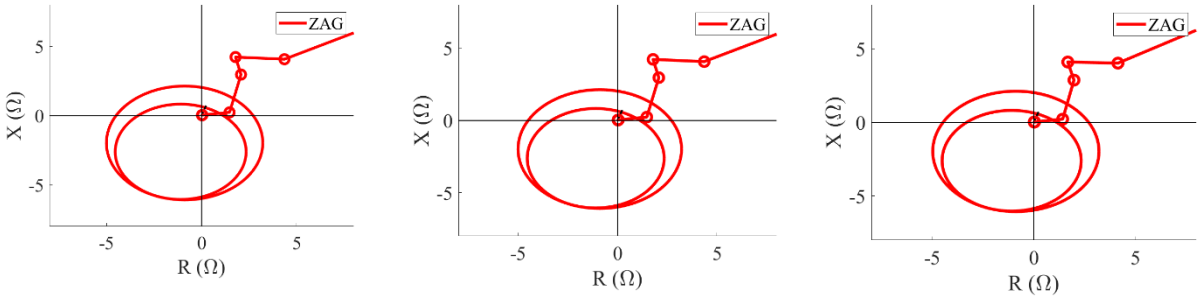

(a) Phase currents—dq domain (b) Phase currents—αβ domain (c) Sequence currents—dq domain

Figure 69. Mho element behavior during an AG fault for different inner-current controllers

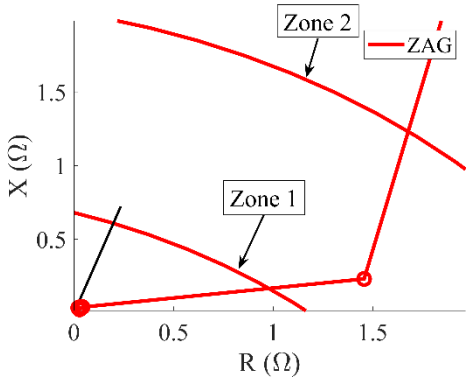

Figure 70 - Mho element behavior during AG fault (zoomed in).

The mho element for phase faults also presented stable behavior. Figure 70 presents the element response with a comparison between the current controllers. The response between the current controllers did not change. An important observation is that for phase faults, the mho circle has an abnormal expansion. This is caused by the current limiters in the inverter and is further explained in Section 5.2.2.2. Figure 71 compares the dynamic mho expansion for the relay connected to the grid at one end of the line with the other end connected to the IBR.

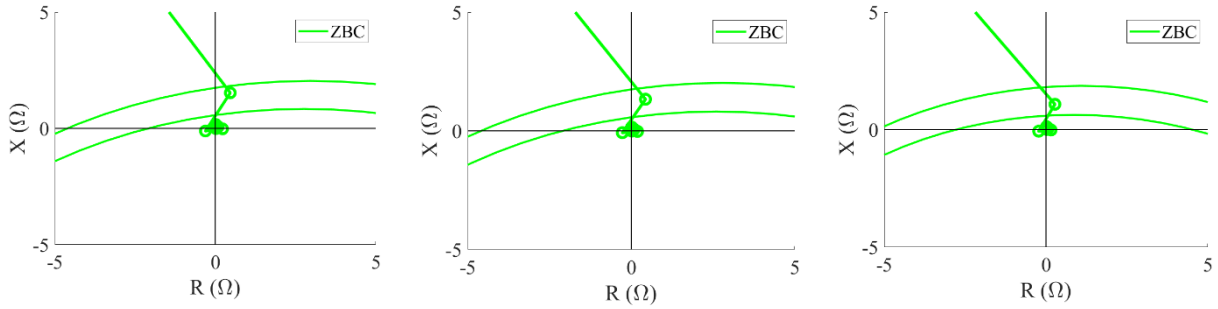

(a) Phase currents—dq domain (b) Phase currents—αβ domain (c) Sequence currents—dq domain

Figure 71. Mho element behavior for a BC fault comparing the inner-current controllers

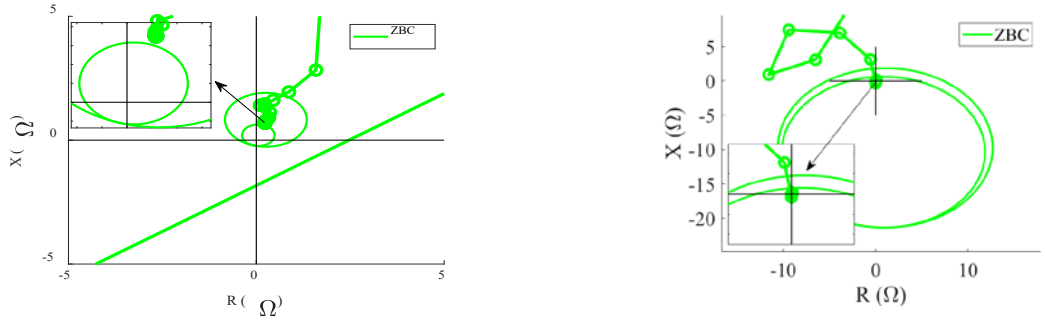

(a) Grid end (b) IBR end

Figure 72. Comparing the dynamic mho expansion between the IBR end and the grid end of the line

5.2.2.1.2 Directional Elements

The different current controllers also affect the response of the directional elements based on the negative-sequence impedance (i.e., 32QG and 32Q elements). Figure 72 presents the element response for each current controller during an AG fault. A forward fault is declared when z2A is more negative than Z2FTH. This response is achieved only when the inverter regulates the sequence currents in the dq domain (i.e., regulating I2 injection in compliance with IEEE Std 2800-2022); therefore, this IBR modeling parameter affects the relay decision.

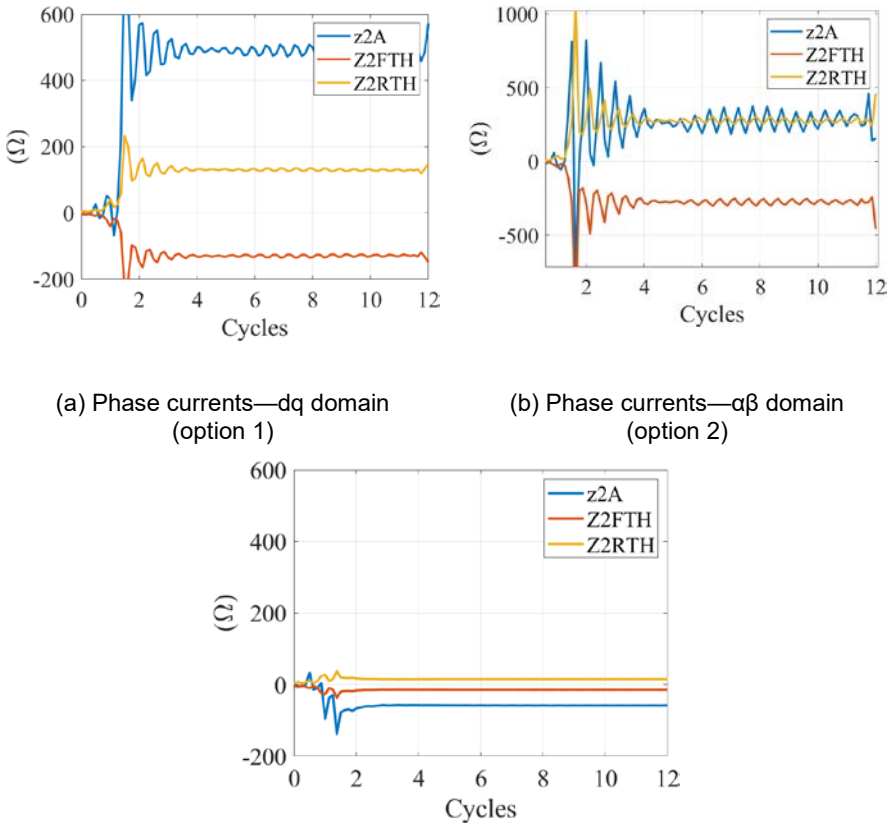

(a) Phase currents—dq domain (option 1)

(b) Phase currents—αβ domain (option 2)

(c) Sequence currents—dq domain

Figure 73. Negative-sequence directional element response comparing the three current controllers

For the negative-sequence directional elements 32QG and 32Q, the first supervises ground faults, and the second supervises phase faults. Their principle of operation is met when the inverter controls the injection of the negative-sequence current I2; however, the 32QG element has a current supervision, called zero-sequence restraining factor, which monitors the ratio |I2|/|I0| and checks if this ratio is greater than its threshold, k2, as expressed by the logic diagram in Figure 73. In this figure, the 32QGE is a digital variable responsible for enabling the 32QG element.

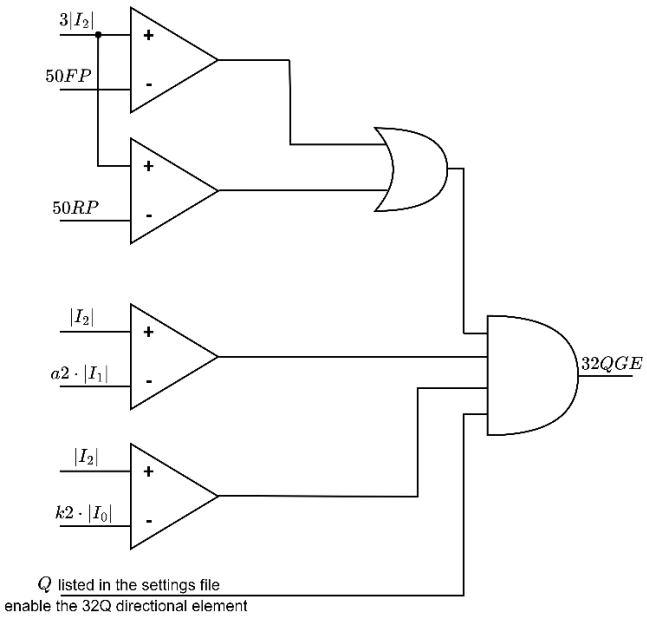

Figure 74. Overcurrent detectors that supervise the 32QG element

For the cases studied in this report, this ratio was always below its threshold; therefore, the 32QG element was never enabled to operate. Figure 74 presents an example of the zero-sequence restraining factor operation.

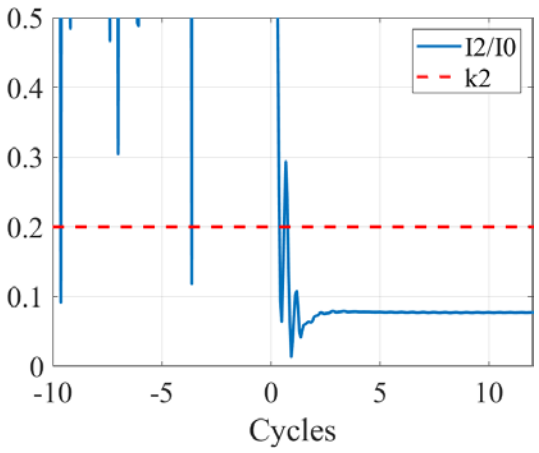

Figure 75. Zero-sequence restraining factor blocking the 32QG element

The zero-sequence direction element (32V) response depends on the transformer connection. The 32V can only operate when the transformer provides a zero-sequence path through an appropriate grounded connection. Figure 75 presents the response for the 32V element. The results show that the computed impedance z0A is smaller than the forward threshold Z0FTH, which indicates a forward fault.

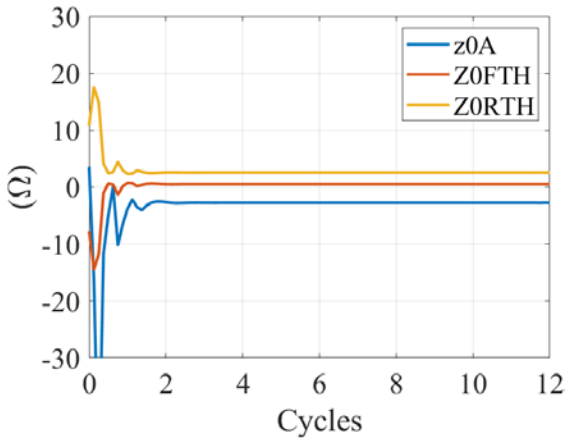

Figure 76. 32V element response

5.2.2.1.3 FID Logic

The sequence current-based FID logic has two main requirements: (1) A ground path behind the relay to allow the zero-sequence current to circulate must be present, and (2) the inverter current controller must regulate the I2 injection in compliance with IEEE Std 2800-2022. As presented in Section 3.2.6, for the relay to classify an AG fault, the angle difference between I0 and I2 needs to be within the region from -30° to 30°. Figure 76 presents the results for the FID logic for the different inner-current controllers considered for the IBR. The proper condition is met only with sequence current controllers in the dq domain.

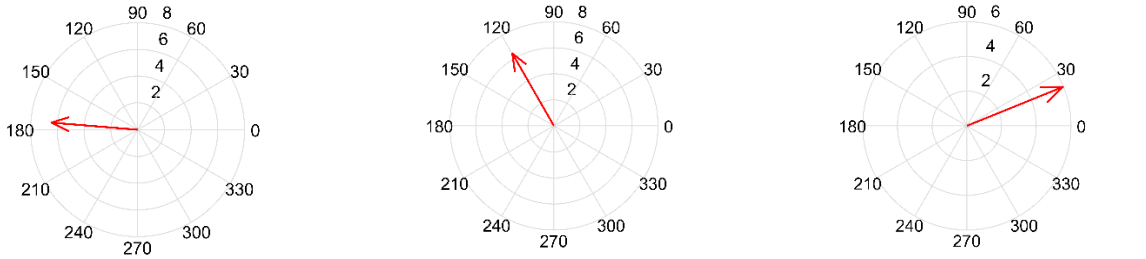

(a) Phase currents—dq domain (b) Phase currents—αβ domain (c) Sequence currents—dq domain

Figure 77. FID logic response for different current controllers

5.2.2.2 Impact of Current Limiter Logic on Protection Element Response

5.2.2.2.1 Effects of Current Limiter Logic Implementation Over Relay Response

This subsection analyzes the effects of the three different current limiter strategies shown in Figure 77 on the protective relay response. We contrast each strategy for different protection elements.

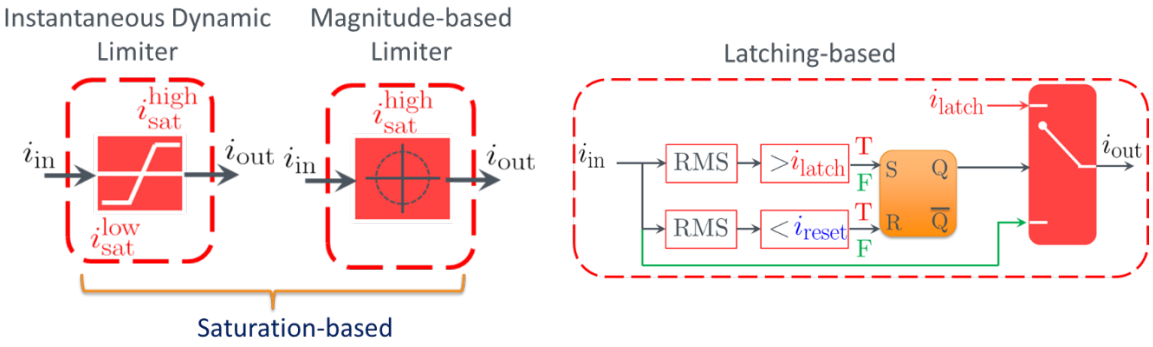

Figure 78. Three Current Limiter strategies for GFL IBRs

Because magnitude-based limiters and latching-based limiters are similar, this evaluation starts from these two current-limiter strategies to narrow the scope. Both current limiters are configured for d/q priority. The GFL IBR has a controlled negative-sequence current, and both the AG and BC faults are applied to evaluate the different protection relay element response times. The following protection functions are chosen according to the fault:

1. Ground faults:
    A. Memory-polarized mho element
    B. I_0-polarized quadrilateral element
    C. I_2-polarized quadrilateral element
    D. Zero-sequence voltage-polarized directional element (32V)
    E. Negative-sequence voltage-polarized directional element (32QG)
    F. Sequence current-based FID logic.
2. Phase faults:
    A. Memory-polarized mho element
    B. I_2-polarized quadrilateral element
    C. Negative-sequence voltage-polarized directional element (32Q).

One concern regarding the different current limiters existing in inverters is whether they impact the time for trip decisions. Figure 78 presents the overall results comparing the magnitude-based versus latching-based limiting, with both using q-axis or d-axis priority. The results prove that current limiters have little impact on the time for the relay response.

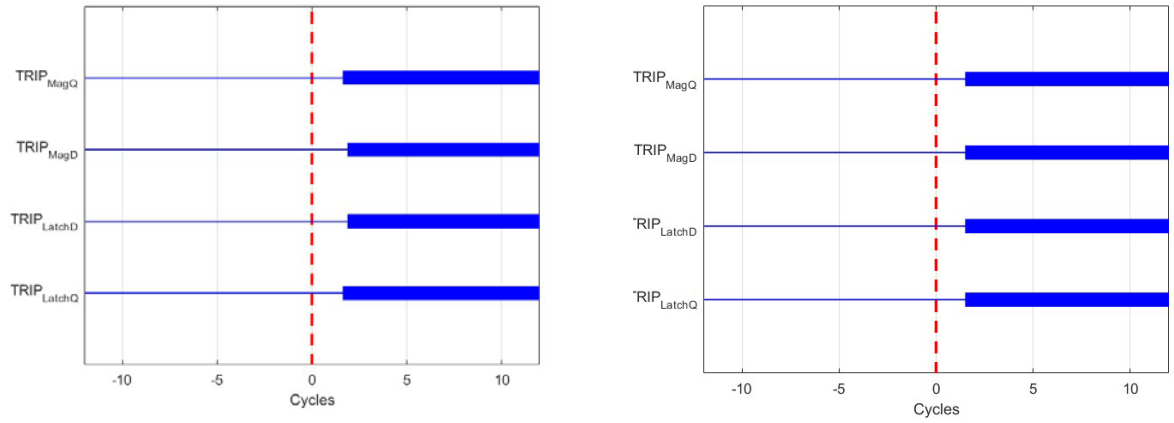

(a) AG fault

(b) BC fault

Figure 79. Example showing relay responses of the magnitude-based and latching-based current-limiting schemes under an (a) AG fault and a (b) BC fault

More tests are carried out to compare the instantaneous dynamic limiter and magnitude-based limiter. Table 19 presents the fixed parameters set in the study case. The only variable parameter is the structure of the current limiter, hereafter referred to as the instantaneous dynamic and magnitude-based current-limiter logic.

Table 19. Fixed Parameters in the Case Study

Fixed Parameter	Description
Transformer TF1 connection	ΔYg connection
Transformer TF2 connection	1. YgΔ connection for ground faults 2. ΔYg connection for phase faults
IBR model	Average
DC source	PV+BESS
Power control	1. PQ dispatch for GFL 2. Droop for GFM
Current control	Sequence currents—dq domain
Current limiter	Instantaneous dynamic and magnitude-based q/d-axis
Fault location	5% of the line (referred to as the IBR bus)
Fault type	1. AG 2. BC

The analysis is performed through simulating ground (AG) and phase (BC) bolted faults at 5% of the line measured from the IBR terminal. The comparison evaluates the instantaneous voltage and current signals, and the protection relay elements for each fault are summarized in the next few pages.

Each current-limiter logic can have its priority set to either the d-axis or the q-axis. Each choice is studied separately to determine their effects on the protection response.

5.2.2.2.2 Phase A-to-Ground Fault—Current Limiter in Q-Axis Priority

Figure 79 presents the instantaneous current signals for the (a) magnitude-based and (b) instantaneous dynamic current-limiter logic. The curves from the top and bottom plots are close

to each other. An important supporting point here is that short circuits fed by IBRs are usually limited to 1.2 p.u. of the inverter's rated current; however, the waveforms for the AG fault show that the faulted current exceeds the 1.2 limit. This is because the power transformer behind the relay in this case had a *Y* grounded connection, allowing the incoming zero-sequence current from the grid to circulate. This current is not controlled by the inverter, so because I0 >> I1 and I0 >> I2, it dominates the fault response.

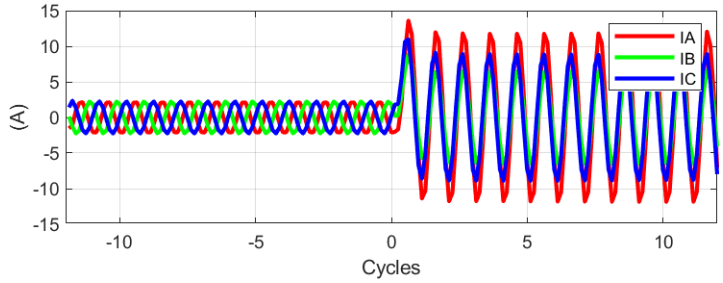

(a) Magnitude-based limiter

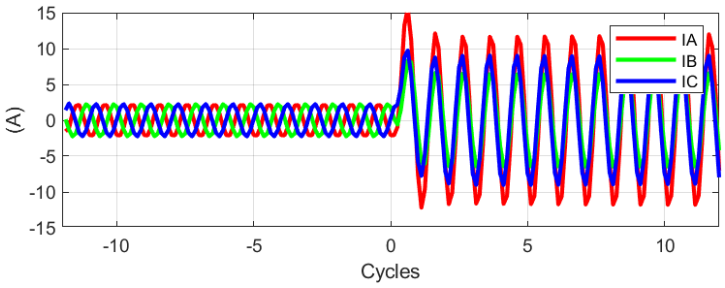

(b) Instantaneous dynamic limiter

Figure 80. Current signals of two commonly used current limiters

Figure 80 presents the response for the mho element using the AG fault loop. It compares the mho response by plotting the estimated impedance for the magnitude-based and instantaneous dynamic limiter logics. There is a slight difference in the apparent impedance computation (Z_{AG}, red line with circles) in regard to its path before reaching the boundary for Z1; however, this difference is not significant enough to affect the relay's final decision. For both current limiters, the mho element properly detects the fault.

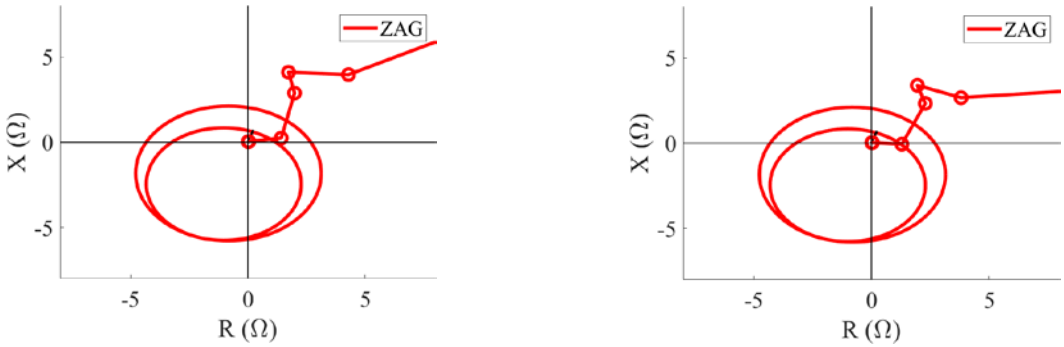

(a) Magnitude-based current limiter

(b) Instantaneous dynamic current limiter

Figure 81. Mho element for ground faults

Figure 81 and Figure 82 present the response for the distance protection using the quadrilateral element polarized by the zero-sequence and the negative-sequence current, respectively. The first polarizing option uses the zero-sequence current; therefore, less effect from the inverter controllers is expected. But there is still a slight difference on the effective impedance computed by the element. For both current-limiting logics, the quadrilateral element detected the fault. In the second case, using the negative-sequence current polarization, the effective impedance computation shows a significant difference between the current-limiter logics, but the final decision was the same, and the relay successfully detected the fault.

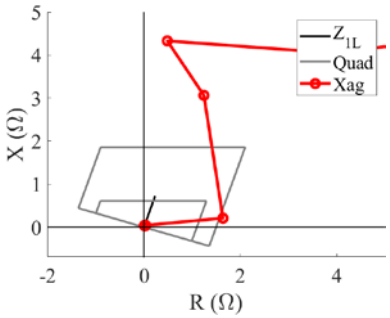

(a) Magnitude-based current limiter

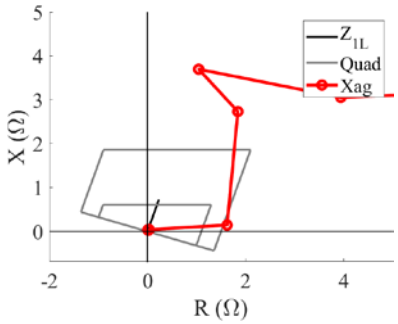

(b) Instantaneous dynamic current limiter

Figure 82. I0-polarized quadrilateral element

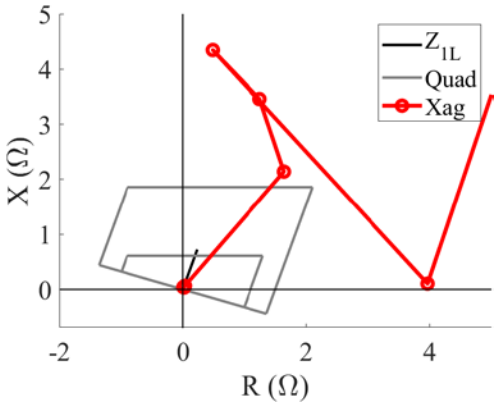

(a) Magnitude-based current limiter

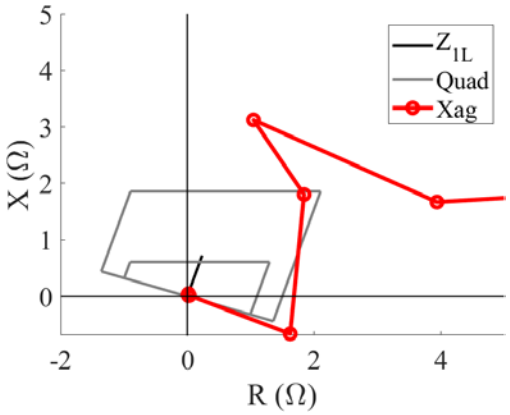

(b) Instantaneous dynamic current limiter

Figure 83. I2-polarized quadrilateral element

Figure 83 presents the fault response for the negative-sequence directional element that supervises ground faults (32QG). The most significant impact shown is during the transient period when the instantaneous dynamic current limiter caused more oscillations in the computed impedances compared to the magnitude-based current limiter; however, the oscillations did not affect the relay decision because z2A < Z2FTH, and thus a forward fault is detected for both current logics.

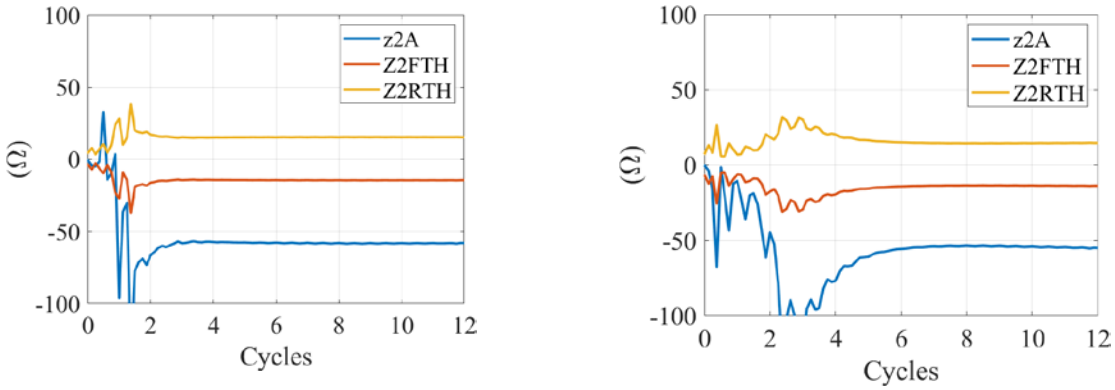

(a) Magnitude-based current limiter

(b) Instantaneous dynamic current limiter

Figure 84. Negative-sequence directional element (32QG)

Figure 84 presents the zero-sequence directional element (32V) behavior for both current limiters. The response of this protection element depends on the zero-sequence injection, which is dominated by the conventional termination and the presence of a ground path in the power transformer behind the relay. No significant difference is present between Figure 84 (a) and (b).

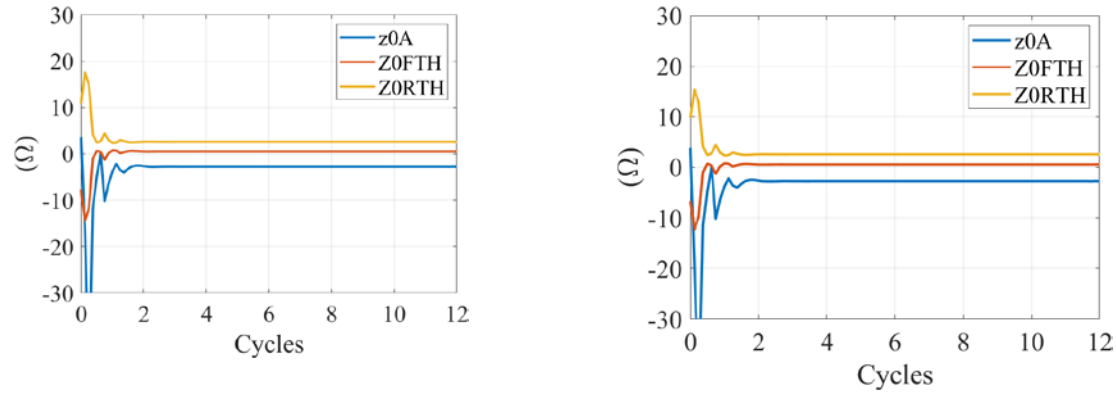

(a) Magnitude-based current limiter

(b) Instantaneous dynamic current limiter

Figure 85. Zero-sequence directional element (32V)

Next, we analyze the effects on the FID logic, as shown in Figure 85. The red arrow is the computation of the angle difference $\angle I_0 - \angle I_2$. This is a snapshot of this angle difference 1.75 cycles after the fault, which is still a transient fault period. For this specific moment, the angle $\angle I_0 - \angle I_2$ differs between the current limiters, but later, in the fault's steady-state condition, they align to the same value; thus, the fault classification decision is the same for both logics.

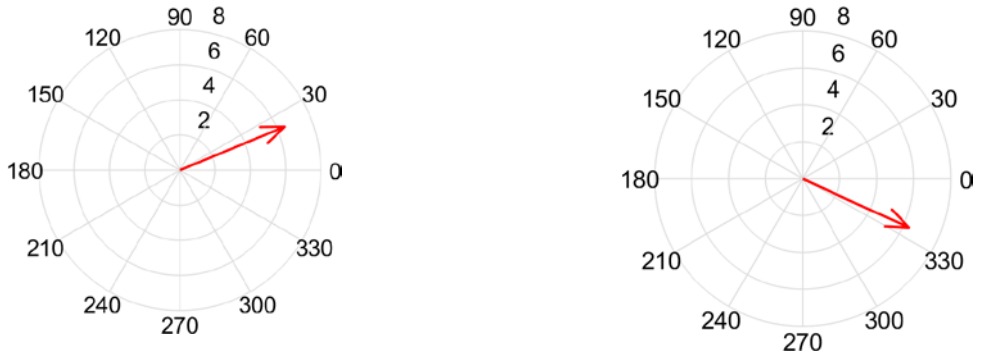

(a) Magnitude-based current limiter

(b) Instantaneous dynamic current limiter

Figure 86. FID logic

Figure 86 presents the timing diagram representing the relay response for the AG fault and comparing the two current-limiter logics. The most important variables to analyze in the relay response refer to the following signals:

- TRIP: final trip signal for the circuit breakers
- Z1G: Zone 1 operation of ground distance elements using either the mho or quadrilateral characteristics
- Z2GT: Zone 2 timing operation of ground distance elements using the mho and quadrilateral characteristics
- XAG1: Zone 1 pickup of the quadrilateral ground element
- XAG2: Zone 2 pickup of the quadrilateral ground element
- MAG1: Zone 1 pickup of the mho ground element
- MAG2: Zone 2 pickup of the mho ground element
- F32QG: forward direction declaration of the 32QG element
- F32V: forward direction declaration of the 32V element
- FSA: AG fault loop selection
- FSB: Phase B-to-ground fault loop selection
- FSC: Phase C-to-ground fault loop selection
- FIDEN: FID logic enabled.

As shown, the relay response is the same for both current limiters, and although their time responses present slight differences for some variables, they are not significant enough for the protection point of view.

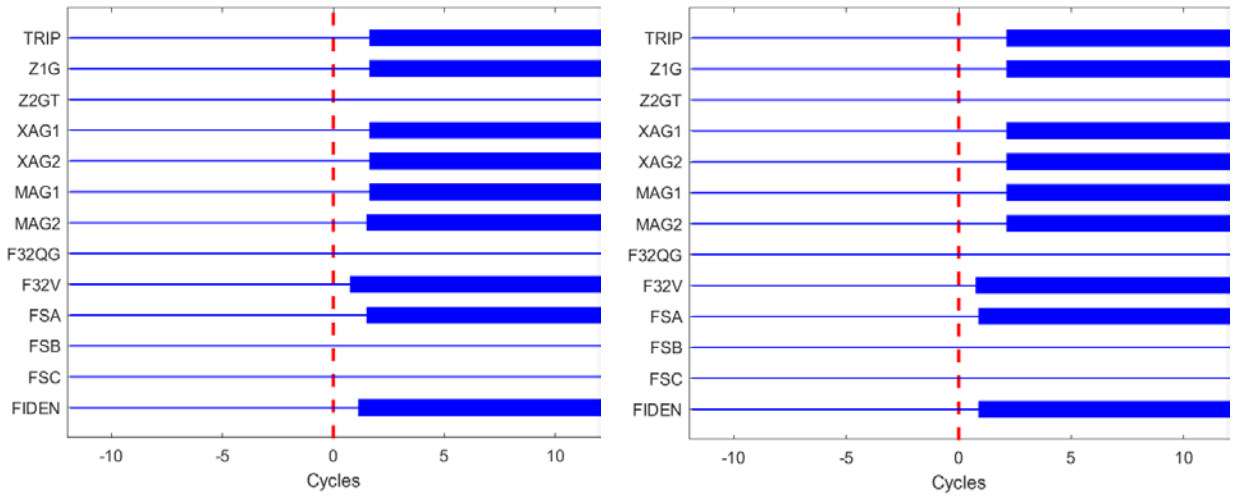

(a) Magnitude-based current limiter

(b) Instantaneous dynamic current limiter

Figure 87. Timing diagram

5.2.2.2.3 Phase-A-to-Ground Fault—Current Limiter in D-Axis Priority

Figure 87 presents the instantaneous current signals comparing the (a) magnitude-based and (b) instantaneous dynamic current-limiter logics. Figure 88 to Figure 93 present the results for the (1) mho element, (2) quadrilateral characteristic with both zero- and negative-sequence current polarization, (3) 32QG directional element, (4) 32-V directional element, and (5) FID logic, respectively. The same conclusions described for the cases with q-axis priority also apply here.

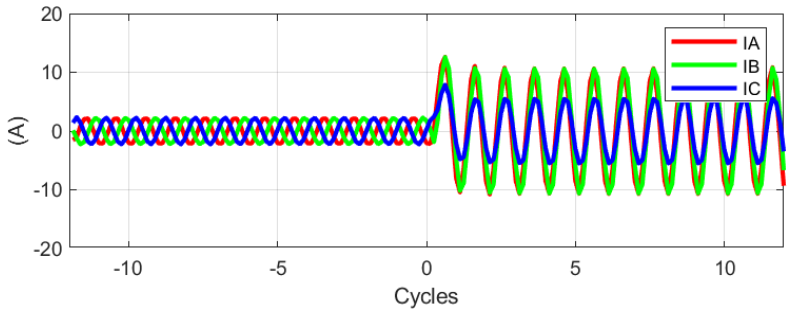

(a) Magnitude-based current limiter

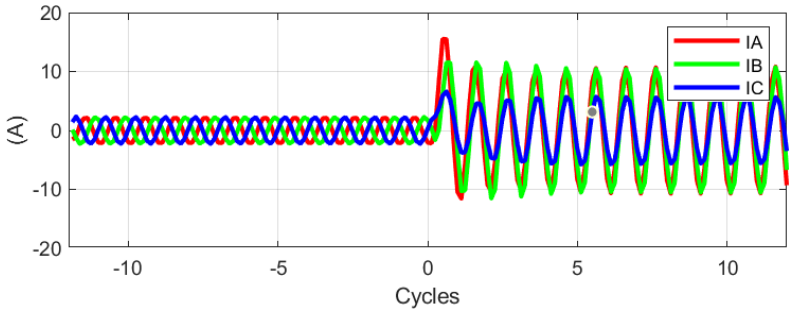

(b) Instantaneous dynamic current limiter

Figure 88. Instantaneous current signals of two typical current limiters

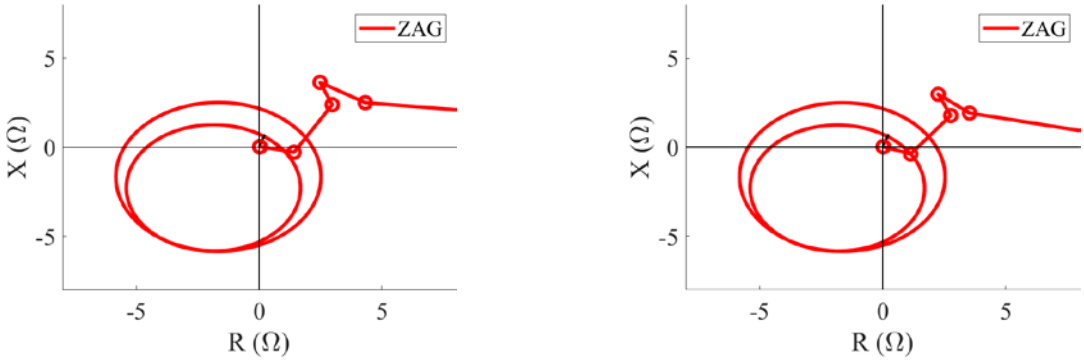

(a) Magnitude-based current limiter

(b) Instantaneous dynamic current limiter

Figure 89. Mho element for ground faults

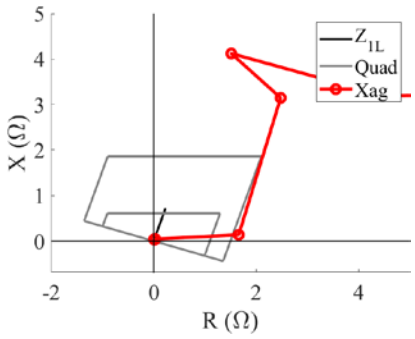

(a) Magnitude-based current limiter

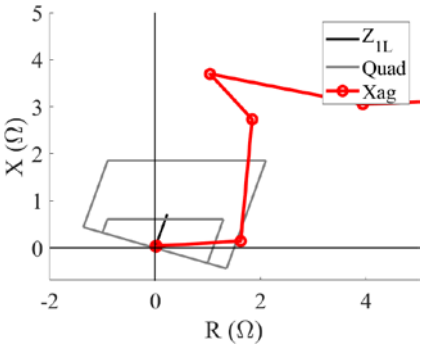

(b) Instantaneous dynamic current limiter

Figure 90. I0-polarized quadrilateral element

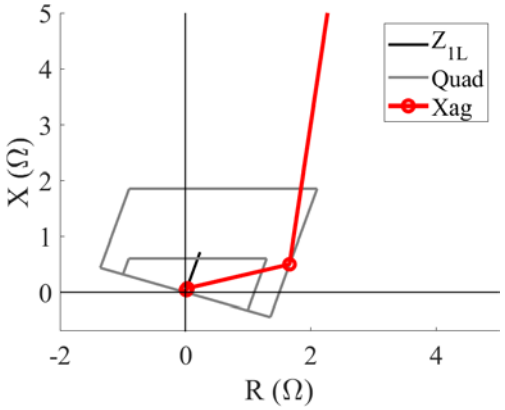

(a) Magnitude-based current limiter

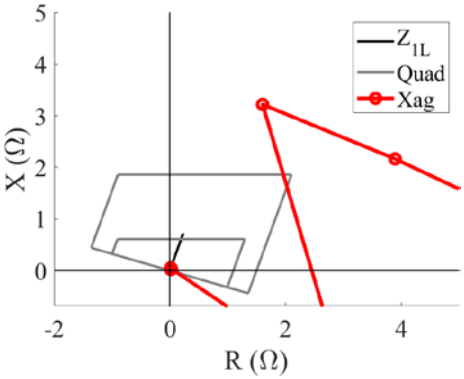

(b) Instantaneous dynamic current limiter

Figure 91. I2-polarized quadrilateral element

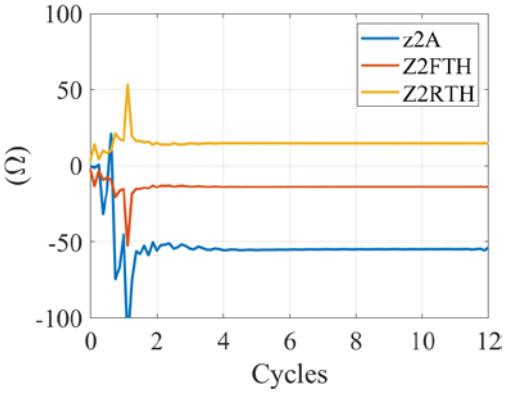

(a) Magnitude-based current limiter

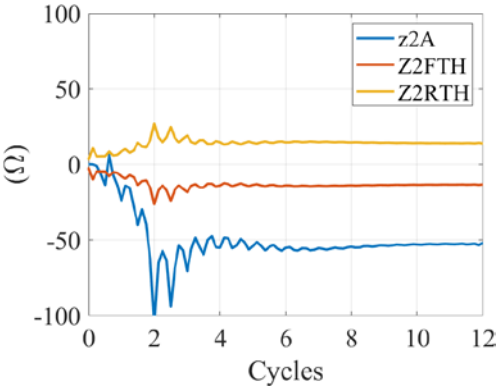

(b) Instantaneous dynamic current limiter

Figure 92. Negative-sequence directional element (32QG)

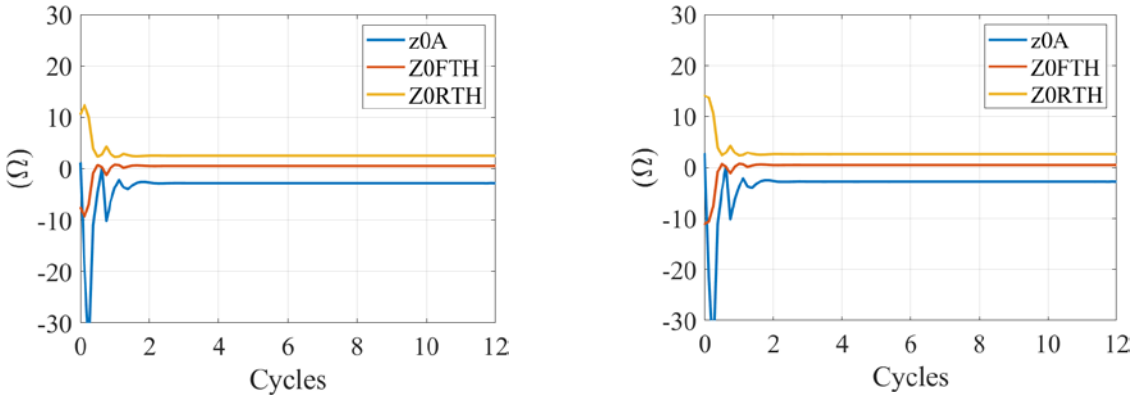

(a) Magnitude-based current limiter

(b) Instantaneous dynamic current limiter

Figure 93. Zero-sequence directional element (32V)

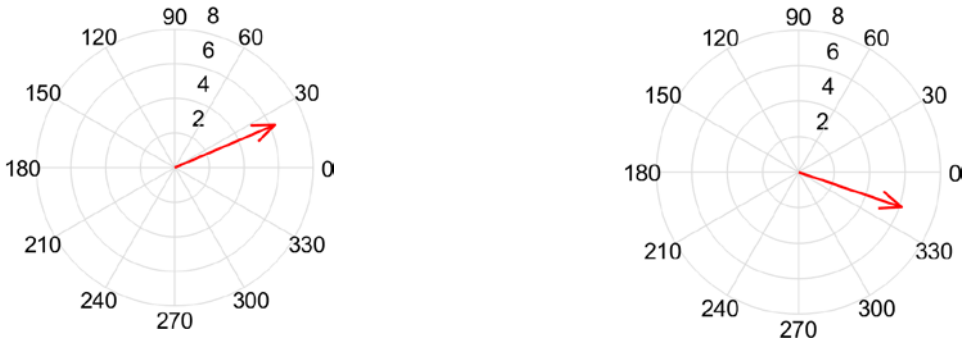

(a) Magnitude-based current limiter

(b) Instantaneous dynamic current limiter

Figure 94. FID logic response

Figure 94 presents the timing diagram for this case. Similar to the previous ground fault case, there is no significant difference in the relay response by varying the current-limiter logic in the IBR control.

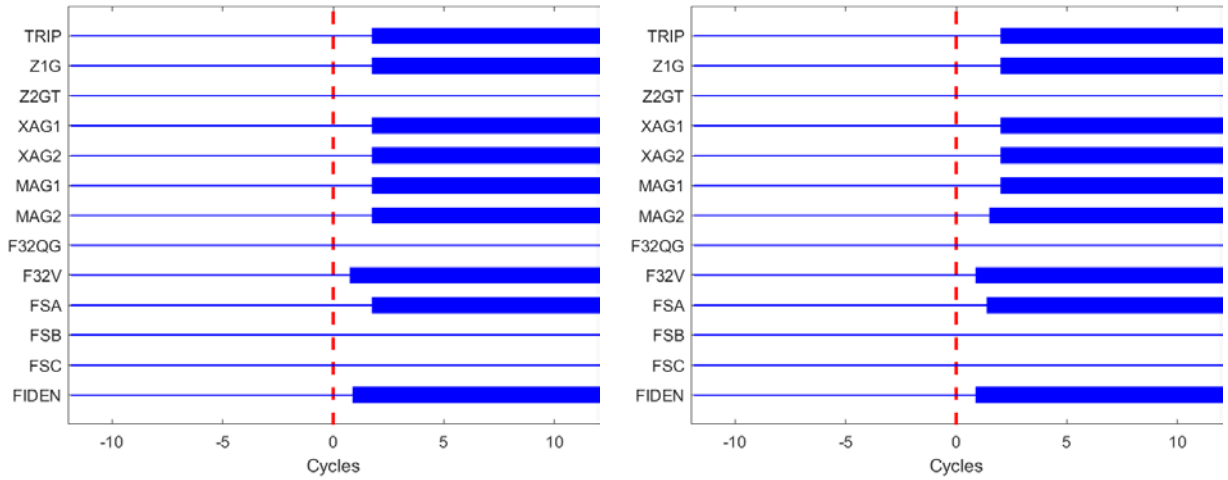

(a) Magnitude-based current limiter

(b) Instantaneous dynamic current limiter

Figure 95. Timing diagram

5.2.2.2.4 BC Fault—Current Limiter in Q-Axis Priority

Figure 95 presents the instantaneous current signals for a BC fault comparing both current-limiter logics. The fault current reaches steady state faster for the (a) magnitude-based current limiter than the (b) instantaneous dynamic limiter. Moreover, the instantaneous dynamic current limiter presents at least one cycle of DC offset before the current reaches steady state, as shown in Figure 95 (b).

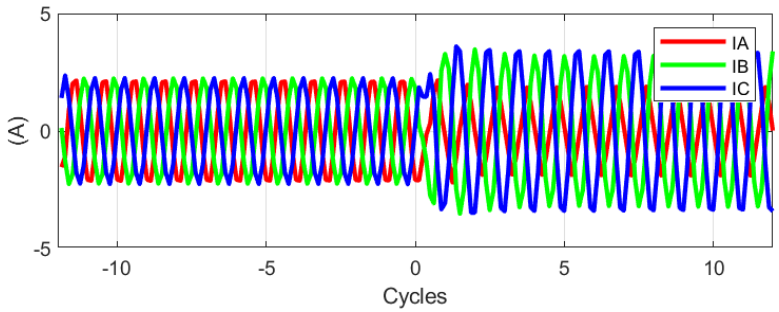

(a) Magnitude-based current limiter

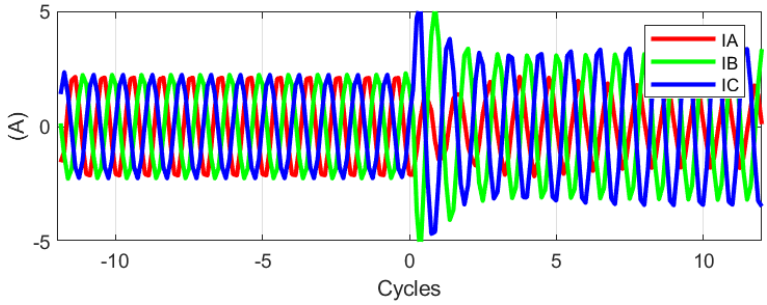

(b) Instantaneous dynamic current limiter

Figure 96. Instantaneous current signals

Figure 96 presents the fault response for the mho element. The apparent impedance computed by the relay is similar between the magnitude-based and the instantaneous dynamic current limiter. A remarkable behavior for both limiters is the mho circle expansion, represented by the two green ellipses. When memory polarization is chosen, the mho circle is designed such that the circle expands up to the effective source impedance behind the relay; however, if this source is an IBR, a virtual impedance source dictated by the controllers affects the circle expansion. The main reason for this is the limited IBR fault contribution (up to 1.2 p.u. by design), resulting in a high source impedance behind the relay, thus producing the abnormal expansion.

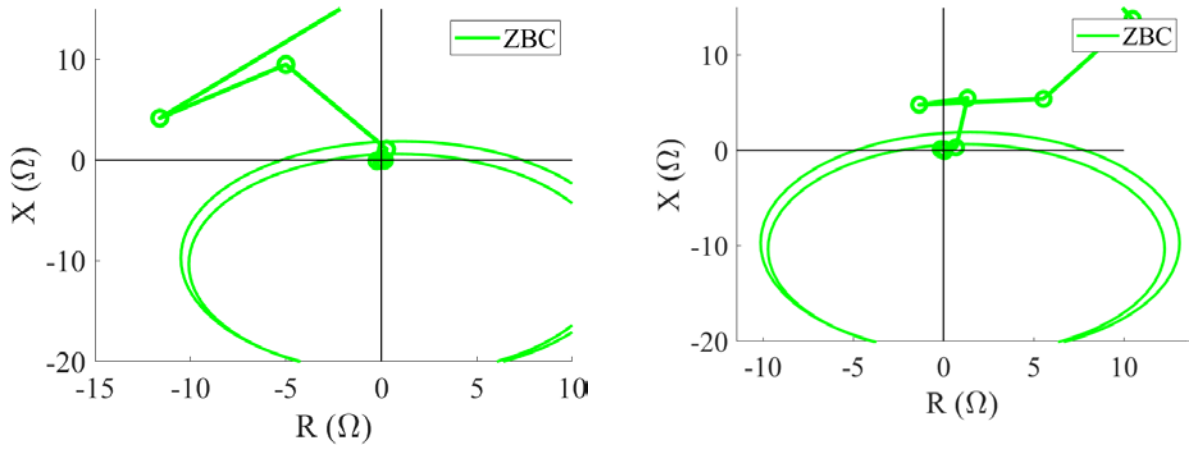

(a) Magnitude-based current limiter

(b) Instantaneous dynamic current limiter

Figure 97. Mho element response for a BC fault

Another effect observed in the mho element for phase faults is that the circle rotation depends on the current priority (d-axis or q-axis) of the inverter during the fault. This behavior occurs to some extent in systems with conventional sources with a high source impedance and a high load flow, but it is much larger in cases with IBRs. In steady state, IBRs are usually set to operate with unit power factor (i.e., maximizing active power); however, during a fault, they can be set to provide voltage support by injecting reactive power into the grid. If the inverter is providing active power during the fault, it is prioritizing d-axis current using the definition of the d-axis in the IBR controls in this study. On the other hand, if it is providing reactive power, it is prioritizing q-axis current. An example of this behavior is shown in Figure 96 where the inverter provides reactive power support (i.e., q-axis priority), causing the circle to expand toward the negative imaginary axis in the R-X plane. If the IBR provided active power during the fault (i.e., d-axis priority), the Mho characteristic expands toward the negative real axis. For comparison, Figure 101 presents the circle expansion when the IBR current-limiter logic operates under d-axis priority. The rotation decreases the fault resistance coverage in the mho characteristic.

Figure 97 presents the quadrilateral characteristic with negative-sequence current polarization for the BC fault. The estimated impedance successfully lies inside the Zone 1 boundary for both current-limiter logics; however, there is a difference in the transient path of the effective impedance computed by the distance element before reaching the Zone 1 boundary.

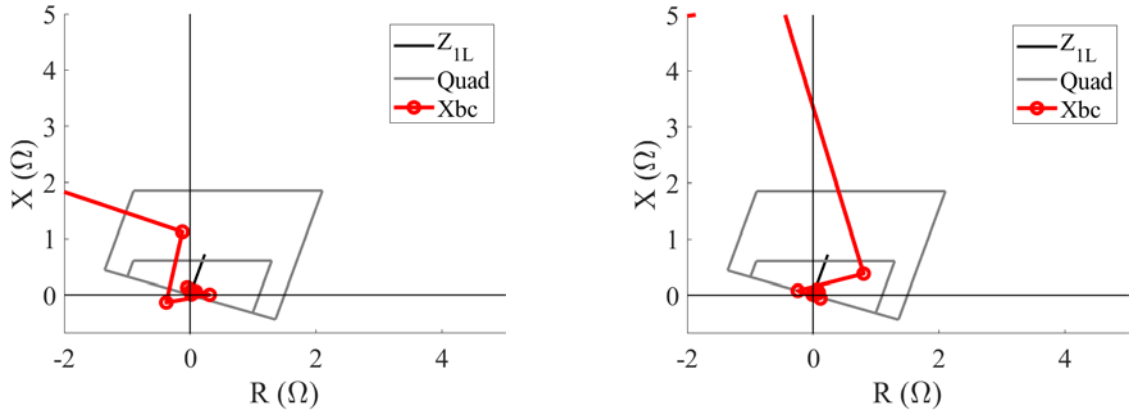

(a) Magnitude-based current limiter (b) Instantaneous dynamic current limiter

Figure 98. Quadrilateral characteristic with I2 polarization

The 32Q directional element response is shown in Figure 98. Similar observations for the case of ground faults apply here. For both current limiters, the element can detect a forward fault, and the only difference is the more oscillatory behavior in the first two cycles after the fault when the instantaneous dynamic current limiter is used.

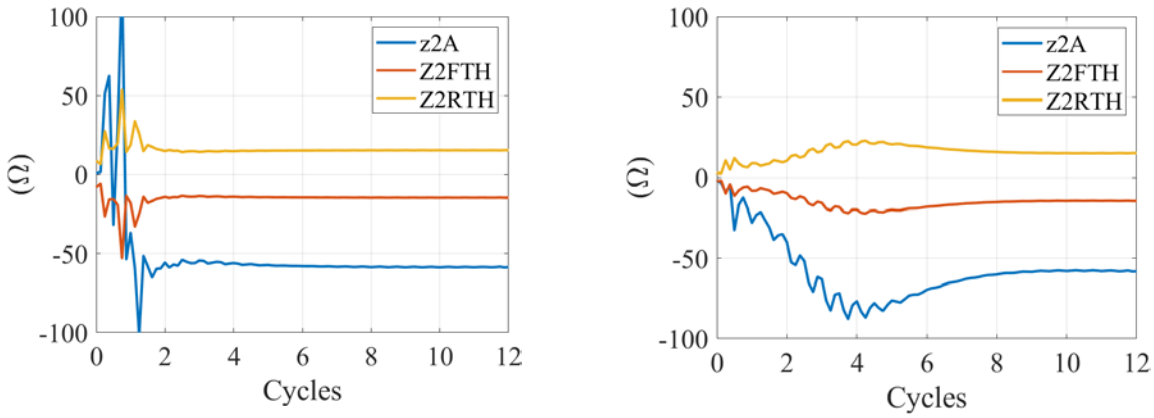

(a) Magnitude-based current limit (b) Instantaneous dynamic current limiter

Figure 99. Negative-sequence directional element (32Q) for phase faults

Figure 99 presents the timing diagram for the BC fault case comparing the magnitude-based and the instantaneous dynamic current limiters. The variables are as follows:

- TRIP: relay final tripping decision
- Z1P: Zone 1 pickup using either the mho or quadrilateral phase elements
- Z2P: Zone 1 timing pickup using the mho or the quadrilateral phase elements (This element operates only after expiring its timer.)
- XBC1: Zone 1 pickup for the quadrilateral phase element (BC fault loop)
- XBC2: Zone 2 pickup for the quadrilateral phase element (BC fault loop)
- MBC1: Zone 1 pickup for the mho phase element (BC fault loop)

- MBC2: Zone 2 pickup for the mho phase element (BC fault loop)
- F32Q: forward fault declaration using the 32Q directional element.

As shown, the relay had the same decisions for both current-limiter logics, and there were no significant timing differences in the element operation; therefore, we can conclude that the current-limiter logics did not significantly affect the protection decisions.

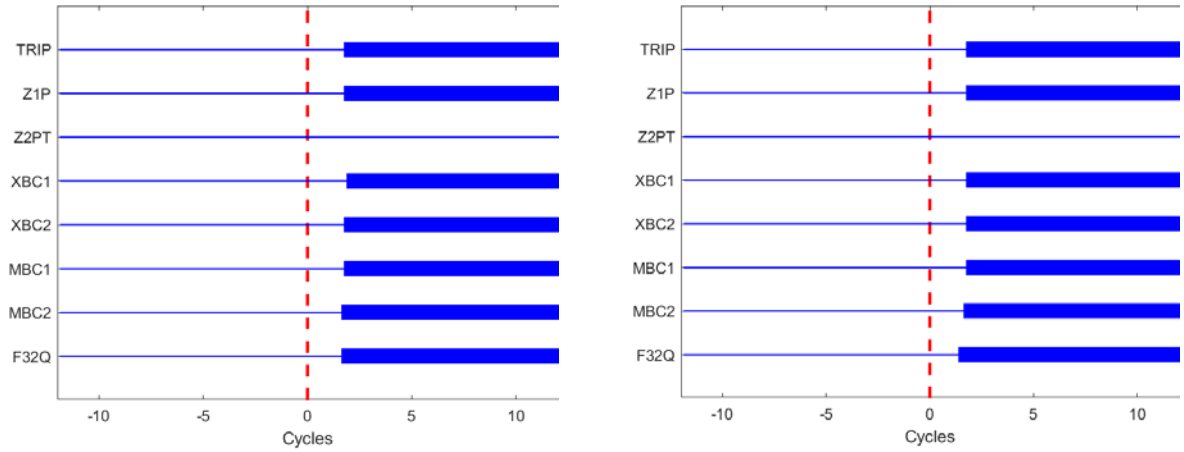

(a) Magnitude-based current limiter

(b) Instantaneous dynamic current limiter

Figure 100. Timing diagram

5.2.2.2.5 BC Fault—Current Limiter in D-Axis Priority

Figure 100 presents the instantaneous current signals when the IBR is operating under d-axis priority. The protection element responses are presented from Figure 101 to Figure 103. Similar conclusions presented in the q-axis priority case apply here. The most significant difference is the mho circle expansion, shown in Figure 101. In this case, the circle expanded toward the real axis.

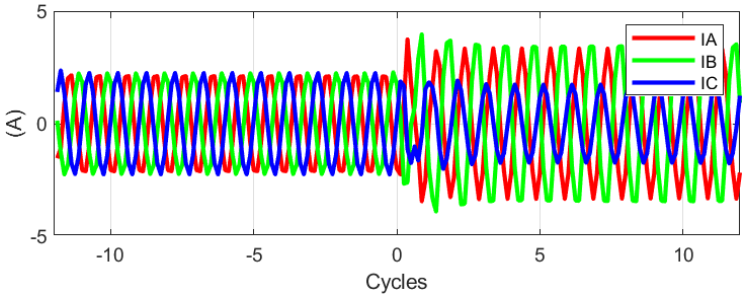

(a) Magnitude-based current limiter

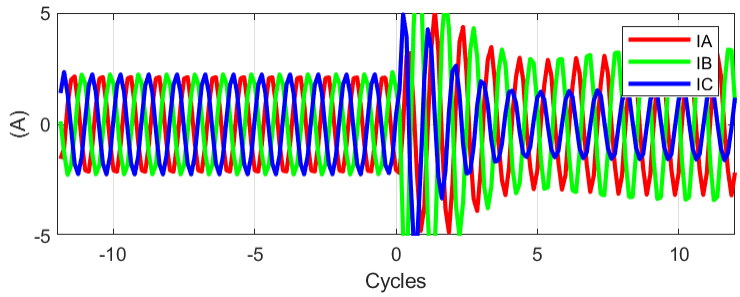

(b) Instantaneous dynamic current limiter

Figure 101. Instantaneous current signals of two typical current limiters

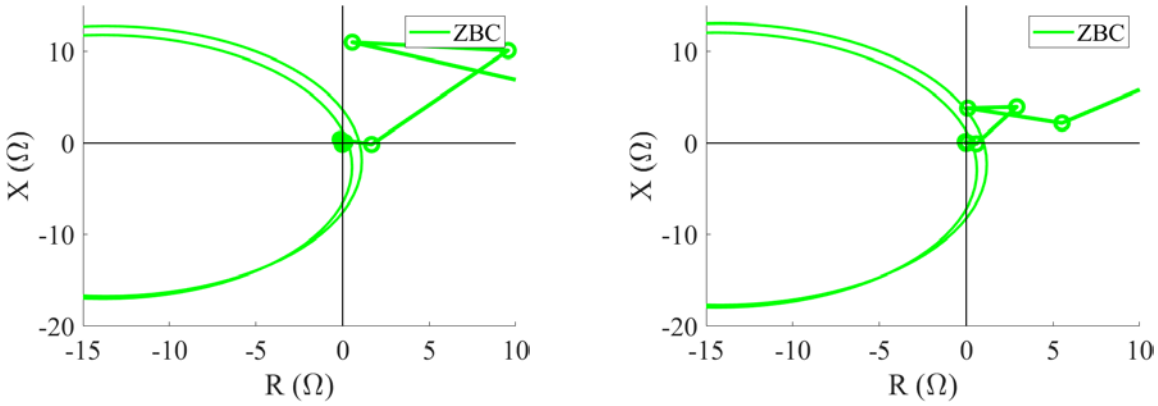

(a) Magnitude-based current limiter

(b) Instantaneous dynamic current limiter

Figure 102. Mho element for a phase fault

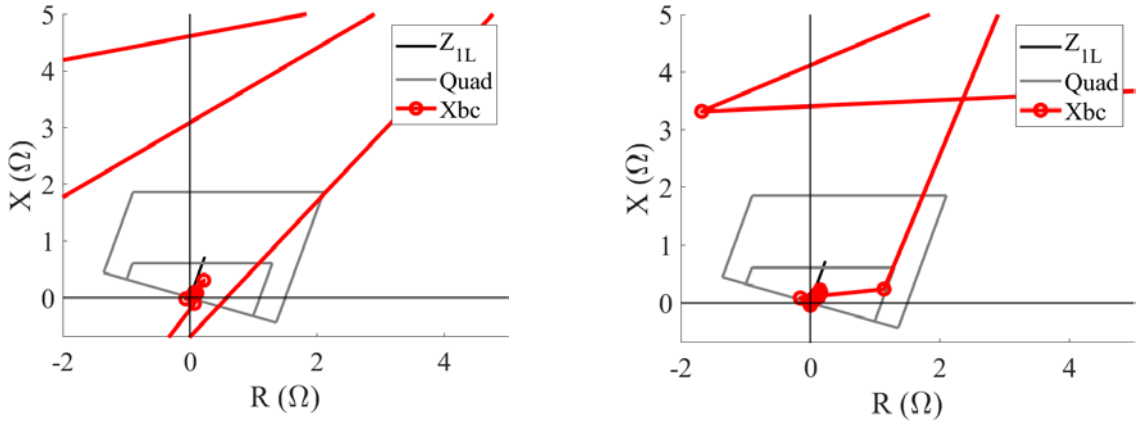

(a) Magnitude-based current limiter (b) Instantaneous dynamic current limiter

Figure 103. Quadrilateral characteristic with I2 polarization

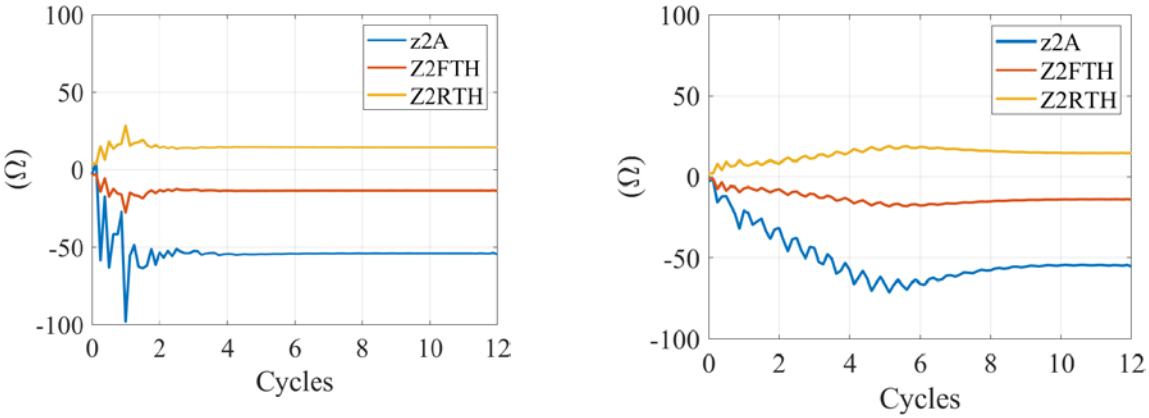

(a) Magnitude-based current limiter (b) Instantaneous dynamic current limiter

Figure 104. Negative-sequence directional element (32Q)

In general, despite the minor differences presented in the computation of each protection element presented in this section, the instantaneous dynamic or the magnitude-based current-limiter logics did not have a significant effect on the protection decisions. The relay's decision was correct in all cases, and only the transient path changed for a few conditions without compromising the protection.

Figure 104 presents the timing diagram for this case. Similar to what was observed for the previous BC fault case, the same conclusions apply here, and there is no significant impact on the relay's operation by varying the current-limiter logic.

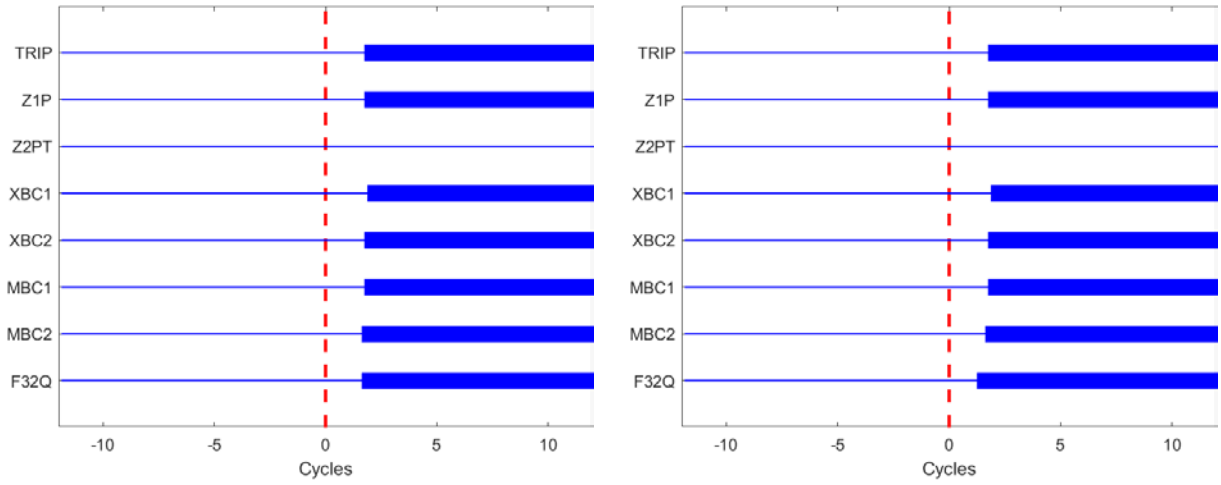

(a) Magnitude-based current limiter

(b) Instantaneous dynamic current limiter

Figure 105. Timing diagram

5.2.2.3 Current-Blocking Schemes and Their Effects on Relaying Decisions

Current-blocking schemes (also called momentary cessation) refer to a temporary interruption of current injection from the inverter after the fault inception. According to IEEE Std 2800-2022, current blocking is only allowed under very low-voltage conditions. This section evaluates the impact of the IBR's time delay to enter current-blocking mode on the protection relay response. Considering the previous analyses of the outer- and inner-current controllers, the cases presented here consider that the inverter controls I2 in compliance with IEEE Std 2800. We evaluate three different time delays after the fault inception that the inverter takes to block the current injection: (1) one cycle, (2) two cycles, and (3) four cycles. In addition, we analyze faults at 5%, 30% and 70% of the line referring to the IBR end. This section shows only a few results, but they are enough to support the general conclusions observed for all the test cases. Figure 105 provides the timing diagrams for the relay response considering the three cases analyzed. The conclusions are as follows: When the IBR took one cycle after the fault inception to block the current injection, the relay did not have enough time to operate; however, for two or more cycles, it had a reliable operation. The longer the inverter stays active during the fault, the more time the relay needs to have a reliable decision. Notice that for the cases where the relay operated, the protection functions remained asserted during the time before the current-blocking scheme is achieved [66].

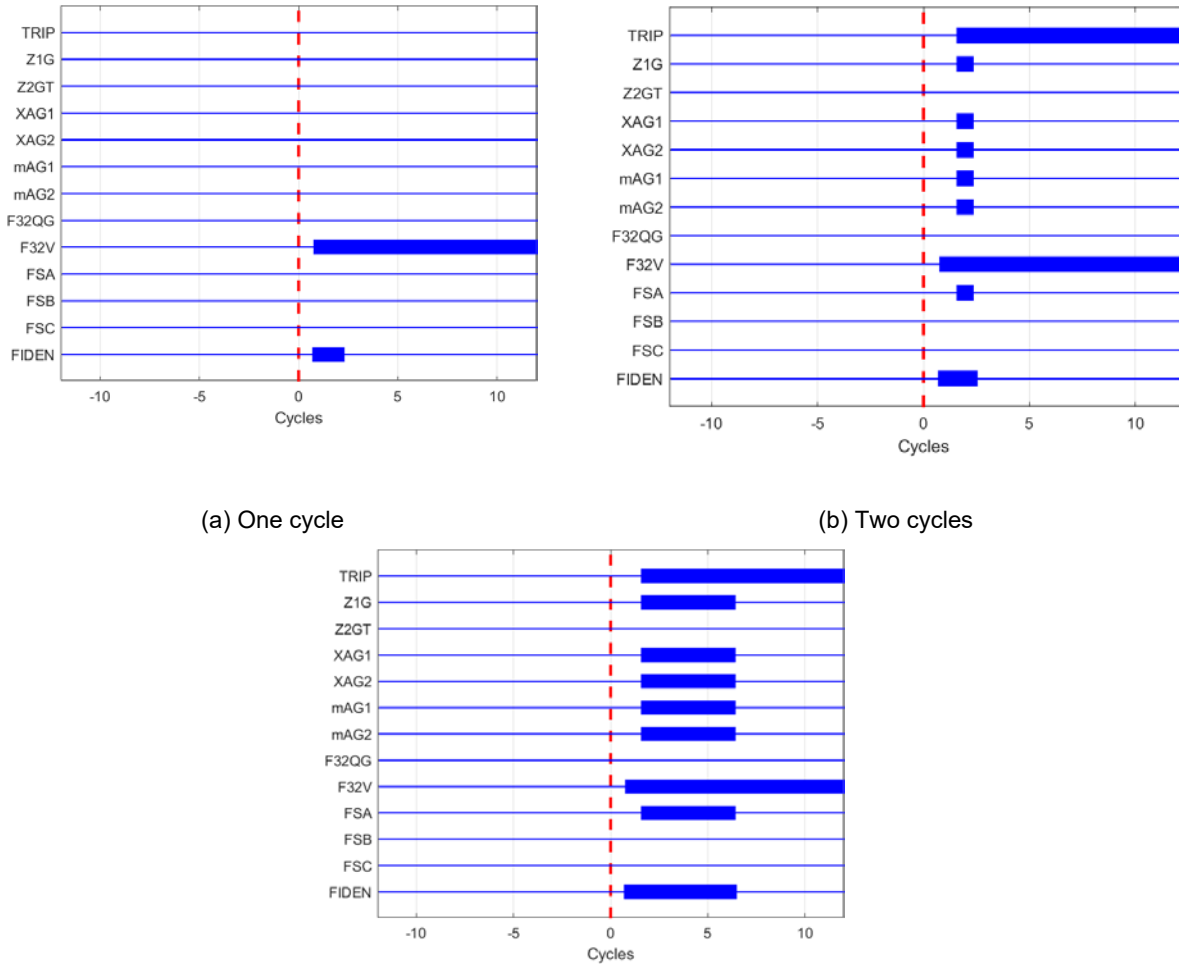

(a) One cycle

(b) Two cycles

(c) Four cycles

Figure 106. Timing diagrams to evaluate the impact of the current-blocking schemes on the relay response

5.2.2.3.1 Ground Distance Elements

The elements that are affected by the current-blocking scheme include the (1) I2-polarized quadrilateral element negative sequence, (2) directional element, and (3) FID logic. Figure 106 presents the response for the quadrilateral characteristic. Notice that the longer the IBR takes to activate the current blocking, the less oscillatory the effective estimated impedance becomes.

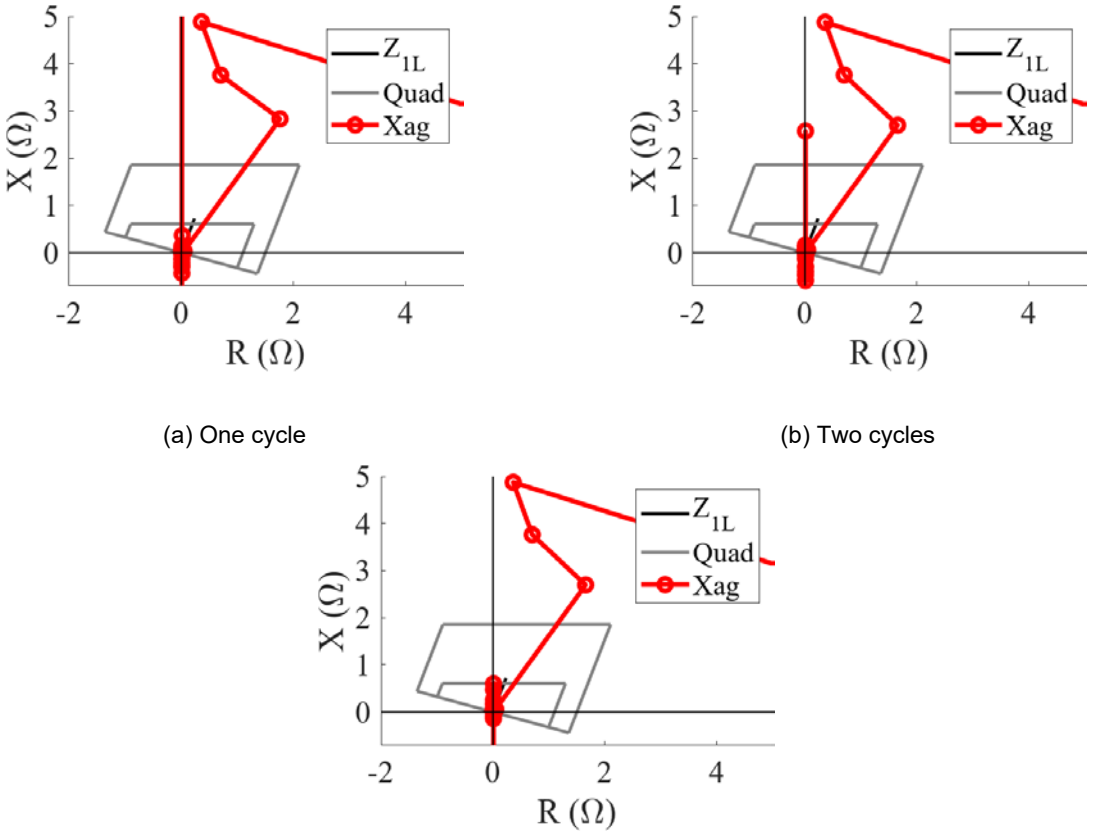

(a) One cycle

(b) Two cycles

(c) Four cycles

Figure 107. I2-polarized quadrilateral element

Figure 107 presents the response for the 32QG element. In this case, this element response is more reliable if the IBR delay for current blocking is set to four cycles. For instance, the directional element properly detected a forward fault two cycles after the fault, as shown in Figure 107 (a); however, this is a critically narrow time window for the relay decision.

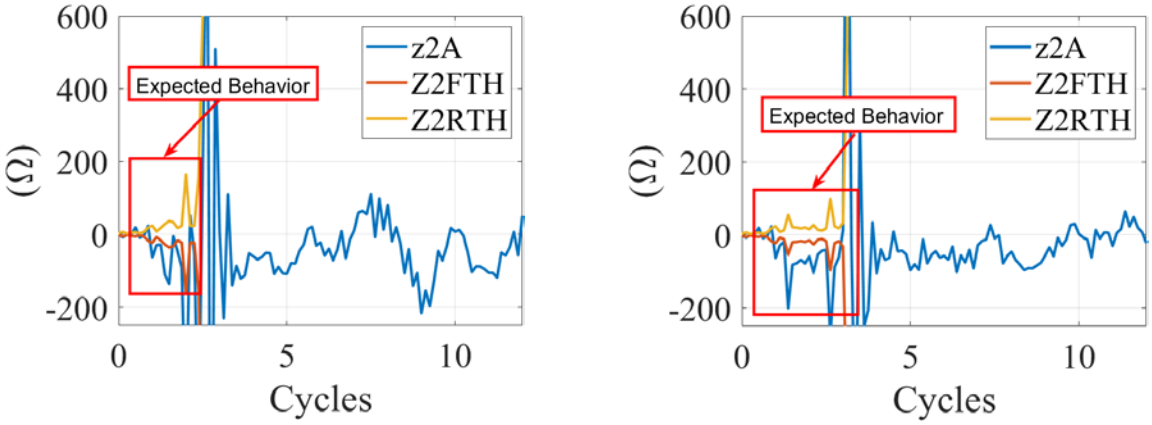

(a) One cycle

(b) Two cycles

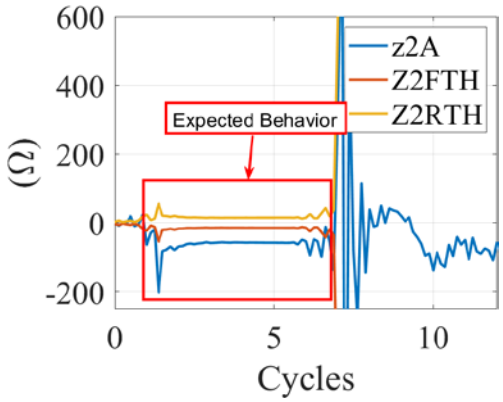

(c) Four cycles

Figure 108. 32QG element response

Figure 108 presents the results for the sequence current-based FID logic considering that the inverter is set to control the negative-sequence current injection. As a reminder, this element decides a forward fault if the angle difference between I0 and I2 is from 330° to 30°. The only condition that caused issues is when the inverter entered current-blocking mode one cycle after the fault inception.

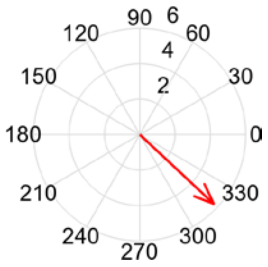

(a) One cycle

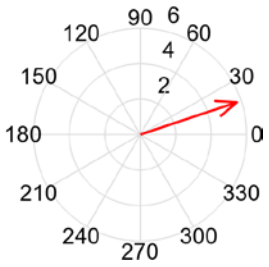

(b) Two cycles

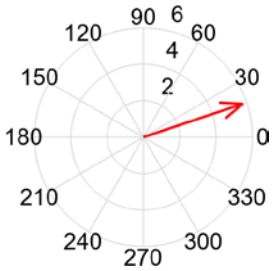

(c) 4 cycles

Figure 109. Sequence current-based FID logic

5.2.2.3.2 Phase Distance Elements

Figure 109 presents the results for the I2-polarized quadrilateral element, Figure 110 presents the results for the 32Q directional element, and Figure 111 presents the results for the mho element using the BC fault loop. The results clearly show that when the current-blocking scheme takes

place after two or four cycles, the relay logic can operate more reliably, whereas one cycle is not enough for the protection elements to make a decision.

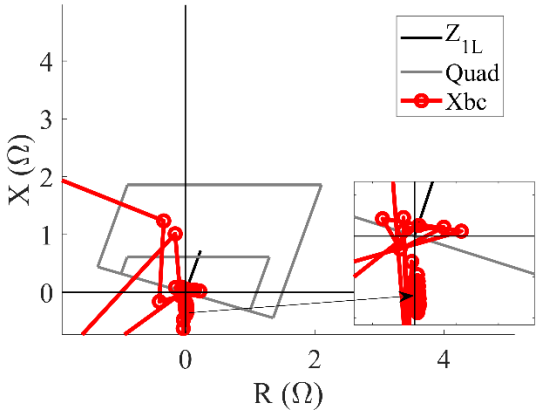

(a) One cycle

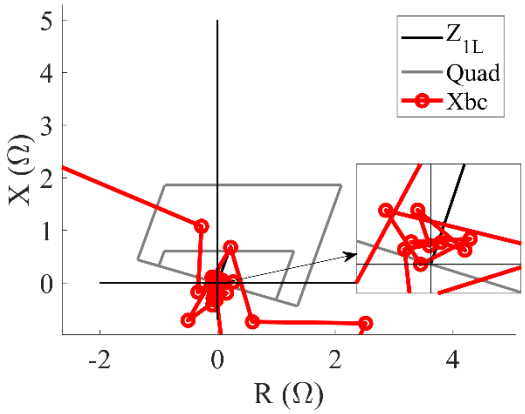

(b) Two cycles

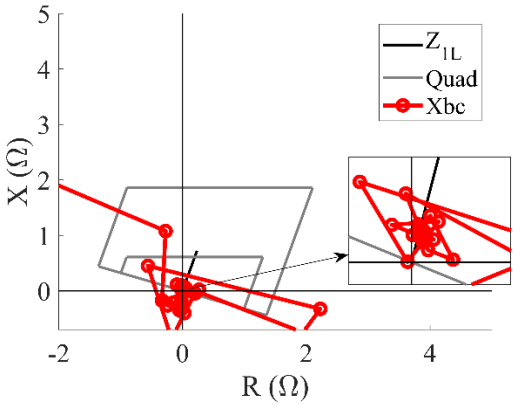

(c) Four cycles

Figure 110. I2-polarized quadrilateral element for phase faults

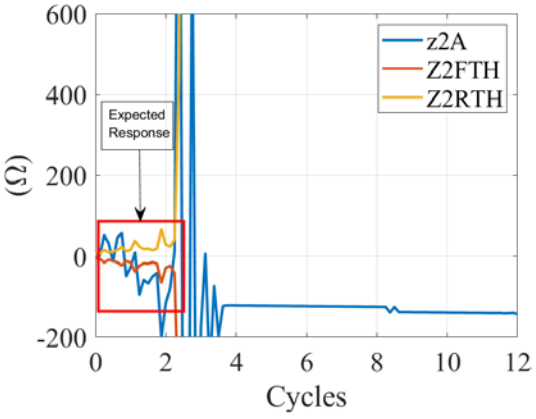

(a) One cycle

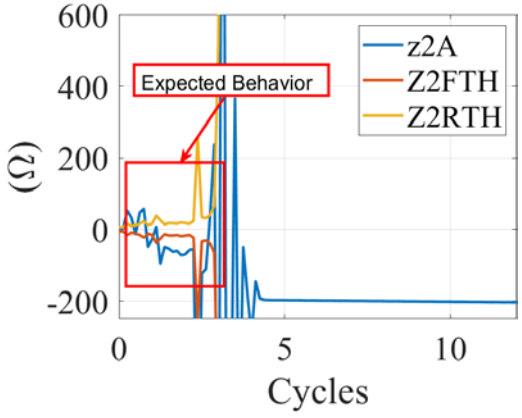

(b) Two cycles

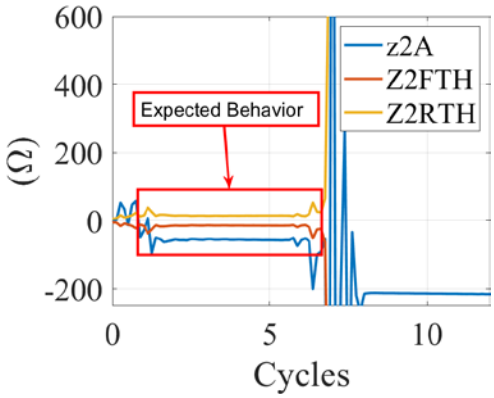

(c) Four cycles

Figure 111. 32Q directional element

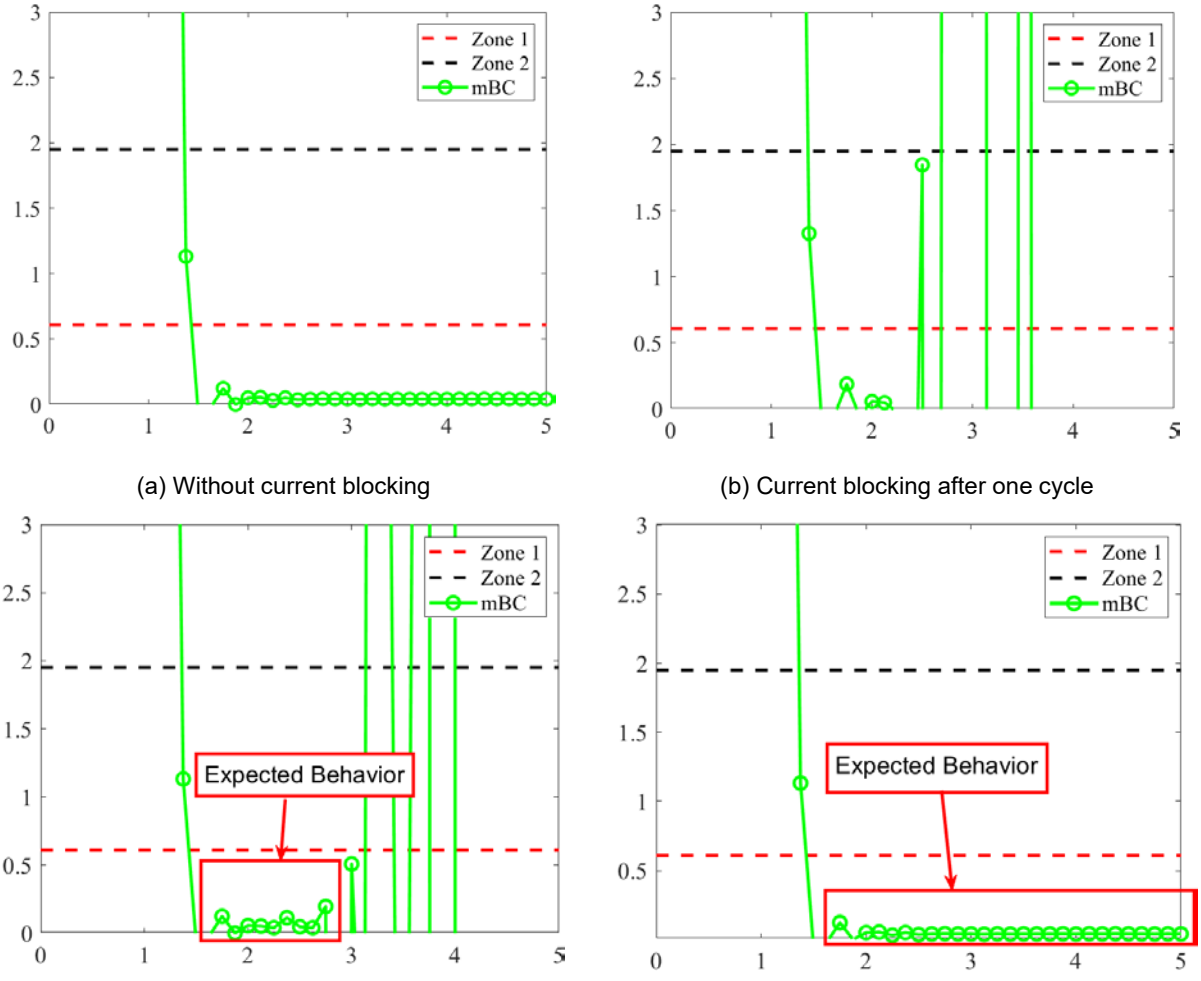

(a) Without current blocking

(b) Current blocking after one cycle

(c) Current blocking after two cycles

(d) Current blocking after four cycles

Figure 112. Mho element response during the current-blocking scheme (BC loop)

5.2.2.4 Slow Versus Fast Response of IBR Controllers (Time Constant)

Another important aspect evaluated in this report is the impact of the speed of the IBR controllers on the protection element response. So, we compare a slow and fast settling time of the controller's response. The elements that are the most impacted are those that depend on the controller's response: the quadrilateral elements, the 32QG directional, and the FID logic, shown in Figure 112 through Figure 114. It is possible that their response changes between the slow and fast settling time of the IBR's controllers. For the cases analyzed, the quadrilateral ground element using the negative-sequence current polarization had a slight difference for close-in bolted faults, but it could still correctly detect the fault. The 32QG element has a faster directional discrimination when the controller has a faster settling time; however, this element is not really used because the zero-sequence restraining factor blocks it. The FID logic might take longer to reach steady state, but for the first cycle after the fault inception, the angle difference between I0 and I2 was already in the proper region to select the AG fault loop. These changes are not significant, as observed by checking the timing diagram in Figure 115, where the tripping decision occurred at almost the same instant for both time constants.

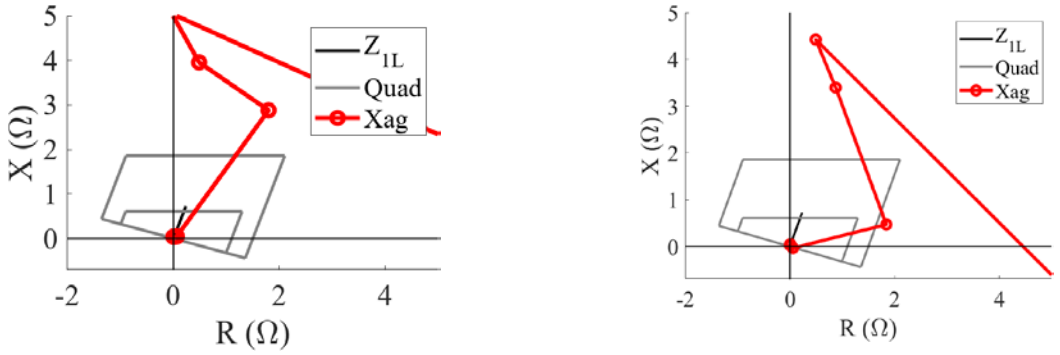

(a) Fast (b) Slow

Figure 113. I2-polarized quadrilateral element

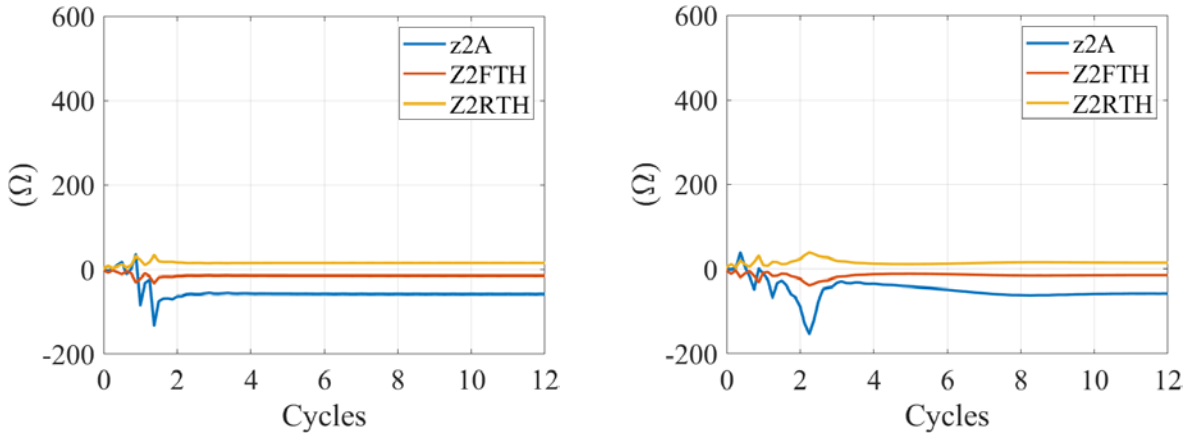

(a) Fast (b) Slow

Figure 114. 32QG directional element response

(a) Fast (b) Slow

Figure 115. FID logic response

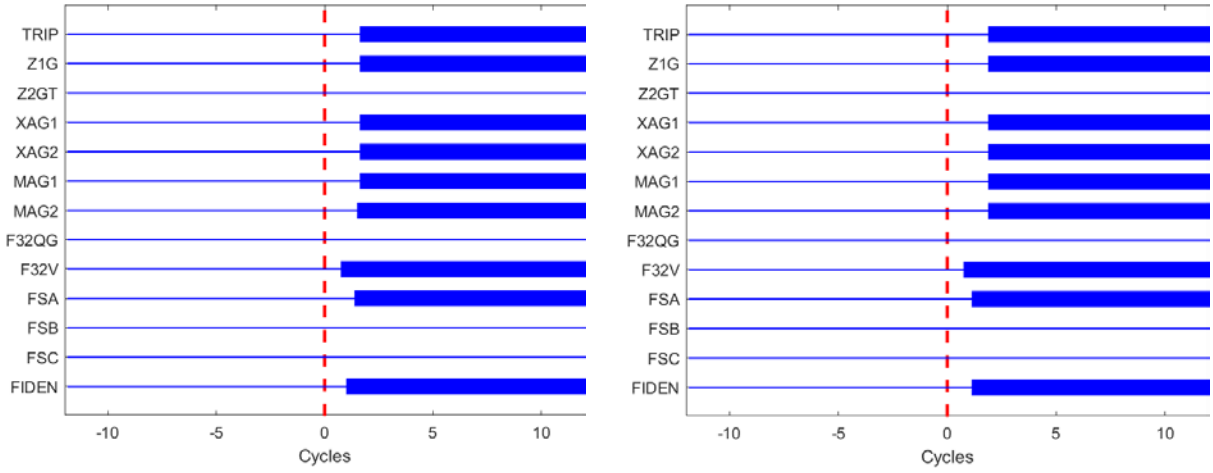

(a) Fast (b) Slow

Figure 116. Timing diagram comparing the fast and slow response of the IBR's controllers

5.2.3 Additional Analysis: Power System Conditions

This section considers additional analysis from different power system conditions, such as different grid strengths; different IBR operating points; and different fault types, locations, and fault impedances. These additional cases are defined for both GFL IBRs and GFM IBRs. The results shown in this section represent generic conclusions for both GFL IBRs and GFM IBRs. It is known that grid strength, power flow conditions, and fault resistance affect the distance protection by affecting the effective impedance estimated by the relay (either using the quadrilateral or mho characteristic); however, it is not clear what additional problems might exist if the fault is fed by IBRs. This section provides insights regarding these classic problems in distance protection fed by nonconventional sources.

5.2.3.1 Effect of Grid Strength

The effect of grid strength is greater during resistive faults. The investigation of these cases aids in checking possible measurement errors caused by system nonhomogeneity and that affect the distance elements—specifically, if these errors will lead to overreaching in distance elements and if they might affect the fault resistance coverage for distance protection. Table 20 presents the scenarios set in the PSCAD simulation.

Table 20. Grid Strength Configuration

IBR operating mode	GFL GFM
Outer-loop control	PQ dispatch
Inner-current control	Phase currents in dq domain Phase currents in αβ domain Sequence currents in dq domain
Transformer TF2 connection	YgΔ (Yg winding facing the transmission system)
Fault type	AG Fault resistance: 0 to 10 Ω in steps of 1 Ω Fault location: 5%, 50%, and 80% of the line (referred to as the IBR end)
Grid strength conditions	Hydro connected Hydro disconnected

The results for the quadrilateral characteristic show oscillatory behavior in the effective impedance if the quadrilateral characteristic is polarized by the I2 current and the fault resistance value increases. Figure 116 presents the results for three different fault resistance cases: bolted, 5 Ω, and 10 Ω, where the oscillations are more critical for the 10 Ω fault.

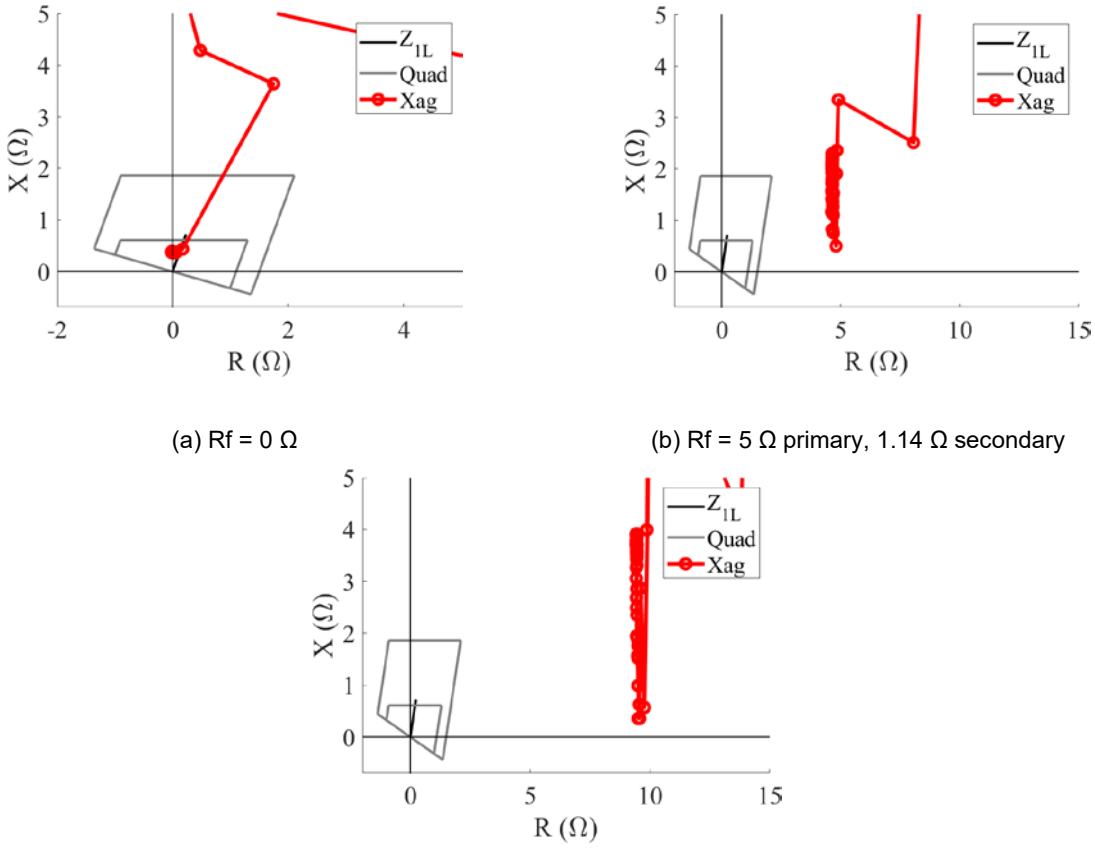

(a) Rf = 0 Ω

(b) Rf = 5 Ω primary, 1.14 Ω secondary

(c) Rf = 10 Ω primary, 2.28 Ω secondary

Figure 117. Quadrilateral relay behavior for resistive faults at 50% of the line with I2 polarization with IEEE Std 2800-compliant controller

Even for smaller fault resistances, the relay did not detect the fault because of the chosen relay settings; however, longer lines than the one tested would have a higher margin to operate because the left and right resistance blinders are set to higher values. In those cases, the quadrilateral characteristic might have unsecured operation in the reactance element because of the oscillations caused by the negative-sequence current control. Note that the fault resistance values are in primary ohms, and what is really shown in the quadrilateral characteristic plot is referred to as secondary ohms. For instance, consider a ground fault with a fault resistance of 10 Ω in primary values. Using a current transformer with a transformation ratio of 80 and a voltage transformer with a transformation ratio of 3500, the relay would theoretically measure the fault resistance as $10 \times \frac{80}{350} = 2.28\ \Omega$ in secondary terms. This calculation highlights an overestimation of fault resistance, a common phenomenon when weak sources interact with stiff systems.

Another challenge with negative-sequence current polarization arises when setting the tilt angle for the relay, particularly if one end of the line is fed by an IBR. In conventional systems, such as the example shown in Figure 27, engineers rely on data related to the equivalent source impedance behind the line end and the line impedance. Using this information, they can use (34) to accurately compute the tilt angle for the reactance element in the quadrilateral characteristic.

In systems fed by IBRs, the equivalent impedance at the IBR termination of the line is not well defined; therefore, the equivalent negative-sequence impedance seen by the relay is influenced by the behavior of the IBR controllers. This dependency introduces challenges in setting the tilt angle, as improper configurations can cause the relay to overreach Zone 1. Currently, to the best of our knowledge, there is no straightforward manner to compute the tilt angle for the quadrilateral element polarized by I2 at the IBR termination. Whereas for the case where the quadrilateral element is polarized by I0, the transformer zero-sequence leakage impedance can be used to compute the tilt angle, T_0. This is exemplified in Figure 117, where Z_{0R} is the remote end equivalent zero-sequence source impedance, Z_{0L} is the zero-sequence line impedance, and Z_{T0} is the zero-sequence leakage impedance for a YgΔ power transformer. The equation for the tilt angle, T_0, results in (48):

$$T_0 = \arg\left[\frac{Z_{T0} + Z_{0L} + Z_{0R}}{(1-m)\cdot Z_{0L} + Z_{0R}}\right] \quad (°) \tag{48}$$

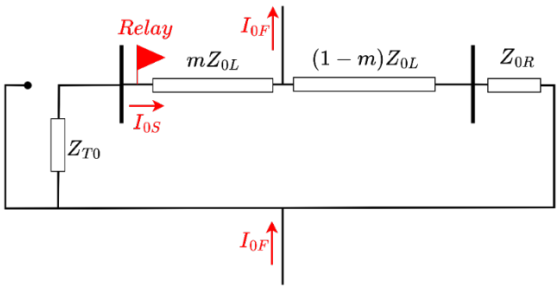

Figure 118. Zero-sequence equivalent network to compute the tilt angle for zero-sequence current polarization

For grid strength, a total of 198 cases were simulated. Among them, 66 cases had the IBR set to regulate the negative-sequence current injection. This provides valuable analysis because the FID logic and the z2-based directional elements are not reliable if the IBR does not regulate I2. Table 21 presents the percentage of operation for the distance elements for the cases where the IBR regulates I2. In summary, there are no significative differences in the behavior of distance elements considering resistive faults with different grid strengths for faults on the line for the scenario studied.

Table 21. Percentage of Operation for Distance Elements in Cases With Resistive Faults and Different Grid Strength Conditions

Fault Location	Hydro	Zone 1 Op (mho) (%)	Zone 1 Op (quad) (%)	Zone 2 Op (mho) (%)	Zone 2 Op (quad) (%)
5 %	On	18	18	36	18
	Off	18	18	36	18
50 %	On	9	18	27.27	18
	Off	9	18	27.27	18
80 %	On	0	0	27.27	18
	Off	0	0	27.27	18

The cases for the evaluation of the effects of grid strength on the mho element are the same as those described in Table 20. The results regarding the performance of the mho element are shown in Table 21. In general, the performance for the mho element during different grid strength conditions remained the same. This can have more impact on faults external to the line. Figure 118 presents the results with the mho element behavior during ground faults for fault resistances with 0 Ω, 5 Ω, and 10 Ω. The mho element presented reliable behavior for the faults that lie inside the circle; however, it has small fault resistance coverage. This is because this line is short, and the infeed effect (i.e., caused by the short-circuit current contribution from the remote and the local source with the fault resistance [18]) limits the resistive coverage by amplifying the resistive part of the apparent impedance measured by the relay.

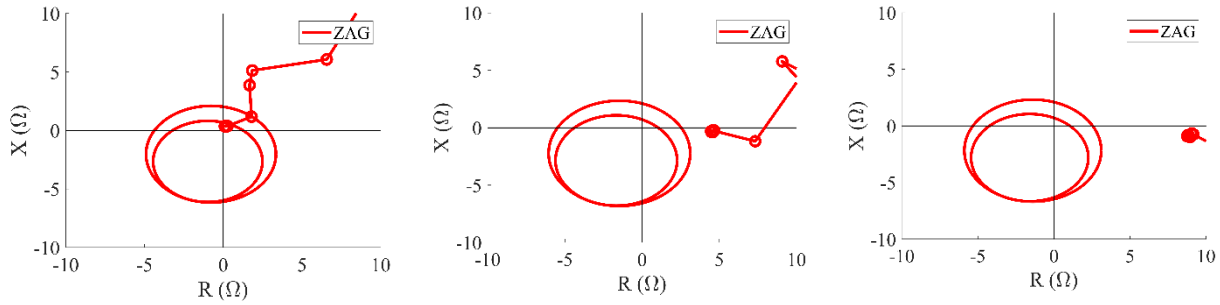

(a) Rf = 0 Ω (b) Rf = 5 Ω (c) Rf = 10 Ω

Figure 119. Mho element behavior for ground faults with different fault resistances

Figure 119 presents a comparison for the mho element behavior for the two grid strength conditions for an AG fault at 50% of the line with 5 Ω of fault resistance. This behavior is similar between the two cases because the hydro plant had little effect on the distance elements because of its small fault current contribution relative to the parallel system connected to the Kekaha bus.

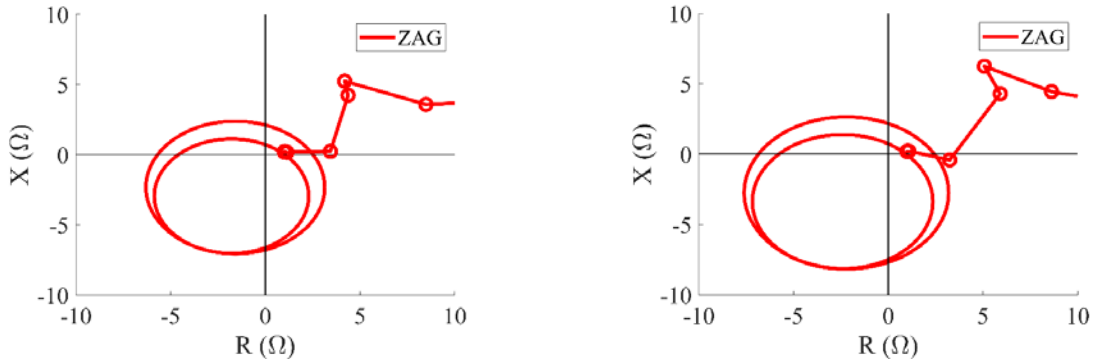

(a) Hydro on

(b) Hydro off

Figure 120. Comparing the effect of grid strength conditions for an AG fault with Rf 5 Ω at 50% of the line

5.2.3.2 Effect of Different Operating Points

Distance relays can be affected by resistive faults according to loading conditions. Depending on whether the relay end is exporting or importing power, the resistive component of the fault can appear to have a reactive component. This can cause the apparent impedance seen by the relay to tilt up or down. This tilt in the apparent impedance can overreach Zone 1 in the distance elements. To evaluate the effect of different power flow conditions in the system fed by IBRs, the cases described in Table 22 were simulated in PSCAD.

Table 22. Scenarios for Different Power Flow Conditions

IBR operating mode	GFL
Outer-loop control	PQ dispatch
Inner-current control	Phase currents in dq domain Phase currents in αβ domain Sequence currents in dq domain
Transformer TF2 connection	YgΔ (Yg winding facing the transmission system)
Fault type	AG Fault resistance: 0 to 10 Ω in steps of 1 Ω Fault location: 5%, 50%, and 80% of the line (referred to the IBR end)
Power flow conditions	1. Fully rated 2. P = 0.1 p.u., Q = 0.0 p.u. 3. P = 0.25 p.u., Q = 0.0 p.u. 4. P = 0.25 p.u., Q = 0.15 p.u.

Table 23 presents the results of comparing the percentage of operation of the quadrilateral element in Zone 1 and Zone 2 for the scenarios that the relay is expected to operate (i.e., the IBR regulates I2 in compliance with IEEE Std 2800-2022, the quadrilateral element uses I0 polarization, it is supervised by the 32V directional element, and the FID logic is enabled).

Table 23. Performance of the Quadrilateral Element Operation for Different Power Flow Conditions and Fault Locations

Fault Location	Power Flow Condition	Zone 1 Op (Quad) (%)	Zone 2 Op (Quad) (%)
5%	1	18.18	18.18
	2	18.18	18.18
	3	18.18	18.18
	4	18.18	18.18
50 %	1	18.18	18.18
	2	18.18	18.18
	3	18.18	18.18
	4	18.18	18.18
80 %	1	0	18.18
	2	0	18.18
	3	0	18.18
	4	0	18.18

The same cases described in Table 22 were used to check the mho element performance for different power flow conditions. Table 24 presents these results. For the cases expected to operate, the different power flow conditions did not have a significant impact on the mho element fault detection.

Table 24. Performance of the Mho Element for Different Power Flow Conditions and Fault Locations

Fault Location	Power Flow Condition	Zone 1 Op (Mho) (%)	Zone 2 Op (Mho) (%)
5%	1	18.18	45
	2	18.18	36
	3	18.18	36
	4	18.18	36
50%	1	9.09	36
	2	9.09	27
	3	9.09	27
	4	9.09	27
80%	1	0	27
	2	0	27
	3	0	27
	4	0	27

The results show that for the cases where the relay is expected to operate, the different power flow conditions did not impact the relay performance. The main limitation of the quadrilateral

characteristic is the sensitivity for fault resistance. Fault resistance greater or equal to 2 Ω prevents fault detection under the chosen relay settings.

6 Guidance and Suggested Requirements for IBR Modeling and Control

This section presents guidance and requirements for modeling IBRs with a protective relay perspective, and it summarizes the recommendations for protection engineers. It also recommends IBR controls that can facilitate proper transmission system protection operation.

6.1 GFL and GFM Modeling Aspects

Table 25 summarizes the impact of various aspects of GFL IBRs models on protection element response.

Table 25. Impact of Various GFL IBR Aspects on the Responses of Various Relay Elements [51]

GFL Modeling Aspect	Observation	Conclusion
Inverter model: average and switching models	The aspect cannot indicate any differences in fault response.	This modeling aspect does not substantially affect the fault response. Recommendation: The average model reduces the simulation time and provides results with enough resolution.
DC source: PV, battery, and PV+battery	The aspect cannot indicate any differences in fault responses. Batteries were charged.	This modeling aspect does not substantially affect the fault response and can be simplified. Note that GFM IBRs require a stiff DC source, while GFL IBRs do not.
Power loop control: PQ dispatch vs. Vdc-Vac control	The power loop control type did not affect the relay response, as shown in Section 5.2.1.3, however, it needs to be considered depending on the control objective of the inverter.	This aspect should be considered when modeling an IBR.
Current control: dq, seq, and αβ	The current loop affects the IBR negative-sequence response. αβ control was the most challenging among the three that challenge the protection reliability. Because it was the one that caused more oscillations in the protection elements calculations (e.g., directional, quadrilateral characteristic, and FID).	This aspect showed substantial influence over the IBR fault response and should be known for proper IBR modeling.
Current limiter: saturation/latching dq or αβ	The current-limiter strategy proved to be critical for proper representation of the IBR fault response.	This aspect showed a critical difference in the IBR fault response and should be included in the model.

Table 26 summarizes the impacts of various aspects related to GFM IBR models on protection element response.

Table 26. Impacts of Various GFM IBR Aspects on the Response of Various Relays Elements [51]

GFM Modeling Aspect	Observation	Conclusion
Outer-loop: droop or VSM	The type of voltage control loop did not affect the fault current response, nor the relay response. But the different outer-loop controllers are needed to have more faithful representation of the inverter in the field.	This aspect should be considered when modeling an IBR. Recommendation: The type of voltage control needs to be provided and included in the simulation, along with the model parameters.
Current control: dq, αβ, and sequence control	There was a noticeable change in the negative-sequence current with the different current control.	This aspect should be considered when modeling an IBR. Recommendation: The type of current control needs to be provided and represented when building the simulation model. If the sequence control is used, the settings for the negative-sequence current magnitude and angle need to be provided and modeled.

The modeling and control of IBR aspects leading to protection problems are summarized in Table 27. For each aspect, the simulation results are provided to verify the description of the problem and recommendation.

Table 27. Recommendations for IBR Modeling and Control from the Perspective of Protection Systems [65][66]

IBR Modeling Aspect	Problem Description	Recommendation
Negative-sequence component control compliance	If the GFL and GFM inverters do not have negative-sequence control implemented or do not comply with IEEE Std 2800, they will not have the appropriate negative-sequence components (V2 and I2). This will affect the protective elements that rely on negative-sequence estimation, mainly the I2-polarized quadrilateral characteristic, the 32Q and 32QG directional elements, and the sequence current-based FID logic.	Negative-sequence control should be included in the GFL and GFM inverter control to support the correct protective relay decision. We suggest disabling the protection elements that need negative-sequence components when negative-sequence current injection is not controlled by the IBR. Along with the magnitude, the correct angle of the negative-sequence current contributed by the inverter with respect to the negative-sequence voltage at the terminal is crucial for the correct operation of any negative-sequence-based directional element. For instance, in Section 5.2.2.1, out of the dq-based, $\alpha\beta$-based, and sequence-based control of the IBR, the negative-sequence-based directional element declares a forward fault (the correct decision under the case study) only if the IBR is IEEE Std 2800 compliant for sequence-domain control.
Negative-sequence magnitude	In some cases, the magnitude of the negative-sequence current is not sufficient to enable negative-sequence directional supervision. Or it has sufficient magnitude initially but decreases below its threshold before the distance element picks up.	The settings for the magnitude of the negative-sequence control or current limiter need to be provided and correctly modeled, including the time constants. The minimal magnitude of negative sequence current depends on the thresholds (a more general requirement would be at least 3I2 > 10% the measured positive sequence current).
Negative-sequence response time or time constant of sequence current regulator	IEEE Std 2800-compliant IBRs (GFL or GFM) from different vendors can have different response times for the sequence current control. This impacts the transients of the negative-sequence current response of the IBR after the inception of the fault. The response of the relays based on the negative-sequence current during this transient period can be impacted.	The sequence controller and the associated feed-forward compensations in the control architecture need to be designed so that during the transient period, the angle convention of the negative-sequence current does not differ too much from the desired response to avoid misoperation of the directional element. The negative-sequence current response should occur within a few cycles (one–three cycles) to enable

IBR Modeling Aspect	Problem Description	Recommendation
		the negative-sequence-based elements to make the correct decisions. For instance, in Figure 113 (a), within one cycle from the fault inception, the directional element observes a forward fault direction (the correct direction in this case study) for the fast response GFL IBR case. But in the slower case, Figure 113 (b), the trajectory of z2A moves inside Z2FTH and Z2RTH after approximately two cycles, and the behavior makes the directional element prone to delaying its decision. It is recommended that both the steady-state value of the sequence current injected by the IBR and the time constant of the transient response should be set by the IBR meet the IEEE 2800-2022 recommendation to support proper protection function operation. The time response characteristics of the magnitude and angle of the negative sequence current response should be made available to protection engineers to determine if they need to delay the Zone 1 tripping response.
Current limiter	The current-limiter strategy proved to be critical for proper representation of the IBR fault response.	The current-limiter logic can affect the IBR fault response, especially in the transient period. Depending on the limiting logic, some elements, such as the directional, can present more oscillatory behavior in the estimated impedance (however, this did not impact the final decision). The negative-sequence polarized quadrilateral element can also present a slight difference in the transient fault period but not in the final relay decision. Depending on the current priority, this affects the mho phase element's circle rotation, which, consequently, might reduce its resistive reach—for example, if the IBR is operating under d-axis priority. This aspect showed a critical difference in the IBR fault

IBR Modeling Aspect	Problem Description	Recommendation
		responses and should be included in the model. Recommendation: The current limiter needs to be provided and correctly represented when building the simulation model. The magnitude-based current limiter is preferred because of the faster response.
Reactive power support	The reactive power support can impact the fault response, especially if starting from a low real power output.	Settings and time constants for the reactive power support should be provided and correctly modeled.
Current-blocking	The duration of the minimum FRT time before current blocking is allowed has an impact on the correct operation of the relay, especially for the negative-sequence-based directional element. If the IBR goes into current blocking too soon, the protection will not have sufficient time to pick up. When the IBR takes longer to block the current injection, the protection can respond properly if other protection criteria are met.	The duration of the minimum time for the IBR to block current injection is crucial in the decision-making of the negative-sequence-based directional element. For instance, Figure 107 (a), (b), and (c), show the negative-sequence-based directional element when the FRT time = one cycle, FRT time = two cycles, and FRT time = four cycles, respectively, and they show how a shorter time can compromise the relay decision. If the blocking time is set to one cycle, the fault direction decision by the relay is significantly affected, whereas for longer times (e.g., four cycles), the relay elements correctly detect the fault direction, and, as a result, the relay is effective. One option is to disable the protection elements that require negative-sequence components if the blocking occurs too fast after the fault inception, but this is at the expense of the protection scheme reliability. It is recommended that making no relay decision is better than making a wrong one. Recommendation: Thresholds and delays related to IBR current blocking need to be considered in the IBR model. Future revisions of IEEE 2800 could require that current blocking, if used for undervoltage response, shall not occur before four cycles.

6.2 Protection Setting Guidance Based on the Characterization Study

This section presents guidance in Table 28 to implement dependable protection schemes for systems fed by IBRs based on the simulation results presented in Section 5.

Table 28. Recommendations for Protection Functions Impacted by IBRs

Transmission System Protective Relay	Impacts Caused by IBR Response	Insights or Recommendation
Distance relay	• Dynamic variations in highly inductive source impedances (magnitude and phase angle) behind the relay (in the third quadrant) for a forward fault influence the mho expansion. • Because the source impedance depends on the IBR control system, the mho expansion can be in the negative-resistance or negative-reactance directions in the R-X plane. • The quadrilateral characteristic polarized by the negative-sequence current is impacted by the IBR current controllers—the effective impedance computed by the relay might have oscillatory behavior, jeopardizing the protection reliability. • Even for current controllers compliant with IEEE Std 2800-2022, the I2-polarized quadrilateral element might not be reliable during resistive fault cases. (This is more likely to happen during single-line-to-ground faults.) • Current-blocking schemes affect the fault detection capability of the relay. • Memory-polarized mho elements might not be reliable during frequency excursion events (not observed in our studies). • System nonhomogeneity is an additional challenge for I2-polarized quadrilateral elements because the equivalent source behind the relay for systems with IBRs is dependent on the IBR controllers.	• The lack of enough supervising current is a risk to distance relay reliability on lines with IBR termination. • The ground distance relay should avoid negative-sequence current polarization, so protection engineers should prefer zero-sequence polarized and positive-sequence voltage-polarized elements. • I2 polarization can be replaced by loop-current polarization for ground and phase distance elements. • Memory-polarized elements in some commercial relays have the feature to reduce the percentage of the voltage memory to avoid problems during frequency excursions while guaranteeing security during zero-voltage faults.
Directional relay	• Negative-sequence directional relays are highly dependent on IBR current controllers, so they might give the wrong fault signature for the direction determination. • If the IBR controls only positive-sequence current, directional elements might fail to pick up due to the lack of supervising current.	• Negative- and zero-sequence directional elements are enabled only when the respective sequence passes a certain minimal threshold to increase the reliability of the directionality decision with this minimum sensitivity.

Transmission System Protective Relay	Impacts Caused by IBR Response	Insights or Recommendation
	• Zero-sequence polarized directional relays are reliable to supervise ground faults in systems dominated by IBRs.	• Negative-sequence directional elements can be used to supervise phase faults if the IBR controls negative-sequence current injection. • Zero-sequence polarized directional elements to supervise ground faults are preferred in grounded systems. • Phase directional elements can be reliable to supervise phase faults in lines with IBR termination.
FID logic	• FID logic based on the angle difference between I0 and I2 depends on a grounded transformer creating a zero-sequence path and on the IBR providing negative-sequence current injection regulation. Proper fault signature and current-level detectors affect this element.	• FID logic can be enabled for grounded systems when the IBR regulates I2, but there is a lack of studies checking the behavior for double-line-to-ground faults in systems dominated by IBRs to check additional logics presented in the FID. • Commercial relays have the option of using voltage-based FID logic, which is an option when ground path or I2 regulation is not present.

7 Conclusions and Future Work

This research study conducted an in-depth EMT simulation study to analyze the impact of various IBR modeling and control aspects on transmission protection relay elements and protection relay decisions. By integrating GFL IBRs and GFM IBRs into a real-world transmission network, the study identifies key aspects of modeling and control that influence traditional protection schemes. The key learnings and findings are summarized as follows:

- Overall, the studies show that protection engineers should not depend on negative-sequence-dependent elements if IBRs do not use explicit sequence current control that complies with IEEE Std 2800.
- GFM IBRs and GFL IBRs primarily impact phasor-protection elements, such as quadrilateral distance elements with negative sequence current polarization, negative sequence directional and fault type selection logic, while differential protection remains reliable (as do time domain elements such as incremental quantities elements and travelling wave). High-resistance faults being the main cause of restrained differential elements, which would also occur in conventional systems without IBRs.
- Protection engineers need to understand the IBR fault response, particularly the negative-sequence current during the transient period (the first three cycles when the protection relays make decisions) to ensure proper relay settings and coordination. Likewise, IBR engineers must understand how specific IBR controls and configurations influence the fault response, and they should design them to ensure consistent fault behavior during the transient period. Generally speaking, conventional generators settle to I2 within a fraction of cycle, allowing relays to take action in approximately 1-1.5 cycles. Thus, IBRs settling down to I2 within 4 cycles helps for some protection elements to respond in approximately the same time frame. If the negative sequence current magnitude exceeds the minimum current threshold more quickly, and the negative sequence current angle does likewise, the protection elements are likely to respond in more quickly.
- The extensive characterization and sensitivity study of IBR modeling and the impacts of control aspects on protection relay elements show that the inverter model (average model versus switching model), DC source (PV, battery and combined), and power loop (PQ-dispatch versus Vdc-Vac control for GFL IBRs and droop versus VSM for GFM IBRs) will not impact the sequence components or the protection elements. However, faster loop (current control), current limiter, and current-blocking time (momentary cessation) do affect the protection elements and can affect the final protection relay decision.
- In particular, negative-sequence current compliance with IEEE Std 2800-2022 is critical for the protection elements, and negative-sequence control should be included in the GFL and GFM inverter control to support the correct decision of the protective relay. We suggest disabling protection elements that need negative-sequence components when the negative-sequence current injection is not controlled by IBR. The negative-sequence current should be higher than a certain threshold (a more general requirement would be at least $3I2 > 10\%$ the positive sequence current supplied by the IBR) so that the supervision elements (current-level detectors) can be enabled. Along with the magnitude, the correct angle of the negative-sequence current contributed by the inverter with respect to the negative-sequence voltage is crucial for the correct operation of any negative-sequence-based directional elements.

- For the IBR fault current settling time, it is straightforward to tune a GFL inverter to meet the four-cycle settling time requirement defined in IEEE Std 2800-2022, but for a GFM inverter it requires difficult tuning and potentially compromising other GFM control objectives. However, IBRs with fault current settling down more than four-cycle still enable the protective relay to make a correct although delayed decision. If the negative-sequence current magnitude is higher than the threshold for the supervision elements and the negative-sequence current phase angle settles in the appropriate range (provided by IEEE Std. 2800 (leading V2 in the range of 90 to 100 degrees for full converters IBRs)) during the first three cycles the relay is likely to trip in the first three cycles. Additionally, some GFM IBRs produce I2 naturally when not on the current limit, which explains the erratic behavior seen in the field.
- The duration of the minimum FRT time before current blocking (momentary cessation) is allowed and has an impact on the correct operation of the relay, especially for negative-sequence-based directional elements. If the IBR goes into current blocking too soon, the protection will not have sufficient time to pick up. When the IBR takes longer to block the current injection, the protection can properly respond if other protection criteria are met. If the blocking time is set to one cycle, the fault direction decision by the relay is significantly affected, whereas for longer times (e.g., four cycles), the relay elements correctly detect the fault direction, and, as a result, the relay is effective. It is recommended that the IBRs be required to avoid current blocking during the first four cycles, if current blocking is used for undervoltage conditions at all.
- Different current-limiting schemes result in different fault responses. More specifically, the current limiter causes instantaneous angle shifts which deceive the relays. The instantaneous dynamic current limiter shows more oscillations and needs more time to settle than the magnitude-based current limiter; therefore, a magnitude-based current limiter is recommended.
- Even though GFM IBRs and GFL IBRs have different control strategies, their fault currents are limited by the current limiter. Both GFL and GFM inverters can contribute a consistent fault current for the protection relay to making timely and correct decisions as long as they produce a reliable negative-sequence current.
- Based on the learnings related to the impacts of the IBR response on the distance element, the directional element, and FID logic, the recommendations are summarized as follows: (1) A ground distance relay should avoid negative-sequence current polarization, so protection engineers should prefer zero-sequence polarized and positive-sequence voltage-polarized elements. Also, negative-sequence current polarization can be replaced by loop-current polarization for ground and phase distance elements in the quadrilateral characteristic. (2) A zero-sequence polarized directional element is preferred to supervise ground faults in grounded systems, and negative-sequence directional elements can be used to supervise the phase fault if the IBR controls the negative-sequence current injection.

The research work conducted in this study contributes to the fundamental understanding of IBR fault responses and their impact on protection elements. Future work will extend the impact study by: (1) offering quantifiable recommendations to IEEE 2800 for relaxing the GFM inverter setting time requirements, based on studies involving both generic and selected OEM models; (2) conducting further analysis to develop recommendations for systems where IBRs provide little or unreliable negative sequence current; (3) identify what type of IBR current limiter methods are

acceptable and which are not; (4) study the protection impact under less severe fault scenarios where the current limiters of GFM and GFL IBRs are not hit.

References

[1] NERC, "NERC Staff Analysis of System Protection Misoperations" (December 2014), https://www.nerc.com/pa/RAPA/PA/Performance%20Analysis%20DL/NERC%20Staff%20Analysis%20of%20Reported%20Misoperations%20-%20Final.pdf.

[2] NERC, *San Fernando Disturbance* (November 2020), https://www.nerc.com/pa/rrm/ea/Documents/San_Fernando_Disturbance_Report.pdf.

[3] G. Benmouyal and K. Zimmerman, "Experience With Subcycle Operating Time Distance Elements in Transmission Line Digital Relays," 37th Annual Western Protective Relay Conference, Spokane, Washington, October 19-21, 2010.

[4] "IEEE standard for interconnection and interoperability of inverter-based resources (IBRs) interconnecting with associated transmission electric power systems," IEEE Std 2800-2022, pp. 1–180, 2022.

[5] IEEE Standard for Interconnection and Interoperability of Distributed Energy Resources with Associated Electric Power Systems Interfaces, IEEE Std 1547-2018, Apr. 2018, doi: 10.1109/IEEESTD.2018.8332112.

[6] J. J. Bian, A. D. Slone, and P. J. Tatro, "Protection System Misoperation Analysis," presented at the 2014 IEEE Power and Energy Society General Meeting (PESGM).

[7] S. Chakraborty et al., "A Generic and Multifunctional Electromagnetic Transient Model for Grid-Following Inverters," 2024 IEEE 52nd Photovoltaic Specialist Conference (PVSC), Seattle, WA, USA, 2024, pp. 1039-1044, doi: 10.1109/PVSC57443.2024.10748997.

[8] P. T. Krein, J. Bentsman, R. M. Bass, and B. L. Lesieutre, "On the Use of Averaging for the Analysis of Power Electronic Systems," *IEEE Transactions on Power Electronics* 5, no. 2 (1990): 182–190.

[9] A. Yazdani and R. Iravani, *Voltage-Sourced Converters in Power Systems: Modeling, Control, and Applications* (John Wiley & Sons, 2010).

[10] S. Golestan, J. M. Guerrero, and J. C. Vasquez, "Three-Phase PLLs: A Review of Recent Advances," *IEEE Transactions on Power Electronics* 32, no. 3 (2016): 1894–1907.

[11] S. Ke and Y. Li, "Grid-Connected Phase-Locked Loop Technology Based on a Cascade Second-Order IIR Filter," *Energies* 16 (2023): 3967.

[12] F. Blaabjerg, R. Teodorescu, M. Liserre, and A. V. Timbus, "Overview of Control and Grid Synchronization for Distributed Power Generation Systems," *IEEE Transactions on Industrial Electronics* 53, no. 5 (2006): 1398–1409.

[13] A. Khan, M. Easley, M. Hosseinzadehtaher, M. B. Shadmand, H. Abu- Rub, and P. Fajri, "PLL-Less Active and Reactive Power Controller for Grid-Following Inverter," *2020 IEEE Energy Conversion Congress and Exposition (ECCE)* (2020): 4322–4328.

[14] N. Kroutikova, C. A. Hernandez-Aramburo, and T. C. Green, "State Space Model of Grid-Connected Inverters Under Current Control Mode," *IET Electric Power Applications* 1, no. 3 (2007): 329–338.

[15] R. Kabiri, D. G. Holmes, and B. P. McGrath, "Control of Active and Reactive Power Ripple to Mitigate Unbalanced Grid Voltages," *IEEE Transactions on Industry Applications* 52 (2015): 1660–1668.

[16] M. A. Elgendy, B. Zahawi, and D. J. Atkinson, "Assessment of Perturb and Observe MPPT Algorithm Implementation Techniques for PV Pumping Applications," *IEEE Transactions on Sustainable Energy* 3 (2012): 21–33.

[17] N. Bottrell and T. C. Green, "Comparison of Current-Limiting Strategies During Fault Ride-Through of Inverters to Prevent Latch-Up and Wind-Up," *IEEE Transactions on Power Electronics* 29 (2013): 3786–3797.
[18] T. Qoria, F. Gruson, F. Colas, X. Kestelyn, and X. Guillaud, "Current Limiting Algorithms and Transient Stability Analysis of Grid-Forming VSCs," *Electric Power Systems Research* 189 (2020): 106726.
[19] L. Huang, H. Xin, Z. Wang, L. Zhang, K. Wu, and J. Hu, "Transient Stability Analysis and Control Design of Droop-Controlled Voltage Source Converters Considering Current Limitation," *IEEE Transactions on Smart Grid* 10, no. 1 (2017): 578–591.
[20] S. Li, L. Xu, and T. A. Haskew, "Control of VSC-based STATCOM using conventional and direct-current vector control strategies," *International Journal of Electrical Power & Energy Systems* (2013): 175–186.
[21] X. Zhao and D. Flynn, "Freezing Grid-Forming Converter Virtual Angular Speed to Enhance Transient Stability Under Current Reference Limiting," presented at the 2020 IEEE 21st Workshop on Control and Modeling for Power Electronics (COMPEL).
[22] X. Zhao and D. Flynn, "Stability Enhancement Strategies for a 100% Grid-Forming and Grid-Following Converter-Based Irish Power System," *IET Renewable Power Generation* 16, no. 1 (2022): 125–138.
[23] M. G. Taul, X. Wang, P. Davari, and F. Blaabjerg, "Current Limiting Control With Enhanced Dynamics of Grid-Forming Converters During Fault Conditions," *IEEE Journal of Emerging and Selected Topics in Power Electronics* 8, no. 2 (2019): 1062–1073.
[24] C. Liu, X. Cai, R. Li, and R. Yang, "Optimal Short-Circuit Current Control of the Grid-Forming Converter During Grid Fault Condition," *IET Renewable Power Generation* 15, no. 10 (2021): 2185–2194.
[25] M. Awal and I. Husain, "Transient Stability Assessment for Current Constrained and Current-Unconstrained Fault Ride Through in Virtual Oscillator-Controlled Converters," *IEEE Journal of Emerging and Selected Topics in Power Electronics* 9, no. 6 (2021): 6935–6946.
[26] C. A. Plet and T. C. Green, "A Method of Voltage Limiting and Distortion Avoidance for Islanded Inverter-Fed Networks Under Fault," presented at the 2011 European Conference on Power Electronics and Applications.
[27] C. A. Plet and T. C. Green, "Fault Response of Inverter Interfaced Distributed Generators in Grid-Connected Applications," *EPSR* 106 (2014): 21–28.
[28] K. G. Saffar, S. Driss, and F. B. Ajaei, "Impacts of Current Limiting on the Transient Stability of the Virtual Synchronous Generator," *IEEE Transactions on Power Electronics* 38, no. 2 (2022): 1509–1521.
[29] B. Fan and X. Wang, "Fault Recovery Analysis of Grid-Forming Inverters With Priority-Based Current Limiters," *IEEE Transactions on Power Systems* (2022).
[30] B. Fan, T. Liu, F. Zhao, H. Wu, and X. Wang, "A Review of Current Limiting Control of Grid-Forming Inverters Under Symmetrical Disturbances," *IEEE Open Journal of Power Electronics* (2022).
[31] B. Bahrani, S. Kenzelmann, and A. Rufer, "Multivariable-Pi-Based dq Current Control of Voltage Source Converters With Superior Axis Decoupling Capability," *IEEE Transactions on Industrial Electronics* 58, no. 7 (2010): 3016–3026.

[32] D. N. Zmood and D. G. Holmes, "Stationary Frame Current Regulation of PWM Inverters With Zero Steady-State Error," *IEEE Transactions on Power Electronics* 18, no. 3 (2003): 814–822.
[33] B. Mahamedi, M. Eskandari, J. E. Fletcher, and J. Zhu, "Sequence Based Control Strategy With Current Limiting for the Fault Ride-Through of Inverter-Interfaced Distributed Generators," *IEEE Transactions on Sustainable Energy* 11, no. 1 (2018): 165–174.
[34] S. Chakraborty et al., "Design of Multifunctional Electromagnetic Transient Model for Grid-Forming Inverters," presented at IECON 2024 – 50th Annual Conference of the IEEE Industrial Electronics Society.
[35] Y. Sun, X. Hou, J. Yang, H. Han, M. Su, and J. M. Guerrero, "New Perspectives on Droop Control in AC Microgrid," *IEEE Transactions on Industrial Electronics* 64, no. 7 (July 2017): 5741-5745, doi.org/10.1109/TIE.2017.2677328.
[36] S. D'Arco and J. A. Suul, "Virtual Synchronous Machines—Classification of Implementations and Analysis of Equivalence to Droop Controllers for Microgrids," presented at the 2013 IEEE Grenoble Conference, Grenoble, France, doi.org/10.1109/PTC.2013.6652456.
[37] B. Mahamedi, M. Eskandari, J. E. Fletcher, and J. Zhu, "Sequence-Based Control Strategy with Current Limiter for the Fault Ride-Through of Inverter-Interfaced Distributed Generators," *IEEE Transactions on Sustainable Energy* 11, no. 1 (Jan. 2020): 165-174, doi.org/10.1109/TSTE.2018.2887149.
[38] M. G. Taul, X. Wang, P. Davari, and F. Blaabjerg, "Current Limiting Control With Enhanced Dynamics of Grid-Forming Converters During Fault Conditions," *IEEE Journal of Emerging and Selected Topics in Power Electronics* 8, no. 2 (2019): 1062–1073.
[39] C. Liu, X. Cai, R. Li, and R. Yang, "Optimal Short-Circuit Current Control of the Grid-Forming Converter During Grid Fault Condition," *IET Renewable Power Generation* 15, no. 10 (2021): 2185–2194.
[40] A. D. Paquette and D. M. Divan, "Virtual Impedance Current Limiting for Inverters in Microgrids With Synchronous Generators," *IEEE Transactions on Industry Applications* 51, no. 2 (2014): 1630–1638.
[41] R. Chowdhury and N. Fischer, "Transmission Line Protection for Systems With Inverter-Based Resources—Part i: Problems," *IEEE Transactions on Power Delivery* 36, no. 4 (2021): 2416–2425.
[42] R. Chowdhury and N. Fischer, "Transmission Line Protection for Systems With Inverter-Based Resources—Part ii: Solutions," *IEEE Transactions on Power Delivery* 36, no. 4 (2021): 2426–2433.
[43] A. S. Zamzam and J. Wang, "Hierarchical Data-Driven Protection for Microgrid With 100% Renewable," *IEEE Energy Conversion Congress and Exposition (ECCE)* (2023): 1–6.
[44] A. A. Aboelnaga, M. A. Azzouz, H. F. Sindi, and A. S. A. Awad, "Fault Ride Through of Inverter-Interfaced Renewable Energy Sources for Enhanced Resiliency and Grid Code Compliance," *IEEE Transactions on Sustainable Energy* 13, no. 4 (2022): 2275–2290.
[45] S. Golestan, J. M. Guerrero, and J. C. Vasquez, "Three-phase PLLs: A review of recent advances," IEEE Transactions on Power Electronics, vol. 32, no. 3, pp. 1894–1907, 2016.
[46] M. Jensen and A. Saeed, "Sensitivity-driven Wide Area Protection (SWAP) Coordination Tools for IBRs," in *2004 IEEE PES T&D*, Anaheim, CA, USA.

[47] F. V. Lopes, M. J. B. B. Davi, M. Oleskovicz, and G. B. Fabris, "Importance of EMT-Type Simulations for Protection Studies in Power Systems With Inverter-Based Resources," presented at the 2022 Workshop on Communication Networks and Power Systems (WCNPS).
[48] A. Haddadi, M. Zhao, I. Kocar, U. Karaagac, K. W. Chan, and E. Farantatos, "Impact of Inverter-Based Resources on Negative-Sequence Quantities-Based Protection Elements," *IEEE Transactions on Power Delivery* 36, no. 1 (2021): 289–298.
[49] E. O. Schweitzer III and J. Roberts, "Distance Relay Element Design," *SEL Journal of Reliable Power* 1, no. 1 (2010): 1–26.
[50] D. Hou, A. Guzman, and J. Roberts, "Innovative Solutions Improve Transmission Line Protection," presented at the 1997 SEL 24th Annual Western Protective Relay Conference, Spokane, WA.
[51] B. Kasztenny and D. Finney, "Fundamentals of Distance Protection," presented at the 2008 IEEE 61st Annual Conference for Protective Relay Engineers, College Station, TX, April, doi.org/10.1109/CPRE.2008.4515045.
[52] K. Dase, A. Guzmán, S. Chase, and B. Smyth, "Applying Dependable and Secure Protection With Quadrilateral Distance Elements," presented at the 2023 SEL Georgia Tech Protective Relaying Conference, Atlanta, GA.
[53] S. Chakraborty et al., "Studying the Impact of IBR Modeling on the Commonly Applied Transmission Line Protective Elements," *IEEE Energy Conversion Congress & Exposition* (2024): 1–9.
[54] S. E. Zocholl, "Three-Phase Circuit Analysis and the Mysterious k0 Factor," prezsented at the 1995 22nd Annual Western Protective Relay Conference, Spokane, WA, April.
[55] M. Washer, J. C. Maun, C. Dzienis, M. Kereit, Y. Yelgin, and J. Blumschein, "Precise Impedance-Based Fault Location Algorithm with Fault Resistance Separation," presented at the 2015 IEEE Eindhoven PowerTech Conference, doi.org/10.1109/PTC.2015.7232595.
[56] C. Dzienis, Y. Yelgin, G. Steynberg, and M. Claus, "Novel Impedance Determination Method for Phase-to-Phase Loops," presented at the 2014 IEEE Power Systems Computation Conference, August, doi.org/10.1109/PSCC.2014.7038393.
[57] H. Altuve, G. Benmouyal, J. Roberts, and D. A. Tziouvaras, "Transmission Line Differential Protection With an Enhanced Characteristic," presented at the 2022 IEE International Conference on Developments in Power System Protection, November, 414–419, doi.org/10.1049/cp:20040150.
[58] H. Miller, J. Burger, N. Fischer, and B. Kasztenny, "Modern Line Current Differential Protection Solutions," presented at the 2010 63rd Annual Conference for Protection Relay Engineers 2, no. 3, doi.org/10.1109/CPRE.2010.5469504.
[59] A. Guzmán, J. Roberts, and D. Hou, "New Ground Directional Elements Operate Reliably for Changing System Conditions," presented at the 1997 SEL Beijing Electric Power International Conference on Transmission and Distribution, Beijing.
[60] Schweitzer Engineering Laboratories Inc., *SEL-411L Relay Instruction Manual Advanced Line Differential Protection, Automation, and Control System* (Pullman, 2016).
[61] D. Costello and K. Zimmerman, "Determining the Faulted Phase," presented at the 2009 SEL 36th Annual Western Protective Relay Conference, Spokane, WA, doi.org/10.1109/CPRE.2010.5469523.

[62] Schweitzer III, E. O., M. V. Mynam, A. Guzman-Casillas, B. Z. Kastenny, V. Skendzic, and D. E. Whitehead, "US10,742,022 B2: Fault Detection in Electric Power Delivery Systems Using Underreach, Directional, and Traveling Wave Elements," U.S. Patent Application Publication US 2017/0146613 A1, filed Feb. 2, 2017, and issued May 25, 2017. https://patents.google.com/patent/US20170146613A1/en?oq=US20170146613A1+
[63] IEEE, *IEEE 2800-2022 – IEEE Standard for Interconnection and Interoperability of Inverter-Based Resources (IBRs) Interconnecting with Associated Transmission Electric Power Systems* (2022), doi.org/10.1109/IEEESTD.2022.9762253.
[64] IEEE, *IEEE Std 1547-2023 – IEEE Standard for Interconnection and Interoperability of Distributed Energy Resources with Associated Electric Power Systems Interfaces* (2023).
[65] Y. Liang, Z. Lu, W. Li, W. Zha, and Y. Huo, "A Novel Fault Impedance Calculation Method for Distance Protection Against Fault Resistance," *IEEE Transactions on Power Delivery* 35, no. 1 (2020): 396–407, doi.org/10.1109/TPWRD.2019.2920690.
[66] S. Chakraborty, et al., "Study Impact of Momentary Cessation of IBRs on Power System Protection Relay Elements," IEEE PESGM 2025 (Accepted).
[67] P. Pinheiro, et al., "Benefits and Recommendations for Using Classic Protection Functions in Transmission Lines Interfacing IBRs Compliant to IEEE 2800," CIGRE US National Committee 2024 Grid of the Future Symposium.
[68] P. Pinheiro, et al., "Analysis of Line Distance Elements for Various IBR Controllers and System Conditions," Journal of Electric Power System Research, 2025 (Accepted).

Appendix

A.1 Grid Strength

The purpose of this test is to examine the impact of grid-following (GFL) and grid-forming (GFM) inverters on protection relay elements, as these effects are not yet fully understood. In this study, GFL and GFM inverters are configured with regulated negative-sequence current control and identical settings to compare their fault responses and the behavior of various protection elements under the same fault conditions: AG (Figure A-1) and BC faults (Figure A-2). The results indicate that both inverter types have a very similar impact on protection elements when regulated negative-sequence current control is implemented.

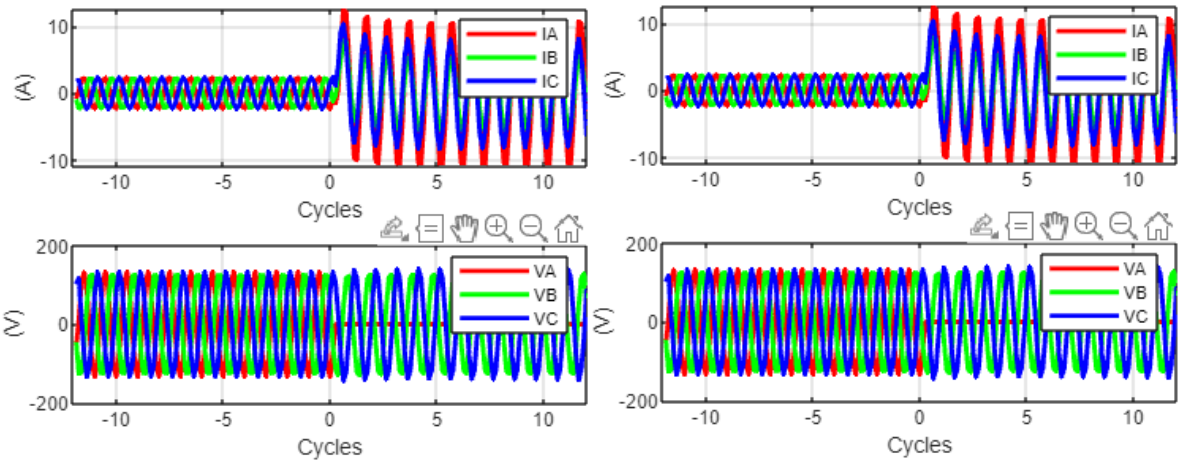

(a)

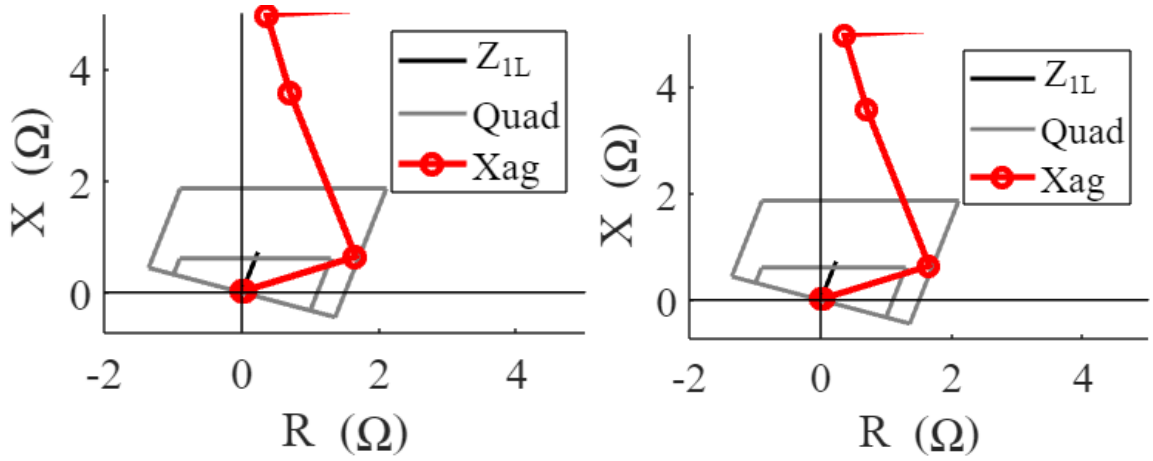

(b)

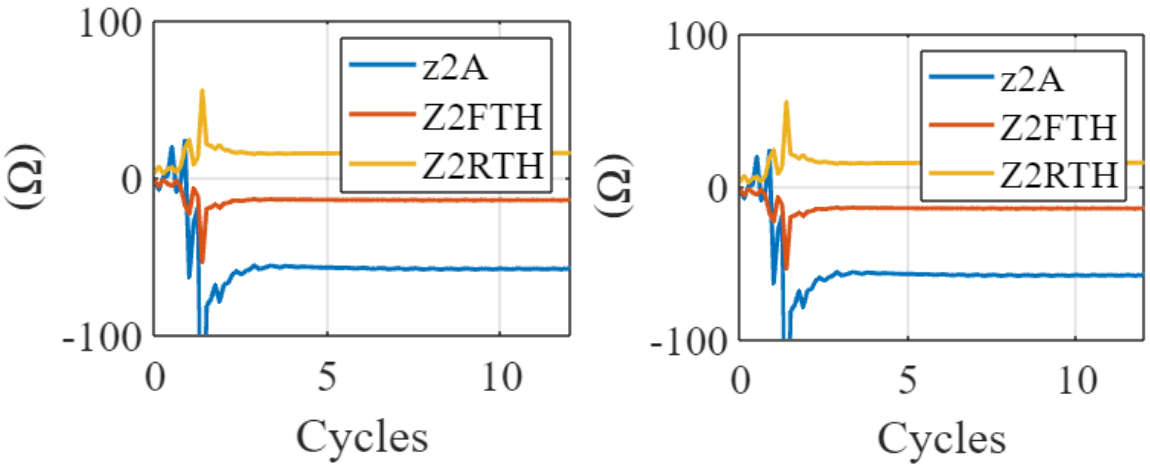

(c)

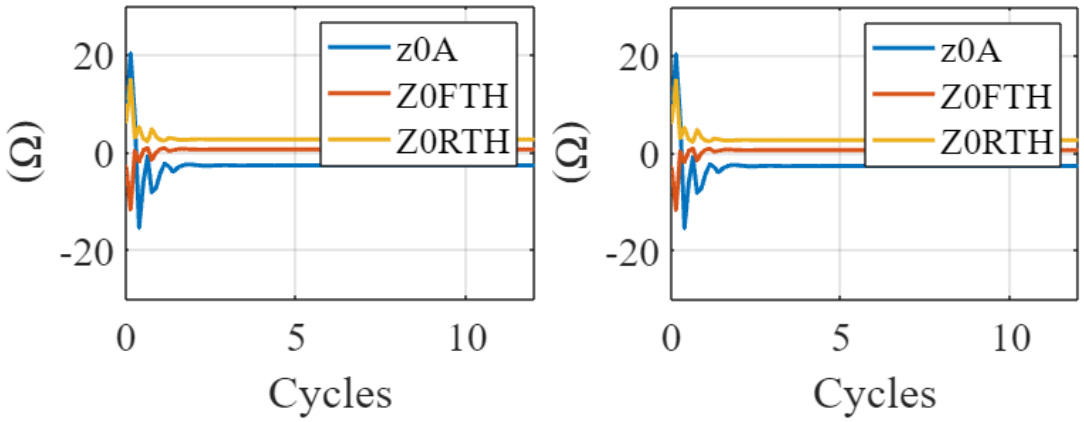

(d)

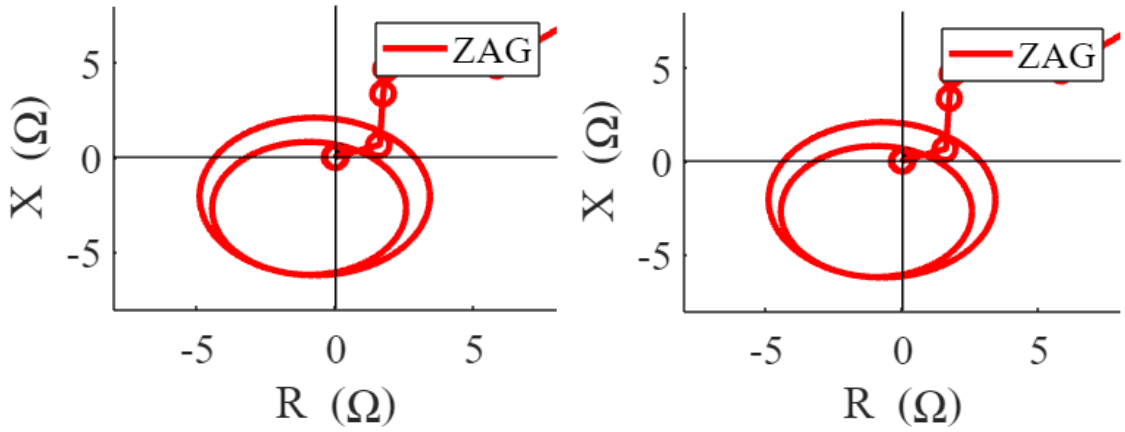

(e)

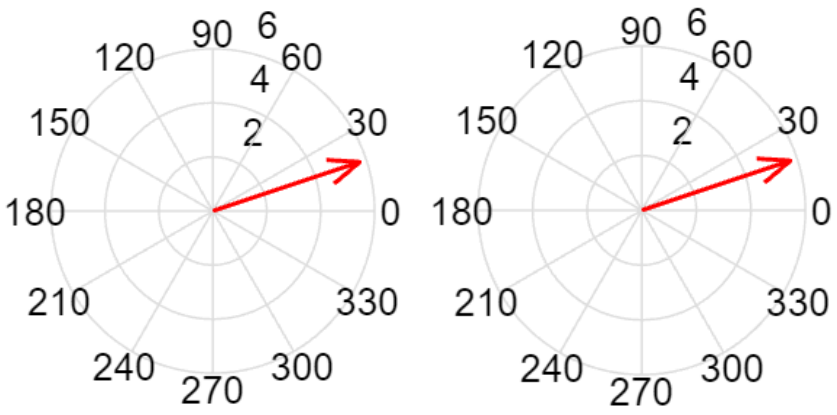

(f)

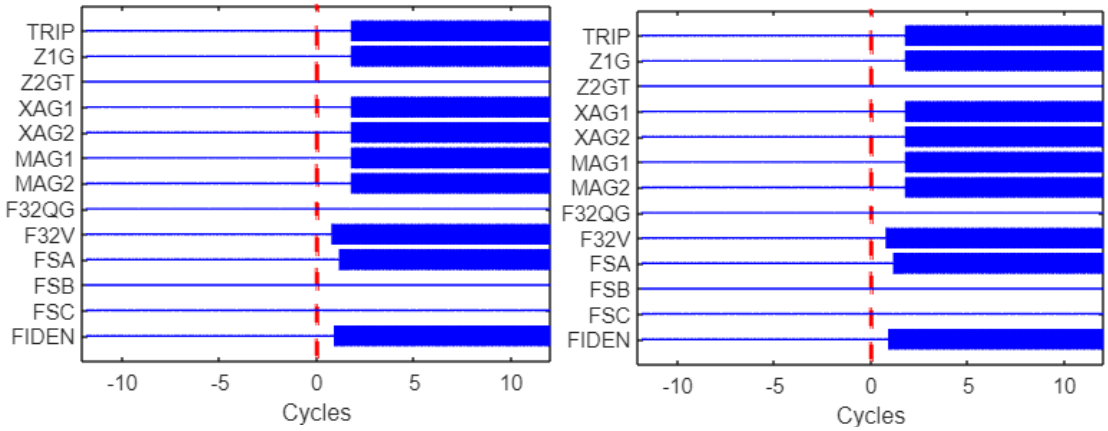

(g)

Figure A-1. GFL (left) and GFM (right) IBR fault responses and the responses of the relay elements under an AG fault: (a) current and voltage, (b) I2-polarized quadrilateral element, (c) negative-sequence voltage-polarized directional element (32QG), (d) zero-sequence voltage-polarized directional element (32V), (e) memory-polarized mho element, (f) fault identification logic; and (g) relay trip signals

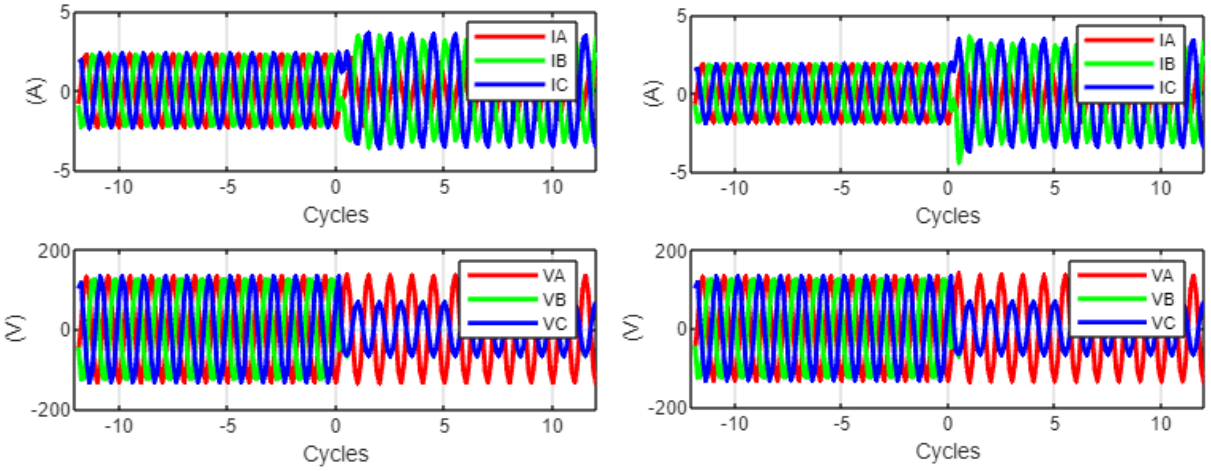

(a)

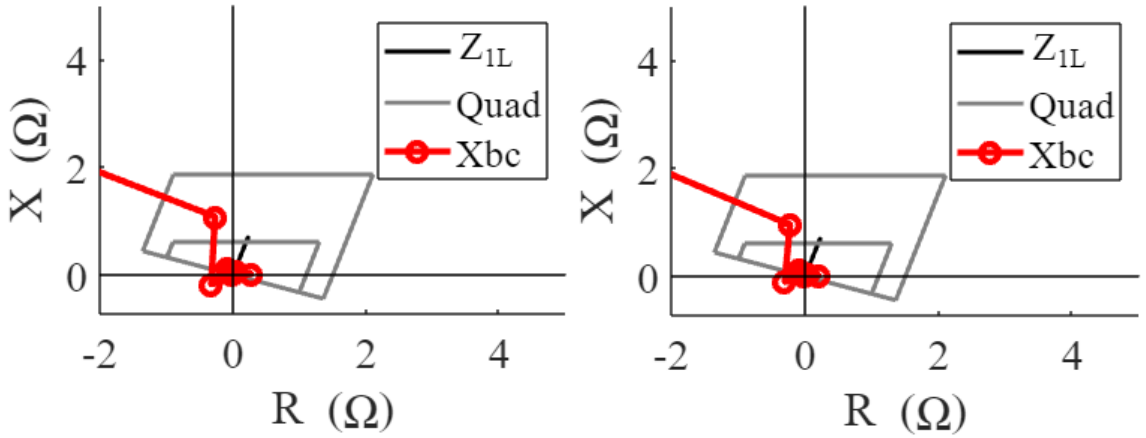

(b)

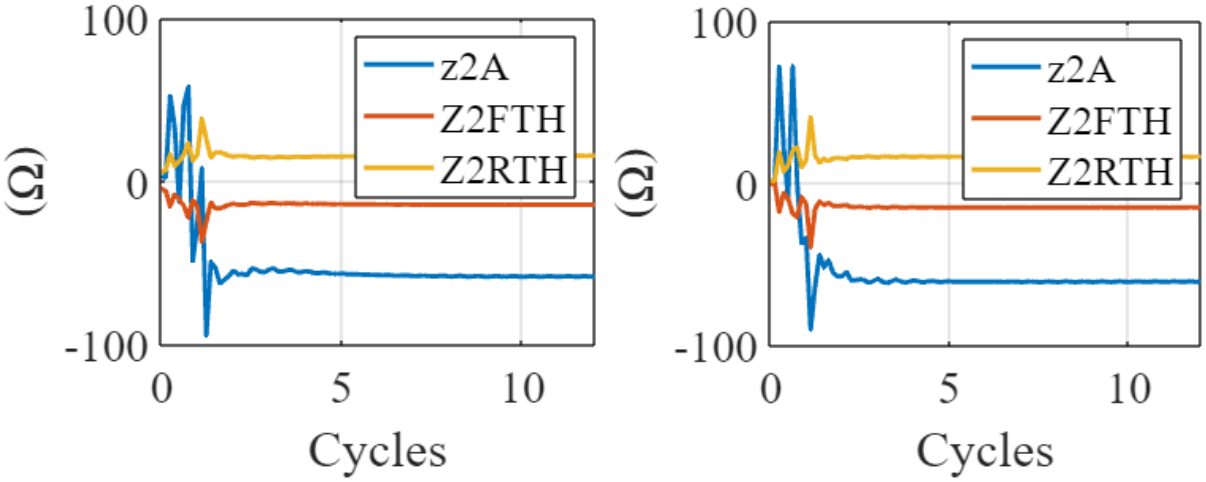

(c)

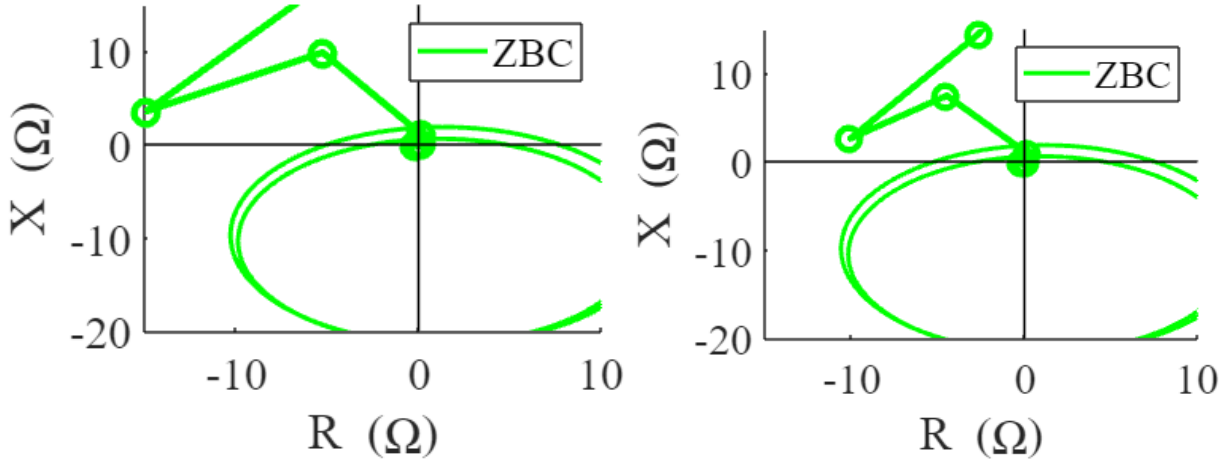

(d)

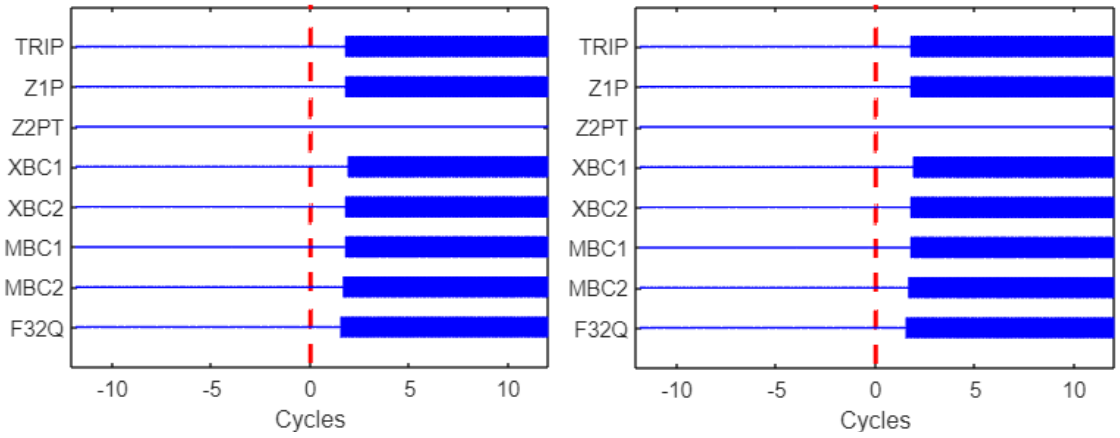

(e)

Figure A-2. GFL (left) and GFM (right) IBR fault responses and the responses of the relay elements under a BC fault: (a) current and voltage, (b) I2-polarized quadrilateral element, (c) negative-sequence voltage-polarized directional element (32QG), (d) memory-polarized mho element, and (e) relay trip signals

A.2 Pre-Fault Operating Point of IBRs

GFL and GFM inverters are configured with regulated negative-sequence current control and settings to compare the fault responses and the responses of different protection elements under different pre-fault operating points (Figure A-3 and Figure A-4). The test results further point out that both inverter types have a very similar impact on protection elements when regulated negative-sequence current control is implemented.

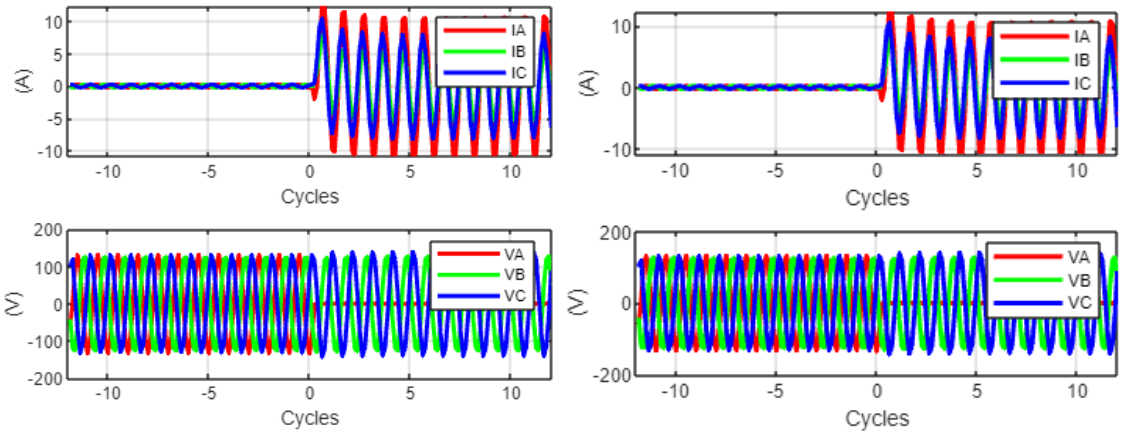

(a)

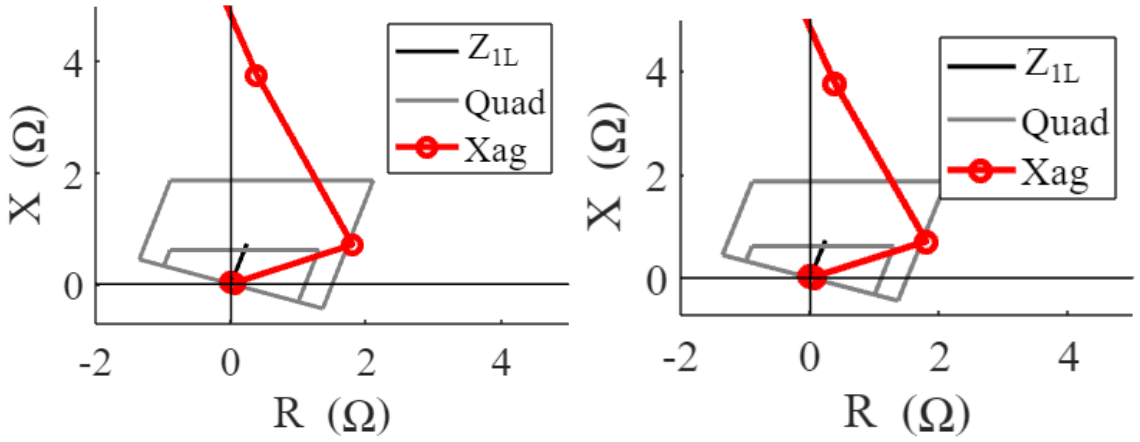

(b)

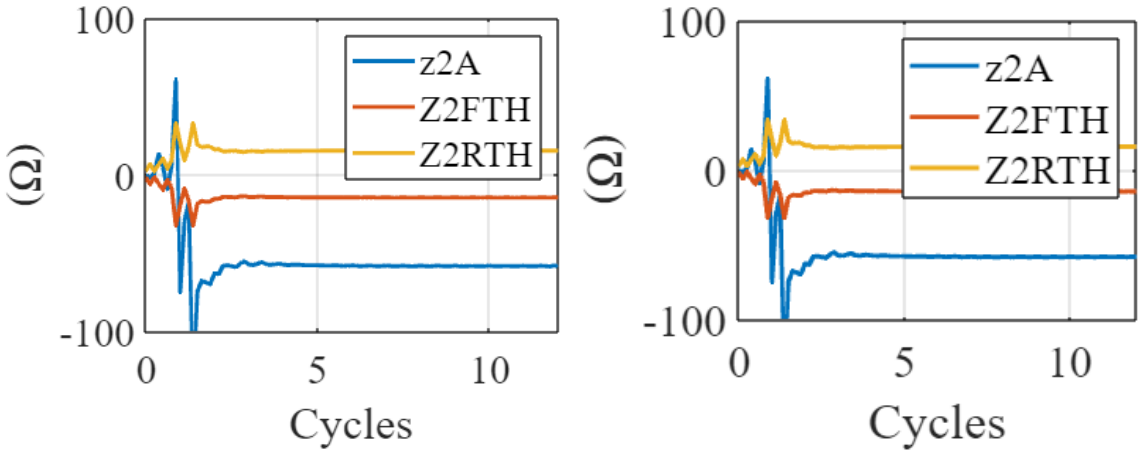

(c)

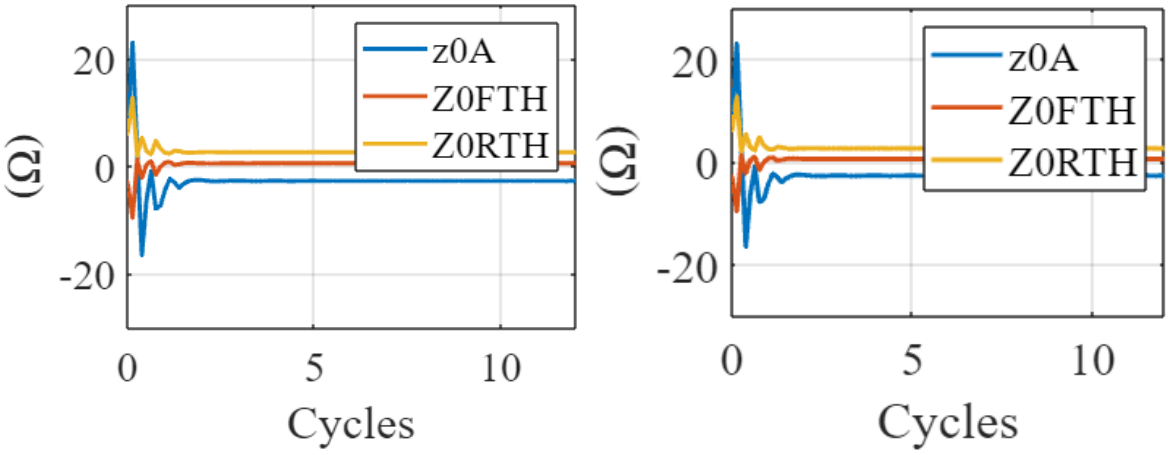

(d)

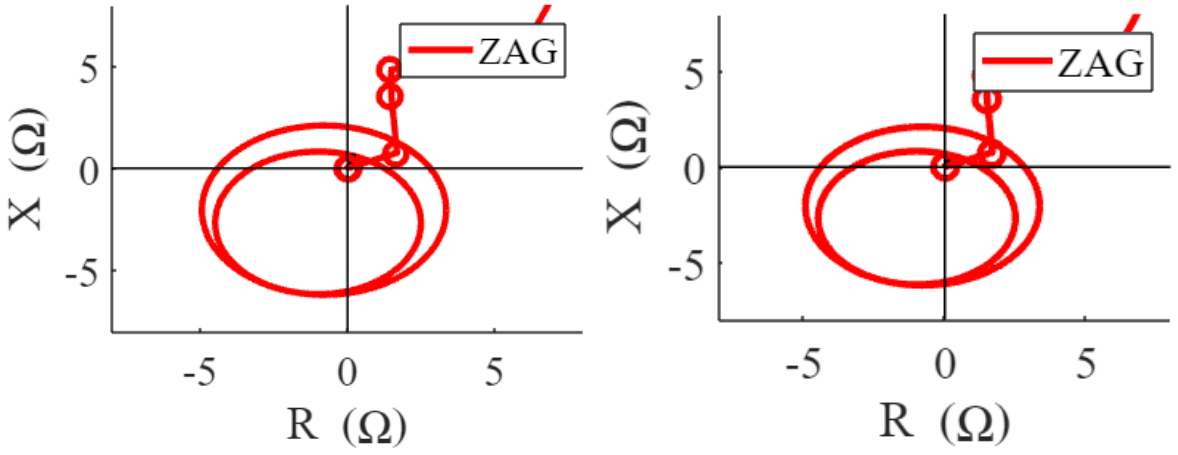

(e)

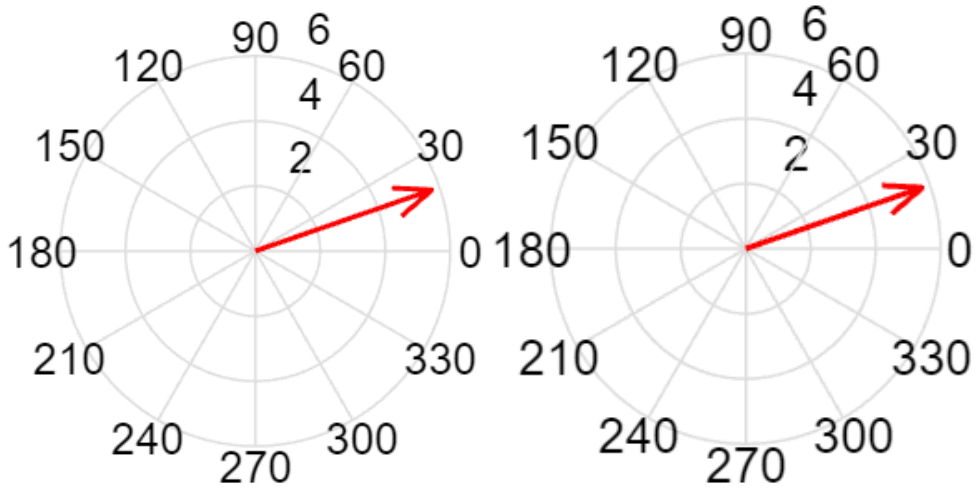

(f)

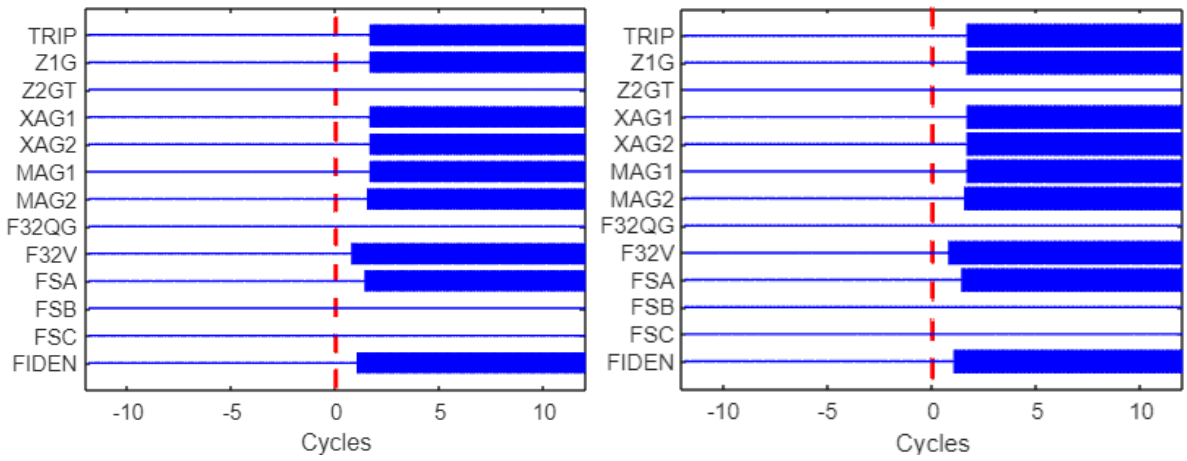

(g)

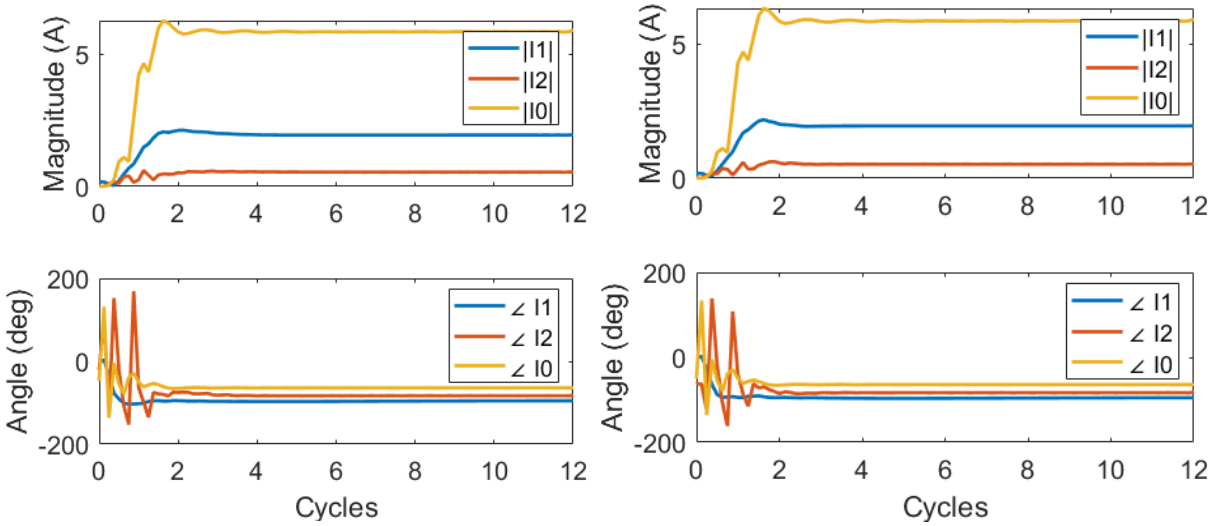

(h)

Figure A-3. GFL (left) and GFM (right) IBR fault responses and the responses of the relay elements under an AG fault (P* = 0.1 p.u. and Q* = 0 p.u.): (a) current and voltage, (b) I2-polarized quadrilateral element, (c) negative-sequence voltage-polarized directional element (32QG), (d) aero-sequence voltage-polarized directional element (32V), (e) memory-polarized mho element, (f) fault identification logic, (g) relay trip signals, and (h) sequence components of the fault current

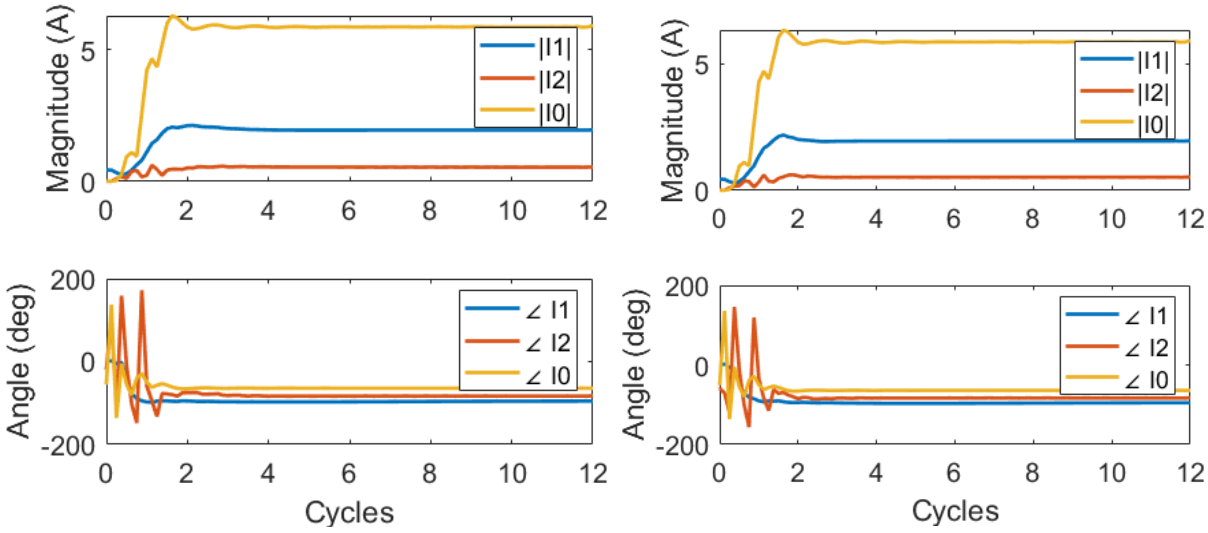

(a)

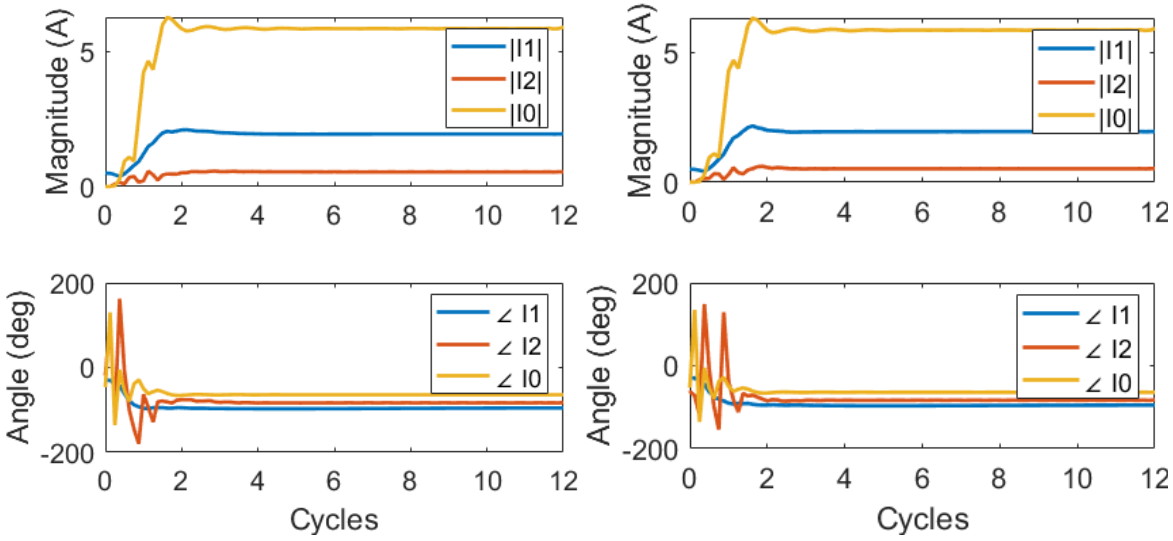

(b)

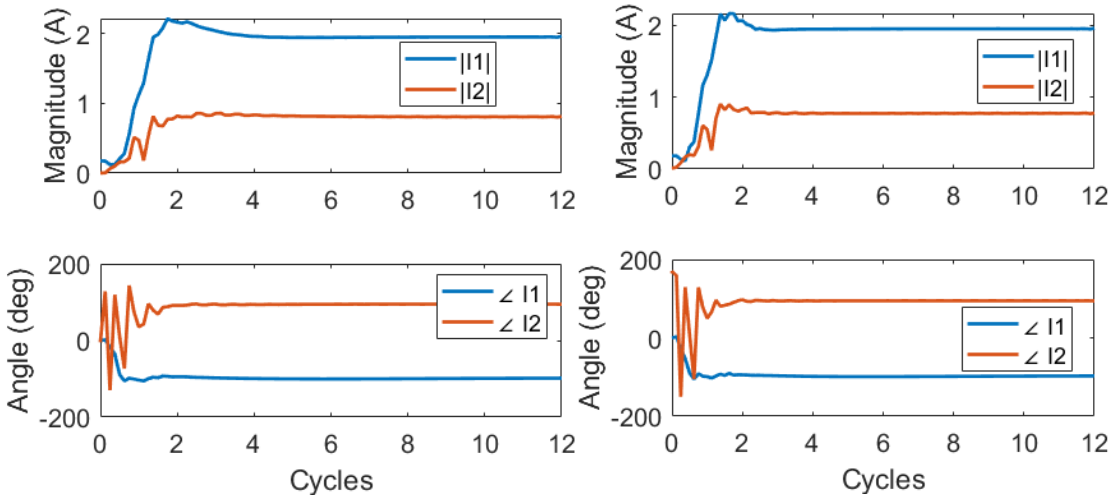

(c)

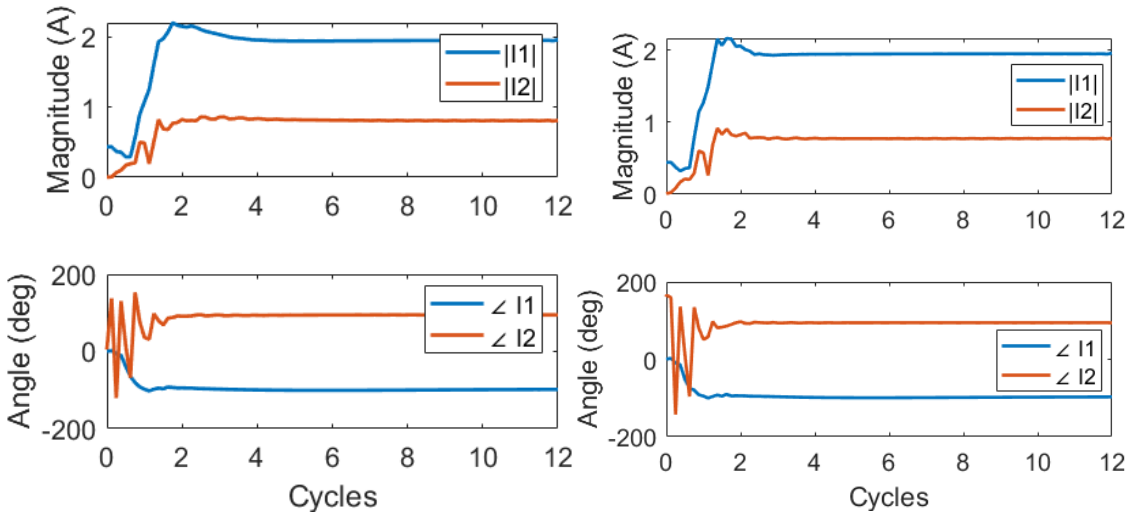

(d)

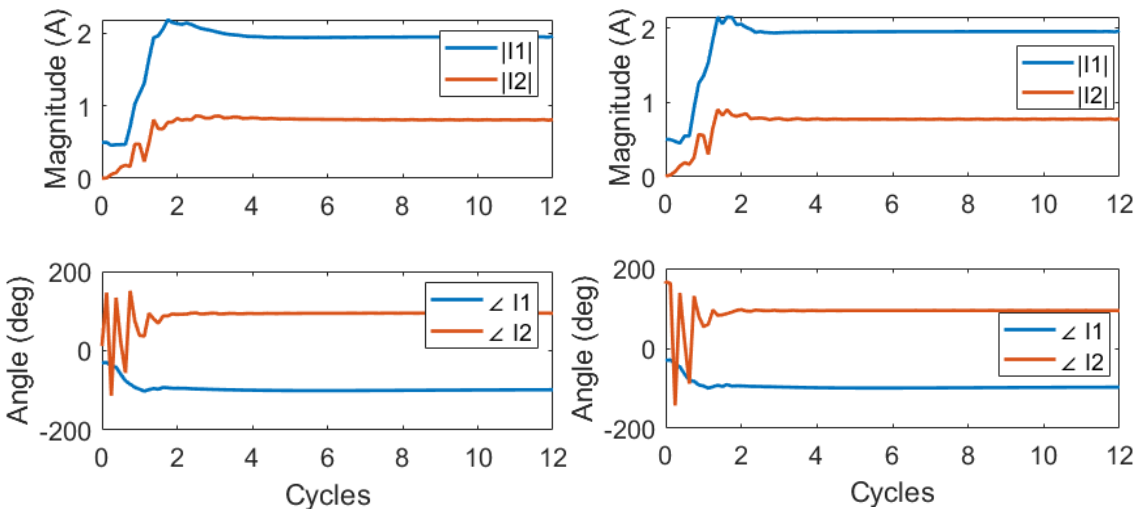

(e)

Figure A-4. Current sequence components of GFL (left) and GFM (right) IBR fault responses under varying pre-fault operating points: (a) P* = 0.25 p.u. and Q*=0 p.u. under an AG fault, (b) P* = 0.25 p.u. and Q* = 0.15 p.u. under an AG fault, (c) P* = 0.1 p.u. and Q* = 0 p.u. under a BC fault, (d) P* = 0.25 p.u. and Q* = 0 p.u. under a BC fault, and (e) P* = 0.25 p.u. and Q* = 0.15 p.u. under a BC fault